UC Irvine

UC Irvine Electronic Theses and Dissertations

Title

Investigating the effects of pandemic SARS-CoV-2 infection on the central nervous system using mouse-adapted SARS-CoV-2 and a preclinical Alzheimer's Disease mouse model

Permalink

https://escholarship.org/uc/item/8f0719wq

Author

Furman, Susana

Publication Date

2024

Copyright Information

This work is made available under the terms of a Creative Commons Attribution-NonCommercial-ShareAlike License, available at https://creativecommons.org/licenses/by-nc-sa/4.0/

Peer reviewed|Thesis/dissertation

eScholarship.org Powered by the California Digital Library
University of California

UNIVERSITY OF CALIFORNIA,
IRVINE

Investigating the effects of pandemic SARS-CoV-2 infection on the central nervous system using mouse-adapted SARS-CoV-2 and a preclinical Alzheimer's Disease mouse model

DISSERTATION

Submitted in partial satisfaction of the requirements for the degree of

DOCTOR OF PHILOSOPHY

in Biological Sciences

by

Susana Furman

Dissertation Committee:
Professor Thomas E. Lane, Chair
Professor Melissa B. Lodoen
Professor Kim N. Green

2024

Portions of Chapter 1 © 2023 John Wiley and Sons, Inc.
Chapter 2 © 2021 American Society for Microbiology
Chapter 3 © 2022 John Wiley and Sons, Inc.
All other materials © 2024 Susana Furman

TABLE OF CONTENTS

Page

LIST OF ABBREVIATIONS……iv
LIST OF FIGURES……...vii
LIST OF TABLES……viii
ACKNOWLEDGEMENTS……ix
VITA……x
ABSTRACT OF THE DISSERTATION……..…xiii
1. BACKGROUND AND INTRODUCTION……1
1.1 Alzheimer's disease……2
1.2 Alzheimer's disease hypothesis……..3
1.3 Alzheimer's disease treatments……..…4
1.4 Risk factors of Alzheimer's disease……...……6
1.5 Animal models of Alzheimer's disease……..……8
1.6 COVID-19……...10
1.7 SARS-CoV-2……...…12
1.8 COVID-19 Risk factors……...……13
1.9 Symptoms and transmission……..……15
1.10 Post-acute Sequelae of SARS-CoV-2 (PASC)……...……16
1.11 COVID-19, neurodegeneration and AD…..……...……17
1.12 Animal models COVID-19…...……23
1.13 Summary……..……...…24
References……..…26
2. MICROGLIA DO NOT RESTRICT SARS-COV-2 REPLICATION FOLLOWING INFECTION OF THE CENTRAL NERVOUS SYSTEM OF K18-HUMAN ACE2 TRANSGENIC MICE.……...…52
Abstract……...…55
Introduction……57
Results……59
Discussion……...…63
Materials and Methods……..……70
References……...…77
Figures and Legends……...…87
3. MAC2 IS A LONG-LASTING MARKER OF PERIPHERAL CELL INFILTRATES INTO THE MOUSE CNS AFTER BONE MARROW TRANSPLANTATION AND CORONAVIRUS INFECTION……..…97
Abstract……..…...…..100
Introduction……...…..……101
Materials and Methods……105

Results……..…108
Discussion……116
References……125
Figures and Legends……140
4. CHARACTERIZING THE EFFECTS OF MOUSE-ADAPTED SARS-COV-2 INFECTION ON AD-ASSOCIATED NEUROPATHOLOGY……..……148
Abstract……150
Introduction……...…152
Materials and Methods……..…155
Results……...…158
Discussion……165
References……172
Figures and Figure legends……...……184
5.SUMMARY…..……..…201
5.1 Summary and Significance……202
5.2 Future Directions…….……...…207
5.3 References……..……209

LIST OF ABBREVIATIONS

ACE2……....angiotensin converting enzyme
Ach……..……..acetylcholine
AchE……..acetylcholinesterase
AD……..Alzheimer's disease
ApoE……..…apolipoprotein
APP……...amyloid precursor protein
ARDS……acute respiratory distress syndrome
ARIA……amyloid-beta imaging abnormalities
Aβ……..amyloid beta
BAM……border-associated macrophages
BBB……..blood brain barrier
BM……bone marrow
BSL3…….……..…….……biosafety level 3
BuChE……..butyrylcholinesterase
CA1……....cornu Ammonis 1; region of hippocampus
CA3……cornu Ammonis 1; region of hippocampus
CCL#.....C-C motif chemokine ligand # (# = interchangeable number)
CNS……..……central nervous system
CoV……...……..coronavirus
COVID-19……....coronavirus disease 19
CSF…….……cerebrospinal fluid
CSF1R…….…colony-stimulating factor 1 receptor
CXCL#.....C-X-C motif chemokine ligand # (# = interchangeable number)
CXCR#.....C-X-C motif chemokine receptor # (# = interchangeable number)
d.p.i……days post infection
DAM……disease-associated microglia
DEG……differentially expressed gene
DNA…….….deoxyribonucleic acid
E……envelope; coronavirus structural protein
EOAD……..early onset Alzheimer's disease
FDA…….……food and drug administration
FDR……..…..false discovery rate
FPKM……..…fragments per kilobase of transcript per million mapped reads
FTD……...……..…frontotemporal dementia
GFAP…….……..….glial fibrillary acidic protein
GFP……..…….green fluorescent protein
GO…….gene ontology
GWAS……..genome-wide association studies

h-MAPT……..human microtubule-associated protein tau
HE……..…..Hemagglutinin esterase; coronavirus structural protein
HHV-6……...human herpesvirus 6
iPSC……..…….induced pluripotent stem cells
HIV……..human immunodeficiency virus
HSV1……..…herpes simplex virus 1
i.n……..…intranasal inoculation
Iba1……..ionized calcium-binding adaptor molecule 1
IFN…….……interferon
Igf-1……..…..insulin-like growth factor 1
IL-1β…….…….interleukin 1 beta
IL-6……...…….interleukin 6
ISH…….……in situ hybridization
JEV…….……japanese encephalitis virus
JHMV……..John Howard Mueller virus
LAMP1……...……lysosome associated membrane protein-1
LOAD……....late onset Alzheimer's disease
M…….membrane; coronavirus structural protein
MCI…….mild cognitive impairment
MERS-CoV……..Middle-East-Respiratory-Syndrome coronavirus
MHV……..……..mouse hepatitis virus
N……..…nucleocapsid; coronavirus structural protein
NfL……....neurofilament light chain
NFT……neurofibrillary tangles
NLRP3……..NOD-like receptor protein 3
NMDA……...….N-methyl-D-aspartate
PET……...…….positron emission tomography
PFU……...……plaque forming units
PLX5622……microglia-depleting drug
PSD95……..Postsynaptic density protein-95
PSEN-1……...presenilin-1
PSEN-2……...presenilin-2
qPCR……...…….quantitative polymerase chain reaction
RAAS…….renin-angiotensin-aldosterone system
RBD……receptor binding domain
RNA……...……..ribonucleic acid
S……..…….spike; coronavirus structural protein
S1……...…..subunit1 of receptor binding domain
S2…….... subunit 2 of receptor binding domain

SARS-CoV-1……..….Severe-Acute-Respiratory-Virus-1
SARS-CoV-2……...……Severe-Acute-Respiratory-Virus-2
SARS2 MA10……... Severe-Acute-Respiratory-Virus-2 (mouse-adapted 10)
scRNAseq……..……..Single-cell RNA-sequencing
Thy1…….. thymocyte differentiation antigen 1
TMEV……...…..Theiler's Murine Encephalomyelitis virus
TMPRSS-2……...…….. transmembrane protease serine protease-2
WAM……white matter-associated microglia
WNV……West Nile Virus
WT……..……wild type

LIST OF FIGURES

Page
2.1 SARS-CoV-2 infects human iPSC-derived neurons……87
2.2 SARS-CoV-2 infection of lungs of K18-hACE2 mice……...……89
2.3 CD8+ T cell infiltration into lungs of SARS-CoV-2-infected mice……...……91
2.4 Widespread neuroinvasion by SARS-CoV-2 of K18 human-ACE2 mice……...…92
2.5 Neurons are targets of infection within the brains of SARS-CoV-2 infected K18-hACE2 mice……93
2.6 SARS-CoV-2 infection of K18 human-ACE2 mice results in microgliosis and myeloid cell infiltration……..……94
2.7 Microglia ablation does not impact control of viral replication in the CNS……95
3.1 *Lgals3*/MAC2 distinguishes infiltrating cells from microglia in the adult CNS……...……140
3.2 MAC2 is a specific and long-lasting marker for bone marrow-derived infiltrating cells….142
3.3 MAC2 is not a ubiquitous marker for plaque-associated microglia during the early stages of disease in 5xFAD mice……144
3.4 The effects of aging on MAC2 staining in WT and 5xFAD mice…….……146
4.1 MA10 infection elicits mild disease in infected mice and genotype does not affect mortality……...……184
4.2 MA10 infection in lungs of WT and 5xFAD mice is associated with differential expression of genes involved in modulation of immune system responses and other inflammatory pathways……..185
4.3 MA10 infection in brains of WT and 5xFAD mice is associated with differential expression of genes involved in regulation of synaptic activity at 7dpi……186
4.4 MA10 infection in brains of WT and 5xFAD mice is associated with differential expression of genes involved in regulation of synaptic activity at 21 dpi…….……188
4.5 Effects of MA10 infection on GFAP staining in WT and 5xFAD mice……190
4.6 Effects of MA10 infection on IBA1 and Mac2 staining in WT and 5xFAD mice……192
4.7 Effects of MA10 infection on dystrophic neurites and amyloid beta plaques in WT and 5xFAD mice…….……194
4.8 Effects of MA10 infection on neurons and cell death in WT and 5xFAD mice……196
4.9 Effects of MA10 infection on synapses in WT and 5xFAD mice…….……198

LIST OF TABLES

Page

4.1 Corresponding primary, secondary antibodies, and associated information……..……200

ACKNOWLEDGEMENTS

I would like to convey my gratitude to my thesis advisor Dr. Thomas E. Lane for his insight, encouragement and patience. I would like to thank him for all of the effort and time he devoted to not only myself, but also the other graduate students. I would also like to thank my committee members Dr. Kim Green, Dr. Melissa Lodoen, and former members Dr. Matt Blurton-Jones, and Dr. Joshua Grill for their feed-back. Additionally, I would like to highlight my gratitude to the Department of Neurobiology and Behavior for their support and guidance, among them my first mentors Dr. Norbert Fortin and Dr. Gabe Elias. I am incredibly grateful to every member of the Lane lab for their constant support and their friendship. I would like to thank my family, my mother Diana Duenas, and my father Gustavo Mesa for their support. Lastly to my husband, David Furman for his unconditional love, unyielding support and encouragement.

Portions of Chapter 1 of this dissertation is a reprint of materials as it appears in the Journal of Neurochemistry, with permission from John Wiley and Sons, Inc. The co-authors listed in this publication aided in the conceptualization as well as editing and reviewing the material. Chapter 2 of this dissertation is a reprint of the materials as it appears in the Journal of Virology, with permission from American Society for Microbiology. The co-authors listed in this publication helped direct and supervise research which forms the basis of this dissertation. Chapter 3 of this dissertation is a reprint as it appears in GLIA, with permission from John Wiley and Sons, Inc. The first-author listed in this publication directed and supervised research which forms the basis for this dissertation. Financial support was provided by the University of California, Irvine, Aging and Alzheimer's Disease NIA Training Grant T32 AG0009.

VITA

Susana Furman

EDUCATION

Graduate Student- University of California, Irvine 2019-2024
Biological Sciences Ph.D Program (Advisor: Thomas E. Lane, Ph.D.) Irvine, CA
Department of Neurobiology and Behavior

B.S. University of California, Irvine 2013-2017
Major- Biological Sciences Irvine, CA

RESEARCH EXPERIENCE

Neuroscience Graduate Student 2019-2024
Graduate Advisor: Thomas E. Lane, Ph.D.- Professor Irvine, CA
Department of Neurobiology and Behavior

- Evaluating the roles of microglia in disease in response to SARS-CoV-2 infection of the CNS in pre-clinical viral mouse models of Alzheimer's Disease.
- Characterizing novel anti-viral treatments in experimental models of SARS-CoV-2 infection.

Staff Research Specialist 2017-2019
Advisor: Norbert Fortin, Ph.D.- Professor Irvine, CA
Department of Neurobiology and Behavior

- Investigated the neural mechanisms underlying episodic memory using a multi-technique approach utilizing high-density electrophysiological recordings paired with complex memory tasks in rodents.
- Supervised undergraduate students and ensured general lab safety compliance
- Ensured all members of lab maintained up to date lab safety and animal handling training

Undergraduate Researcher 2016-2017
Advisor: Norbert Fortin, Ph.D.- Professor Irvine, CA
Department of Neurobiology and Behavior

- Trained and assessed rodents on a complex memory task to assess the role of hippocampus and prefrontal cortex in episodic memory

CLINICAL EXPERIENCE

COPE Health Solutions: Clinical Care Extender Program 2014-2016
Hoag Hospital, Newport Beach

- Assisted patients and patient care teams in various departments within the hospital
- Assisted patients bathing, feeding, repositioning, ambulation, transfer and discharge. As well as, room cleaning/ bed changing, preparing supplies for staff and sample delivery to appropriate labs.
- Completed 300+ hours in the Oncology Unit, Labor and Delivery Unit, Mother Baby Care Unit and Medical-Surgical Unit

TEACHING AND LEADERSHIP EXPERIENCE

Teaching Assistant for Neurobiology undergraduate course, UCI 2020-2021

- Assisted in grading assignments and writing exam questions, as well as holding office hours and answering student questions via email.

Education and Outreach ambassador, Center for the Neurobiology of Learning, UCI 2016-2022

- Assisted community outreach and education to advance interest in neuroscience

Co-Chair for Beall Scholar Program, UCI 2022-2024

- Assisted in development of outreach and the Beall Scholar program targeting underrepresented minority high school students to advance interest in research and education on Alzheimer's disease and dementia
- Planned and helped execute the yearly Emerging Scientists Symposium to exhibit neurodegenerative disease research
- Mentored Beall Scholar high school students yearly and provided guidance on college applications and career

POSTERS

UCI Undergraduate Research Symposium Irvine - CA 2017
UCI Center for Virus Research Symposium Irvine - CA 2022
13th Annual Emerging Scientists Symposium Irvine - CA 2022
Southern California Alzheimer's Disease Centers Research Symposium Irvine - CA 2022
16th Annual SoCal Glial-Neural Interactions in Health and Disease Symposium Riverside - CA 2023

14th Annual Emerging Scientists Symposium	Irvine - CA 2023
Southern California Alzheimer's Disease Centers Research Symposium	Irvine - CA 2023
15th Annual Emerging Scientists Symposium	Irvine - CA 2024

PUBLICATIONS

1. Olivarria GM*, Cheng Y*, Furman S*, Pachow C, Hohsfield LA, Smith-Geater C, Miramontes R, Wu J, Burns MS, Tsourmas KI, Stocksdale J, Manlapaz C, Yong WH, Teijaro J, Edwards R, Green KN, Thompson LM, Lane TE. Microglia do not restrict SARS-CoV-2 replication following infection of the central nervous system of K18-hACE2 transgenic mice. bioRxiv [Preprint]. 2021 Nov 17:2021.11.15.468761. doi: 10.1101/2021.11.15.468761. Update in: J Virol. 2021 Dec 22;:jvi0196921. PMID: 34816260; PMCID: PMC8609895. * Authors equally contributed to this work.
2. Hohsfield LA, Tsourmas KI, Ghorbanian Y, Syage AR, Jin Kim S, Cheng Y, Furman S, Inlay MA, Lane TE, Green KN. MAC2 is a long-lasting marker of peripheral cell infiltrates into the mouse CNS after bone marrow transplantation and coronavirus infection. Glia. 2022 Jan 13. doi: 10.1002/glia.24144. Epub ahead of print. PMID: 35025109.
3. Furman S, Green K, Lane TE. COVID-19 and the impact on Alzheimer's disease pathology. J Neurochem. 2023 Oct 18. doi: 10.1111/jnc.15985. PMID: 37850241.

ABSTRACT OF THE DISSERTATION

Investigating the effects of pandemic SARS-CoV-2 infection on the central nervous system using mouse-adapted SARS-CoV-2 and a preclinical Alzheimer's Disease mouse model

By

Susana Furman

Doctor of Philosophy in Biological Sciences

University of California, Irvine, 2024

Professor Thomas E. Lane, Chair

Alzheimer's disease (AD) is the most prevalent form of dementia among elderly individuals, and although our understanding of some of the genetic causes of AD has improved, other risk factors contributing to the progression of AD require further evaluation. Accumulating evidence indicates that infections significantly exacerbate AD-like pathological changes, suggesting that infection-mediated inflammation may increase the susceptibility of developing AD later in life. This is further highlighted in the face of the ongoing COVID-19 pandemic, as COVID-19 patients exhibit a spectrum of neurologic disease symptoms. COVID-19 appears to impact brain structure and function, and while definitive mechanisms between COVID-19 and neurodegeneration remain poorly understood, several suggest that COVID-19 may induce or accelerate neurodegenerative processes. Microglia play a role not only in host defense to infection, but contribute to disease pathogenesis in AD. They are the resident immune cells in the CNS, monitor homeostasis and respond to injury and inflammation and can release proinflammatory chemokines and cytokines, triggering both innate and adaptive immune

responses. Therefore, understanding the influence of SARS-CoV-2 on the CNS and AD pathology is crucial, and necessitates further research. To address this, experiments were carried out to evaluate the immune response in SARS-CoV-2 susceptible mice (k18-hACE2) and the contributions of microglia in host defense and neuroinflammation in this context.

Intranasal inoculation of k18-hACE2 mice with SARS-CoV-2 resulted in significant weight loss, viral replication within the lungs, and severe disease. Examination of the brains of infected mice revealed extensive viral replication and spread within neurons, with evidence of microglial activation, contributing to the neuroinflammatory environment. We showed that pharmacological depletion of microglia with CSF1R inhibitor in chow (PLX5622) prior to SARS-CoV-2 infection, did not affect viral replication, but resulted in a marked reduction in proinflammatory chemokine and cytokine expression within the brains compared to infected control chow animals. These findings support the notion that microglia do contribute to the neuroinflammatory response, in part, through influencing expression of chemokines/cytokines in response in the k18-hACE2 mouse model of SARS-CoV-2 infection. The ability of the virus to efficiently infect and replicate within the CNS in this model contrasts with clinical findings in COVID-19 patients, where extensive CNS infection is rare, and so we found the k18-hACE2 mouse to not be the best model to accurately recapitulate COVID-19 disease presentation and pathogenesis. To better model COVID-19 clinical symptoms observed in human patients, we utilized a mouse-adapted SARS-CoV-2 -MA10 (MA10) to infect mice. This virus is able to recognize and bind to mouse ACE2, therefore it does not rely on the use of genetically-modified mice expressing human ACE2 for infection. Intranasal inoculation of C57BL/6 mice with MA10 results in lung infection associated inflammation and respiratory disease similar to COVID-19. Importantly, MA10 does not readily infect the CNS of infected mice which makes use of this virus a more reliable and accurate model of COVID-19. We utilized MA10 to evaluate the long-term effect of

infection on neurodegenerative processes in laboratory mice and an established preclinical transgenic mouse models of AD.

Intranasal inoculation of WT and 5xFAD mice with SARS-CoV-2- MA10 resulted in a dramatic increase in expression of gene transcripts associated with modulation of the immune system and other inflammatory pathways in the lungs of infected animals during initial phases of infection that eventually returned to baseline levels of expression after infection had resolved. In the brains, we observed lasting gene expression changes in the absence of viral RNA. These changes were associated with neuronal and synaptic dysfunction**,** and lasted well beyond viral clearance. These lasting changes in gene expression did not translate to detectable changes in neuropathology associated with neuroinflammation (astrocytes, microglia, and inflammatory monocytes) or other AD-associated pathology indicative or neuronal dysfunction (Aβ plaques or dystrophic neurites) in the brains of 5xFAD mice. No evidence of overt neuronal degeneration was found; moreover, no overt changes in synapse number were noted. These findings indicate that experimental infection of mice with MA10 is associated with detectable and enduring changes in the brain associated with neuronal dysfunction, even though gene expression changes do not directly translate into altered neuropathological changes. However, these long-lasting changes in gene expression provide some mechanistic insights that aid in our understanding how cognitive dysfunction may result from COVID-19. Moreover, this study provides evidence that viral infection that results from a lower viral dose or less severe variants of SARS-CoV-2 may not necessarily lead to permanent or long-term deleterious consequences in the brain.

CHAPTER 1

BACKGROUND AND INTRODUCTION

1.1 Alzheimer's disease

Alzheimer's disease (AD) is the leading cause of age- related dementia and is defined as a slowly progressive neurodegenerative disease. It is characterized by an initial impaired ability to form recent memories, inevitably affecting all intellectual functions and impairing the ability to perform daily activities. Patients with AD progress from normal cognition to Mild Cognitive Impairment (MCI) and then follow stages of increasing severity: mild, moderate, and severe [1]. The neuropathological hallmarks of AD can be characterized by the accumulation of amyloid plaques, neurofibrillary tangles (NFTs), neuronal loss and neuroinflammation [2]. The presymptomatic stages and neuropathology can occur years before initial symptom onset and involve early pathological changes in the cortex and hippocampus [3,4]. Extracellular amyloid plaques are predominantly present in the neocortex and hippocampus [5] and are due to the accumulation of amyloid beta (Aβ) peptides as a result of amyloidogenic processing involving the sequential proteolytic cleavage of amyloid precursor protein (APP) by the enzymes β- and γ-secretase [6,7]. NFTs are abnormal filaments composed of misfolded and abnormally hyperphosphorylated tau that can accumulate in the axon and dendrites resulting in neuronal loss due to increased levels of the tau protein. Accumulation of NFTs occurs in the entorhinal cortex, the CA1 and subiculum regions of the hippocampus, whereas other regions such as CA3 and dentate gyrus seem to be unaffected. Furthermore, other limbic structures such as the amygdala contain a high density of tangles [5,8]

Aβ accumulation results in glial cell activation [9] that has also been demonstrated to play a role by contributing to inflammation observed in AD [10–13]. Other studies have demonstrated the co-localization of astrocytes and microglia with Aβ deposition [14,15]. Microglia are the resident immune cells in the central nervous system (CNS), constituting around 10% of CNS cells [16,17]

and arise from progenitor cells in the embryonic yolk sac during development [18]. They monitor the CNS and play a role in homeostasis as well as respond to injury and inflammation. Under normal conditions they exist in a resting state that allows them to surveil the brain parenchyma [19,20]. When activated, microglia can undergo a series of morphological changes associated with a transition from an arborized state to a more ameboid morphology with a larger soma and fewer branched processes [21,22]. In response to CNS injury or infection, activated microglia respond by producing proinflammatory cytokines/chemokines that promote neuroinflammation and/or release anti-inflammatory cytokines that aid in tissue repair and angiogenesis [11,21-,24]. During the progression of AD, these reactive inflammatory microglia also have the capacity to convert other glial cells such as resting astrocytes to reactive astrocytes [25]. Astrocytes are the most abundant glial cell type in the CNS [26]. In a healthy environment, they perform several roles including ion homeostasis, synapse remodeling, neurotransmission, oxidative stress regulation, and maintenance and permeability of the blood brain barrier (BBB) [27–30]. Upon activation, astrocytes as well as microglia secrete pro-inflammatory cytokines: interferon-γ (IFN-γ), tissue necrosis factor-α (TNF-α), interleukins-1 and 6 (IL-1 and IL-6) which can induce neuronal damage and the production of Aβ [31,32].

1.2 Alzheimer's disease hypothesis

The underlying mechanisms by which accumulation of Aβ within the brains has not definitively been identified; however, there are several causes associated with this process. The amyloid hypothesis proposes that there is an increase of Aβ, due to the accumulation of its peptides (Aβ40 and Aβ42). With the accumulation of these peptides, there is also an increase in Aβ42/Aβ40 ratio leading to fibril formation and resulting neurotoxicity, neuronal death and tau

pathology [33]. This version of the amyloid hypothesis is more closely associated with inherited/familial forms of AD associated with genetic mutations that affect processing and production of Aβ. It is important to note that amyloid deposits are also found in the aged brain [34] but given that plaque accumulation can occur years before clinical symptoms, it is possible that cognitively normal patients with amyloid deposits may have had early preclinical AD.

1.3 Alzheimer's disease treatments

Currently the Food and Drug Administration (FDA) has approved several drugs for the treatment of AD. Categories of these drugs include cholinesterase inhibitors, N-methyl-D-aspartate (NMDA)antagonists, and antibodies targeting and removing Aβ plaques. Acetylcholinesterase (AChE) inhibitors block the action of the cholinesterase enzyme from degrading acetylcholine (ACh) and therefore increasing ACh levels in the synaptic cleft. ACh is an essential neurotransmitter for cognitive function and the degeneration of cholinergic neurons in the basal forebrain and loss of cholinergic transmission in the cortex has been associated with impaired cognitive function of AD [35] . Of these inhibitors donepezil, rivastigmine, and galantine are currently approved to use for managing the symptoms of AD.

Donepezil is a well-tolerated, reversible drug that binds to AChE and inhibits the breakdown of ACh, therefore increasing its concentration [36]. Rivastigmine binds to two sites of AChE and butyrylcholinesterase (BuChE), and prevents ACh metabolism. It is used for mild to moderate symptoms and also improves cognitive function. However, oral administration of this drug is associated with adverse effects, including vomiting and nausea and given that AD patients suffer from swallowing problems in addition to memory loss, compliance with this drug becomes difficult to manage. To bypass this problem, rivastigmine can be delivered by skin

patches for continuous delivery [37,38]. Lastly,galantamine is an oral medication approved for the treatment of mild to moderate dementia, including AD. It acts via a dual-mechanism; inhibition of AChE activity to prevent ACh breakdown, and via allosteric modulation of nicotinic receptors leading to a conformational change causing increased release of Ach [39]. Both mechanisms work to increase Ach availability in the brain. Similar to other cholinesterase inhibitors, galantamine is associated with gastrointestinal symptoms like nausea and vomiting.

Overactive NMDA receptors cause abnormal Ca^{2+} signaling and increased glutamate release, resulting in neuronal cell death and decline in cognitive function [40]. Memantine, used to treat moderate to severe AD, is an NMDA receptor antagonist that works by decreasing abnormal glutaminergic activity that leads to neurotoxicity in the AD brain. It is a low-affinity, well tolerated drug that interferes with the receptor without impairing normal synaptic transmission [41].

Unfortunately, most of the drugs approved to treat AD only target symptoms, but they do not reverse or halt disease progression. However, 2 new FDA approved drugs- aducanumab and lecanemab-aim at targeting the underlying biological processes driving AD. Both treatments are humanized monoclonal antibodies approved for those with MCI due to AD with confirmed Aβ pathology via PET scans. Aducanumab binds to both soluble and insoluble Aβ aggregates, and was the first FDA-approved drug that addresses some of the underlying biology rather than the symptoms of AD leading to a decrease in Aβ plaques [42,43]. The dose, manner of administration, and intervals between doses are stringently monitored and controlled due to an increased risk of amyloid-beta imaging abnormalities (ARIA) [44]. Lecanemab binds to soluble Aβ, and has exhibited a decrease in brain Aβ plaques as well as leading to slower cognitive decline [45] . Alternative nonpharmacologic treatments also exist, but they do not target the underlying biology

of AD. However these treatments can aid in the maintenance and improvements of quality of life.

1.4 Risk factors of Alzheimer's disease

Although many theories have been proposed to explain the development of AD, no single theory has gained universal acceptance. As a result, AD is proposed to be a more complex multifactorial disease where multiple risk factors are likely to contribute to its onset. AD can be divided into early-onset AD (EOAD) and late-onset AD (LOAD). EOAD can either be familial or sporadic, while LOAD is sporadic. Familial AD is a rare form of AD only accounting for 1-6% of cases usually associated with family members in more than one generation with AD, and usually occurring earlier in life from 30-65 years [46]. All familial cases of AD are linked to mutations in genes such as APP [47] Presenilin-1 (PSEN-1) [48], and Presenilin-2 (PSEN-2) [49].

While mutations in disease-associated genes are thought to influence onset of familial AD; other genetic polymorphisms have been associated with the more common sporadic form. In LOAD, age is the most important risk factor [50] as cases usually develop after 65 years of age [51]. Arguably the strongest genetic risk factor in LOAD is the apolipoprotein E (ApoE) gene. Each person has two ApoE alleles, and human ApoE has three different alleles: ε2, ε3, and ε4. Alleles ε2, ε3 are associated with a lower risk or are protective, while ε4 is associated with an increased risk [52]. The presence of one ε4 allele increases the risk of AD by threefold, while the presence of two ε4 alleles increases risk by eightfold [53]. Additionally ε4 is also associated with an earlier age of disease onset [54]. A definite sex-linked effect for ApoE has not been established; however, ApoE4 carrier status and CSF tau levels have been more strongly correlated in women than in

men [55], providing supporting evidence that ApoE4 may have a sex- specific effect on risk for neurodegeneration.

The ApoE protein helps carry cholesterol and other types of fat in the bloodstream and is found in the liver and in the brain, including astrocytes and microglia [56]. Both astrocytes and microglia have roles on Aβ clearance [57] and ApoE4 expression alters normal function of both cell types. ApoE4 specifically, increases AD risk through impairing their ability to efficiently clear Aβ compared to ApoE3 and ApoE2 [58–60]. ApoE4 is also correlated with tau pathology where amyloid pathology is also present [61] and has also been shown to worsen tau pathology in tau mouse models as well as in human primary tauopathies [62].

Aging, genetic risk factors and sex cannot account for all AD cases. Environmental risk factors linked to an increased risk of AD include: inflammation and other medical comorbidities [63–65], air pollution and oxidative stress [66], diet and nutrition [67], head injury [68] and heavy metal exposure [69]. Microbial and viral exposures have been suggested to be correlated with an increased risk of neurodegeneration including AD [70,71]. The possible involvement of infectious agents has been suggested as an emerging risk factor in the etiology of AD and many past studies have implicated several infectious agents in AD, including: human immunodeficiency virus (HIV), West Nile virus (WNV) , *Chlamydia pneumoniae*, *Borrelia burgdorferi* spirochetes, *Troponema pallidum*, Epstein-Barr virus (EBV), herpes simplex virus- 1 (HSV1) and human herpesvirus- 6 (HHV-6) [72–77]. The increasing number of studies associating infections necessitates serious re-evaluation of the contribution of infections to AD and other associated dementias.

1.5 Animal models of Alzheimer's disease

There are numerous preclinical animal AD models available today. It is important to emphasize that no existing model recapitulates all features observed in AD. An ideal animal model would display the full spectrum of both pathological and clinical features observed in human AD. The majority of AD cases are characterized as LOAD with unknown etiology. However, many of the preferred AD models today are generated through genetic manipulation of AD-associated mutations that drive the more rare and genetically driven form of AD. Therefore, use of a specific AD model should be carefully determined based on the goals of each individual study. A wide variety of vertebrates have been used as models, these include: rat, sea lamprey, zebrafish, pig, sheep, mice and non-human primates; invertebrate species also include the fruit fly and roundworm [78]. However, due to the low cost, ease of breeding and genetic manipulation, mouse models of AD are more widely preferred and available.

It is important to note that there are physiological and behavioral differences in background strains used in AD mouse models that can influence phenotype [79–81]. Therefore careful selection of the AD mouse model with respect to its background strain should also be considered depending on the particular study. The list of types of AD mouse models is extensive, but many common models express human APP, presenilin genes (PSEN1 and 2), tau, or apolipoprotein E.

Amyloid/Aβ models are based on the expression of APP and PSEN mutations. PSEN1 or PS1, is the most common autosomal dominant gene associated with familial forms of AD. PS1 mutant mice have increased levels of Aβ42 but not Aβ40 [82]. These mice develop robust amyloid pathology, as well as learning and memory impairments. It is important to note that PSEN1 mutations alone are not enough to drive pathology or cognitive impairments because mouse and

human APP (hAPP) and Aβ are different in 17 amino acids with three key residues that make human APP more likely to aggregate [80,83,84]. hAPP and therefore Aβ appear necessary to drive the AD associated phenotype in mice. Within these lines, there can be variable promoters, isoforms and mutations driving the expression of hAPP.

With this in mind, a widely accepted mouse model, the 5xFAD, recapitulates Aβ pathology in an accelerated manner. It expresses five mutations driven by the thymocyte differentiation antigen 1 (Thy1), that provides high levels of expression of these mutations selectively in neurons. The 5xFAD expresses the Swedish, Florida (1716V) and London (V717I) mutations in hAPP and the M146L and L286V PSEN1 mutation. 5xFAD mice exhibit robust pathology including increased levels of Aβ42, development of Aβ plaques at four months of age, inflammation, microgliosis, reactive astrocytes and dystrophic neurites, with notable sex differences in pathology. They also have a variety of physiological, behavioral and cognitive deficits [85,86]. It is important to note that although models like this recapitulate the Aβ pathology of AD, but do not present tau pathology.

Murine tau does not naturally aggregate into NFTs in the same manner that human tau does [87]. Due to this, tau mouse models utilize human-MAPT that induces NFT formation and develop tau pathology [88–92], but mutations in *h-MAPT* cause (FTD) and not AD [93,94]. Given the observed relationship between amyloid and tau pathologies in AD, mouse models that recapitulate both have also been developed [95–97]. Tau pathology in AD mouse models depends on the expression of human tau with mutations associated with frontotemporal dementia FTD [98]. One notable and well characterized example is the 3xTg which combines hAPP with the Swedish mutation, PSEN1, and P301L. P301L is the most common FTD associated tau mutation that favors tau aggregation [99–101]. As previously stated, ApoE is the greatest risk factor for AD, and

mouse models have been developed expressing familial AD (FAD) mutations along mouse-ApoE (mApoE). ApoE knock-in mice are available, with ApoE4 mice exhibiting synaptic plasticity and cognitive deficits [102–105].

AD mouse models are often criticized because they do not completely recapitulate all aspects of AD associated pathology, or because often, preclinical studies that had success with these models largely failed in human clinical trials. However, it is important to note there are limitations in using mouse models to make conclusions about sporadic AD, as most of these mice more closely model familial AD.

1.6 COVID-19

Coronaviruses (CoVs) belong to the order Nidovirales and include the Arteriviridae, Roniviridae, Mesoniviridae, and Coronaviridae families. The Coronaviridae family is further divided into alpha-α, beta-β, delta-δ, and gamma-γ subfamilies based on phylogeny. CoVs are nonsegmented positive-sense RNA viruses with the largest RNA genomes, identified to date which can be up to 30 kilobases [106]. They contain a 5' cap structure with a 3' poly(A) tail that allows them to be directly translated into protein. The defining physical feature of CoVs is the spike projections that protrude from the surface of the virion that give the appearance of a solar corona, hence the name coronavirus.

CoVs contain four main structural proteins encoded in the 3' end of the viral genome. These proteins include the spike (S), membrane (M), envelope (E), and nucleocapsid (N). The S protein on the surface of CoV is what gives the virion its crown-like appearance, and it is composed from a trimer of molecules. In some CoVs, the S monomer is cleaved by a cellular furin-like protease into two subunits; S1 forms the head and contains a variable receptor binding

domain (RBD) and S2 forms the stalk [106]. Initial virion attachment is initiated by the S1 subunit which mediates binding a particular host cell receptor, while the S2 subunit undergoes conformational changes that result in fusion to the cell membrane. The M protein is the most abundant structural protein and defines the shape of the virion [107]. It plays a role in assembly by interacting with other structural proteins and in the budding of virus particles [106,107] as well as playing a role in the induction of an interferon (IFN) response [108]. The E protein is the smallest structural protein and has a role in assembly and budding [109]. However, in some CoVs, the E protein has additional roles. In Severe Acute Respiratory Syndrome (SARS-CoV-1) it is required for pathogenesis, as SARS-CoV-1 lacking the E protein exhibited lower viral titers and has an attenuated phenotype in SARS-CoV-1 rodent models [110–113]. The N protein has an important role in interacting, packaging and protecting the genomic viral RNA and plays a critical role in transcription and virion assembly by interacting with the M protein [114]. Lastly, Hemagglutinin esterase (HE) is only present in some β-CoVs that include murine hepatitis virus (MHV) and human CoVs HCoV-OC43 and HCoV-HKU1 and it is thought to enhance S-protein mediated entry and spread [115].

In general,α and β-CoVs primarily infect and originate from mammals, primarily bats, whereas γ and δ-CoVs originate from birds [116]. In the majority of animal hosts, most CoVs cause respiratory and gastrointestinal symptoms. CoV infections in humans also involve gastrointestinal and mild to severe respiratory symptoms from the common cold to pneumonia [117]. To date, seven different CoVs are known to infect humans. These include two α-CoVs (HCoV-229E and HCoV-NL63) and 5 β-CoVs (HCoV-HKU1, HCoV-OC43, SARS-CoV-1, MERS-CoV, and more recently SARS-CoV-2 [118]). Four of these endemic HCoVs: 229E, NL63, HKU1, and OC43 are responsible for 10-30% of common cold cases [119].

SARS-CoV-1 and MERS-CoV have been responsible for epidemics in 2003 and 2012 respectively [118,120,121] with survivors experiencing lingering symptoms after acute disease [122]. More recently, severe acute respiratory syndrome coronavirus 2 (SARS-CoV-2) was identified as the infectious agent responsible for coronavirus disease 2019 (COVID-19) which has developed into a global and ongoing pandemic since early 2020 [118] and has affected hundreds of millions of people worldwide [123].

1.7 SARS-CoV-2

SARS-CoV-2 shares about 80% of its genetic identity with SARS-CoV [124] and both viruses use angiotensin converting enzyme 2 (ACE2) as its receptor [125,126]. The SARS-CoV-2 RBD differs in several key amino acid residues from SARS-CoV RBD, allowing for a documented 10-20 fold higher binding affinity with the human ACE2 (hACE2) receptor, which may account for the greater infectivity of SARS-CoV-2 [127].The S1 subunit of the RBD in the S protein binds to hACE2 and the transmembrane protease serine protease-2 (TMPRSS-2) and ADAM metallopeptidase domain 17 (ADAM17) of the host cells aid in the priming the S protein to allow fusion of both the host and viral membranes through S2 subunit so the virus can enter the host cell via endocytosis [128]. The expression of these molecules in cells determines the viral tropism of SARS-CoV-2 and identifies tissues and organs most susceptible to infection.

ACE2 is thought to play a role in regulation of the renin-angiotensin-aldosterone system (RAAS) and be a regulator of cardiac function and blood pressure [129,130]. It is mainly expressed in alveolar epithelial cells of the lungs and enterocytes of the small intestine [131] but can be expressed in other tissues. High expression levels of ACE2 were noted in the testis, kidneys,

heart, thyroid, and adipose tissue, as well as in the blood, spleen, bone marrow, brain, blood vessels, and muscle at lower expression.

1.8 COVID-19 Risk Factors

There are several risk factors that increase disease severity and mortality related to COVID-19 and these comorbidities include conditions such as obesity, hypertension, cardiovascular disease, and diabetes [132,133]. Genome-wide association studies (GWAS) have identified genes coinciding with ABO blood groups [134], and immune function [135]. Additionally, the presence of neutralizing auto-antibodies against type 1 interferons with either several or fatal disease have been reported [136,137] and this is correlated with increased age which is arguably the biggest contributing risk factor for COVID-19 [138]. To date, overwhelming evidence indicates that increased age is associated with not only a higher risk of disease severity, but also mortality [139–141].

Similar to COVID-19, age is a key factor associated with dementia [142] Interestingly, pre-existing dementia has also been identified as a prominent risk factor for COVID-19. In a recent study it was discovered that among patients with dementia, Alzheimer's disease (AD) was the most prevalent cognitive impairment observed in those who succumbed to COVID-19 [143]. Additionally, patients with dementia typically experience more severe clinical disease and increased mortality due to infection [144,145]. Whether this is due to those with dementia being less able to modify behavior to prevent infection or the majority of those with dementia being elderly, and therefore have a muted immune response rendering them more prone to infection [146]. However recent studies have found other links to risk genetic risk factors associated with AD to also be tied to COVID-19 risk.

Previous studies have reported on the ApoE4 mutations and its effects on susceptibility to other viral infections such as HIV, HSV and hepatitis C [147–149]. ApoE4 is also widely recognized to be the strongest genetic risk associated with the onset of sporadic AD [52], but it recently has also been identified as a genetic factor implicated in risk of infection, disease severity and mortality due to COVID-19. Recent studies have found that ApoE4 homozygous carriers have a two-fold increase in risk for SARS-CoV-2 infection and a quadrupled increase in risk of death due to COVID-19, even controlling for other existing comorbidities including pre-existing dementia [150,151]. Additionally, ApoE4 carrier status also correlated with higher mental fatigue post-infection compared to noncarriers and reported that these effects could partly be due to cerebrovascular damage [152]. This could partly explain its effects, given ApoE dysfunction has been associated with cardiovascular disease and other comorbidities that increase vulnerability to COVID-19 [153]. *In vitro* experiments have also generated data supporting greater susceptibility to SARS-CoV-2 infection in ApoE4 human-induced pluripotent stem cell (hiPSC) derived neurons and astrocytes, demonstrating an increase in astrocytic nuclear fragmentation due to infection [154]. Lastly, *in vivo* mouse experiments indicate an increase in viral loads, worsened survival, and a dampened immune response in infected ApoE4 knockin mice [155].

The mechanisms by which ApoE4 increases risk of COVID-19 infection and outcomes are still not fully understood; however, ApoE4 is known to affect a variety of processes that are likely to facilitate infection and clinical disease outcomes. ApoE4 is associated with increased BBB permeability and loss of integrity [156] which could facilitate viral entry into the CNS. Other studies have postulated that ApoE4 may enhance infection via the regulation of cholesterol homeostasis by elevating cholesterol levels [157] which may facilitate binding of the viral S protein to its receptor ACE2 [158,159]. Additionally, ApoE4 is reported to promote the production of some

pro-inflammatory cytokines [160–163] increasing the likelihood of a cytokine storm, often associated with more severe COVID-19 [164–167].

1.9 Symptoms and transmission

SARS-CoV-2 is primarily transmitted via respiratory droplets and aerosols, with a median incubation period of 4-5 days before symptom onset in the majority of individuals [168]. Although some cases are asymptomatic, infection in the majority of patients presents with mild-to-moderate respiratory disease and other flu-like symptoms including fever, headache and gastrointestinal manifestations like diarrhea [166,169]. The most common symptom is dyspnoea that can, in some severe cases, lead to hypoxaemia [170]. In more severe cases this can result in acute respiratory distress syndrome (ARDS). which is an inflammatory form of lung injury associated with alveolar damage that ultimately leads to respiratory failure [171]. While infection is more highly associated with respiratory symptoms and disease, other organ systems including cardiac, renal, gastrointestinal, and neurologic [172–174] are targets of infection given the widespread expression of ACE2, with multiple organ failure observed in some patients [175].

While COVID-19 presents primarily with respiratory symptoms, neurological symptoms and complications have been extensively documented [176,177,177–180], with the majority of neurological manifestations occurring in patients with severe disease [181]. Additionally, neurological symptoms can manifest before, during or after the onset of respiratory symptoms [182] including confusion and delirium which can present without respiratory symptoms [183]. More common neurological symptoms include myalgia (muscle pain or ache), headache, dizziness, as well as olfactory and gustatory dysfunction that includes anosmia and ageusia [184,185]. Anosmia is thought to result from damage to olfactory epithelium, rather than neuronal injury [186]. Other

complications have also been observed with more severe disease including higher probability of ischemic strokes, cerebrovascular disease, coagulation abnormalities/hypercoagulation, seizures, meningitis and encephalitis [179,187–194].

1.10 Post-acute Sequelae of SARS-CoV2 (PASC)

Most patients with COVID-19 recover with no symptoms associated with infection; however some report lingering symptoms and other health problems after the initial acute infection has resolved that vary from mild to severe. This is not unprecedented for individuals infected with coronaviruses as individuals infected with SARS-CoV and MERS-CoV have exhibited persistent lingering symptoms after acute disease [122]. Moreover, Influenza is another RNA virus that is associated with re-occuring pandemics and infection is associated with a variety of effects on the nervous system [195,196]. Overwhelming evidence indicates that long-term cognitive impairments are commonly followed by those that have experienced ARDS [197]. More recent studies, however, have indicated that even non-hospitalized patients with mild disease also experience prolonged symptoms post COVID-19 infection [198]. Additionally, other human CoVs such as OC43, more commonly associated with the common cold, have been reported to affect the hippocampus, especially regions associated with memory and cognition [199,200]. Given that the hippocampus plays a pivotal role in learning and memory, there could be long-term negative consequences to cognition resulting from CoV infections. Long-term effects post COVID-19 are new and not yet fully understood and more studies are required to determine if SARS-COV-2 leads to hippocampal degeneration and if this can possibly induce or worsen the onset of neurodegenerative diseases such as AD.

1.11 COVID-19, neurodegeneration and AD

Given that viral infections already have been implicated with an increased risk of cognitive impairment and other neurodegenerative diseases [70], it is not surprising that COVID-19 has also recently been associated with the development of rapidly progressive dementia with an increased risk of a new AD diagnosis within 360 days after initial COVID-19 diagnosis [201]. COVID-19 appears to affect brain structure and function in a variety of different manners, some of which could explain the association between COVID-19 infection and neurodegeneration. Although definitive causal links between COVID-19 and neurodegeneration have not been established, several mechanisms have been proposed by which COVID-19 could induce or accelerate changes related to neurodegeneration, dementia and ultimately AD.

Numerous neurodegenerative disorders, including AD, are linked to abnormal folding and aggregation of proteins. Additionally, being exposed to infectious agents—both viral and bacterial—appears to increase the risk of these disorders [70,72–77,202]. Recently, there is established evidence that many viruses including Influenza A, murine cytomegalovirus and SARS-CoV and their viral proteins have amyloidogenic properties and are prone to the formation of amyloid aggregates [203–205]. Given the previously stated genetic similarity between SARS-CoV and SARS-CoV-2 [124], there is a possibility that SARS-CoV-2 viral proteins, which are shared by other CoVs [106] could be prone to aggregation. Supporting this, a study has indicated that SARS-CoV-2 viral proteins have been shown to form amyloid aggregates [206].

Recent evidence also suggests that SARS-CoV-2 infection appears to disrupt Aβ42 and tau homeostasis. Hyperphosphorylation and altered distribution of tau has been observed in *in vitro* organoid models infected with SARS-CoV-2 [207]. Studies also indicated that infection has shown to enhance Aβ42 neurotoxicity in the brain, impair clearance in blood serum, and induce

amyloid aggregation of proteins in CSF [208–210]. Specifically the presence of Aβ42 has been observed to increase binding of ACE2 to the S1 viral subunit, possibly resulting in increased facilitation of viral entry, as well as increased production of proinflammatory mediators such as IL-6 [210] which is associated with impaired hippocampal neurogenesis [211].

Enhancement of ACE2 activity in AD mouse models has indicated a reduction in hippocampal Aβ42 deposition, as well as reduction in hyperphosphorylated tau and inflammatory cytokines in the brain, and improved cognition [212,213]; therefore inhibition of ACE2 activity might implicate worsened AD- associated pathology and neuroinflammation. Animal experiments have shown that infection with SARS-CoV or injection of SARS S glycoprotein is associated with a significant downregulation of ACE2 activity [214]. Given that SARS-CoV and SARS-CoV-2 share ACE2 as a functional receptor this implies that ACE2 activity and function can also be inhibited by SARS-CoV-2 infection. An important function of ACE2 includes the regulation of brain-derived neurotrophic factor (BDNF) release [215] and BDNF has important roles in neurogenesis, as well as other processes in neurodegenerative diseases, like cognition, neurodevelopment and plasticity [216–218]. BDNF reduction has been linked with Aβ accumulation, tau phosphorylation, and neuroinflammation [219]. Given this evidence, some hypothesize that downstream inhibition of BDNF via an ACE2 mechanism in COVID-19 can instigate neurodegeneration [215].

In the context of COVID-19, microglia and other CNS cells including astrocytes, oligodendrocytes and neurons have been identified as potential targets for infection as these cells express ACE2 [220,221]. It is also known that experimental CNS infection of susceptible mice with neurotropic strains of murine coronaviruses induce widespread activation of microglia and astrocytes associated with the release of pro-inflammatory chemokines and cytokines as well as

the activation of both the innate and adaptive immune responses [222–224]. More recently, experimental infection of mice with mouse-adapted SARS-CoV-2 results in glial activation associated with cytokine production and neuroinflammation in the absence of viral infection of the CNS emphasizing that lung infection can induce changes within the CNS [225]. Additionally, the N protein of SARS-CoV-2 has been co-localized in microglia, astrocytes and oligodendrocytes in the cortex of some COVID-19 patients [226] as well as in microglia in the brains of other animal models [227]. Other studies have reported that SARS-CoV-2 infection of microglia, *in vitro* and as well as in vivo have elicited pro-inflammatory activation in microglia [228]. The systemic inflammation that results from infection is mediated partly by NLRP3 inflammasome. NLRP3 activation can affect microglial function by facilitating the polarization of microglia towards an inflammatory phenotype leading to a reduction in phagocytic function and impairing Aβ clearance [229,230]. Additionally, an inflammatory phenotype in microglia has been shown to induce expression of genes that contribute to neuroinflammation [231] which is also associated with neuronal damage [232,233].

Post-mortem analysis of brains from COVID-19 patients have reported gliosis and immune cell accumulation linked to axonal damage and BBB disruption and leakage [234]; [235,236]. The BBB consists of endothelial cells, pericytes and astrocytes and infection results in endothelial damage and increased capillary permeability [237,238]. Astrocytes, already vulnerable to the effects of infection [220,221] secrete pro-inflammatory cytokines and contribute to production of Aβ [31,32]. These detrimental effects to BBB permeability and integrity can then contribute to the development of neuroinflammatory diseases of the CNS, such as AD[239,240].Although cytokine storm is considered to be a major cause of ARDS and multiple organ failure [241], it has also been recently associated as a major contributing factor of neurological complications of COVID-19. It

has been observed that patients with more severe COVID-19 have a more drastic inflammatory immune response [164,166] leading to the release of proinflammatory cytokines [165,167,242]. Some of these inflammatory markers including IL-6 and IL-1β are also elevated in animal models [243] and associated with impaired neurogenesis and hippocampal dependent memory [211,244] . Elevated levels of IL-6 are associated with increased viral loads and disease severity [245,246] and have been demonstrated to be involved in neurodegenerative diseases mediated by neuroinflammation [247]. Elevated levels of IL-1β have also been correlated with Aβ accumulation and NFTs [248]. Elevated cytokine levels have also been seen in patients experiencing pneumonia and hypoxia [249] and hypoxic changes in vitro and in patients have been associated with neuronal death and loss (in cortex and hippocampus) respectively [118,250]. Additionally, evidence of neuronal degeneration and changes in glial cell morphology are also present in some hippocampal tissues derived from COVID-19 patients [251].

Galectins are a family of animal β-galactoside binding lectins that aid in a variety of different cellular functions including cell adhesion, proliferation, differentiation, migration and growth [252]. However they can also modulate neuroinflammation and potentially contribute to neurodegeneration [253]. Many galectins are expressed in the CNS, including GAL-3 and GAL-9, where GAL-3 is primarily expressed in microglia and GAL-9 in astrocytes [254]. Recent evidence suggests that SARS-CoV-2 infection is associated with increased plasma levels of GAL-3 and GAL-9 in COVID-19 patients in comparison to controls [255–257]. NLRP3 activation has also been shown to drive serum levels of GAL-3 [258]. It has been established that systemic inflammation resulting from infection is in part, mediated by NLRP3 inflammasome, and NLRP3 activation can facilitate the polarization of microglia towards an M1 phenotype and impairing Aβ clearance [229,230]. GAL-3 has been established to have a role in neuroinflammation and a critical contributor

to cognitive impairment and a variety of neurodegenerative diseases including AD [259–262]; [263,264]. In the context of AD, GAL-3 has been shown to be elevated in the cortex, hippocampus and CSF of AD patients, as CSF levels have been shown to be strongly correlated with tau pathology (p-tau181 and t-tau) as well as other synaptic markers like neurogranin [265]. Additionally elevated levels have been shown to contribute to Aβ oligomerization and toxicity [266] and negatively associated with memory function, especially hippocampal dependent memory formation [266,267]. GAL-9 is believed to facilitate astrocyte-microglia communication and promote microglia cytokine production [268], and increased GAL-9 levels in CSF have been associated with CNS immune activation and poor cognitive performance [269] as well as in patients with MCI and AD [270]. It is possible that elevated levels of these galectins, as a result of COVID-19 in some patients, may exacerbate neurodegenerative processes and contribute to an increased risk of neurodegenerative diseases, including AD.

In addition to elevated inflammatory markers, there are other elevated markers of neurodegeneration that result from COVID-19. Elevated blood plasma markers for Glial fibrillary acidic protein (GFAP) and Neurofilament Light Chain (NfL) have been observed in patients with moderate to severe COVID-19 indicating astrocytic and neuronal injury [271]. Additionally, a significant increase in both total and phosphorylated tau (t-tau and p-tau-181), and UCHL1 were also observed in infected patient plasma[272]. A separate study found that the increase in these markers was also associated with the presence of neurological symptoms [273] and interestingly, plasma levels of Aβ, NfL, neurogranin, t-tau, p-tau-181 remained elevated post-COVID-19 recovery [274]. Overall, given evidence linking COVID-19 with neuroinflammation and distinct neurodegenerative processes, it is possible that some neurological manifestations of COVID-19 are likely to result, in part from hippocampal injury and neuronal death and may be

contributing to long-term neurological sequelae such as cognitive impairment in patients with Long COVID.

One study investigated white matter changes one year after initial COVID-19 diagnosis and found that those that had recovered from COVID-19 had decreased axonal density compared to healthy controls, and this was more pronounced in patients that had experienced severe disease versus mild disease. The specific areas affected included the corona radiata, corpus callosum, and superior longitudinal fasciculus, which play important roles in connection between different brain regions as well as hemispheres. While these structural changes persisted in recovered patients even after one year, interestingly they were not associated with decline in cognitive function [275].

Other changes in brain structure have been associated with even mild COVID-19. A recent study has found changes in the limbic and olfactory cortical system, including tissue damage and reductions in gray matter thickness, specifically orbitofrontal cortex and parahippocampal gyrus, as well as other regions functionally connected to olfactory cortex and a greater reduction in global brain size. Interestingly in this study, infection was associated with greater cognitive decline measured by a variety of cognitive tests [276]. However, other studies have reported contradicting results, reporting significant increases in bilateral gray matter volumes in district anatomical regions in the brains of patients post-COVID-19 [277,278]. These contradicting results could be due to differences in methodology, participant characteristics, severity of disease, as well as temporal trajectories in pathophysiological mechanisms related to the presence of neurological symptoms in their cohort of participants.

1.12 Animal models of COVID-19

Several animal models have been shown to be susceptible to SARS-CoV-2 infection and display mild to moderate disease pathogenesis and transmission. These include ferrets, non-human primates, minks, cats, dogs and bats [283–290]. However given the cost, availability, and the difficulty in handling these animals under BSL-3 conditions, rodent models are favored.

One rodent model naturally susceptible to SARS-CoV-2 infection is the Syrian hamster (*Mesocricetus auratus*). Syrian hamsters intranasally infected with SARS-CoV-2 display mild to moderate disease, including weight loss and respiratory distress. They also mirror the effects of other risk factors in human disease such as age, with aged hamsters developing more severe disease than young ones [291–293]. Although experiments with these animals can be performed with ease, due to the limited genetic manipulations and availability of compatible reagents, experiments with these models can be limited .

Although rodents allow for more accessible studies, the main obstacle in modeling SARS-CoV-2 infection in the common laboratory mouse (*Mus musculus*) is the inability of the virus to bind effectively to murine ACE2 [294]. Several modifications to the laboratory mouse have been employed to address this limitation.

Transgenic mouse models have been created to express the human ACE2 (hACE2) receptors under the regulation of a global promoter, the krt18 promoter for epithelial cells or an endogenous mouse ACE2 promoter [295–297]. These mice develop severe disease, including lethal encephalitis and experience CNS and widespread neuronal infection [298,299]. Other models utilize Crispr/Cas9 technology to knockin the human ACE2 gene, rather than driving expression via a specific promoter. This model displays mild to moderate disease that includes pneumonia and elevated cytokine levels along with high viral loads in lungs, trachea and brains [300].

Unfortunately, the severe disease pathogenesis in some of these models renders them less useful in recapitulating the presentation of COVID-19 in humans, therefore other approaches have also been utilized.

Adenovirus or adeno-associated viruses (AAVs) have been utilized to allow for the expression of hACE2 in the respiratory tract of laboratory mice, making them susceptible to SARS-CoV-2 infection and replication temporarily. These mice develop clinical disease and widespread infection of the lungs. However, expression of hACE in these models is abnormal which could alter cellular tropism, and target tissues [301,302]. Although to date, no mouse model has been adapted well enough to capture all aspects of COVID-19 presentation in humans, other avenues are available. These include the adaptation of the native SARS-CoV-2 virus to a standard laboratory mouse.

Viral models which include mouse-adapted SARS-CoV-2 were created by modification of the S protein of SARS-CoV-2 to allow for effective binding to murine ACE2. This was achieved by sequential passage of the virus in mouse lung tissue and modifying the RBD. Mice infected with this mouse-adapted (MA) strain, SARS-CoV-2-MA10, typically display mild disease. This viral model causes acute lung injury in infected BALB/c mice, and more ameliorated disease in C57BL/6J mice. It also recapitulates the effects of age, with increased morbidity and mortality in older mice [303,304]. This model allows for the use of standard laboratory mice and their transgenic counterparts, expanding the scope of many experiments.

1.13 Summary

Alzheimer's disease (AD) is linked to a variety of risk factors including genetic mutations, aging, and other environmental factors such as viral and bacterial infections.

SARS-CoV-2, the viral pathogen responsible for COVID-19, has been linked to a variety of comorbidities and risk factors shared by AD. While COVID-19 usually results in a wide range of symptoms, including respiratory distress, infection has been associated with changes in brain structure and function which are also associated with neuroinflammation and potential neurodegeneration. Additionally, long-term cognitive impairments have been observed post-COVID-19.

Age is the biggest contributing factor to AD and COVID-19, and both - regardless of their etiology- appear to enhance the effects of one another. With an increasing aging population, paired with an increase in the prevalence of age-related dementia and other neurodegenerative diseases, the public health consequences are likely to be dire. Regardless of how these processes occur, the long-term consequences of two colliding diseases (AD and COVID-19) and their synergistic effects on neurodegeneration are yet to be seen and further research is needed to understand the impact of COVID-19 on neurodegenerative diseases like AD. Ongoing research investigating this holds promise, with the potential to offer interventions that could improve public health outcomes amid an aging population.

The goal of this research was to better understand the molecular and cellular mechanisms by which SARS-CoV-2 affects the brain and, specifically the state of glial cells and neuronal function and the contributing changes that may influence neurodegeneration in the context of AD.

References

1. Sperling, R. A. *et al.* Toward defining the preclinical stages of Alzheimer's disease: recommendations from the National Institute on Aging-Alzheimer's Association workgroups on diagnostic guidelines for Alzheimer's disease. *Alzheimers Dement. J. Alzheimers Assoc.* **7**, 280–292 (2011).
2. De-Paula, V. J., Radanovic, M., Diniz, B. S. & Forlenza, O. V. Alzheimer's Disease. in *Protein Aggregation and Fibrillogenesis in Cerebral and Systemic Amyloid Disease* (ed. Harris, J. R.) 329–352 (Springer Netherlands, Dordrecht, 2012). doi:10.1007/978-94-007-5416-4_14.
3. Dubois, B. *et al.* Preclinical Alzheimer's disease: Definition, natural history, and diagnostic criteria. *Alzheimers Dement.* **12**, 292–323 (2016).
4. Kumar, A., Sidhu, J., Goyal, A. & Tsao, J. W. Alzheimer Disease. in *StatPearls* (StatPearls Publishing, Treasure Island (FL), 2022).
5. Casanova, M. F. *et al.* A topographical study of senile plaques and neurofibrillary tangles in the hippocampi of patients with Alzheimer's disease and cognitively impaired patients with schizophrenia. *Psychiatry Res.* **49**, 41–62 (1993).
6. Joshi, G. & Wang, Y. Golgi defects enhance APP amyloidogenic processing in Alzheimer's disease. *BioEssays News Rev. Mol. Cell. Dev. Biol.* **37**, 240–247 (2015).
7. Chen, G. *et al.* Amyloid beta: structure, biology and structure-based therapeutic development. *Acta Pharmacol. Sin.* **38**, 1205–1235 (2017).
8. Arnold, S. E., Hyman, B. T., Flory, J., Damasio, A. R. & Van Hoesen, G. W. The topographical and neuroanatomical distribution of neurofibrillary tangles and neuritic plaques in the cerebral cortex of patients with Alzheimer's disease. *Cereb. Cortex N. Y. N 1991* **1**, 103–116 (1991).
9. Selkoe, D. J. Alzheimer's Disease Is a Synaptic Failure. *Science* **298**, 789–791 (2002).
10. González-Reyes, R. E., Nava-Mesa, M. O., Vargas-Sánchez, K., Ariza-Salamanca, D. & Mora-Muñoz, L. Involvement of Astrocytes in Alzheimer's Disease from a Neuroinflammatory and Oxidative Stress Perspective. *Front. Mol. Neurosci.* **10**, 427 (2017).

11. Wang, W.-Y., Tan, M.-S., Yu, J.-T. & Tan, L. Role of pro-inflammatory cytokines released from microglia in Alzheimer's disease. *Ann. Transl. Med.* **3**, 136 (2015).

12. Shao, Y., Gearing, M. & Mirra, S. S. Astrocyte-apolipoprotein E associations in senile plaques in Alzheimer disease and vascular lesions: a regional immunohistochemical study. *J. Neuropathol. Exp. Neurol.* **56**, 376–381 (1997).

13. McGeer, P. L., Itagaki, S., Tago, H. & McGeer, E. G. Reactive microglia in patients with senile dementia of the Alzheimer type are positive for the histocompatibility glycoprotein HLA-DR. *Neurosci. Lett.* **79**, 195–200 (1987).

14. Frackowiak, J. *et al.* Ultrastructure of the microglia that phagocytose amyloid and the microglia that produce beta-amyloid fibrils. *Acta Neuropathol. (Berl.)* **84**, 225–233 (1992).

15. Bolmont, T. *et al.* Dynamics of the microglial/amyloid interaction indicate a role in plaque maintenance. *J. Neurosci. Off. J. Soc. Neurosci.* **28**, 4283–4292 (2008).

16. Lawson, L. J., Perry, V. H., Dri, P. & Gordon, S. Heterogeneity in the distribution and morphology of microglia in the normal adult mouse brain. *Neuroscience* **39**, 151–170 (1990).

17. Lawson, L. J., Perry, V. H. & Gordon, S. Turnover of resident microglia in the normal adult mouse brain. *Neuroscience* **48**, 405–415 (1992).

18. Ginhoux, F., Lim, S., Hoeffel, G., Low, D. & Huber, T. Origin and differentiation of microglia. *Front. Cell. Neurosci.* **7**, (2013).

19. Tremblay, M.-È. *et al.* The role of microglia in the healthy brain. *J. Neurosci. Off. J. Soc. Neurosci.* **31**, 16064–16069 (2011).

20. Nimmerjahn, A., Kirchhoff, F. & Helmchen, F. Resting microglial cells are highly dynamic surveillants of brain parenchyma in vivo. *Science* **308**, 1314–1318 (2005).

21. Colonna, M. & Butovsky, O. Microglia Function in the Central Nervous System During Health and Neurodegeneration. *Annu. Rev. Immunol.* **35**, 441–468 (2017).

22. Woodburn, S. C., Bollinger, J. L. & Wohleb, E. S. The semantics of microglia activation: neuroinflammation, homeostasis, and stress. *J. Neuroinflammation* **18**, 258 (2021).

23. Solito, E. & Sastre, M. Microglia function in Alzheimer's disease. *Front. Pharmacol.* **3**, 14 (2012).

24. Tang, Y. & Le, W. Differential Roles of M1 and M2 Microglia in Neurodegenerative Diseases. *Mol. Neurobiol.* **53**, 1181–1194 (2016).

25. Liddelow, S. A. *et al.* Neurotoxic reactive astrocytes are induced by activated microglia. *Nature* **541**, 481–487 (2017).

26. Colombo, E. & Farina, C. Astrocytes: Key Regulators of Neuroinflammation. *Trends Immunol.* **37**, 608–620 (2016).

27. Kim, Y., Park, J. & Choi, Y. K. The Role of Astrocytes in the Central Nervous System Focused on BK Channel and Heme Oxygenase Metabolites: A Review. *Antioxidants* **8**, 121 (2019).

28. Sofroniew, M. V. Molecular dissection of reactive astrogliosis and glial scar formation. *Trends Neurosci.* **32**, 638–647 (2009).

29. Scimemi, A. The Role of Astrocytes in Neurotransmitter Uptake and Brain Metabolism. in *Computational Glioscience* (eds. De Pittà, M. & Berry, H.) 309–328 (Springer International Publishing, Cham, 2019). doi:10.1007/978-3-030-00817-8_12.

30. Abbott, N. J., Rönnbäck, L. & Hansson, E. Astrocyte-endothelial interactions at the blood-brain barrier. *Nat. Rev. Neurosci.* **7**, 41–53 (2006).

31. Zhao, J., O'Connor, T. & Vassar, R. The contribution of activated astrocytes to Aβ production: implications for Alzheimer's disease pathogenesis. *J. Neuroinflammation* **8**, 150 (2011).

32. Blasko, I. *et al.* Costimulatory effects of interferon-gamma and interleukin-1beta or tumor necrosis factor alpha on the synthesis of Abeta1-40 and Abeta1-42 by human astrocytes. *Neurobiol. Dis.* **7**, 682–689 (2000).

33. Paroni, G., Bisceglia, P. & Seripa, D. Understanding the Amyloid Hypothesis in Alzheimer's Disease. *J. Alzheimers Dis. JAD* **68**, 493–510 (2019).

34. Imhof, A. *et al.* Morphological substrates of cognitive decline in nonagenarians and centenarians: a new paradigm? *J. Neurol. Sci.* **257**, 72–79 (2007).

35. Davies, P. & Maloney, A. J. Selective loss of central cholinergic neurons in Alzheimer's disease.

Lancet Lond. Engl. **2**, 1403 (1976).

36. Cacabelos, R. Donepezil in Alzheimer's disease: From conventional trials to pharmacogenetics. *Neuropsychiatr. Dis. Treat.* **3**, 303–333 (2007).
37. Annicchiarico, R., Federici, A., Pettenati, C. & Caltagirone, C. Rivastigmine in Alzheimer's disease: Cognitive function and quality of life. *Ther. Clin. Risk Manag.* **3**, 1113–1123 (2007).
38. Nguyen, K., Hoffman, H., Chakkamparambil, B. & Grossberg, G. T. Evaluation of rivastigmine in Alzheimer's disease. *Neurodegener. Dis. Manag.* **11**, 35–48 (2021).
39. Prvulovic, D., Hampel, H. & Pantel, J. Galantamine for Alzheimer's disease. *Expert Opin. Drug Metab. Toxicol.* **6**, 345–354 (2010).
40. Huang, Y.-J., Lin, C.-H., Lane, H.-Y. & Tsai, G. E. NMDA Neurotransmission Dysfunction in Behavioral and Psychological Symptoms of Alzheimer's Disease. *Curr. Neuropharmacol.* **10**, 272–285 (2012).
41. Folch, J. *et al.* Memantine for the Treatment of Dementia: A Review on its Current and Future Applications. *J. Alzheimers Dis.* **62**, 1223–1240 (2018).
42. Dhillon, S. Aducanumab: First Approval. *Drugs* **81**, 1437–1443 (2021).
43. Sevigny, J. *et al.* The antibody aducanumab reduces Aβ plaques in Alzheimer's disease. *Nature* **537**, 50–56 (2016).
44. Padda, I. S. & Parmar, M. Aducanumab. in *StatPearls* (StatPearls Publishing, Treasure Island (FL), 2022).
45. van Dyck Christopher H. *et al.* Lecanemab in Early Alzheimer's Disease. *N. Engl. J. Med.* **388**, 9–21 (2023).
46. Kvello-Alme, M., Bråthen, G., White, L. R. & Sando, S. B. The Prevalence and Subtypes of Young Onset Dementia in Central Norway: A Population-Based Study. *J. Alzheimers Dis. JAD* **69**, 479–487 (2019).
47. Goate, A. *et al.* Segregation of a missense mutation in the amyloid precursor protein gene with familial Alzheimer's disease. *Nature* **349**, 704–706 (1991).

48. St George-Hyslop, P. *et al.* Genetic evidence for a novel familial Alzheimer's disease locus on chromosome 14. *Nat. Genet.* **2**, 330–334 (1992).

49. Sherrington, R. *et al.* Alzheimer's Disease Associated with Mutations in Presenilin 2 is Rare and Variably Penetrant. *Hum. Mol. Genet.* **5**, 985–988 (1996).

50. Henderson, A. S. The risk factors for Alzheimer's disease: a review and a hypothesis. *Acta Psychiatr. Scand.* **78**, 257–275 (1988).

51. Guerreiro, R. & Bras, J. The age factor in Alzheimer's disease. *Genome Med.* **7**, 106 (2015).

52. Kim, J., Basak, J. M. & Holtzman, D. M. The Role of Apolipoprotein E in Alzheimer's Disease. *Neuron* **63**, 287–303 (2009).

53. Bertram, L., McQueen, M. B., Mullin, K., Blacker, D. & Tanzi, R. E. Systematic meta-analyses of Alzheimer disease genetic association studies: the AlzGene database. *Nat. Genet.* **39**, 17–23 (2007).

54. Corder, E. H. *et al.* Gene dose of apolipoprotein E type 4 allele and the risk of Alzheimer's disease in late onset families. *Science* **261**, 921–923 (1993).

55. Hohman, T. J. *et al.* Sex-Specific Association of Apolipoprotein E With Cerebrospinal Fluid Levels of Tau. *JAMA Neurol.* **75**, 989–998 (2018).

56. Fernandez, C. G., Hamby, M. E., McReynolds, M. L. & Ray, W. J. The Role of APOE4 in Disrupting the Homeostatic Functions of Astrocytes and Microglia in Aging and Alzheimer's Disease. *Front. Aging Neurosci.* **11**, (2019).

57. Ries, M. & Sastre, M. Mechanisms of Aβ Clearance and Degradation by Glial Cells. *Front. Aging Neurosci.* **8**, 160 (2016).

58. Deane, R. *et al.* apoE isoform-specific disruption of amyloid beta peptide clearance from mouse brain. *J. Clin. Invest.* **118**, 4002–4013 (2008).

59. Koistinaho, M. *et al.* Apolipoprotein E promotes astrocyte colocalization and degradation of deposited amyloid-beta peptides. *Nat. Med.* **10**, 719–726 (2004).

60. Simonovitch, S. *et al.* Impaired Autophagy in APOE4 Astrocytes. *J. Alzheimers Dis. JAD* **51**, 915–927 (2016).

61. Farfel, J. M., Yu, L., De Jager, P. L., Schneider, J. A. & Bennett, D. A. Association of APOE with tau-tangle pathology with and without β-amyloid. *Neurobiol. Aging* **37**, 19–25 (2016).

62. Shi, Y. *et al.* ApoE4 markedly exacerbates tau-mediated neurodegeneration in a mouse model of tauopathy. *Nature* **549**, 523–527 (2017).

63. Newman, A. B. *et al.* Dementia and Alzheimer's disease incidence in relationship to cardiovascular disease in the Cardiovascular Health Study cohort. *J. Am. Geriatr. Soc.* **53**, 1101–1107 (2005).

64. Alford, S., Patel, D., Perakakis, N. & Mantzoros, C. S. Obesity as a risk factor for Alzheimer's disease: weighing the evidence. *Obes. Rev.* **19**, 269–280 (2018).

65. Lee, H. J. *et al.* Diabetes and Alzheimer's Disease: Mechanisms and Nutritional Aspects. *Clin. Nutr. Res.* **7**, 229–240 (2018).

66. Moulton, P. V. & Yang, W. Air Pollution, Oxidative Stress, and Alzheimer's Disease. *J. Environ. Public Health* **2012**, 472751 (2012).

67. Hu, N. *et al.* Nutrition and the Risk of Alzheimer's Disease. *BioMed Res. Int.* **2013**, e524820 (2013).

68. Ramos-Cejudo, J. *et al.* Traumatic Brain Injury and Alzheimer's Disease: The Cerebrovascular Link. *EBioMedicine* **28**, 21–30 (2018).

69. Huat, T. J. *et al.* Metal Toxicity Links to Alzheimer's Disease and Neuroinflammation. *J. Mol. Biol.* **431**, 1843–1868 (2019).

70. Levine, K. S. *et al.* Virus exposure and neurodegenerative disease risk across national biobanks. *Neuron* **111**, 1086-1093.e2 (2023).

71. Lotz, S. K., Blackhurst, B. M., Reagin, K. L. & Funk, K. E. Microbial Infections Are a Risk Factor for Neurodegenerative Diseases. *Front. Cell. Neurosci.* **15**, 691136 (2021).

72. Carbone, I. *et al.* Herpes virus in Alzheimer's disease: relation to progression of the disease. *Neurobiol. Aging* **35**, 122–129 (2014).

73. Dhingra, V., Li, Q., Allison, A. B., Stallknecht, D. E. & Fu, Z. F. Proteomic Profiling and Neurodegeneration in West-Nile-Virus-Infected Neurons. *J. Biomed. Biotechnol.* **2005**, 271–279

(2005).

74. Esiri, M. M., Biddolph, S. C. & Morris, C. S. Prevalence of Alzheimer plaques in AIDS. *J. Neurol. Neurosurg. Psychiatry* **65**, 29–33 (1998).

75. Little, C. S., Hammond, C. J., MacIntyre, A., Balin, B. J. & Appelt, D. M. Chlamydia pneumoniae induces Alzheimer-like amyloid plaques in brains of BALB/c mice. *Neurobiol. Aging* **25**, 419–429 (2004).

76. Miklossy, J. Historic evidence to support a causal relationship between spirochetal infections and Alzheimer's disease. *Front. Aging Neurosci.* **7**, 46 (2015).

77. Miklossy, J. *et al.* Beta-amyloid deposition and Alzheimer's type changes induced by Borrelia spirochetes. *Neurobiol. Aging* **27**, 228–236 (2006).

78. Götz, J., Bodea, L.-G. & Goedert, M. Rodent models for Alzheimer disease. *Nat. Rev. Neurosci.* **19**, 583–598 (2018).

79. Qosa, H. & Kaddoumi, A. Effect of mouse strain as a background for Alzheimer's disease models on the clearance of amyloid-β. *J. Syst. Integr. Neurosci.* **2**, 135–140 (2016).

80. Hall, A. M. & Roberson, E. D. Mouse Models of Alzheimer's Disease. *Brain Res. Bull.* **88**, 3–12 (2012).

81. Jankowsky, J. L. & Zheng, H. Practical considerations for choosing a mouse model of Alzheimer's disease. *Mol. Neurodegener.* **12**, 89 (2017).

82. Duff, K. *et al.* Increased amyloid-beta42(43) in brains of mice expressing mutant presenilin 1. *Nature* **383**, 710–713 (1996).

83. Zhu, F., Nair, R. R., Fisher, E. M. C. & Cunningham, T. J. Humanising the mouse genome piece by piece. *Nat. Commun.* **10**, 1845 (2019).

84. Xu, G. *et al.* Murine Aβ over-production produces diffuse and compact Alzheimer-type amyloid deposits. *Acta Neuropathol. Commun.* **3**, 72 (2015).

85. Oakley, H. *et al.* Intraneuronal β-Amyloid Aggregates, Neurodegeneration, and Neuron Loss in Transgenic Mice with Five Familial Alzheimer's Disease Mutations: Potential Factors in Amyloid

Plaque Formation. *J. Neurosci.* **26**, 10129–10140 (2006).

86. Forner, S. *et al.* Systematic phenotyping and characterization of the 5xFAD mouse model of Alzheimer's disease. *Sci. Data* **8**, 270 (2021).

87. Kampers, T., Pangalos, M., Geerts, H., Wiech, H. & Mandelkow, E. Assembly of paired helical filaments from mouse tau: implications for the neurofibrillary pathology in transgenic mouse models for Alzheimer's disease. *FEBS Lett.* **451**, 39–44 (1999).

88. Roberson, E. D. Mouse models of frontotemporal dementia. *Ann. Neurol.* **72**, 837–849 (2012).

89. Mocanu, M.-M. *et al.* The Potential for β-Structure in the Repeat Domain of Tau Protein Determines Aggregation, Synaptic Decay, Neuronal Loss, and Coassembly with Endogenous Tau in Inducible Mouse Models of Tauopathy. *J. Neurosci.* **28**, 737–748 (2008).

90. Ramsden, M. *et al.* Age-dependent neurofibrillary tangle formation, neuron loss, and memory impairment in a mouse model of human tauopathy (P301L). *J. Neurosci. Off. J. Soc. Neurosci.* **25**, 10637–10647 (2005).

91. Yoshiyama, Y. *et al.* Synapse loss and microglial activation precede tangles in a P301S tauopathy mouse model. *Neuron* **53**, 337–351 (2007).

92. Koss, D. J. *et al.* Mutant Tau knock-in mice display frontotemporal dementia relevant behaviour and histopathology. *Neurobiol. Dis.* **91**, 105–123 (2016).

93. Poorkaj, P. *et al.* Tau is a candidate gene for chromosome 17 frontotemporal dementia. *Ann. Neurol.* **43**, 815–825 (1998).

94. Spillantini, M. G. & Goedert, M. Tau Gene Mutations and Tau Pathology in Frontotemporal Dementia and Parkinsonism Linked to Chromosome 17. in *Neuropathology and Genetics of Dementia* (eds. Tolnay, M. & Probst, A.) 21–37 (Springer US, Boston, MA, 2001). doi:10.1007/978-1-4615-1249-3_3.

95. Jackson, R. J. *et al.* Human tau increases amyloid β plaque size but not amyloid β-mediated synapse loss in a novel mouse model of Alzheimer's disease. *Eur. J. Neurosci.* **44**, 3056–3066 (2016).

96. Lippi, S. L. P., Smith, M. L. & Flinn, J. M. A Novel hAPP/htau Mouse Model of Alzheimer's

Disease: Inclusion of APP With Tau Exacerbates Behavioral Deficits and Zinc Administration Heightens Tangle Pathology. *Front. Aging Neurosci.* **10**, 382 (2018).

97. Saito, T. *et al.* Humanization of the entire murine Mapt gene provides a murine model of pathological human tau propagation. *J. Biol. Chem.* **294**, 12754–12765 (2019).

98. Lewis, J. *et al.* Enhanced neurofibrillary degeneration in transgenic mice expressing mutant tau and APP. *Science* **293**, 1487–1491 (2001).

99. Javonillo, D. I. *et al.* Systematic Phenotyping and Characterization of the 3xTg-AD Mouse Model of Alzheimer's Disease. *Front. Neurosci.* **15**, 785276 (2022).

100. Oddo, S., Caccamo, A., Kitazawa, M., Tseng, B. P. & LaFerla, F. M. Amyloid deposition precedes tangle formation in a triple transgenic model of Alzheimer's disease. *Neurobiol. Aging* **24**, 1063–1070 (2003).

101. Oddo, S. *et al.* Triple-transgenic model of Alzheimer's disease with plaques and tangles: intracellular Abeta and synaptic dysfunction. *Neuron* **39**, 409–421 (2003).

102. Balu, D. *et al.* The role of APOE in transgenic mouse models of AD. *Neurosci. Lett.* **707**, 134285 (2019).

103. Neustadtl, A. *et al.* Reduced cortical excitatory synapse number in APOE4 mice is associated with increased calcineurin activity. *Neuroreport* **28**, 618–624 (2017).

104. Sun, G. *et al.* Hippocampal synaptic and neural network deficits in young mice carrying the human APOE4 gene. *CNS Neurosci. Ther.* **23**, 748–758 (2017).

105. Holtzman, D. M. *et al.* Apolipoprotein E isoform-dependent amyloid deposition and neuritic degeneration in a mouse model of Alzheimer's disease. *Proc. Natl. Acad. Sci. U. S. A.* **97**, 2892–2897 (2000).

106. Weiss, S. R. & Navas-Martin, S. Coronavirus Pathogenesis and the Emerging Pathogen Severe Acute Respiratory Syndrome Coronavirus. *Microbiol. Mol. Biol. Rev.* **69**, 635–664 (2005).

107. Neuman, B. W. *et al.* A structural analysis of M protein in coronavirus assembly and morphology. *J. Struct. Biol.* **174**, 11–22 (2011).

108. Laude, H., Gelfi, J., Lavenant, L. & Charley, B. Single amino acid changes in the viral glycoprotein M affect induction of alpha interferon by the coronavirus transmissible gastroenteritis virus. *J. Virol.* **66**, 743–749 (1992).

109. Nieto-Torres, J. L. *et al.* Subcellular location and topology of severe acute respiratory syndrome coronavirus envelope protein. *Virology* **415**, 69–82 (2011).

110. Nieto-Torres, J. L. *et al.* Severe Acute Respiratory Syndrome Coronavirus Envelope Protein Ion Channel Activity Promotes Virus Fitness and Pathogenesis. *PLOS Pathog.* **10**, e1004077 (2014).

111. DeDiego, M. L. *et al.* A severe acute respiratory syndrome coronavirus that lacks the E gene is attenuated in vitro and in vivo. *J. Virol.* **81**, 1701–1713 (2007).

112. Netland, J. *et al.* Immunization with an attenuated severe acute respiratory syndrome coronavirus deleted in E protein protects against lethal respiratory disease. *Virology* **399**, 120–128 (2010).

113. Lamirande, E. W. *et al.* A Live Attenuated Severe Acute Respiratory Syndrome Coronavirus Is Immunogenic and Efficacious in Golden Syrian Hamsters. *J. Virol.* **82**, 7721–7724 (2008).

114. McBride, R., van Zyl, M. & Fielding, B. C. The Coronavirus Nucleocapsid Is a Multifunctional Protein. *Viruses* **6**, 2991–3018 (2014).

115. Langereis, M. A., van Vliet, A. L. W., Boot, W. & de Groot, R. J. Attachment of mouse hepatitis virus to O-acetylated sialic acid is mediated by hemagglutinin-esterase and not by the spike protein. *J. Virol.* **84**, 8970–8974 (2010).

116. Su, S. *et al.* Epidemiology, Genetic Recombination, and Pathogenesis of Coronaviruses. *Trends Microbiol.* **24**, 490–502 (2016).

117. Wevers, B. A. & van der Hoek, L. Recently discovered human coronaviruses. *Clin. Lab. Med.* **29**, 715–724 (2009).

118. Solomon, M. & Liang, C. Human coronaviruses: The emergence of SARS-CoV-2 and management of COVID-19. *Virus Res.* **319**, 198882 (2022).

119. Paules, C. I., Marston, H. D. & Fauci, A. S. Coronavirus Infections—More Than Just the Common Cold. *JAMA* **323**, 707–708 (2020).

120. Peiris, J. S. M. *et al.* Coronavirus as a possible cause of severe acute respiratory syndrome. *Lancet Lond. Engl.* **361**, 1319–1325 (2003).

121. Raj, V. S., Osterhaus, A. D. M. E., Fouchier, R. A. M. & Haagmans, B. L. MERS: emergence of a novel human coronavirus. *Curr. Opin. Virol.* **5**, 58–62 (2014).

122. Ahmed, H. *et al.* Long-term clinical outcomes in survivors of severe acute respiratory syndrome and Middle East respiratory syndrome coronavirus outbreaks after hospitalisation or ICU admission: A systematic review and meta-analysis. *J. Rehabil. Med.* **52**, jrm00063 (2020).

123. COVID - Coronavirus Statistics - Worldometer. https://www.worldometers.info/coronavirus/.

124. Zhou, P. *et al.* A pneumonia outbreak associated with a new coronavirus of probable bat origin. *Nature* **579**, 270–273 (2020).

125. Li, W. *et al.* Angiotensin-converting enzyme 2 is a functional receptor for the SARS coronavirus. *Nature* **426**, 450–454 (2003).

126. Tai, W. *et al.* Characterization of the receptor-binding domain (RBD) of 2019 novel coronavirus: implication for development of RBD protein as a viral attachment inhibitor and vaccine. *Cell. Mol. Immunol.* **17**, 613–620 (2020).

127. Wrapp, D. *et al.* Cryo-EM structure of the 2019-nCoV spike in the prefusion conformation. *Science* **367**, 1260–1263 (2020).

128. Hoffmann, M. *et al.* SARS-CoV-2 Cell Entry Depends on ACE2 and TMPRSS2 and Is Blocked by a Clinically Proven Protease Inhibitor. *Cell* **181**, 271-280.e8 (2020).

129. Crackower, M. A. *et al.* Angiotensin-converting enzyme 2 is an essential regulator of heart function. *Nature* **417**, 822–828 (2002).

130. Gheblawi, M. *et al.* Angiotensin-Converting Enzyme 2: SARS-CoV-2 Receptor and Regulator of the Renin-Angiotensin System. *Circ. Res.* **126**, 1456–1474 (2020).

131. Hamming, I. *et al.* Tissue distribution of ACE2 protein, the functional receptor for SARS coronavirus. A first step in understanding SARS pathogenesis. *J. Pathol.* **203**, 631–637 (2004).

132. Karagiannidis, C. *et al.* Case characteristics, resource use, and outcomes of 10 021 patients with

COVID-19 admitted to 920 German hospitals: an observational study. *Lancet Respir. Med.* **8**, 853–862 (2020).

133. Parohan, M. *et al.* Risk factors for mortality in patients with Coronavirus disease 2019 (COVID-19) infection: a systematic review and meta-analysis of observational studies. *Aging Male Off. J. Int. Soc. Study Aging Male* **23**, 1416–1424 (2020).
134. Severe Covid-19 GWAS Group *et al.* Genomewide Association Study of Severe Covid-19 with Respiratory Failure. *N. Engl. J. Med.* **383**, 1522–1534 (2020).
135. Pairo-Castineira, E. *et al.* Genetic mechanisms of critical illness in COVID-19. *Nature* **591**, 92–98 (2021).
136. Bastard, P. *et al.* Autoantibodies against type I IFNs in patients with life-threatening COVID-19. *Science* **370**, eabd4585 (2020).
137. Koning, R. *et al.* Autoantibodies against type I interferons are associated with multi-organ failure in COVID-19 patients. *Intensive Care Med.* **47**, 704–706 (2021).
138. Bastard, P. *et al.* Autoantibodies neutralizing type I IFNs are present in ~4% of uninfected individuals over 70 years old and account for ~20% of COVID-19 deaths. *Sci. Immunol.* **6**, eabl4340 (2021).
139. Chen, Y. *et al.* Aging in COVID-19: Vulnerability, immunity and intervention. *Ageing Res. Rev.* **65**, 101205 (2021).
140. Mueller, A. L., McNamara, M. S. & Sinclair, D. A. Why does COVID-19 disproportionately affect older people? *Aging* **12**, 9959–9981 (2020).
141. O'Driscoll, M. *et al.* Age-specific mortality and immunity patterns of SARS-CoV-2. *Nature* **590**, 140–145 (2021).
142. Flier, W. M. van der & Scheltens, P. Epidemiology and risk factors of dementia. *J. Neurol. Neurosurg. Psychiatry* **76**, v2–v7 (2005).
143. Martín-Jiménez, P. *et al.* Cognitive Impairment Is a Common Comorbidity in Deceased COVID-19 Patients: A Hospital-Based Retrospective Cohort Study. *J. Alzheimers Dis. JAD* **78**, 1367–1372

(2020).

144. Atkins, J. L. *et al.* Preexisting Comorbidities Predicting COVID-19 and Mortality in the UK Biobank Community Cohort. *J. Gerontol. A. Biol. Sci. Med. Sci.* **75**, 2224–2230 (2020).

145. Wang, Q., Davis, P. B., Gurney, M. E. & Xu, R. COVID-19 and dementia: Analyses of risk, disparity, and outcomes from electronic health records in the US. *Alzheimers Dement. J. Alzheimers Assoc.* **17**, 1297–1306 (2021).

146. Dewan, S. K., Zheng, S., Xia, S. & Bill, K. Senescent remodeling of the immune system and its contribution to the predisposition of the elderly to infections. *Chin. Med. J. (Engl.)* **125**, 3325–3331 (2012).

147. Burt, T. D. *et al.* Apolipoprotein (apo) E4 enhances HIV-1 cell entry in vitro, and the APOE epsilon4/epsilon4 genotype accelerates HIV disease progression. *Proc. Natl. Acad. Sci. U. S. A.* **105**, 8718–8723 (2008).

148. Linard, M. *et al.* Interaction between APOE4 and herpes simplex virus type 1 in Alzheimer's disease. *Alzheimers Dement. J. Alzheimers Assoc.* **16**, 200–208 (2020).

149. Mueller, T. *et al.* Apolipoprotein E allele frequencies in chronic and self-limited hepatitis C suggest a protective effect of APOE4 in the course of hepatitis C virus infection. *Liver Int. Off. J. Int. Assoc. Study Liver* **36**, 1267–1274 (2016).

150. Kuo, C.-L. *et al.* ApoE e4e4 Genotype and Mortality With COVID-19 in UK Biobank. *J. Gerontol. A. Biol. Sci. Med. Sci.* **75**, 1801–1803 (2020).

151. Kuo, C.-L. *et al.* APOE e4 Genotype Predicts Severe COVID-19 in the UK Biobank Community Cohort. *J. Gerontol. A. Biol. Sci. Med. Sci.* **75**, 2231–2232 (2020).

152. Kurki, S. N. *et al.* APOE ε4 associates with increased risk of severe COVID-19, cerebral microhaemorrhages and post-COVID mental fatigue: a Finnish biobank, autopsy and clinical study. *Acta Neuropathol. Commun.* **9**, 199 (2021).

153. Kulminski, A. M. *et al.* Protective role of the apolipoprotein E2 allele in age-related disease traits and survival: Evidence from the Long Life Family Study. *Biogerontology* **17**, 893–905 (2016).

154. Wang, C. *et al.* ApoE-Isoform-Dependent SARS-CoV-2 Neurotropism and Cellular Response. *Cell Stem Cell* **28**, 331-342.e5 (2021).

155. Ostendorf, B. N. *et al.* Common human genetic variants of APOE impact murine COVID-19 mortality. *Nature* 1–3 (2022) doi:10.1038/s41586-022-05344-2.

156. Montagne, A. *et al.* APOE4 leads to blood-brain barrier dysfunction predicting cognitive decline. *Nature* **581**, 71–76 (2020).

157. Dallongeville, J., Lussier-Cacan, S. & Davignon, J. Modulation of plasma triglyceride levels by apoE phenotype: a meta-analysis. *J. Lipid Res.* **33**, 447–454 (1992).

158. Wang, H. *et al.* The role of high cholesterol in age-related COVID19 lethality. *bioRxiv* 2020.05.09.086249 (2021) doi:10.1101/2020.05.09.086249.

159. Zhu, H. *et al.* A Chinese host genetic study discovered IFNs and causality of laboratory traits on COVID-19 severity. *iScience* **24**, 103186 (2021).

160. de Leeuw, S. M. *et al.* APOE2, E3, and E4 differentially modulate cellular homeostasis, cholesterol metabolism, and inflammatory response in isogenic iPSC-derived astrocytes. *Stem Cell Rep.* **17**, 110–126 (2022).

161. Konttinen, H. *et al.* PSEN1ΔE9, APPswe, and APOE4 Confer Disparate Phenotypes in Human iPSC-Derived Microglia. *Stem Cell Rep.* **13**, 669–683 (2019).

162. Vitek, M. P., Brown, C. M. & Colton, C. A. APOE genotype-specific differences in the innate immune response. *Neurobiol. Aging* **30**, 1350–1360 (2009).

163. Zhang, H., Wu, L.-M. & Wu, J. Cross-talk between apolipoprotein E and cytokines. *Mediators Inflamm.* **2011**, 949072 (2011).

164. Chen, G. *et al.* Clinical and immunological features of severe and moderate coronavirus disease 2019. *J. Clin. Invest.* **130**, 2620–2629 (2020).

165. Hu, B., Huang, S. & Yin, L. The cytokine storm and COVID-19. *J. Med. Virol.* **93**, 250–256 (2021).

166. Huang, C. *et al.* Clinical features of patients infected with 2019 novel coronavirus in Wuhan, China. *The Lancet* **395**, 497–506 (2020).

167. Ragab, D., Salah Eldin, H., Taeimah, M., Khattab, R. & Salem, R. The COVID-19 Cytokine Storm; What We Know So Far. *Front. Immunol.* **11**, 1446 (2020).

168. Lauer, S. A. *et al.* The Incubation Period of Coronavirus Disease 2019 (COVID-19) From Publicly Reported Confirmed Cases: Estimation and Application. *Ann. Intern. Med.* **172**, 577–582 (2020).

169. Guan, W. *et al.* Clinical Characteristics of Coronavirus Disease 2019 in China. *N. Engl. J. Med.* **382**, 1708–1720 (2020).

170. Zhou, F. *et al.* Clinical course and risk factors for mortality of adult inpatients with COVID-19 in Wuhan, China: a retrospective cohort study. *The Lancet* **395**, 1054–1062 (2020).

171. Diamond, M., Peniston, H. L., Sanghavi, D. & Mahapatra, S. Acute Respiratory Distress Syndrome. in *StatPearls* (StatPearls Publishing, Treasure Island (FL), 2022).

172. Gupta, A. *et al.* Extrapulmonary manifestations of COVID-19. *Nat. Med.* **26**, 1017–1032 (2020).

173. Tavazzi, G. *et al.* Myocardial localization of coronavirus in COVID-19 cardiogenic shock. *Eur. J. Heart Fail.* **22**, 911–915 (2020).

174. Xiao, F. *et al.* Evidence for Gastrointestinal Infection of SARS-CoV-2. *Gastroenterology* **158**, 1831-1833.e3 (2020).

175. Du, Y. *et al.* Clinical Features of 85 Fatal Cases of COVID-19 from Wuhan. A Retrospective Observational Study. *Am. J. Respir. Crit. Care Med.* **201**, 1372–1379 (2020).

176. Chen, T. *et al.* Clinical characteristics of 113 deceased patients with coronavirus disease 2019: retrospective study. *BMJ* **368**, m1091 (2020).

177. Harapan, B. N. & Yoo, H. J. Neurological symptoms, manifestations, and complications associated with severe acute respiratory syndrome coronavirus 2 (SARS-CoV-2) and coronavirus disease 19 (COVID-19). *J. Neurol.* **268**, 3059–3071 (2021).

178. Johansson, A., Mohamed, M. S., Moulin, T. C. & Schiöth, H. B. Neurological manifestations of COVID-19: A comprehensive literature review and discussion of mechanisms. *J. Neuroimmunol.* **358**, 577658 (2021).

179. Mao, L. *et al.* Neurologic Manifestations of Hospitalized Patients With Coronavirus Disease 2019 in

Wuhan, China. *JAMA Neurol.* **77**, 683–690 (2020).

180. Zubair, A. S. *et al.* Neuropathogenesis and Neurologic Manifestations of the Coronaviruses in the Age of Coronavirus Disease 2019 A Review. *JAMA Neurol.* **77**, 1018–1027 (2020).

181. Liotta, E. M. *et al.* Frequent neurologic manifestations and encephalopathy-associated morbidity in Covid-19 patients. *Ann. Clin. Transl. Neurol.* **7**, 2221–2230 (2020).

182. Keyhanian, K. *et al.* SARS-CoV-2 and nervous system: From pathogenesis to clinical manifestation. *J. Neuroimmunol.* **350**, 577436 (2020).

183. Butt, I., Sawlani, V. & Geberhiwot, T. Prolonged confusional state as first manifestation of COVID-19. *Ann. Clin. Transl. Neurol.* **7**, 1450–1452 (2020).

184. Cooper, K. W. *et al.* COVID-19 and the Chemical Senses: Supporting Players Take Center Stage. *Neuron* **107**, 219–233 (2020).

185. Karadaş, Ö., Öztürk, B. & Sonkaya, A. R. A prospective clinical study of detailed neurological manifestations in patients with COVID-19. *Neurol. Sci. Off. J. Ital. Neurol. Soc. Ital. Soc. Clin. Neurophysiol.* **41**, 1991–1995 (2020).

186. Brann, D. H. *et al.* Non-neuronal expression of SARS-CoV-2 entry genes in the olfactory system suggests mechanisms underlying COVID-19-associated anosmia. *Sci. Adv.* **6**, eabc5801 (2020).

187. Duong, L., Xu, P. & Liu, A. Meningoencephalitis without respiratory failure in a young female patient with COVID-19 infection in Downtown Los Angeles, early April 2020. *Brain. Behav. Immun.* **87**, 33 (2020).

188. Fan, H., Tang, X., Song, Y., Liu, P. & Chen, Y. Influence of COVID-19 on Cerebrovascular Disease and its Possible Mechanism. *Neuropsychiatr. Dis. Treat.* **16**, 1359–1367 (2020).

189. Favas, T. T. *et al.* Neurological manifestations of COVID-19: a systematic review and meta-analysis of proportions. *Neurol. Sci. Off. J. Ital. Neurol. Soc. Ital. Soc. Clin. Neurophysiol.* **41**, 3437–3470 (2020).

190. Lyons, S. *et al.* Seizure with CSF lymphocytosis as a presenting feature of COVID-19 in an otherwise healthy young man. *Seizure* **80**, 113–114 (2020).

191. Merkler, A. E. *et al.* Risk of Ischemic Stroke in Patients With Coronavirus Disease 2019 (COVID-19) vs Patients With Influenza. *JAMA Neurol.* (2020) doi:10.1001/jamaneurol.2020.2730.

192. Moriguchi, T. *et al.* A first case of meningitis/encephalitis associated with SARS-Coronavirus-2. *Int. J. Infect. Dis. IJID Off. Publ. Int. Soc. Infect. Dis.* **94**, 55–58 (2020).

193. Sohal, S. & Mansur, M. COVID-19 Presenting with Seizures. *IDCases* **20**, e00782 (2020).

194. Tang, N., Li, D., Wang, X. & Sun, Z. Abnormal coagulation parameters are associated with poor prognosis in patients with novel coronavirus pneumonia. *J. Thromb. Haemost. JTH* **18**, 844–847 (2020).

195. Cárdenas, G. *et al.* Neurological events related to influenza A (H1N1) pdm09. *Influenza Other Respir. Viruses* **8**, 339–346 (2014).

196. Robinson, C. P. & Busl, K. M. Neurologic Manifestations of Severe Respiratory Viral Contagions. *Crit. Care Explor.* **2**, e0107 (2020).

197. Chrousos, G. P. & Kaltsas, G. Post‐SARS sickness syndrome manifestations and endocrinopathy: how, why, and so what? *Clin. Endocrinol. (Oxf.)* **63**, 363–365 (2005).

198. Dennis, A. *et al.* Multiorgan impairment in low-risk individuals with post-COVID-19 syndrome: a prospective, community-based study. *BMJ Open* **11**, e048391 (2021).

199. Jacomy, H., Fragoso, G., Almazan, G., Mushynski, W. E. & Talbot, P. J. Human coronavirus OC43 infection induces chronic encephalitis leading to disabilities in BALB/C mice. *Virology* **349**, 335–346 (2006).

200. Ritchie, K., Chan, D. & Watermeyer, T. The cognitive consequences of the COVID-19 epidemic: collateral damage? *Brain Commun.* **2**, fcaa069 (2020).

201. Wang, L. *et al.* Association of COVID-19 with New-Onset Alzheimer's Disease. *J. Alzheimers Dis.* **89**, 411–414 (2022).

202. de Souza Rolim, T. *et al.* Oral infections and orofacial pain in Alzheimer's disease: a case-control study. *J. Alzheimers Dis. JAD* **38**, 823–829 (2014).

203. Chevalier, C. *et al.* PB1-F2 Influenza A Virus Protein Adopts a β-Sheet Conformation and Forms

Amyloid Fibers in Membrane Environments. *J. Biol. Chem.* **285**, 13233–13243 (2010).

204. Ghosh, A. *et al.* Self-assembly of a nine-residue amyloid-forming peptide fragment of SARS corona virus E-protein: mechanism of self aggregation and amyloid-inhibition of hIAPP. *Biochemistry* **54**, 2249–2261 (2015).
205. Pham, C. L. *et al.* Viral M45 and necroptosis-associated proteins form heteromeric amyloid assemblies. *EMBO Rep.* **20**, e46518 (2019).
206. Bhardwaj, T. *et al.* Amyloidogenic proteins in the SARS-CoV and SARS-CoV-2 proteomes. *Nat. Commun.* **14**, 945 (2023).
207. Ramani, A. *et al.* SARS-CoV-2 targets neurons of 3D human brain organoids. *EMBO J.* **39**, e106230 (2020).
208. Chiricosta, L., Gugliandolo, A. & Mazzon, E. SARS-CoV-2 Exacerbates Beta-Amyloid Neurotoxicity, Inflammation and Oxidative Stress in Alzheimer's Disease Patients. *Int. J. Mol. Sci.* **22**, 13603 (2021).
209. Christ, W. *et al.* SARS-CoV-2 and HSV-1 Induce Amyloid Aggregation in Human CSF. 2022.09.15.508120 Preprint at https://doi.org/10.1101/2022.09.15.508120 (2022).
210. Hsu, J. T.-A. *et al.* The Effects of Aβ1-42 Binding to the SARS-CoV-2 Spike Protein S1 Subunit and Angiotensin-Converting Enzyme 2. *Int. J. Mol. Sci.* **22**, 8226 (2021).
211. Kong, X. *et al.* JAK2/STAT3 signaling mediates IL-6-inhibited neurogenesis of neural stem cells through DNA demethylation/methylation. *Brain. Behav. Immun.* **79**, 159–173 (2019).
212. Duan, R. *et al.* ACE2 activator diminazene aceturate ameliorates Alzheimer's disease-like neuropathology and rescues cognitive impairment in SAMP8 mice. *Aging* **12**, 14819–14829 (2020).
213. Evans, C. E. *et al.* ACE2 activation protects against cognitive decline and reduces amyloid pathology in the Tg2576 mouse model of Alzheimer's disease. *Acta Neuropathol. (Berl.)* **139**, 485–502 (2020).
214. Kuba, K. *et al.* A crucial role of angiotensin converting enzyme 2 (ACE2) in SARS coronavirus-induced lung injury. *Nat. Med.* **11**, 875–879 (2005).

215. Motaghinejad, M. & Gholami, M. Possible Neurological and Mental Outcomes of COVID-19 Infection: A Hypothetical Role of ACE-2\Mas\BDNF Signaling Pathway. *Int. J. Prev. Med.* **11**, 84 (2020).

216. Edelmann, E. *et al.* Theta Burst Firing Recruits BDNF Release and Signaling in Postsynaptic CA1 Neurons in Spike-Timing-Dependent LTP. *Neuron* **86**, 1041–1054 (2015).

217. Mizui, T. *et al.* BDNF pro-peptide actions facilitate hippocampal LTD and are altered by the common BDNF polymorphism Val66Met. *Proc. Natl. Acad. Sci. U. S. A.* **112**, E3067-3074 (2015).

218. Motaghinejad, M. *et al.* Neuroprotective effects of various doses of topiramate against methylphenidate-induced oxidative stress and inflammation in isolated rat amygdala: the possible role of CREB/BDNF signaling pathway. *J. Neural Transm. Vienna Austria 1996* **123**, 1463–1477 (2016).

219. Gao, L., Zhang, Y., Sterling, K. & Song, W. Brain-derived neurotrophic factor in Alzheimer's disease and its pharmaceutical potential. *Transl. Neurodegener.* **11**, 4 (2022).

220. Singh, M., Bansal, V. & Feschotte, C. A Single-Cell RNA Expression Map of Human Coronavirus Entry Factors. *Cell Rep.* **32**, 108175 (2020).

221. Chen, R. *et al.* The spatial and cell-type distribution of SARS-CoV-2 receptor ACE2 in human and mouse brain. 2020.04.07.030650 Preprint at https://doi.org/10.1101/2020.04.07.030650 (2020).

222. Hosking, M. P., Liu, L., Ransohoff, R. M. & Lane, T. E. A protective role for ELR+ chemokines during acute viral encephalomyelitis. *PLoS Pathog.* **5**, e1000648 (2009).

223. Lane, T. E., Hardison, J. L. & Walsh, K. B. Functional diversity of chemokines and chemokine receptors in response to viral infection of the central nervous system. *Curr. Top. Microbiol. Immunol.* **303**, 1–27 (2006).

224. Skinner, D., Marro, B. S. & Lane, T. E. Chemokine CXCL10 and Coronavirus-Induced Neurologic Disease. *Viral Immunol.* **32**, 25–37 (2019).

225. Amruta, N. *et al.* Mouse Adapted SARS-CoV-2 (MA10) Viral Infection Induces Neuroinflammation in Standard Laboratory Mice. *Viruses* **15**, 114 (2022).

226. Cama, V. F. *et al.* The microglial NLRP3 inflammasome is involved in human SARS-CoV-2 cerebral pathogenicity: A report of three post-mortem cases. *J. Neuroimmunol.* **361**, 577728 (2021).

227. de Melo, G. D. *et al.* COVID-19–related anosmia is associated with viral persistence and inflammation in human olfactory epithelium and brain infection in hamsters. *Sci. Transl. Med.* **13**, eabf8396 (2021).

228. Jeong, G. U. *et al.* SARS-CoV-2 Infection of Microglia Elicits Proinflammatory Activation and Apoptotic Cell Death. *Microbiol. Spectr.* **10**, e0109122 (2022).

229. Jones, H. D. *et al.* The NLRP3 inflammasome is required for the development of hypoxemia in LPS/mechanical ventilation acute lung injury. *Am. J. Respir. Cell Mol. Biol.* **50**, 270–280 (2014).

230. Tejera, D. *et al.* Systemic inflammation impairs microglial Aβ clearance through NLRP3 inflammasome. *EMBO J.* **38**, e101064 (2019).

231. Murta, V., Villarreal, A. & Ramos, A. J. Severe Acute Respiratory Syndrome Coronavirus 2 Impact on the Central Nervous System: Are Astrocytes and Microglia Main Players or Merely Bystanders? *ASN Neuro* **12**, 1759091420954960 (2020).

232. Rock, R. B. *et al.* Role of Microglia in Central Nervous System Infections. *Clin. Microbiol. Rev.* **17**, 942–964 (2004).

233. Ising, C. & Heneka, M. T. Functional and structural damage of neurons by innate immune mechanisms during neurodegeneration. *Cell Death Dis.* **9**, 1–8 (2018).

234. Matschke, J. *et al.* Neuropathology of patients with COVID-19 in Germany: a post-mortem case series. *Lancet Neurol.* **19**, 919–929 (2020).

235. Bellon, M. *et al.* Cerebrospinal Fluid Features in Severe Acute Respiratory Syndrome Coronavirus 2 (SARS-CoV-2) Reverse Transcription Polymerase Chain Reaction (RT-PCR) Positive Patients. *Clin. Infect. Dis. Off. Publ. Infect. Dis. Soc. Am.* **73**, e3102–e3105 (2021).

236. Schwabenland, M. *et al.* Deep spatial profiling of human COVID-19 brains reveals neuroinflammation with distinct microanatomical microglia-T-cell interactions. *Immunity* **54**, 1594-1610.e11 (2021).

237. Helms, J. *et al.* Neurologic Features in Severe SARS-CoV-2 Infection. *N. Engl. J. Med.* NEJMc2008597 (2020) doi:10.1056/NEJMc2008597.

238. Magro, C. *et al.* Complement associated microvascular injury and thrombosis in the pathogenesis of severe COVID-19 infection: A report of five cases. *Transl. Res. J. Lab. Clin. Med.* **220**, 1–13 (2020).

239. Daneman, R. & Prat, A. The Blood–Brain Barrier. *Cold Spring Harb. Perspect. Biol.* **7**, a020412 (2015).

240. Knox, E. G., Aburto, M. R., Clarke, G., Cryan, J. F. & O'Driscoll, C. M. The blood-brain barrier in aging and neurodegeneration. *Mol. Psychiatry* **27**, 2659–2673 (2022).

241. Chousterman, B. G., Swirski, F. K. & Weber, G. F. Cytokine storm and sepsis disease pathogenesis. *Semin. Immunopathol.* **39**, 517–528 (2017).

242. Ye, Q., Wang, B. & Mao, J. The pathogenesis and treatment of the `Cytokine Storm' in COVID-19. *J. Infect.* **80**, 607–613 (2020).

243. Klein, R. *et al.* COVID-19 induces neuroinflammation and loss of hippocampal neurogenesis. *Res. Sq.* rs.3.rs-1031824 (2021) doi:10.21203/rs.3.rs-1031824/v1.

244. Garber, C. *et al.* Astrocytes decrease adult neurogenesis during virus-induced memory dysfunction via IL-1. *Nat. Immunol.* **19**, 151–161 (2018).

245. Chen, X. *et al.* Detectable Serum Severe Acute Respiratory Syndrome Coronavirus 2 Viral Load (RNAemia) Is Closely Correlated With Drastically Elevated Interleukin 6 Level in Critically Ill Patients With Coronavirus Disease 2019. *Clin. Infect. Dis. Off. Publ. Infect. Dis. Soc. Am.* **71**, 1937–1942 (2020).

246. Chen, L. Y. C., Hoiland, R. L., Stukas, S., Wellington, C. L. & Sekhon, M. S. Assessing the importance of interleukin-6 in COVID-19. *Lancet Respir. Med.* **9**, e13 (2021).

247. Strafella, C. *et al.* Investigation of Genetic Variations of IL6 and IL6R as Potential Prognostic and Pharmacogenetics Biomarkers: Implications for COVID-19 and Neuroinflammatory Disorders. *Life* **10**, 351 (2020).

248. Griffin, W. S. T. & Mrak, R. E. Interleukin-1 in the genesis and progression of and risk for development of neuronal degeneration in Alzheimer's disease. *J. Leukoc. Biol.* **72**, 233–238 (2002).

249. Arnaldez, F. I. *et al.* The Society for Immunotherapy of Cancer perspective on regulation of interleukin-6 signaling in COVID-19-related systemic inflammatory response. *J. Immunother. Cancer* **8**, e000930 (2020).

250. Song, E. *et al.* Neuroinvasion of SARS-CoV-2 in human and mouse brain. *J. Exp. Med.* **218**, e20202135 (2021).

251. Bayat, A.-H. *et al.* COVID-19 causes neuronal degeneration and reduces neurogenesis in human hippocampus. *Apoptosis* **27**, 852–868 (2022).

252. Ramírez Hernández, E. *et al.* The therapeutic potential of galectin-1 and galectin-3 in the treatment of neurodegenerative diseases. *Expert Rev. Neurother.* **20**, 439–448 (2020).

253. Yang, R.-Y., Rabinovich, G. A. & Liu, F.-T. Galectins: structure, function and therapeutic potential. *Expert Rev. Mol. Med.* **10**, e17 (2008).

254. Chen, H.-L., Liao, F., Lin, T.-N. & Liu, F.-T. Galectins and Neuroinflammation. in *Glycobiology of the Nervous System* (eds. Yu, R. K. & Schengrund, C.-L.) 517–542 (Springer, New York, NY, 2014). doi:10.1007/978-1-4939-1154-7_24.

255. Bai, G. *et al.* High Levels of the Cleaved Form of Galectin-9 and Osteopontin in the Plasma Are Associated with Inflammatory Markers That Reflect the Severity of COVID-19 Pneumonia. *Int. J. Mol. Sci.* **22**, 4978 (2021).

256. Bozorgmehr, N. *et al.* Galectin-9, a Player in Cytokine Release Syndrome and a Surrogate Diagnostic Biomarker in SARS-CoV-2 Infection. *mBio* **12**, e00384-21 (2021).

257. De Biasi, S. *et al.* Marked T cell activation, senescence, exhaustion and skewing towards TH17 in patients with COVID-19 pneumonia. *Nat. Commun.* **11**, 3434 (2020).

258. Chen, Y. *et al.* Gasdermin D Drives the Nonexosomal Secretion of Galectin-3, an Insulin Signal Antagonist. *J. Immunol. Baltim. Md 1950* **203**, 2712–2723 (2019).

259. Ma, S. *et al.* Prevalence of mild cognitive impairment in type 2 diabetes mellitus is associated with

serum galectin‐3 level. *J. Diabetes Investig.* **11**, 1295–1302 (2020).

260. Siew, J. J. *et al.* Galectin-3 is required for the microglia-mediated brain inflammation in a model of Huntington's disease. *Nat. Commun.* **10**, 3473 (2019).

261. Yan, J. *et al.* Increased Expressions of Plasma Galectin-3 in Patients with Amyotrophic Lateral Sclerosis. *Chin. Med. J. (Engl.)* **129**, 2797–2803 (2016).

262. Yazar, H. O., Yazar, T. & Cihan, M. A preliminary data: Evaluation of serum Galectin-3 levels in patients with Idiopathic Parkinson's Disease. *J. Clin. Neurosci. Off. J. Neurosurg. Soc. Australas.* **70**, 164–168 (2019).

263. Ashraf, G. M. & Baeesa, S. S. Investigation of Gal-3 Expression Pattern in Serum and Cerebrospinal Fluid of Patients Suffering From Neurodegenerative Disorders. *Front. Neurosci.* **12**, (2018).

264. Yazar, T., Olgun Yazar, H. & Cihan, M. Evaluation of serum galectin-3 levels at Alzheimer patients by stages: a preliminary report. *Acta Neurol. Belg.* **121**, 949–954 (2021).

265. Boza-Serrano, A. *et al.* Galectin-3 is elevated in CSF and is associated with Aβ deposits and tau aggregates in brain tissue in Alzheimer's disease. *Acta Neuropathol. (Berl.)* **144**, 843–859 (2022).

266. Tao, C.-C. *et al.* Galectin-3 promotes Aβ oligomerization and Aβ toxicity in a mouse model of Alzheimer's disease. *Cell Death Differ.* **27**, 192–209 (2020).

267. Chen, Y.-C. *et al.* Galectin-3 Negatively Regulates Hippocampus-Dependent Memory Formation through Inhibition of Integrin Signaling and Galectin-3 Phosphorylation. *Front. Mol. Neurosci.* **10**, (2017).

268. Steelman, A. J. & Li, J. Astrocyte galectin-9 potentiates microglial TNF secretion. *J. Neuroinflammation* **11**, 144 (2014).

269. Premeaux, T. A. *et al.* Elevated Cerebrospinal Fluid Galectin-9 is Associated with Central Nervous System Immune Activation and Poor Cognitive Performance in Older HIV-infected Individuals. *J. Neurovirol.* **25**, 150–161 (2019).

270. Wang, X., Niu, Y., Yue, C.-X., Fu, S. & Wang, R.-T. Increased ileal bile acid binding protein and

galectin-9 are associated with mild cognitive impairment and Alzheimer's disease. *J. Psychiatr. Res.* **119**, 102–106 (2019).

271. Kanberg, N. *et al.* Neurochemical evidence of astrocytic and neuronal injury commonly found in COVID-19. *Neurology* **95**, e1754–e1759 (2020).

272. Frontera, J. A. *et al.* Comparison of serum neurodegenerative biomarkers among hospitalized COVID-19 patients versus non-COVID subjects with normal cognition, mild cognitive impairment, or Alzheimer's dementia. *Alzheimers Dement. J. Alzheimers Assoc.* **18**, 899–910 (2022).

273. Boutajangout, A. *et al.* Plasma biomarkers of neurodegeneration and neuroinflammation in hospitalized COVID‐19 patients with and without new neurological symptoms. *Alzheimers Dement.* **17**, e057892 (2021).

274. Sun, B. *et al.* Characterization and Biomarker Analyses of Post-COVID-19 Complications and Neurological Manifestations. *Cells* **10**, 386 (2021).

275. Huang, S. *et al.* Persistent white matter changes in recovered COVID-19 patients at the 1-year follow-up. *Brain* **145**, 1830–1838 (2022).

276. Douaud, G. *et al.* SARS-CoV-2 is associated with changes in brain structure in UK Biobank. *Nature* **604**, 697–707 (2022).

277. Besteher, B. *et al.* Larger gray matter volumes in neuropsychiatric long-COVID syndrome. *Psychiatry Res.* **317**, 114836 (2022).

278. Lu, Y. *et al.* Cerebral Micro-Structural Changes in COVID-19 Patients – An MRI-based 3-month Follow-up Study. *EClinicalMedicine* **25**, 100484 (2020).

279. Paniz-Mondolfi, A. *et al.* Central nervous system involvement by severe acute respiratory syndrome coronavirus-2 (SARS-CoV-2). *J. Med. Virol.* **92**, 699–702 (2020).

280. Solomon, I. H. *et al.* Neuropathological Features of Covid-19. *N. Engl. J. Med.* **383**, 989–992 (2020).

281. Stein, S. R. *et al.* SARS-CoV-2 infection and persistence in the human body and brain at autopsy. *Nature* **612**, 758–763 (2022).

282. Thakur, K. T. *et al.* COVID-19 neuropathology at Columbia University Irving Medical Center/New York Presbyterian Hospital. *Brain* **144**, 2696–2708 (2021).

283. Kim, Y.-I. *et al.* Infection and Rapid Transmission of SARS-CoV-2 in Ferrets. *Cell Host Microbe* **27**, 704-709.e2 (2020).

284. Munster, V. J. *et al.* Respiratory disease in rhesus macaques inoculated with SARS-CoV-2. *Nature* **585**, 268–272 (2020).

285. Rockx, B. *et al.* Comparative pathogenesis of COVID-19, MERS, and SARS in a nonhuman primate model. *Science* **368**, 1012–1015 (2020).

286. Yu, P. *et al.* Age-related rhesus macaque models of COVID-19. *Anim. Models Exp. Med.* **3**, 93–97 (2020).

287. Oreshkova, N. *et al.* SARS-CoV-2 infection in farmed minks, the Netherlands, April and May 2020. *Euro Surveill. Bull. Eur. Sur Mal. Transm. Eur. Commun. Dis. Bull.* **25**, (2020).

288. Shi, J. *et al.* Susceptibility of ferrets, cats, dogs, and other domesticated animals to SARS–coronavirus 2. *Science* **368**, 1016–1020 (2020).

289. Li, W. *et al.* Bats are natural reservoirs of SARS-like coronaviruses. *Science* **310**, 676–679 (2005).

290. Andersen, K. G., Rambaut, A., Lipkin, W. I., Holmes, E. C. & Garry, R. F. The proximal origin of SARS-CoV-2. *Nat. Med.* **26**, 450–452 (2020).

291. Chan, J. F.-W. *et al.* Simulation of the Clinical and Pathological Manifestations of Coronavirus Disease 2019 (COVID-19) in a Golden Syrian Hamster Model: Implications for Disease Pathogenesis and Transmissibility. *Clin. Infect. Dis. Off. Publ. Infect. Dis. Soc. Am.* **71**, 2428–2446 (2020).

292. Osterrieder, N. *et al.* Age-Dependent Progression of SARS-CoV-2 Infection in Syrian Hamsters. *Viruses* **12**, E779 (2020).

293. Imai, M. *et al.* Syrian hamsters as a small animal model for SARS-CoV-2 infection and countermeasure development. *Proc. Natl. Acad. Sci. U. S. A.* **117**, 16587–16595 (2020).

294. Wan, Y., Shang, J., Graham, R., Baric, R. S. & Li, F. Receptor Recognition by the Novel

Coronavirus from Wuhan: an Analysis Based on Decade-Long Structural Studies of SARS Coronavirus. *J. Virol.* **94**, e00127-20 (2020).

295. Tseng, C.-T. K. *et al.* Severe acute respiratory syndrome coronavirus infection of mice transgenic for the human Angiotensin-converting enzyme 2 virus receptor. *J. Virol.* **81**, 1162–1173 (2007).
296. McCray, P. B. *et al.* Lethal infection of K18-hACE2 mice infected with severe acute respiratory syndrome coronavirus. *J. Virol.* **81**, 813–821 (2007).
297. Bao, L. *et al.* The pathogenicity of SARS-CoV-2 in hACE2 transgenic mice. *Nature* **583**, 830–833 (2020).
298. Netland, J., Meyerholz, D. K., Moore, S., Cassell, M. & Perlman, S. Severe acute respiratory syndrome coronavirus infection causes neuronal death in the absence of encephalitis in mice transgenic for human ACE2. *J. Virol.* **82**, 7264–7275 (2008).
299. Olivarria, G. M. *et al.* Microglia Do Not Restrict SARS-CoV-2 Replication following Infection of the Central Nervous System of K18-Human ACE2 Transgenic Mice. *J. Virol.* **96**, e0196921 (2022).
300. Sun, S.-H. *et al.* A Mouse Model of SARS-CoV-2 Infection and Pathogenesis. *Cell Host Microbe* **28**, 124-133.e4 (2020).
301. Rathnasinghe, R. *et al.* Comparison of transgenic and adenovirus hACE2 mouse models for SARS-CoV-2 infection. *Emerg. Microbes Infect.* **9**, 2433–2445 (2020).
302. Israelow, B. *et al.* Mouse model of SARS-CoV-2 reveals inflammatory role of type I interferon signaling. *J. Exp. Med.* **217**, e20201241 (2020).
303. Dinnon, K. H. *et al.* A mouse-adapted model of SARS-CoV-2 to test COVID-19 countermeasures. *Nature* **586**, 560–566 (2020).
304. Leist, S. R. *et al.* A Mouse-Adapted SARS-CoV-2 Induces Acute Lung Injury and Mortality in Standard Laboratory Mice. *Cell* **183**, 1070-1085.e12 (2020).

CHAPTER 2

MICROGLIA DO NOT RESTRICT SARS-COV-2 REPLICATION FOLLOWING INFECTION OF THE CENTRAL NERVOUS SYSTEM OF K18-HUMAN ACE2 TRANSGENIC

Journal of Virology, 2021

Microglia Do Not Restrict SARS-CoV-2 Replication following Infection of the Central Nervous System of K18-Human ACE2 Transgenic Mice

Gema M. Olivarria[a], Yuting Cheng[b], Susana Furman[a], Collin Pachow[b], Lindsay A. Hohsfield[a], Charlene Smith-Geater[c], Ricardo Miramontes[d], Jie Wu[e], Mara S. Burns[a], Kate I. Tsourmas[a], Jennifer Stocksdale[a], Cynthia Manlapaz[a], William H. Yong[f], John Teijaro[g], Robert Edwards[f], Kim N.Green[a], Leslie M. Thompson[a,c,e,f], Thomas E. Lane[a,b,h]

[a]Department of Neurobiology and Behavior, University of California, Irvine, Irvine, California, USA

[b]Department of Molecular Biology and Biochemistry, School of Biological Sciences, University of California, Irvine, Irvine, California, USA

[c]Department of Psychiatry and Human Behavior, University of California, Irvine School of Medicine, Irvine, California, USA

[d]Institute for Memory Impairments and Neurological Disorders, School of Biological Sciences, University of California, Irvine, Irvine, California, USA

[e]Department of Biological Chemistry, University of California, Irvine School of Medicine, Irvine, California, USA

[f]Department of Pathology & Laboratory Medicine, University of California, Irvine School of Medicine, Irvine, California, USA

[g]Department of Immunology and Microbiology, The Scripps Research Institute, La Jolla California, USA

[h]Center for Virus Research, University of California, Irvine, Irvine, California, USA

ABSTRACT

Unlike SARS-CoV-1 and MERS-CoV, infection with SARS-CoV-2, the viral pathogen responsible for COVID-19, is often associated with neurologic symptoms that range from mild to severe, yet increasing evidence argues the virus does not exhibit extensive neuroinvasive properties. We demonstrate SARS-CoV-2 can infect and replicate in human iPSC-derived neurons and that infection shows limited antiviral and inflammatory responses but increased activation of EIF2 signaling following infection as determined by RNA sequencing. Intranasal infection of K18 human ACE2 transgenic mice (K18-hACE2) with SARS-CoV-2 resulted in lung pathology associated with viral replication and immune cell infiltration. In addition, ~50% of infected mice exhibited CNS infection characterized by wide-spread viral replication in neurons accompanied by increased expression of chemokine (*Cxcl9, Cxcl10, Ccl2, Ccl5* and *Ccl19*) and cytokine (*Ifn-λ* and *Tnf-α*) transcripts associated with microgliosis and a neuroinflammatory response consisting primarily of monocytes/macrophages. Microglia depletion via administration of colony-stimulating factor 1 receptor inhibitor, PLX5622, in SARS-CoV-2 infected mice did not affect survival or viral replication but did result in dampened expression of proinflammatory cytokine/chemokine transcripts and a reduction in monocyte/macrophage infiltration. These results argue that microglia are dispensable in terms of controlling SARS-CoV-2 replication in the K18-hACE2 model but do contribute to an inflammatory response through expression of pro-inflammatory genes. Collectively, these findings contribute to previous work demonstrating the ability of SARS-CoV-2 to infect neurons as well as emphasizing the potential use of the K18-hACE2 model to study immunological and neuropathological aspects related to SARS-CoV-2-induced neurologic disease.

IMPORTANCE

Understanding the immunological mechanisms contributing to both host defense and disease following viral infection of the CNS is of critical importance given the increasing number of viruses that are capable of infecting and replicating within the nervous system. With this in mind, the present study was undertaken to evaluate the role of microglia in aiding in host defense following experimental infection of the central nervous system (CNS) of K18-hACE2 with SARS-CoV-2, the causative agent of COVID-19. Neurologic symptoms that range in severity are common in COVID-19 patients and understanding immune responses that contribute to restricting neurologic disease can provide important insight into better understanding consequences associated with SARS-CoV-2 infection of the CNS.

INTRODUCTION

The clinical spectrum of COVID-19 is complex, and numerous risk factors and comorbidities are considered important in affecting disease severity, including age, obesity, chronic respiratory disease, and cardiovascular disease (1). In addition, neurological symptoms are common in COVID-19 patients, suggesting the virus can potentially infect and replicate in the central nervous system (CNS). Indeed, encephalitis and meningitis have been reported in COVID-19 patients, and viral RNA and protein have been detected within the CSF of infected patients (2–4). Additionally, human brain organoids are susceptible to SARS-CoV-2 infection (2, 5), yet demonstration of extensive CNS penetrance by SARS-CoV-2 has remained elusive. It is imperative to develop pre-clinical animal models of COVID-19 that capture consistent and reproducible clinical and histologic readouts of many disease-associated symptoms following experimental infection with clinical isolates of SARS-CoV-2 (6). Importantly, these models should be able to reliably evaluate interventional therapies to limit viral replication and mute immune-mediated pathology, as well as evaluate effectiveness of novel vaccines, all while remaining cost-effective. To date, the most common animal models employed to evaluate COVID-19 pathogenesis include mice, nonhuman primates (rhesus macaques, cynomolgus macaques and African green monkeys), Syrian hamsters, ferrets, and cats (6).

Human ACE2 (hACE2) transgenic mouse models have provided important insights into the pathogenesis of COVID-19. Perlman and colleagues (7) developed the K18-hACE2 mice, initially used as a mouse model of SARS-CoV-1, which has been successfully employed as a model of COVID-19 (8). Intranasal inoculation of SARS-CoV-2 in K18-hACE2 mice results in a dose-dependent increase in weight loss and mortality with the lung being the major site of viral infection, while smaller amounts of virus are detected in the heart, liver, spleen, kidney, small

intestine, and colon (8). Examination of lungs revealed distribution of viral antigen associated with alveolar damage, interstitial lesions, edema, and inflammation. Lung infection resulted in an increase in expression of interferons as well as inflammatory cytokines and chemokines associated with neutrophil, macrophage/monocyte, and T cell infiltration. Viral RNA was also detected within the sinonasal epithelium, and viral antigen was present in sustentacular cells associated with anosmia (8).

Examination of brains of SARS-CoV-2 infected hACE2 transgenic mice has indicated that infection of the CNS is not consistent, and in some cases, virus is rarely detected (8–12). This may reflect the SARS-CoV-2 isolate being studied as well as the dose of virus being administered. However, in those animals in which virus penetrates the brain, there can be extensive spread of the virus throughout different anatomic regions accompanied by cell death (8), and these results are consistent with early studies examining SARS-CoV-1 infection of K18-hACE2 mice (7). High-level of CNS infection in K18-hACE2 is accompanied by meningeal inflammation associated with immune cell infiltration into the brain parenchyma and microglia activation (11). Enhanced CNS penetrance and replication of SARS-CoV-2 within the CNS of K18-hACE2 is associated with increased mortality, although the mechanisms by which this occurs remain unclear. The present study was undertaken to (i) expand on earlier studies examining SARS-CoV-2 infection of human CNS resident cells, (ii) evaluate the immune response that occurs in response to SARS-CoV-2 infection of the CNS of K18-hACE2 mice, and (iii) assess the contributions of microglia in host defense following CNS infection by SARS-CoV-2.

RESULTS

SARS-CoV-2 infection of human neurons. Previous studies have indicated neurons are susceptible to infection by SARS-CoV-2 (2); therefore, we infected human iPSC-derived neurons with SARS-CoV-2. Similar to earlier reports, SARS-CoV-2 was able to infect and replicate within neurons as determined by staining for nucleocapsid protein (Fig. 1A and B). By 48h pi., viral nucleocapsid protein had spread from the neuron cell body and extended down dendritic and axonal projections (Fig. 1C and D). Notably, we did not detect syncytium formation in neuron cultures at any time following infection with SARS-CoV-2, suggesting that virus may not spread via fusion with neighboring cells. RNA sequencing analysis revealed that expression of both antiviral and inflammatory responses in infected neurons was limited relative to the genes within the heatmap at both 24h and 48h postinfection (Fig. 1E). We then evaluated pathways that may progressively change between 24h and 48h postinfection comparing the Transcripts per million (TPMs) as input for Ingenuity Pathway Analysis (IPA). Figure 1F shows the top 12 IPA canonical pathways that are overrepresented. eIF2 signaling is the predominant pathway induced upon SARS-CoV-2 infection of neurons, followed by pathways associated with oxidative phosphorylation, eIF4, MTOR signaling and mitochondrial dysfunction, the latter with no prediction of activity. Notably, the Coronavirus Pathogenesis Pathway is also overrepresented; however, is inhibited in response to neuronal infection by SARS-CoV-2 over the time frame tested with the majority of the genes represented encoding ribosomal proteins (Fig. 1F).

SARS-CoV-2 infection of lungs of K18-hACE2 mice.K18-hACE2 mice were intranasally infected with either 1×10^4, 5×10^4 or 1×10^5 PFU of SARS-CoV-2, and weight loss and mortality were recorded. Consistent with other reports (8–12), we observed a general trend toward dose-dependent increase in weight loss and mortality out to day 7 post infection (pi.)

(Fig. 2A). qPCR indicated the presence of viral RNA in lungs of infected K18-hACE2 (Fig. 2B). *In situ* hybridization of lungs of mice infected with 5×10^4 PFU of virus at day 7 pi. revealed localized areas of viral infection as determined by expression of spike RNA (Fig. 2C). Hematoxylin and eosin staining of lungs demonstrated both alveolar and interstitial lesions, with alveolar hemorrhage and edema (Fig. 2D), interstitial congestion (Fig. 2E) and lymphocytic infiltrates (Fig. 2F). qPCR analysis of proinflammatory cytokines and chemokines indicated increased expression of *Ifn-λ*, *Cxcl10*, *Cxcr2*, and *Ccl2* yet varied expression of *Il-10*, *TNF-α*, *Ccl19*, *and Ccl5* and limited expression of transcripts for *Ifn-β1* (Fig. 2G). Hematoxylin and eosin staining showed immune cell infiltrates in SARS-CoV-2-infected lungs containing inflammatory $CD8^+$ T cells as determined by immunofluorescent staining (Fig. 3A to D). In addition, germinal center-like structures were detected within the lungs of SARS-CoV-2-infected mice with enriched $CD8^+$ T cell accumulation (Fig. 3E and F). Collectively, our findings are consistent with previous studies employing SARS-CoV-2 infection of K18-hACE2 mice in terms of development of interstitial pneumonia and immune cell infiltration associated with viral RNA present within the lungs (8–12).

Neuroinvasion by SARS-CoV-2. Following intranasal infection of mice with 5×10^4 PFU of SARS-CoV-2, virus was detected in the brain as determined by qPCR and RNAscope compared to sham-infected mice (Fig. 4A to C). Using a Spike-specific probe, we observed wide-spread expansion of viral mRNA throughout the brain with many distinct anatomical regions infected as well as spared. By day 7 pi., viral RNA was present within the cortex (CTX), striatum (STR), pallidum (PAL), thalamus (TH), hypothalamus (HY), midbrain (MB), pons (P), and medulla (MD), whereas areas that were relatively spared included the olfactory bulb (OB), white matter (WM) tracts, hippocampus (HC) and cerebellum (CB) (Fig. 4B); no viral RNA was

detected in sham-infected K18-hACE2 mice (Fig. 4C). Demyelinating lesions have been detected in postmortem brains of COVID-19 patients (13); however, we did not detect any evidence of demyelination within the brains of SARS-CoV-2-infected mice as determined by luxol-fast blue (LFB) staining (Fig. 4D and E). The predominant cellular target for SARS-CoV-2 infection was neurons as determined by cellular morphology of cells positive for viral RNA (Fig. 5A and B). In a small percentage of infected mice, we were able to detect viral RNA in the olfactory bulb with primary targets being mitral and glomerular neurons (Fig. 5C and D). Prominent neuropathological changes detected included perivascular cuffing (Fig. 5E), subventricular inflammation (Fig. 5F) and leptomeningitis (Fig. 5G), consistent with previous studies (2, 3).

Analysis of CNS myeloid cells showed increased IBA1 soma size and shortened/thickened processes, indicative of microglial activation in SARS-CoV-2-infected mice compared to sham-infected mice (Fig. 6A and B). In addition, immunofluorescent co-staining for Mac2/galectin-3+ cells, a marker recently identified in peripheral cell infiltrates, and IBA1 (Hohsfield et al. *manuscript in revision*), revealed increased monocyte/macrophage infiltration within the brains of infected mice compared to sham-infected mice (Fig. 6A and B). Mac2+ cells enter the CNS parenchyma from different anatomic areas, including the ventricles, leptomeninges and vasculature (Fig. 6C and D) compared to uninfected control mice (Fig. 6E).

Microglia ablation does not affect disease or control of viral replication in the CNS. Previous studies have implicated the importance of microglia in aiding in control of neuroadapted murine beta-coronaviruses by enhancing antiviral T cell responses through augmenting antigen presentation (11–13). Notably, microglia are dependent on signaling through the colony-stimulating factor 1 receptor (CSF1R) for their survival and can be effectively

eliminated with CSF1R inhibitors that cross the blood brain barrier (14). K18-hACE2 mice were fed pre-formulated chow containing either the CSF1R inhibitor PLX5622 (1,200 ppm) (15) or control chow 7 days prior to intranasal infection with 5×10^4 PFU of SARS-CoV-2, and remained on drug for the duration of the experiment (6). No notable differences were detected in weight loss between experimental groups (Fig. 7A). SARS-CoV-2-infected mice treated with either PLX5622 or control chow were sacrificed at day 7 pi., and viral mRNA levels in lungs and brains were determined. As shown in Fig. 7B, we detected no significant differences in the Spike mRNA transcripts in either the lung or the brain between experimental groups. Quantification of Iba1-positive cells revealed a >95% reduction ($P < 0.01$) in microglia in PLX5622-treated mice compared to control mice. Overall, PLX5622-mediated ablation of microglia resulted in a dramatic reduction in expression of proinflammatory cytokine/chemokine genes within the brains of SARS-CoV-2 infected mice compared to infected mice fed control chow (Fig. 7D). By day 7 pi., SARS-CoV-2 infection resulted in increased expression of proinflammatory cytokines and chemokines in mice treated with control chow. The highest transcript levels were for the T cell chemoattractants CXCL9 and CXCL10; monocyte/macrophage chemoattractants, CCL2 and CCL5; and TNF-α (Fig. 7D). Transcripts encoding the neutrophil chemoattractant CXCL1, and B cell chemoattractant CCL19 were also increased, as well as IFN-λ type 3 and IL-10 compared to uninfected controls (Fig. 7D). Depletion of microglia resulted in a marked reduced expression of the majority chemokine/cytokines transcripts. While not significant, there was a marked reduction in Mac2/galactin3+ cells in PLX5622-treated mice compared to control chow and this correlated with reduced expression of monocyte/macrophage chemoattractant chemokines CCL2 and CCL5 (Fig. 7E) that have previously been shown to attract these cells into the CNS of mice infected with a neurotropic mouse coronavirus (16–21).

DISCUSSION

In the face of the ongoing COVID-19 pandemic, it is imperative to develop pre-clinical animal models of COVID-19 that capture consistent and reproducible clinical and histologic readouts of many disease-associated symptoms following experimental infection with SARS-CoV-2 [1]. For both SARS-CoV-2 and SARS-CoV-1, the surface-bound viral spike glycoprotein uses the cellular surface receptor protein, ACE2, to bind and enter cells. However, mouse ACE2 does not efficiently bind the spike glycoprotein of either SARS-CoV-1 or SARS-CoV-2, rendering wild-type mice not useful in the study of SARS or COVID-19 pathogenesis, respectively, due to an inefficient ability to infect and replicate in host cells. Human ACE2 (hACE2) transgenic mouse models have provided important insights into the pathogenesis of COVID-19 in terms of evaluating the efficacy and duration of immune responses elicited in response to infection as well as testing vaccines, antiviral drugs and monoclonal antibody therapies to restrict viral replication and limit disease severity (8).

Intranasal inoculation of K18-hACE2 mice with SARS-CoV-2 resulted in weight loss along with viral infection and replication within the lungs that was associated with a robust inflammatory response. These findings are consistent with other reports that demonstrated the presence of neutrophils, monocytes/macrophages and T cells within the lungs of SARS-CoV-2-infected K18-hACE2 mice (8, 11). In response to infection, expression of proinflammatory cytokines/chemokines was increased and correlated with the presence of inflammatory cells. We detected inflammatory $CD8^+$ T cells in the lungs of infected mice and these cells are presumably responding to the T cell chemoattractant CXCL10. Our lab has previously shown that induction of CXCL10 expression following experimental infection of mice with a neuroadapted strain of murine coronavirus is critical in host defense and acts by

attracting virus-specific T cells into the CNS (22–24). Similarly, inflammatory monocyte/macrophages are likely recruited in response to expression of CCL2 as this has been shown to attract these cells following murine coronavirus infection of mice (16–19). The increased expression of transcripts encoding CXCR2 most likely reflects the presence of inflammatory neutrophils (25). Therapeutic targeting of these chemokines may therefore alter immune cell trafficking into the lungs of infected mice and alleviate the severity of lung pathology. How blocking chemokine signaling would affect SARS-CoV-2-induced lung pathology in COVID-19 patients is under investigation.

Clinical reports of COVID-19 patients cite a dysregulated immune response characterized by elevated chemokine expression as key in the development of pathogenesis (26, 27). Similar to our findings using the K18-hACE2 model, these reports have found upregulation of CCL2 (MCP1), CXCL8 (IL-8), and CXCL10 (IP10) to correlate with severity of disease and have suggested evaluation of these as biomarkers for disease and as targets for therapeutic intervention (28–30). Leronlimab, a CCR5-blocking antibody, is currently in phase 2 clinical trials in the United States. for treatment of mild, moderate, and severe COVID-19 (NCT04343651, NCT04347239). In addition, limiting neutrophil infiltration into the lungs of COVID-19 patients may help prevent disease progression and outcome. With this in mind, the monoclonal antibody BMS-986253 that blocks CXCL8 as well as Reparixin, an oral inhibitor of CXCR1/2, are both currently undergoing clinical trials in the United States. for reducing the severity of COVID-19-related pneumonia by reducing neutrophil accumulation within the lungs of infected patients (NCT04878055, NCT04347226). A clinical trial was recently completed using measurement of CXCL10 in a Clinical Decision Support Protocol in COVID-19 patients

(NCT04389645) that positively correlated CXCL10 levels with mortality suggesting that targeting CXCL10 signaling may also be beneficial in managing disease severity (31).

Examination of brains of SARS-CoV-2-infected K18-hACE2 mice, as well as brains from other hACE2 transgenic mice, has revealed that virus is able to infect, replicate and spread within the parenchyma and this is considered important in contributing to mortality (2, 5, 8, 9). Virus can be detected in different anatomic regions of the brain and is accompanied by cell death (5) and these observations are consistent with early studies examining SARS-CoV-1 infection of K18-hACE2 mice (7). Our results indicate that neurons are primary targets for SARS-CoV-2 infection within the brains of K18-hACE2 mice which is consistent with other studies (10, 32, 33). Furthermore, human iPSC-derived neurons were susceptible to SARS-CoV-2 infection and virus was able to replicate in these cells. The detection of viral antigen within dendrites extending from the cell body suggests this may offer a unique mechanism of viral replication and spread in neurons and this is further emphasized by the absence of cell death and/or syncytium formation. RNA sequencing of infected neurons revealed that expression of most inflammatory and antiviral response genes were reduced in SARS-CoV-2-infected neurons, consistent with a previously published study highlighting the muted immune response in neurons infected with SARS-CoV-2 compared to Zika virus (2). However, IPA analysis determined that despite the lack of induced immune and inflammatory response in infected neurons, there was a significant overrepresentation of pathways associated with eIF2, oxidative phosphorylation, regulation of eIF4 and mTOR signaling. eIF2, which mediates initiation of eukaryotic translation by binding Met-tRNA$_i^{Met}$ to the ribosomal subunit, can be activated via phosphorylation by various kinases, including protein kinase-RNA-dependent (PKR), PKR-like endoplasmic reticulum kinase (PERK), and heme regulated inhibitor (HRI) (34). Upregulation of eIF2 phosphorylation by

these can occur in response to various types of stressors, including viral infection, ER stress, or oxidative stress, respectively (34). Upregulation of eIF4, which mediates recruitment of ribosomes to mRNA for translation, alongside overactivation of mTOR signaling, which modulates eIF4 activity, suggests infection of neurons with SARS-CoV-2 induces increased cellular activity and protein production even in the absence of inflammatory and antiviral gene induction (35). Whether this increase in protein production pathways corresponds to viral hijacking of cellular machinery for viral reproduction or if it corresponds to other induced mechanisms of neuronal stress/survival response remains to be determined.

Resident cells of the CNS are important in host defense following viral infection through either secretion of antiviral cytokines like type I interferon (IFN-I) and pro-inflammatory cytokines/chemokines, and presentation of antigen to infiltration of antigen-sensitized T cells. We found the transcripts encoding the T cell chemoattractant chemokines, including CXCL9 and CXCL10 were expressed along with monocyte/macrophage chemokines CCL2 and CCL5 and CXCL1 which attracts neutrophils. In addition, transcripts specific for the B cell chemoattractant CCL19 were also detected. The chemokine elicited in response to CNS infection of K18-hACE2 by SARS-CoV-2 infection is remarkably similar to the chemokine response following CNS infection of mice with the neuroadapted strains of murine coronaviruses (36, 37). This is interesting in that murine coronaviruses are primarily tropic for glial cells, e.g., astrocytes, microglia and oligodendrocytes with relative sparing of neurons while neurons appear to be exclusively targeted by SARS-CoV-2. These findings argue that expression of chemokines following coronavirus infection of the CNS may not be influenced by the cellular target of infection and this may reflect a localized response to expression of interferons (IFN) expressed in response to viral infection. With this in mind, we did detect IFNλ3 transcripts within the brains

of SARS-CoV-2 infected mice yet IFNβ1 transcripts were noticeably reduced. The inflammatory response consisted primarily of monocytes/macrophages as determined by immunofluorescent staining for Mac2 and these cells are most likely migrating into the CNS in response to CCL2 and CCL5 expression (18–21). We did not detect a robust T cell response and this was surprising given the expression levels of CXCL9 and CXCL10 transcripts. Whether this simply reflected that T cells had yet to migrate into the brains of infected mice at the time of sacrifice or if efficient translation of these transcripts is compromised is not known at this time.

We have recently determined that in response to JHMV infection of the CNS of immunocompetent mice, there are inflammatory monocyte/macrophage subpopulations that differentially express CD115/CSF-1R and this highlights the highly inflammatory nature of these cells in models of neurodegeneration (37). Expression of CD115-expressing macrophages and microglia have also been detected in other models of neuroinflammation demonstrating important roles for these cells in contributing to inflammatory responses (38–40). More recently, microglia are recognized to be important in host defense in response to viral infection of the CNS (41–45). Targeted depletion of microglia via CSF1R inhibition leads to increased mortality in mice infected with West Nile Virus (WNV) and is associated with diminished activation of antigen-presenting cells (APCs) and limited reactivation of virus-specific T cells that leads to reduced viral clearance (42, 44). Similar findings have been reported for other neurotropic viruses, including Japanese encephalitis virus (JEV) (44) and Theiler's murine encephalomyelitis virus (TMEV) (43, 45). Moreover, microglia have also been shown to enhance host defense following CNS infection by the neurotropic JHM strain of mouse hepatitis virus (JHMV, a murine coronavirus) and this was related to inefficient T cell-mediated control of viral replication (41, 46). Additionally, the absence of microglia also results in an increase in the severity of

demyelination, accompanied by a decrease in remyelination (46, 47). In response to SARS-CoV-2 CNS infection, we did detect microgliosis indicating these cells are responding to infection and may be involved in host defense. Ablation of microglia via PLX5622 administration did not affect clinical disease nor viral burden within the brain, indicating these cells are dispensable in terms of controlling SARS-CoV-2 replication within the brain in the K18-hACE2 model. There was a marked reduction in expression of proinflammatory cytokines/chemokines, including monocyte/macrophage chemoattractants CCL2 and CCL5 and this corresponded with an overall reduction in numbers of these cells in the brains of PLX5622-treated mice. These findings support the notion that microglia do contribute to the neuroinflammatory response, in part, through influencing expression of chemokines/cytokines in response to SARS-CoV-2 infection of the CNS of K18-hACE2 mice.

Very early in the COVID-19 pandemic, it became apparent that an abundant number of patients exhibited a variety of neurologic conditions that ranged in severity. Although numerous neurological symptoms have been associated with COVID-19, the most common neurologic symptoms include anosmia/dysgeusia, delirium, encephalopathy, and stroke (48–50). The overwhelming evidence indicates that SARS-CoV-2 is not readily detected within the CNS by either PCR and/or immunohistochemical staining (2, 51) suggesting that neurologic complications associated with COVID-19 patients may occur through alternative mechanisms, including the potential development of autoreactive antibodies specific for neural antigens (52). COVID-19 patients have anti-SARS-CoV-2 IgG antibodies in the cerebral spinal fluid (CSF) that recognized target epitopes that differ from serum antibodies. Moreover, a portion of COVID-19 patients exhibited CSF antibodies that targeted self-antigens, arguing for the possibility that neurologic disease may be associated with CNS autoimmunity (52). Nonetheless, neurons and

cells of the vasculature have been shown to be targets of infection (53–57). Despite increasing evidence indicating extensive SARS-CoV-2 infection of the CNS does not occur, autopsy findings indicate the presence of microglia nodules, astrocyte activation and $CD8^+$ T cell infiltration in the brain, providing evidence for immune responses occurring within the CNS of infected patients (3, 58, 59). Related to this, a recent study indicated microglia nodules interacting with inflammatory $CD8^+$ T cells within distinct anatomical regions of the brains of COVID-19 patients and this correlated with altered systemic inflammation (60). It is incontrovertible that transgenic hACE2 models, particularly the K18-hACE2 model, have provided a better understanding of the pathogenesis of COVID-19 yet the one notable and consistent drawback of many of these models is the ability of virus to infect, efficiently replicate, and spread within the parenchyma, which contributes to increased mortality. These findings emphasize the importance of working with animal models in which SARS-CoV-2 entry into the CNS is more consistent with what has been observed in COVID-19 patients.

MATERIALS AND METHODS

Mice and viral infection. All experiments were performed in accordance with animal protocols approved by the University of California, Irvine Institutional Animal Care and Use Committee.8–16 week-old heterozygous K18-hACE2 C57BL/6 (strain: B6.Cg-Tg[K18-ACE2]2Prlmn/J) mice were obtained from Jackson Laboratory. Animals were housed by sex in single use disposable plastic cages and provided ad-libitum water. SARS-CoV-2 isolate USA-WA1/2020 was obtained from BEI. Mice were inoculated with between 104 and 105 PFU of SARS-CoV-2 in 10 μl of DMEM or sham inoculated. Inoculations were performed under deep anesthesia through an intraperitoneal injection of a mixture of ketamine and xylazine. Infected and uninfected mice were examined and weighed daily. Animals were euthanized early if they reached predetermined euthanasia criteria.

iPSC-neuronal differentiation.iPSC line iCS83iCTR33n1 was previously derived, characterized (61) and maintained as described at 37°C, 5% CO_2. on hESC Matrigel (Fisher Scientific catnumber 08774552) with daily feeding of mTeSR1™ (Stem Cell Technologies catnumber 85850) (62). Neuronal differentiation was performed using the protocol as described (62) with a modification that the cells were frozen at the neural progenitor stage at day 8 in CryoStor CS10 (Stem Cell Technologies number 07931). Cells were thawed into LIA medium (ADF supplemented with 2 mM Glutamax, 2% B27 without vitamin A, 0.2 μM LDN 193189 and 1.5 μM IWR1 20 ng/ml Activin A [Peprotech number 120-14E]) containing 10 μM Y-27632 dihydrochloride for the first day post-thaw for further neural differentiation and subsequent daily feeds with LIA without Y-27632 dihydrochloride. Differentiated neurons were plated at 1×10^6 cells per well in 6-well plate format or at $8x10^4$cells per chamberslide well for imaging. Cells were infected with either pseudovirus or SARS-CoV-2 at d46-50 after start of differentiation.

SARS-CoV-2 infection of iPSC-derived neurons.SARS-CoV-2 isolate USA-WA1/2020 was obtained from BEI. Media was removed from cells and replaced with virus-containing media (or nonvirus media for mock-infection wells) at 500 µl per well of a 6-well plate or 200 µl per chamberslide well for 1 h adsorption at 37°C, 5% CO_2, for infection of cells at MOI = 0.1. Culture plates and chamber slides were gently rocked every 15 min to ensure even distribution of infection media. Following 1 h adsorption, nonvirus containing medium was added to all cells for final volume of 2 ml per well of a 6-well plate or 700 µl per chamberslide well and were allowed to incubate with virus for 24 or 48h and then fixed with 4% PFA for subsequent immunocytochemical staining. Cells in 6-well plates were allowed to incubate with virus for 24, 48, or 72h; supernatants were then collected, and cells harvested using 700 µl of cold TRIzol Reagent (Ambion, 15596018) for subsequent qPCR analysis.

PLX5622 treatment. Rodent chow (AIN-76A) formulated with CSF1R inhibitor-PLX5622 at a dose of 1,200 ppm was provided by Plexxikon, Inc. (Berkeley, CA). Mice were fed either PLX5622 chow or control chow 7 days prior to viral infection, and chow was continued until mice were sacrificed at defined time points postinfection.

RNA extraction. All RNA from VSV experiments with iPSC neurons, astrocytes, and microglia was extracted via the RNeasy minikit (Qiagen, 74106) using the “Purification of Total RNA from Animal Cells using Spin Technology” protocol. Homogenization was performed using QIAshredder spin columns (Qiagen, 79656). RNA from SARS-CoV-2 infected neurons was extracted via the RNeasy minikit using the “Purification of Total RNA, Including Small RNAs, from Animal Cells' ' protocol. TRIzol was substituted for QIAzol, and Buffer RW1 was substituted for Buffer RWT. Homogenization was performed using QIAshredder spin columns. All RNA from mouse tissues was extracted via the RNeasy minikit using the “Purification of

Total RNA, Including Small RNAs, from Animal Tissues" protocol. TRIzol was substituted for QIAzol, and Buffer RW1 was substituted for Buffer RWT. Homogenization was performed using the Bead Ruptor 12 (Omni International) and 1.4 mm ceramic beads (Omni International, 19-627). For brain tissue, the machine was set to 2 cycles at 2.25m/s for 15 s with a 1 s pause between cycles. For lungs, the machine was set to 2 cycles at 2.4m/s for 20 s with a 1 s pause between cycles.

cDNA synthesis. All cDNA was made by following the "First Strand cDNA Synthesis" standard protocol provided by New England Biolabs with their AMV Reverse Transcriptase (New England Biolabs, M0277L). Random hexamers (Invitrogen, N8080127) were used for the reactions. RNase inhibitors were not used in the cDNA synthesis.

Gene expression analysis via quantitative PCR. All qPCRs were performed using the Bio-Rad iQ5 and iTaq Universal SYBR Green Supermix (Bio-Rad, 1725120). The standard protocol by Bio-Rad for iTaq Universal SYBR Green Supermix was used unless otherwise stated. Reactions were 10 µl, and the machine was set to run for 1 cycle (95°C for 3 min), followed by 40 cycles (95°C for 10 s, then 55°C for 30 s). The following primer sequences were used—mouse GAPDH, forward primer: AACTTTGGCATTGTGGAAGG, reverse primer: GGATGCAGGGATGATGTTCT; human GAPDH, forward primer: CAGCCTCAAG ATCATCAGCA, reverse primer: TGTGGTCATGAGTCCTTCCA; SARS-CoV-2 Spike, forward primer: TAGTGCGTGATCTCCCTCAG, reverse primer: CCAGCTGTCCAA CCTGAAGA. For the brain cytokine and chemokine qPCR, Qiagen's custom qPCR arrays were employed, following the protocol, "Real-Time PCR for RT^2 Profiler PCR Arrays Formats A, C, D, E, F, G." The plates were pre-aliquoted with primers for the following murine genes: Glyceraldehyde-3-phosphate dehydrogenase (GAPDH), beta actin, chemokine ligand 10

(CXCL10), chemokine ligand 9 (CXCL9), chemokine ligand 2 (CCL2), chemokine ligand 5 (CCL5), interferon gamma (IFN-γ), interferon beta-1 (IFN-B1), tumor necrosis factor (TNF-α), interleukin 10 (IL-10), chemokine ligand 1 (CXCL1), interleukin 28B (IFN-L3), chemokine ligand 19 (CCL19). Reactions were 25 µl (1 µl cDNA, 11.5 µl UltraPure Distilled Water [Invitrogen, 10977-015], 12.5 µl iTaq Universal SYBR Green Supermix). The machine was set to run for 1 cycle (95°C for 10 min), followed by 40 cycles (95°C for 15 s, then 60°C for 1 min). Ct values for each sample were normalized to an internal control (GAPDH), yielding the dCt values. dCt values of infected or PLX-treated samples were compared to appropriate control samples, as indicated, to produce ddCt values. The relative fold change between samples used in the ddCt calculation was calculated (2^{-ddCt}).

qPCR statistical analysis. Statistical analysis was performed in Prism (GraphPad Software). The Brown-Forsythe and Welch's ANOVA tests were used to compare the means between groups. Dunnett's test to correct for multiple comparisons was performed when necessary.

mRNA-Seq. Total RNA was isolated using the Qiagen RNeasy kit and QIAshredders for cell lysis. One microgram of RNA with RNA integrity number values >9 was used for library preparation using the strand-specific Illumina TruSeq mRNA protocol. Libraries were sequenced on the NovaSeq 6000 platform using 100 cycles to obtain paired-end 100 reads at >30 million reads per sample. For RNA-seq analysis, fastq files were trimmed using a base quality score threshold of >20 and aligned to the hg38 genome with Hisat 2. Reads passing quality control were used for quantification using featureCounts and analyzed with the R package DESeq2 to identify DEGs. Genes passing an FDR of 10% were used for GO enrichment analysis using GOrilla (27) (http://cbl-gorilla.cs.technion.ac.il/). For the heatmaps, a list of genes from

GO:0006955 immune response and GO:0006954 inflammatory response was used. From those lists, the genes with the top 100 most variable TPM were plotted using the R package pheatmap. For the 48h versus 24h IPA, the TPM of all genes in the 1_Infected_24h sample were subtracted from the TPM of all genes in the 2_Infected_48h sample. The list of genes was sorted by the difference and the top 400 and bottom 400 selected to use as input for IPA's core analysis.

Histology and immunohistochemical staining. Mice were euthanized at defined time points postinfection and tissues harvested according to IACUC-approved guidelines. Tissues were collected and placed in either cold TRIzol for qPCR analysis or 4% PFA for fixation and subsequent histological analysis. Following fixation, the24–48h brains were either cryoprotected in 30% sucrose, embedded in O.C.T. (Fisher HealthCare), and sliced via Cryostat in 10 μm sagittal sections. Alternatively, tissues were dehydrated and paraffin-embedded and subsequently use for RNAscope or hematoxylin/eosin (H&E) in combination with luxol fast blue (LFB) to assess demyelination within the brains of experimental mice. For immunohistochemical staining of O.C.T.-embedded tissues, slides were rinsed with PBS to remove residual O.C.T., and antigen retrieval (incubation with 10 mM sodium Citrate at 95°C for 15 min) was performed if required for specific antigens at which point samples were incubated with 5% normal goat serum and 0.1% Triton-X, followed by overnight incubation at 4°C with primary antibodies. Several primary antibodies were used, including Iba1 (1:500 Wako), GFAP (1:1000 Abcam), Mac2/Galactin-3 (1:500, CL8942AP Cedarlane), CD4 (1:200 Abcam), CD8 (1:200 Abcam), MHC I (1:200 Abcam), and MHC II (1:200 Abcam). On the second day, slides were treated with appropriate secondary antibodies (1:1000 goat anti-rat/rabbit Invitrogen, 1:1000 goat anti-chicken, Abcam) following PBS rinsing. Slides were then mounted with DAPI Fluoromount-G (SouthernBiotech). High-resolution fluorescent images were obtained using a

Leica TCS SPE-II confocal microscope and LAS-X software. For whole brain stitches, automated slide scanning was performed using a Zeiss AxioScan.Z1 equipped with a Colibri camera and Zen AxioScan 2.3 software. Microglial morphology was determined using the filaments module in Bitplane Imaris 7.5, as described previously (Elmore, Lee, West, & Green, 2015). Cell quantities were determined using the spots module in Imaris.

RNAscope *in situ* hybridization of SARS-CoV-2 spike RNA.RNA *in situ* hybridization was performed via RNAscope 2.5 HD Red assay kit (Advanced Cell Diagnostics, Cat: 322350) in accordance with manufacturer's instructions. Fixed tissue sections were treated with the manufacturer's Fresh Frozen Tissue Sample Preparation Protocol, fixed in chilled 4% PFA, dehydrated, and treated with H_2O_2 and Protease IV before probe hybridization. Paraffinized sections were deparaffinized and treated with H_2O_2 and Protease Plus prior to hybridization. Probes targeting SARS-CoV-2 spike (Cat: 848561), positive-control Hs-PPIB (Cat: 313901), or negative control DapB (Cat: 310043) were hybridized followed by proprietary assay signal amplification and detection. Tissues were counterstained with Gill's hematoxylin. An uninfected mouse was used as a negative control and stained in parallel. Tissues were visualized using an Olympus BX60 microscope and imaged with a Nikon (Model number) camera.

Immunocytochemical staining for SARS-CoV-2.iPSC-derived neurons on glass-bottomed 4-well chamberslides were gently washed with 1X PBS and fixed for 1 h with 4% paraformaldehyde for removal from BSL-3 facility. Wells were subsequently washed 3 times with 1X PBS, permeabilized for 15 min at RT in 0.1% Triton-X in PBS and blocked for 2 h in a 2% BSA-5% NDS blocking solution. Cells were incubated overnight at 4°C in blocking solution with primary antibodies anti-MAP2 (EnCor Biotech. Cat:NC0388389) and anti-SARS-CoV-2 nucleocapsid (Sino Bio. Cat: 40143-R019). Cells were then washed with 1X PBS and incubated

in blocking solution for 2 h at RT with secondary antibodies, Alexa Fluor 594-conjugated goat anti-chicken and Alexa Fluor 488-conjugated goat anti-rabbit. After staining, cells were imaged for presence of SARS-CoV-2 nucleocapsid staining and quantified using the Revolve D75.

ACKNOWLEDGMENTS

This work was supported by a COVID CRAFT grant from UC Irvine Office of Research, NIH-NINDS R35 NS116835, NIH-NINDS NS041249, National Multiple Sclerosis Society grant CA-1607-25040, and support from the Ray and Tye Noorda Foundation to T.E.L. L.M.T. was supported by NIH-NINDS R35 NS116872 and K.N.G. was supported by NIH-NINDS R01NS083801. G.M.O. was supported by Immunology Research Training Grant 5T32AI060573-15, and C.S.-G. was supported by the Hereditary Disease Foundation. We acknowledge the support of the Chao Family Comprehensive Cancer Center Experimental Tissue Shared Resource supported by the National Cancer Institute of the National Institutes of Health under award number P30CA062203.

REFERENCES

1. Channappanavar R, Perlman S. 2020. Age-related susceptibility to coronavirus infections: role of impaired and dysregulated host immunity. *J Clin Invest* 130:6204–6213.
2. Song E, et al. 2021. Neuroinvasion of SARS-CoV-2 in human and mouse brain. *J Exp Med* 218.
3. Lou JJ, et al. 2021. Neuropathology of COVID-19 (neuro-COVID): clinicopathological update. *Free Neuropathol*2.
4. Virhammar J, Kumlien E, Fällmar D, Frithiof R, Jackmann S, Sköld MK, Kadir M, Frick J, Lindeberg J, Olivero-Reinius H, Ryttlefors M, Cunningham JL, Wikström J, Grabowska A, Bondeson K, Bergquist J, Zetterberg H, Rostami E. 2020. Acute necrotizing encephalopathy with SARS-CoV-2 RNA confirmed in cerebrospinal fluid. *Neurology* 95:445–449.
5. Pellegrini L, Albecka A, Mallery DL, Kellner MJ, Paul D, Carter AP, James LC, Lancaster MA. 2020. SARS-CoV-2 Infects the brain choroid plexus and disrupts the blood-CSF barrier in human brain organoids. *Cell Stem Cell*27:951–961.
6. Munoz-Fontela C, et al. 2020. Animal models for COVID-19. *Nature* 586:509–515.
7. McCray PB, Pewe L, Wohlford-Lenane C, Hickey M, Manzel L, Shi L, Netland J, Jia HP, Halabi C, Sigmund CD, Meyerholz DK, Kirby P, Look DC, Perlman S. Jr. 2007. Lethal infection of K18-hACE2 mice infected with severe acute respiratory syndrome coronavirus. *J Virol* 81:813–821.
8. Zheng J, Wong L-YR, Li K, Verma AK, Ortiz ME, Wohlford-Lenane C, Leidinger MR, Knudson CM, Meyerholz DK, McCray PB, Perlman S. 2021. COVID-19 treatments and pathogenesis including anosmia in K18-hACE2 mice. *Nature* 589:603–607.

9. Bao L, Deng W, Huang B, Gao H, Liu J, Ren L, Wei Q, Yu P, Xu Y, Qi F, Qu Y, Li F, Lv Q, Wang W, Xue J, Gong S, Liu M, Wang G, Wang S, Song Z, Zhao L, Liu P, Zhao L, Ye F, Wang H, Zhou W, Zhu N, Zhen W, Yu H, Zhang X, Guo L, Chen L, Wang C, Wang Y, Wang X, Xiao Y, Sun Q, Liu H, Zhu F, Ma C, Yan L, Yang M, Han J, Xu W, Tan W, Peng X, Jin Q, Wu G, Qin C. 2020. The pathogenicity of SARS-CoV-2 in hACE2 transgenic mice. *Nature* 583:830–833.
10. Sun S-H, Chen Q, Gu H-J, Yang G, Wang Y-X, Huang X-Y, Liu S-S, Zhang N-N, Li X-F, Xiong R, Guo Y, Deng Y-Q, Huang W-J, Liu Q, Liu Q-M, Shen Y-L, Zhou Y, Yang X, Zhao T-Y, Fan C-F, Zhou Y-S, Qin C-F, Wang Y-C. 2020. A mouse model of SARS-CoV-2 infection and pathogenesis. *Cell Host Microbe* 28:124–133.
11. Winkler ES, Bailey AL, Kafai NM, Nair S, McCune BT, Yu J, Fox JM, Chen RE, Earnest JT, Keeler SP, Ritter JH, Kang L-I, Dort S, Robichaud A, Head R, Holtzman MJ, Diamond MS. 2020. Publisher correction: SARS-CoV-2 infection of human ACE2-transgenic mice causes severe lung inflammation and impaired function. *Nat Immunol* 21:1470.
12. Jiang R-D, Liu M-Q, Chen Y, Shan C, Zhou Y-W, Shen X-R, Li Q, Zhang L, Zhu Y, Si H-R, Wang Q, Min J, Wang X, Zhang W, Li B, Zhang H-J, Baric RS, Zhou P, Yang X-L, Shi Z-L. 2020. Pathogenesis of SARS-CoV-2 in transgenic mice expressing human angiotensin-converting enzyme 2. *Cell* 182:50–58.
13. Reichard RR, Kashani KB, Boire NA, Constantopoulos E, Guo Y, Lucchinetti CF. 2020. Neuropathology of COVID-19: a spectrum of vascular and acute disseminated encephalomyelitis (ADEM)-like pathology. *Acta Neuropathol* 140:1–6.
14. Elmore MRP, Najafi AR, Koike MA, Dagher NN, Spangenberg EE, Rice RA, Kitazawa M, Matusow B, Nguyen H, West BL, Green KN. 2014. Colony-stimulating factor 1 receptor

signaling is necessary for microglia viability, unmasking a microglia progenitor cell in the adult brain. *Neuron* 82:380–397.

15. Spangenberg E, Severson PL, Hohsfield LA, Crapser J, Zhang J, Burton EA, Zhang Y, Spevak W, Lin J, Phan NY, Habets G, Rymar A, Tsang G, Walters J, Nespi M, Singh P, Broome S, Ibrahim P, Zhang C, Bollag G, West BL, Green KN. 2019. Sustained microglial depletion with CSF1R inhibitor impairs parenchymal plaque development in an Alzheimer's disease model. *Nat Commun* 10:3758.
16. Trujillo JA, Fleming EL, Perlman S. 2013. Transgenic CCL2 expression in the central nervous system results in a dysregulated immune response and enhanced lethality after coronavirus infection. *J Virol* 87:2376–2389.
17. Kim TS, Perlman S. 2005. Viral expression of CCL2 is sufficient to induce demyelination in RAG1−/− mice infected with a neurotropic coronavirus. *J Virol* 79:7113–7120.
18. Held KS, Chen BP, Kuziel WA, Rollins BJ, Lane TE. 2004. Differential roles of CCL2 and CCR2 in host defense to coronavirus infection. *Virology* 329:251–260.
19. Chen BP, Kuziel WA, Lane TE. 2001. Lack of CCR2 results in increased mortality and impaired leukocyte activation and trafficking following infection of the central nervous system with a neurotropic coronavirus. *J Immunol* 167:4585–4592.
20. Glass WG, Hickey MJ, Hardison JL, Liu MT, Manning JE, Lane TE. 2004. Antibody targeting of the CC chemokine ligand 5 results in diminished leukocyte infiltration into the central nervous system and reduced neurologic disease in a viral model of multiple sclerosis. *J Immunol* 172:4018–4025.

21. Glass WG, Liu MT, Kuziel WA, Lane TE. 2001. Reduced macrophage infiltration and demyelination in mice lacking the chemokine receptor CCR5 following infection with a neurotropic coronavirus. *Virology* 288:8–17.

22. Liu MT, Chen BP, Oertel P, Buchmeier MJ, Armstrong D, Hamilton TA, Lane TE. 2000. Cutting edge: the T cell chemoattractant IFN-inducible protein 10 is essential in host defense against viral-induced neurologic disease. *J Immunol* 165:2327–2330.

23. Stiles LN, Hardison JL, Schaumburg CS, Whitman LM, Lane TE. 2006. T cell antiviral effector function is not dependent on CXCL10 following murine coronavirus infection. *J Immunol* 177:8372–8380.

24. Stiles LN, Liu MT, Kane JAC, Lane TE. 2009. CXCL10 and trafficking of virus-specific T cells during coronavirus demyelination. *Autoimmunity* 42:484–491. In Press.

25. Hosking MP, Liu L, Ransohoff RM, Lane TE. 2009. A protective role for ELR+ chemokines during acute viral encephalomyelitis. *PLoS Pathog* 5:e1000648.

26. Lowery SA, Sariol A, Perlman S. 2021. Innate immune and inflammatory responses to SARS-CoV-2: implications for COVID-19. *Cell Host Microbe* 29:1052–1062.

27. Channappanavar R, Perlman S. 2017. Pathogenic human coronavirus infections: causes and consequences of cytokine storm and immunopathology. *Semin Immunopathol* 39:529–539.

28. Alosaimi B, Mubarak A, Hamed ME, Almutairi AZ, Alrashed AA, AlJuryyan A, Enani M, Alenzi FQ, Alturaiki W. 2021. Complement anaphylatoxins and inflammatory cytokines as prognostic markers for COVID-19 severity and in-hospital mortality. *Front Immunol* 12:668725.

29. Huang C, Wang Y, Li X, Ren L, Zhao J, Hu Y, Zhang L, Fan G, Xu J, Gu X, Cheng Z, Yu T, Xia J, Wei Y, Wu W, Xie X, Yin W, Li H, Liu M, Xiao Y, Gao H, Guo L, Xie J, Wang G,

Jiang R, Gao Z, Jin Q, Wang J, Cao B. 2020. Clinical features of patients infected with 2019 novel coronavirus in Wuhan, China. *Lancet* 395:497–506.

30. Laudanski K, Jihane H, Antalosky B, Ghani D, Phan U, Hernandez R, Okeke T, Wu J, Rader D, Susztak K. 2021. Unbiased analysis of temporal changes in immune serum markers in acute COVID-19 infection with emphasis on organ failure, anti-viral treatment, and demographic characteristics. *Front Immunol* 12:650465.
31. Lev S, Gottesman T, Sahaf Levin G, Lederfein D, Berkov E, Diker D, Zaidman A, Nutman A, Ilan Ber T, Angel A, Kellerman L, Barash E, Navon R, Boico O, Israeli Y, Rosenberg M, Gelman A, Kalfon R, Simon E, Avni N, Hainrichson M, Zarchin O, Gottlieb TM, Oved K, Eden E, Tadmor B. 2021. Observational cohort study of IP-10's potential as a biomarker to aid in inflammation regulation within a clinical decision support protocol for patients with severe COVID-19. *PLoS One* 16:e0245296.
32. Kumari P, Rothan HA, Natekar JP, Stone S, Pathak H, Strate PG, Arora K, Brinton MA, Kumar M. 2021. Neuroinvasion and encephalitis following intranasal inoculation of SARS-CoV-2 in K18-hACE2 mice. *Viruses*13:132.
33. Carossino M, et al. 2021. Fatal neuroinvasion of SARS-CoV-2 in K18-hACE2 mice is partially dependent on hACE2 expression. *bioRxiv*.
34. Schmitt E, Naveau M, Mechulam Y. 2010. Eukaryotic and archaeal translation initiation factor 2: a heterotrimeric tRNA carrier. *FEBS Lett* 584:405–412.
35. Showkat M, Beigh MA, Andrabi KI. 2014. mTOR signaling in protein translation regulation: implications in cancer genesis and therapeutic interventions. *Mol Biol Int* 2014:686984.

36. Lane TE, Asensio VC, Yu N, Paoletti AD, Campbell IL, Buchmeier MJ. 1998. Dynamic regulation of alpha- and beta-chemokine expression in the central nervous system during mouse hepatitis virus-induced demyelinating disease. *J Immunol* 160:970–978.
37. Syage AR, Ekiz HA, Skinner DD, Stone C, O'Connell RM, Lane TE. 2020. Single-cell RNA sequencing reveals the diversity of the immunological landscape following central nervous system infection by a murine coronavirus. *J Virol* 94.
38. Hagan N, Kane JL, Grover D, Woodworth L, Madore C, Saleh J, Sancho J, Liu J, Li Y, Proto J, Zelic M, Mahan A, Kothe M, Scholte AA, Fitzgerald M, Gisevius B, Haghikia A, Butovsky O, Ofengeim D. 2020. CSF1R signaling is a regulator of pathogenesis in progressive MS. *Cell Death Dis* 11:904.
39. Knight AC, Brill SA, Solis CV, Richardson MR, McCarron ME, Queen SE, Bailey CC, Mankowski JL. 2020. Differential regulation of TREM2 and CSF1R in CNS macrophages in an SIV/macaque model of HIV CNS disease. *J Neurovirol* 26:511–519.
40. Zuroff LR, Torbati T, Hart NJ, Fuchs D-T, Sheyn J, Rentsendorj A, Koronyo Y, Hayden EY, Teplow DB, Black KL, Koronyo-Hamaoui M. 2020. Effects of IL-34 on macrophage immunological profile in response to alzheimer's-related Abeta42 assemblies. *Front Immunol* 11:1449.
41. Wheeler DL, Sariol A, Meyerholz DK, Perlman S. 2018. Microglia are required for protection against lethal coronavirus encephalitis in mice. *J Clin Invest* 128:931–943.
42. Funk KE, Klein RS. 2019. CSF1R antagonism limits local restimulation of antiviral CD8(+) T cells during viral encephalitis. *J Neuroinflammation* 16:22.

43. Sanchez JMS, DePaula-Silva AB, Doty DJ, Truong A, Libbey JE, Fujinami RS. 2019. Microglial cell depletion is fatal with low level picornavirus infection of the central nervous system. *J Neurovirol* 25:415–421.

44. Seitz S, Clarke P, Tyler KL. 2018. Pharmacologic depletion of microglia increases viral load in the brain and enhances mortality in murine models of flavivirus-induced encephalitis. *J Virol* 92.

45. Waltl I, Käufer C, Gerhauser I, Chhatbar C, Ghita L, Kalinke U, Löscher W. 2018. Microglia have a protective role in viral encephalitis-induced seizure development and hippocampal damage. *Brain Behav Immun* 74:186–204.

46. Mangale V, Syage AR, Ekiz HA, Skinner DD, Cheng Y, Stone CL, Brown RM, O'Connell RM, Green KN, Lane TE. 2020. Microglia influence host defense, disease, and repair following murine coronavirus infection of the central nervous system. *Glia* 68:2345–2360.

47. Sariol A, Mackin S, Allred M-G, Ma C, Zhou Y, Zhang Q, Zou X, Abrahante JE, Meyerholz DK, Perlman S. 2020. Microglia depletion exacerbates demyelination and impairs remyelination in a neurotropic coronavirus infection. *Proc Natl Acad Sci USA* 117:24464–24474.

48. Glatzel M, Hagel C, Matschke J, Sperhake J, Deigendesch N, Tzankov A, Frank S. 2021. Neuropathology associated with SARS-CoV-2 infection. *Lancet* 397:276.

49. Leven Y, Bosel J. 2021. Neurological manifestations of COVID-19 - an approach to categories of pathology. *Neurol Res Pract* 3:39.

50. Johansson A, Mohamed MS, Moulin TC, Schiöth HB. 2021. Neurological manifestations of COVID-19: a comprehensive literature review and discussion of mechanisms. *J Neuroimmunol* 358:577658.

51. Matschke J, Lütgehetmann M, Hagel C, Sperhake JP, Schröder AS, Edler C, Mushumba H, Fitzek A, Allweiss L, Dandri M, Dottermusch M, Heinemann A, Pfefferle S, Schwabenland M, Sumner Magruder D, Bonn S, Prinz M, Gerloff C, Püschel K, Krasemann S, Aepfelbacher M, Glatzel M. 2020. Neuropathology of patients with COVID-19 in Germany: a post-mortem case series. *Lancet Neurol* 19:919–929.

52. Song E, Bartley CM, Chow RD, Ngo TT, Jiang R, Zamecnik CR, Dandekar R, Loudermilk RP, Dai Y, Liu F, Sunshine S, Liu J, Wu W, Hawes IA, Alvarenga BD, Huynh T, McAlpine L, Rahman N-T, Geng B, Chiarella J, Goldman-Israelow B, Vogels CBF, Grubaugh ND, Casanovas-Massana A, Phinney BS, Salemi M, Alexander JR, Gallego JA, Lencz T, Walsh H, Wapniarski AE, Mohanty S, Lucas C, Klein J, Mao T, Oh J, Ring A, Spudich S, Ko AI, Kleinstein SH, Pak J, DeRisi JL, Iwasaki A, Pleasure SJ, Wilson MR, Farhadian SF. 2021. Divergent and self-reactive immune responses in the CNS of COVID-19 patients with neurological symptoms. *Cell Rep Med* 2:100288.

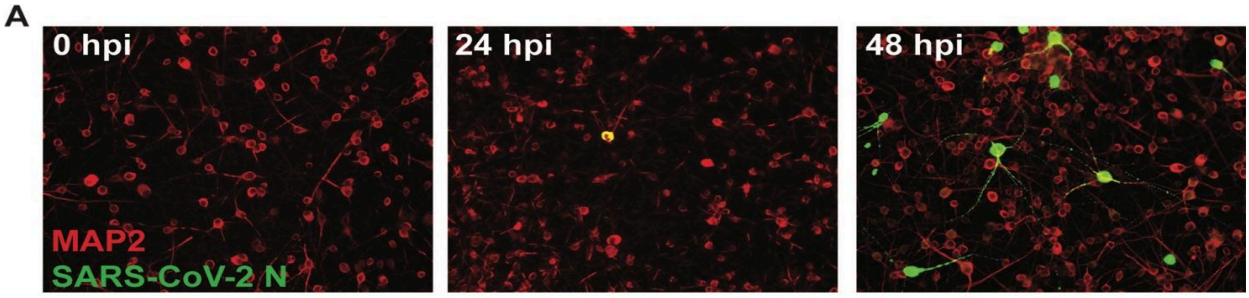
53. Yang AC, Kern F, Losada PM, Agam MR, Maat CA, Schmartz GP, Fehlmann T, Stein JA, Schaum N, Lee DP, Calcuttawala K, Vest RT, Berdnik D, Lu N, Hahn O, Gate D, McNerney MW, Channappa D, Cobos I, Ludwig N, Schulz-Schaeffer WJ, Keller A, Wyss-Coray T. 2021. Dysregulation of brain and choroid plexus cell types in severe COVID-19. *Nature* 595:565–571.

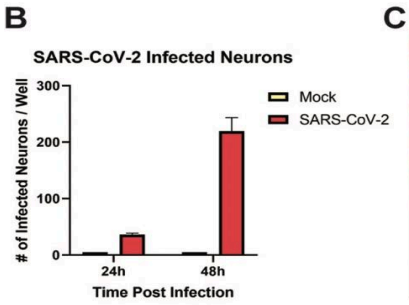
54. Karuppan MKM, Devadoss D, Nair M, Chand HS, Lakshmana MK. 2021. SARS-CoV-2 infection in the central and peripheral nervous system-associated morbidities and their potential mechanism. *Mol Neurobiol* 58:2465–2480.

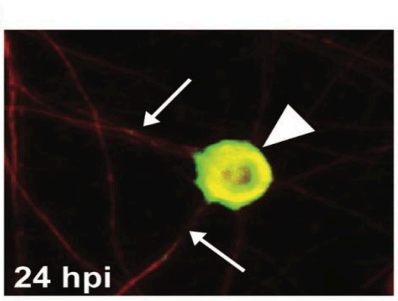
55. Akhter N, Ahmad S, Alzahrani FA, Dar SA, Wahid M, Haque S, Bhatia K, Sr Almalki S, Alharbi RA, Sindi AAA. 2020. Impact of COVID-19 on the cerebrovascular system and the prevention of RBC lysis. *Eur Rev Med Pharmacol Sci* 24:10267–10278.
56. Chia KX, Polakhare S, Bruno SD. 2020. Possible affective cognitive cerebellar syndrome in a young patient with COVID-19 CNS vasculopathy and stroke. *BMJ Case Rep* 13:e237926.
57. MacLean MA, Kamintsky L, Leck ED, Friedman A. 2020. The potential role of microvascular pathology in the neurological manifestations of coronavirus infection. *Fluids Barriers CNS* 17:55.
58. Thakur KT, Miller EH, Glendinning MD, Al-Dalahmah O, Banu MA, Boehme AK, Boubour AL, Bruce SS, Chong AM, Claassen J, Faust PL, Hargus G, Hickman RA, Jambawalikar S, Khandji AG, Kim CY, Klein RS, Lignelli-Dipple A, Lin C-C, Liu Y, Miller ML, Moonis G, Nordvig AS, Overdevest JB, Prust ML, Przedborski S, Roth WH, Soung A, Tanji K, Teich AF, Agalliu D, Uhlemann A-C, Goldman JE, Canoll P. 2021. COVID-19 neuropathology at Columbia University Irving Medical Center/New York Presbyterian Hospital. *Brain* 144:2696–2708.
59. Al-Dalahmah O, Thakur KT, Nordvig AS, Prust ML, Roth W, Lignelli A, Uhlemann A-C, Miller EH, Kunnath-Velayudhan S, Del Portillo A, Liu Y, Hargus G, Teich AF, Hickman RA, Tanji K, Goldman JE, Faust PL, Canoll P. 2020. Neuronophagia and microglial nodules in a SARS-CoV-2 patient with cerebellar hemorrhage. *Acta Neuropathol Commun* 8:147.
60. Schwabenland M, Salié H, Tanevski J, Killmer S, Lago MS, Schlaak AE, Mayer L, Matschke J, Püschel K, Fitzek A, Ondruschka B, Mei HE, Boettler T, Neumann-Haefelin C, Hofmann M, Breithaupt A, Genc N, Stadelmann C, Saez-Rodriguez J, Bronsert P, Knobeloch K-P, Blank T, Thimme R, Glatzel M, Prinz M, Bengsch B. 2021. Deep spatial profiling of human

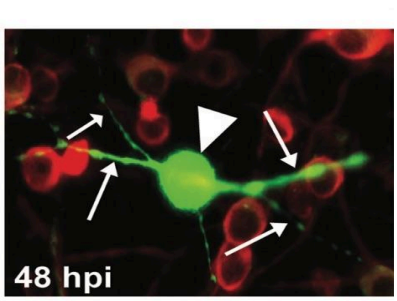
COVID-19 brains reveals neuroinflammation with distinct microanatomical microglia-T-cell interactions. *Immunity* 54:1594–1610.

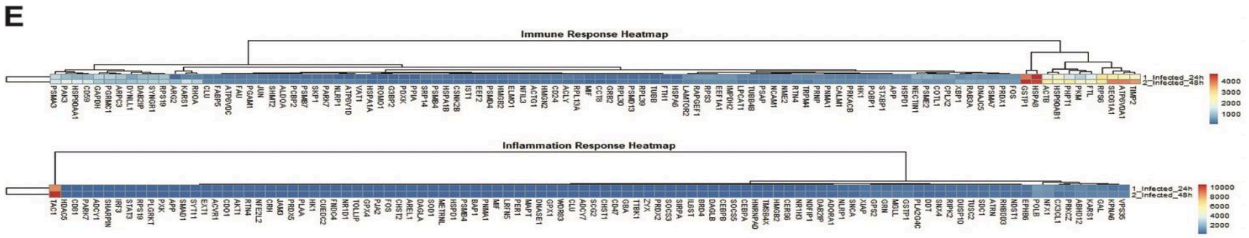
61. Consortium, H.D.i. 2012. Induced pluripotent stem cells from patients with Huntington's disease show CAG-repeat-expansion-associated phenotypes. *Cell Stem Cell* 11:264–278.
62. Smith-Geater C, Hernandez SJ, Lim RG, Adam M, Wu J, Stocksdale JT, Wassie BT, Gold MP, Wang KQ, Miramontes R, Kopan L, Orellana I, Joy S, Kemp PJ, Allen ND, Fraenkel E, Thompson LM. 2020. Aberrant development corrected in adult-onset huntington's disease iPSC-derived neuronal cultures via WNT signaling modulation. *Stem Cell Rep* 14:406–419.


A
0 hpi
24 hpi
48 hpi
MAP2
SARS-CoV-2 N


B
SARS-CoV-2 Infected Neurons
# of Infected Neurons / Well
300
200
100
0
24h
48h
Time Post Infection
Mock
SARS-CoV-2


C
24 hpi


D
48 hpi


E
Immune Response Heatmap
Inflammation Response Heatmap

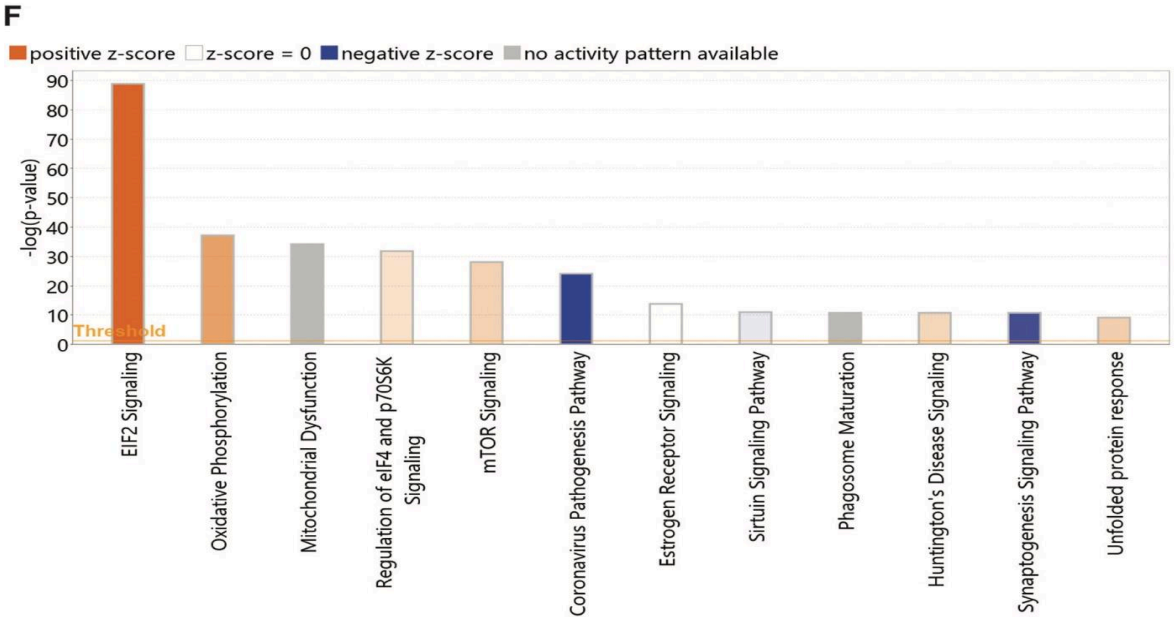

F
positive z-score
z-score = 0
negative z-score
no activity pattern available
-log(p-value)
90
80
70
60
50
40
30
20
10
0
Threshold
EIF2 Signaling
Oxidative Phosphorylation
Mitochondrial Dysfunction
Regulation of eIF4 and p70S6K Signaling
mTOR Signaling
Coronavirus Pathogenesis Pathway
Estrogen Receptor Signaling
Sirtuin Signaling Pathway
Phagosome Maturation
Huntington's Disease Signaling
Synaptogenesis Signaling Pathway
Unfolded protein response

Figure 1. SARS-CoV-2 infects human iPSC-derived neurons. (A) hiPSC-derived neurons were infected with SARS-CoV-2 at an MOI of 0.1, immunostained with anti-MAP2 and anti-SARS-CoV-2 N, and imaged at 0, 24, and 48 h postinfection. (B) Quantification of SARS-CoV-2 GFP fluorescence of mock-infected and SARS-CoV-2-infected hiPSC-derived neurons; data are derived from triplicate wells for each time point analyzed. (C) Perinuclear replication of SARS-CoV-2 in neuronal soma (arrowhead) but no viral axonal (arrows) transport at 24 h postinfection. (D) Perinuclear presence of SARS-CoV-2 in soma (arrowhead) and axon (arrows) at 24 h postinfection. (E) Heat map of genes expressed 24 and 48h postinfection. (F) Top 12 canonical pathways showing progressive changes from 24 to 48 h postinfection.

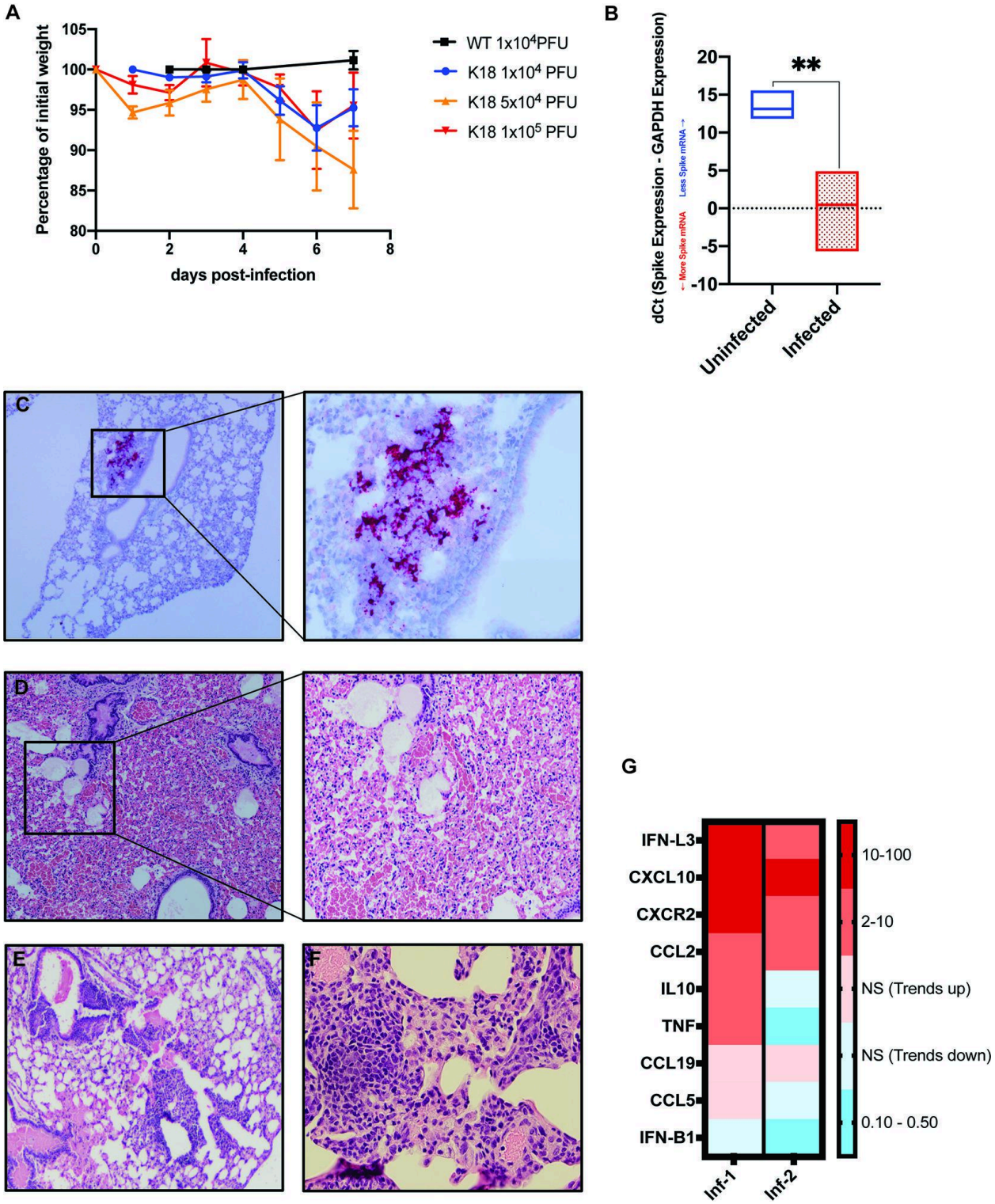

A
Percentage of initial weight
105
100
95
90
85
80
0
2
4
6
8
days post-infection
WT 1x10^4PFU
K18 1x10^4 PFU
K18 5x10^4 PFU
K18 1x10^5 PFU
B
dCt (Spike Expression - GAPDH Expression)
← More Spike mRNA
Less Spike mRNA →
20
15
10
5
0
-5
-10
**
Uninfected
Infected
C
D
E
F
G
IFN-L3
CXCL10
CXCR2
CCL2
IL10
TNF
CCL19
CCL5
IFN-B1
Inf-1
Inf-2
10-100
2-10
NS (Trends up)
NS (Trends down)
0.10 - 0.50

Figure 2. SARS-CoV-2 infection of lungs of K18-hACE2 mice. (A) Percent weight change of K18-hACE2 and WT mice infected with indicated dose of SARS-CoV-2. C57BL/6 wild-type (WT) mice ($n = 3$) were infected with 1 × 104 PFU. K18-hACE2 mice were infected intranasally with SARS-CoV-2 at either 1 × 104 PFU ($n = 17$), 5 × 104PFU ($n = 4$), or 1x105PFU ($n = 8$). (B) Quantitative PCR with primers for Spike mRNA on uninfected and SARS-CoV-2-infected mouse lung tissue. dCt values are derived from the difference between the Ct values of Spike mRNA and a housekeeping gene, GAPDH. Lower dCt values indicate increased viral mRNA. (C) K18-hACE2 mouse lung tissue at day 7 pi. with 5 × 104 PFU SARS-CoV-2 showing localized Spike mRNA expression as determined by RNAscope. Representative H&E images from lungs of SARS-CoV-2-infected mice (5 × 104 PFU) showing (D) airway edema, vascular congestion and intra-alveolar hemorrhage, (E) peri-bronchiolar lymphocytic cuffing, and (F) interstitial vascular congestion and lymphocytic infiltrates. (G) Quantitative PCR shows the fold changes of the indicated genes in two infected mouse lungs compared to uninfected mice. Data presented in *A* are representative of two independent experiments.

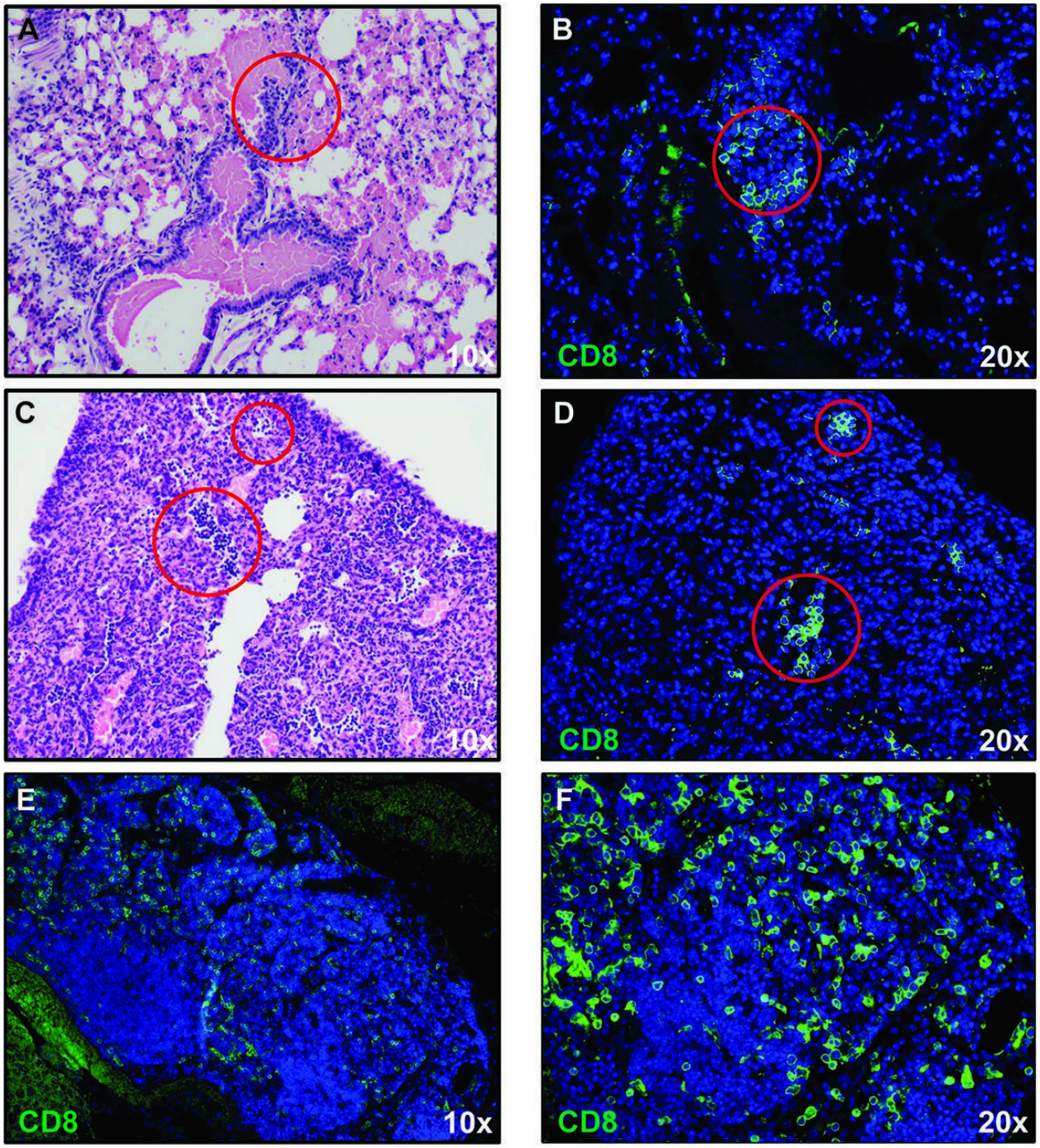


Figure 3. CD8+ T cell infiltration into lungs of SARS-CoV-2-infected mice. H&E staining of lungs of SARS-CoV-2 infected mice at day 7 post infection reveal inflammation (A and C) associated with CD8+ T cell infiltration (B and D) as determined by immunofluorescent staining. Lymph node-like structures were also detected containing CD8+ T cells (E and F). Panels *A*, *C*, and *E* ×10 magnification; panels *B*, *D*, and *F* ×20 magnification.

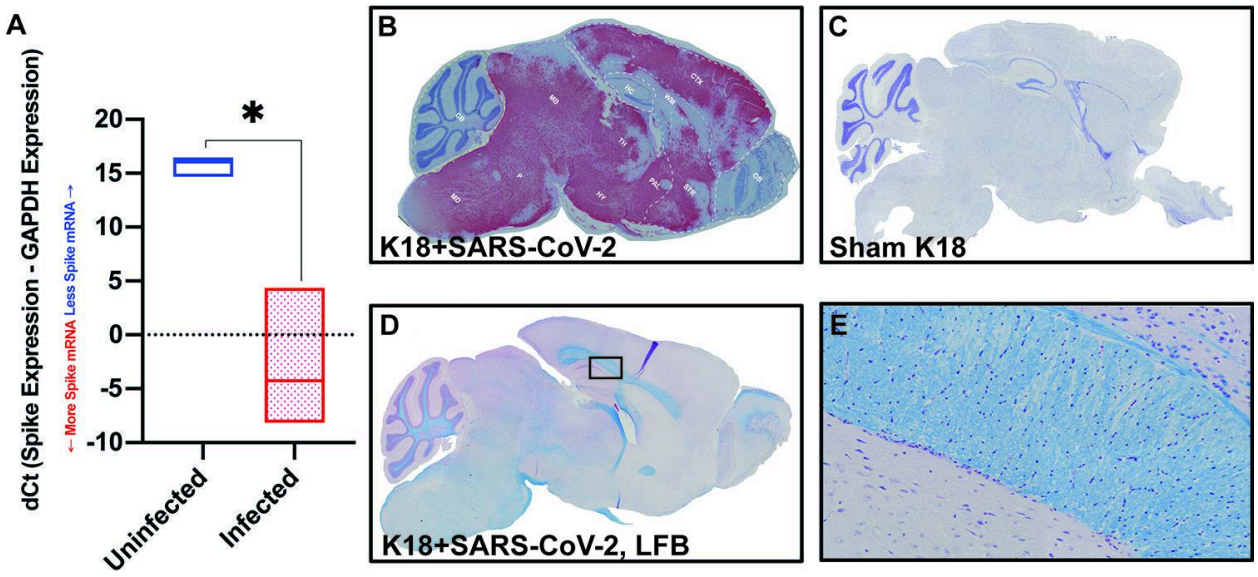


Figure 4. Widespread neuroinvasion by SARS-CoV-2 of K18 human-ACE2 mice. (A) Quantitative PCR with primers for Spike mRNA on uninfected ($n = 5$) and SARS-CoV-2-infected mouse brain tissue ($n = 4$) at day 7 pi. dCt values are derived from the difference between the Ct values of Spike mRNA and the housekeeping gene, GAPDH. *In situ* hybridization for Spike viral mRNA in (B) SARS-CoV-2-infected and (C) sham-infected K18-hACE2 mice. Anatomical regions in which viral RNA is detected (indicated in red) are indicated: cortex (CTX), striatum (STR), pallidum (PAL), thalamus (TH), hypothalamus (HY), midbrain (MB), Pons (P), and medulla (MD), whereas areas that were relatively spared included the olfactory bulb (OB), white matter (WM) tracts and hippocampus (HC) (D) Representative brain from SARS-CoV-2 infected brain from panel *B* stained with LFB demonstrates lack of demyelination with (E) high-power image of myelin tract showing no inflammation or demyelination. Data presented in *A* are representative of two independent experiments.

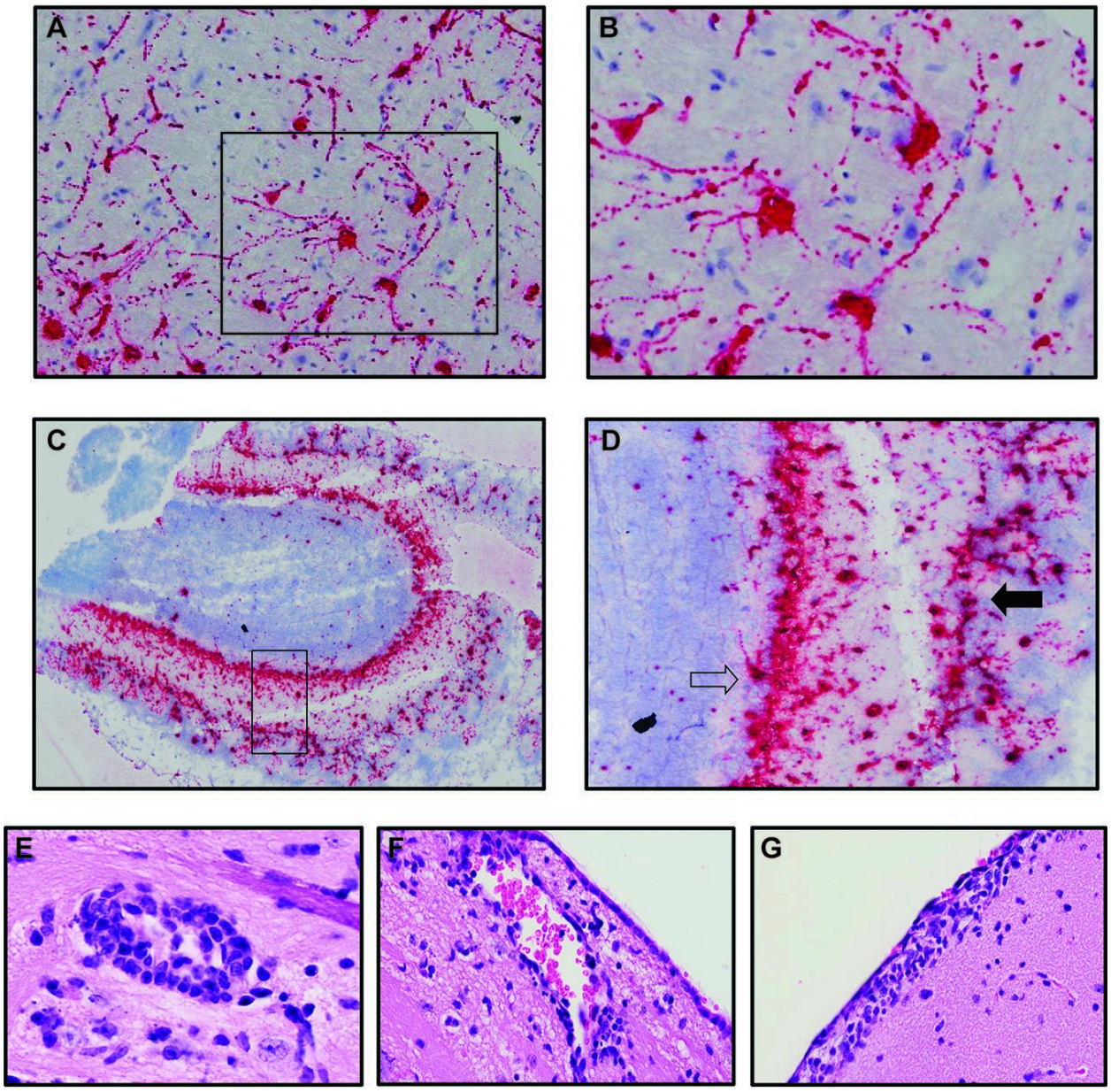


Figure 5. Neurons are targets of infection within the brains of SARS-CoV-2 infected K18-hACE2 mice. Brains of SARS-CoV-2 infected mice at day 7 pi. were analyzed to assess cellular targets of infection through *in situ hybridization* using RNAscope *in situ hybridization* using Spike-specific probes. (A) Cells within the cortex with neuron morphology were primary targets of infection; (B) high-power image of cells boxed in panel *A* show viral RNA present within the cell body as well as extending down dendrites extending from the cell body. (C) Viral RNA was also detected in olfactory bulbs at day 7 pi. (D) high-power image cells boxed in panel *C* reveal neurons in the mitral (open arrow) and glomerular (closed arrow) are infected by virus. Representative H&E images from the brains of infected K18-hACE2 mice at day 7 pi. depicting (E) perivascular cuffing, (F) subventricular inflammation, and (G) leptomeningitis.

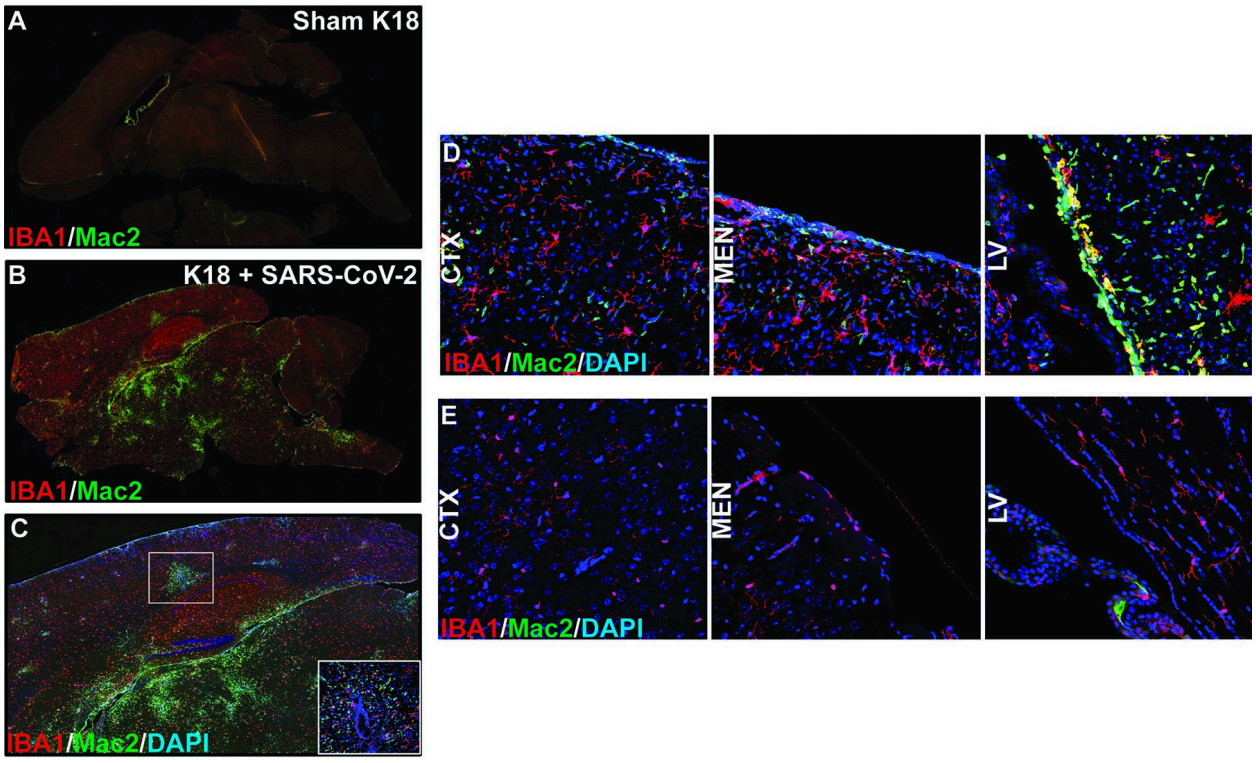


Figure 6. SARS-CoV-2 infection of K18 human-ACE2 mice results in microgliosis and myeloid cell infiltration. Brains from either SARS-CoV-2 or sham-infected mice were removed at day 7 pi. to evaluate immune cell infiltration. Microglia activation and monocyte infiltration were determined in sham-infected mice (A) and SARS-CoV2 infected mice (B) by staining for expression of Iba1 (red) and Mac2/galectin 3 (green), respectively. Infiltration of peripheral monocytes into the SARS-CoV-2 infected brain parenchyma occurs via the vasculature (C) as well as ventricular and leptomeningeal spaces (D) compared to uninfected control mice (E).

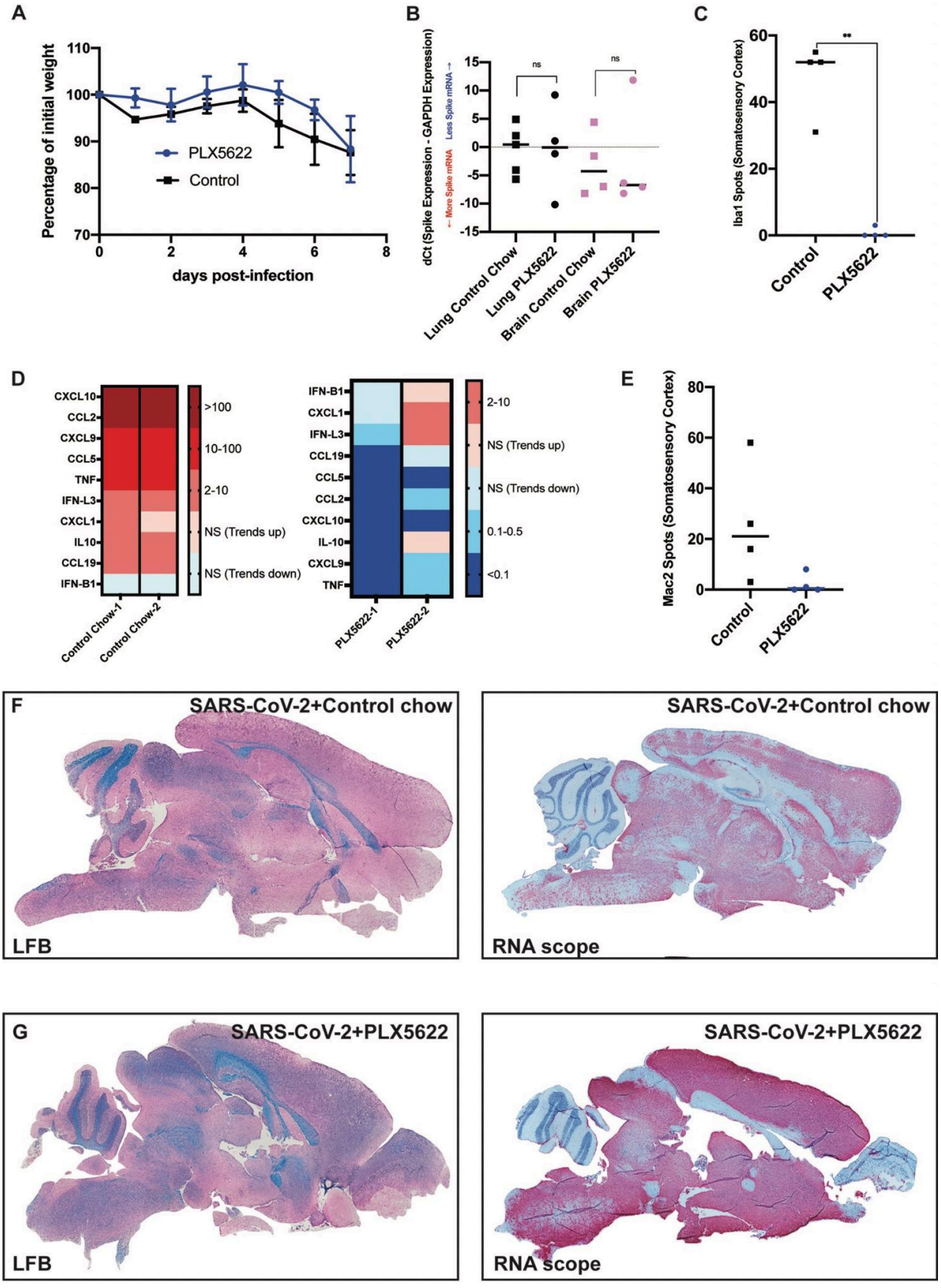

A
Percentage of initial weight
110
100
90
80
70
0
2
4
6
8
days post-infection
PLX5622
Control
B
dCt (Spike Expression - GAPDH Expression)
← More Spike mRNA Less Spike mRNA →
15
10
5
0
-5
-10
-15
ns
ns
Lung Control Chow
Lung PLX5622
Brain Control Chow
Brain PLX5622
C
Iba1 Spots (Somatosensory Cortex)
60
40
20
0
**
Control
PLX5622
D
CXCL10
CCL2
CXCL9
CCL5
TNF
IFN-L3
CXCL1
IL10
CCL19
IFN-B1
>100
10-100
2-10
NS (Trends up)
NS (Trends down)
Control Chow-1
Control Chow-2
IFN-B1
CXCL1
IFN-L3
CCL19
CCL5
CCL2
CXCL10
IL-10
CXCL9
TNF
2-10
NS (Trends up)
NS (Trends down)
0.1-0.5
<0.1
PLX5622-1
PLX5622-2
E
Mac2 Spots (Somatosensory Cortex)
80
60
40
20
0
Control
PLX5622
F
SARS-CoV-2+Control chow
LFB
SARS-CoV-2+Control chow
RNA scope
G
SARS-CoV-2+PLX5622
LFB
SARS-CoV-2+PLX5622
RNA scope

Figure 7. Microglia ablation does not impact control of viral replication in the CNS. (A) Weight loss of K18-hACE2 mice infected intranasally with 5 × 104 PFU of SARS-CoV-2 that were fed either control chow ($n = 4$) of PLX5622-formulated chow ($n = 4$). (B) Quantitative PCR in the brains and lungs of infected PLX-treated and non-PLX-treated mice shows no significant difference in the levels of Spike mRNA in either lung or brain tissue as a result of PLX5622 treatment. (C) Quantification of Iba1-positive cells in the somatosensory cortex shows a significant (**$P < 0.01$) depletion of microglia from PLX5622 treated mice compared to control mice. (D) qPCR analysis of brains of experimental mice indicated a reduction in expression of pro-inflammatory cytokines/chemokines in the brains of PLX5622-treated mice compared to control mice. (E) Quantification of Mac2-positive cells in the somatosensory cortex an overall trend in reduced numbers in PLX5622-treated mice compared to controls. Brains from SARS-CoV-2-infected mice treated with either (F) control chow or (G) PLX5622 were stained with LFB to assess demyelination or the presence of viral RNA determined by RNAscope. Representative brain sections are from experimental mice at day 7 pi. Data in *A* and *B* are representative of two independent experiments.

CHAPTER 3

MAC2 IS A LONG-LASTING MARKER OF PERIPHERAL CELL INFILTRATES INTO THE MOUSE CNS AFTER BONE MARROW TRANSPLANTATION AND CORONAVIRUS INFECTION

Glia, 2022: 1-17

MAC2 is a long-lasting marker of peripheral cell infiltrates into the mouse CNS after bone marrow transplantation and coronavirus infection

Lindsay A. Hohsfield[1] , Kate Inman Tsourmas[1] , Yasamine Ghorbanian[2 3] , Amber R. Syage[1] , Sung Jin Kim[1] , Yuting Cheng , Susana Furman[1] , Matthew A. Inlay[2 3] , Thomas E. Lane [1]* and Kim N. Green[1]*

[1]Department of Neurobiology and Behavior, University of California, Irvine, CA 92697, USA

[2]Sue and Bill Gross Stem Cell Research Center, University of California, Irvine, CA 92697, USA

[3]Department of Molecular Biology and Biochemistry, University of California, Irvine, CA 92697, USA

Correspondence

Kim N. Green, Ph.D.

3208 Biological Sciences III, University of California, Irvine, CA 92697-4545, USA. Email: kngreen@uci.edu

Thomas E. Lane, Ph.D.

Department of Neurobiology & Behavior, School of Biological Sciences, University of California, Irvine, CA 92697-4545, USA.

Email: tlane@uci.edu

Funding information

K.N.G was supported by the National Institutes of Health (NIH) under awards: R01NS083801 (NINDS), R01AG056768 (NIA), and P50AG016573 (NIA). L.A.H. was supported by the Alzheimer's Association Research Fellowship (AARF-16-442762). T.E.L. was supported by the National Institutes of Health (NIH) under awards: R01NS041249 (NINDS) and R35NS116835 (NINDS), the National Multiple Sclerosis Society (NMSS) Collaborative Research Center grant CA-1607-25040 and The Ray and Tye Noorda Foundation. Y.G. was supported by NIH T32 training grant (NS082174).

ABSTRACT

Microglia are the primary resident myeloid cells of the brain responsible for maintaining homeostasis and protecting the central nervous system (CNS) from damage and infection. Monocytes and monocyte-derived macrophages arising from the periphery have also been implicated in CNS pathologies, however, distinguishing between different myeloid cell populations in the CNS has been difficult. Here, we set out to develop a reliable histological marker that can assess distinct myeloid cell heterogeneity and functional contributions, particularly in the context of disease and/or neuroinflammation. scRNAseq from brains of mice infected with the neurotropic JHM strain of the mouse hepatitis virus (JHMV), a mouse coronavirus, revealed that *Lgals3* is highly upregulated in monocyte and macrophage populations, but not in microglia. Subsequent immunostaining for galectin-3 (encoded by *Lgals3*), also referred to as MAC2, highlighted the high expression levels of MAC2 protein in infiltrating myeloid cells in JHMV- infected and bone marrow (BM) chimeric mice, in stark contrast to microglia, which expressed little to no staining in these models. Expression of MAC2 was found even 6-10 months following BM-derived cell infiltration into the CNS. We also demonstrate that MAC2 is not a specific label for plaque-associated microglia in the 5xFAD mouse model, but only appears in a distinct subset of these cells in the presence of JHMV infection or during aging. Our data suggest that MAC2 can serve as a reliable and long-lasting histological marker for monocyte/macrophages in the brain, identifying an accessible approach to distinguishing resident microglia from infiltrating cells in the CNS under certain conditions.

Keywords

Alzheimer's disease, brain, Lgals3, MAC2, microglia, monocytes, mouse coronavirus

INTRODUCTION

Myeloid cells of the innate immune system are comprised of two distinct populations: tissue-resident and monocyte-derived macrophages. In the central nervous system (CNS), the macrophage compartment consists of parenchymal macrophages, known as microglia, and non-parenchymal macrophages, known as CNS (or border)-associated macrophages (CAMs or BAMs) (Katrin Kierdorf, Masuda, Jordão, & Prinz, 2019; Mrdjen et al., 2018). Microglia reside in the brain parenchyma spatially arranged in discrete non-overlapping territories, while BAMs reside within specialized CNS border interfaces that separate the CNS from the periphery, including the choroid plexus, meninges, and perivascular spaces. Recent studies indicate that microglia and non- parenchymal macrophages represent ontologically, phenotypically, and functionally distinct cell populations (Jordao et al., 2019; Masuda et al., 2019; Mrdjen et al., 2018; Munro et al., 2020; Anat Shemer et al., 2018; Utz et al., 2020; Van Hove et al., 2019); however, inflammation-induced phenotypic changes in these cells have made distinguishing and assessing different myeloid cell populations and their diverse functions during disease difficult.

In mice, studies have shown that microglia derive from erythromyeloid precursors in the yolk sac, entering the brain as primitive or pre-macrophages to colonize the CNS during embryonic development (Ginhoux et al., 2010; K. Kierdorf et al., 2013). Once the blood-brain barrier (BBB) is formed, myeloid cell infiltration into the CNS is restricted and microglial population maintenance relies on local self-proliferation without contributions from peripheral monocytes (A. Shemer, Erny, Jung, & Prinz, 2015). While studies have shown that specific BAM subsets (e.g. perivascular and leptomeningeal macrophages) also derive from the yolk sac (Gomez Perdiguero et al., 2015; Utz et al., 2020), it appears that choroid plexus and dural macrophage populations can also be replenished by bone marrow (BM)-derived monocytes under steady-state

conditions (Goldmann et al., 2016; Van Hove et al., 2019). Under inflammatory or disease conditions (e.g. facial nerve axotomy, amyotrophic lateral sclerosis, experimental autoimmune encephalomyelitis), studies have shown that peripheral-derived monocytes enter the brain, but do not contribute significantly to the microglial pool unless under defined experimental circumstances (e.g. irradiation, myeloablative chemotherapy, BBB disruption) (B. Ajami, Bennett, Krieger, McNagny, & Rossi, 2011; B. Ajami, Bennett, Krieger, Tetzlaff, & Rossi, 2007; Cronk et al., 2018; Ginhoux et al., 2010; Hohsfield et al., 2020; Jordao et al., 2019; Lund et al., 2018; Mildner et al., 2007; Reed-Geaghan, Croxford, Becher, & Landreth, 2020).

Despite their distinct origins and functions, assessing the individual contributions of infiltrated myeloid cells and activated microglia remains one of the major challenges in neuroimmunology, particularly within the context of neuroinflammatory diseases (Herz, Filiano, Smith, Yogev, & Kipnis, 2017; Honarpisheh et al., 2020; Prinz & Priller, 2014). Monocytes and microglia share substantial transcriptional and phenotypic overlap. Several of the genes and proteins used to separate these two populations are not exclusively expressed but instead only relatively enriched in one population (e.g. CD45, CX3CR1, CCR2) (Haage et al., 2019; Honarpisheh et al., 2020; Ransohoff & Cardona, 2010; A. Shemer et al., 2015). Microglial-specific genes and proteins have been identified; however, microglia downregulate their homeostatic signature (e.g. *P2ry12*, *Tmem119, Sall1, Siglech*) and upregulate monocyte/macrophage- associated (e.g. *Apoe*, *Itgax*, *Lyz2*) markers during disease (M. L. Bennett et al., 2016; Butovsky et al., 2014; Buttgereit et al., 2016; Keren-Shaul et al., 2017; Konishi et al., 2017). Studies have also identified genes and proteins that are highly expressed in BM-derived myeloid cells, including brain engrafted macrophages (e.g. *Ms4a7*, *Clec12a*, *Ccr2*, *Apoe*, *CD38*, *Mrc1, Cd11a*), but many of these genes are also found in other CNS myeloid

subsets or fail to label cells during immunohistochemical investigations on fixed brain sections (F. C. Bennett et al., 2018; Mrdjen et al., 2018; Anat Shemer et al., 2018; Shukla et al., 2019). As such, there is no histological marker that can reliably identify peripheral myeloid cell infiltrates vs. activated microglia in the CNS to date.

Researchers currently utilize a number of experimental approaches to identify peripheral myeloid cells in the CNS. However, many of these paradigms pose concerning caveats. The generation of GFP BM chimeras provides labeling of BM-derived cells, but this approach involves irradiation, which can induce BBB damage and non-homeostatic peripheral contributions to the microglial niche (B. Ajami et al., 2007; Mildner et al., 2007). Parabiosis avoids these irradiation- induced effects but can involve complicated surgery and result in host-graft rejection. Despite the usefulness of mice genetically labeled for monocyte markers (e.g. *Ccr2*^{RFP} mice), studies have shown that these cells may downregulate CCR2 as they mature/differentiate and enter the brain (Gschwandtner, Derler, & Midwood, 2019; Saederup et al., 2010). Furthermore, these mice are haploinsufficient for CCR2, a critical factor for monocyte migration and entry into the CNS (Chu et al., 2014). Fate mapping techniques have allowed for unprecedented exploration and manipulation of monocytes, but again these techniques are not without their limitations (H.-R. Chen et al., 2020; Liu et al., 2019). The use of lineage tracing from BM-expressed drivers involves the use of tamoxifen, which has recently been identified as a neutral agonist in macrophage lineage tracing studies. A recent study has shown that tamoxifen treatment of pregnant mice induces a significant expansion of the embryonic macrophage population (Rojo, Sauter, Lefevre, Hume, & Pridans, 2018).

Given the lack of reliable markers that can distinguish between monocyte-derived cells and activated microglia, we set out to develop a new histological tool for peripheral myeloid cell

studies in the mouse CNS. To accomplish this, we employed infection of C57BL/6 mice with the neuroadapted JHM strain of mouse hepatitis virus (JHMV), a mouse coronavirus and a robust mouse model for monocyte infiltration in the CNS. Studies indicate that JHMV-infected mice exhibit substantial infiltration by monocytes along with other peripheral immune cells (Held, Chen, Kuziel, Rollins, & Lane, 2004; Savarin, Stohlman, Atkinson, Ransohoff, & Bergmann, 2010). We recently employed single-cell RNA sequencing (scRNAseq) on flow-sorted CD45+ cells infiltrating into the CNS of JHMV-infected mice to better understand the immunological landscape at defined times following infection with a neurotropic virus (Syage et al., 2020). Using this approach, we identified *Lgals3* as a highly enriched gene for monocytes. We then validated the expression of this marker at the protein level via galectin-3/MAC2 staining in BM-derived myeloid cells, and its utility in distinguishing between monocyte and microglia populations in response to JHMV infection as well as in young transgenic mouse models of Alzheimer's disease (AD). This approach not only provides a reliable marker for peripheral-derived cells, but also eliminates the necessity of complex transgenic mouse lines to discern myeloid cell populations, broadening the study of myeloid cell spatial and phenotypic profiles during disease and neuroinflammation.

MATERIALS AND METHODS

Compounds. Pexidartinib (PLX3397) was provided by Plexxikon Inc. and formulated in AIN-76A standard chow at a dose of 600 ppm by Research Diets Inc.

Mice. All mice were obtained from The Jackson Laboratory. For transplant studies, bone marrow cells were isolated from CAG-EGFP mice (Stock No. 006567). Male and female 5xFAD mice were obtained from MMRRC-JAX (Stock No. 34848) and have been previously described in detail (Oakley et al., 2006). For 5xFAD genotyping, the primer sequences used were PS1 Forward 5′ - AAT AGA GAA CGG CAG GAG CA – 3′ and PS1 Reverse 5′ - GCC ATG AGG GCA CTA ATC AT – 3′. All other mice were male C57BL/6 (000664) mice. Animals were housed with open access to food and water under 12h/12h light-dark cycles.

Animal Treatments. All rodent experiments were performed in accordance with animal protocols approved by the Institutional Animal Care and Use Committee at the University of California, Irvine (UCI). *JHMV infection*: Six-week-old C57BL/6 mice (males and females) and four-month- old 5xFAD mice (males and females) were infected intracranially (i.c.) with 200-250 PFU of JHMV in 30 μl of sterile Hanks balanced sterile solution (HBSS); control mice received an i.c. injection of HBSS. JHMV-infected C57BL/6 mice were sacrificed at 7, 14, and 21 days post- infection (d.p.i.) and brains and spinal cords isolated to assess viral titers and perform immunohistochemical staining to assess monocyte infiltration. JHMV-infected 5xFAD mice were sacrificed at 10 d.p.i. and brains removed to determine viral titers, evaluate β-amyloid (Aβ) burden and perform immunohistochemical staining to assess monocyte infiltration. scRNAseq was conducted on male animals. *Microglial depletion:* Mice were administered ad libitum with PLX3397 at a dosage of 600 ppm (to eliminate microglia) or vehicle (control) for

14d. *Bone marrow transplant:* Tissue from a previous study by Hohsfield et. al were employed for analyses performed in the present report (Hohsfield et al., 2020). In brief, C57BL/6 mice were anesthetized with isoflurane and then irradiated with 1000 cGy (whole body) and reconstituted via retroorbital injection with 2 x 10_6 whole BM cells from CAG-EGFP mice. Blood was measured at 4, 8, and/or 12 weeks post transplantation to track granulocyte chimerism. At time of sacrifice, mice were euthanized, and BM was harvested and analyzed by flow cytometry for HSC chimerism. This established an average percent chimerism of >95% in whole body irradiated mice as previously reported (Hohsfield et al., 2020). *Tissue collection:* Following treatments, adult mice were sacrificed via carbon dioxide inhalation and perfused transcardially with 1X PBS. Brains were extracted and dissected down the midline, with one half flash-frozen for subsequent RNA and protein analyses, and the other half drop-fixed in 4% paraformaldehyde. Fixed brains were cryopreserved in PBS + 0.05% sodium azide + 30% sucrose, frozen, and sectioned at 40 m on a Leica SM2000 R sliding microtome for subsequent immunohistochemical analyses. For brains and spinal cords from JHMV-infected mice, half brains dissected down the midline and the length of spinal cord extending from thoracic vertebrate 6-10 was cryoprotected in 30% sucrose, cut into 1- mm transverse blocks and processed to preserve the craniocaudal orientation and subsequently embedded in O.C.T. (VWR, Radnor, PA, USA). For spinal cords, eight micron (mm)-thick coronal sections were cut and sections were stained following standard immunofluorescence protocols; for brains, eight micron sagittal sections were cut(Blanc et al., 2015; Dickey, Worne, Glover, Lane, & O'Connell, 2016; Marro, Grist, & Lane, 2016).

Histology and confocal microscopy. Fluorescent immunolabeling followed a standard indirect technique as described previously (Elmore et al., 2014). Brain sections were stained with

antibodies against the following defined antigens: ionized calcium binding adaptor molecule 1 (IBA1; 1:1000; 019-19741, Wako and ab5076, Abcam) and MAC2/Galectin-3 (1:500; CL8942AP Cedarlane). For DAPI staining, mounted brain sections were cover-slipped using Fluoromount-G with DAPI (00-4959-52, Invitrogen). Amylo-Glo (TR-300-AG; Biosensis) staining was performed according to the manufacturer's instructions. High resolution fluorescent images were obtained using a Leica TCS SPE-II confocal microscope and LAS-X software. For confocal imaging, one field of view (FOV) per brain region was captured per mouse unless otherwise indicated. For whole brain stitches, automated slide scanning was performed using a Zeiss AxioScan.Z1 equipped with a Colibri camera and Zen AxioScan 2.3 software. Microglial morphology was determined using the filaments module in Bitplane Imaris 7.5, as described previously (Elmore, Lee, West, & Green, 2015). Cell quantities were determined using the spots module in Imaris. MAC1+ IBA1+ staining was quantified by using a standardized algorithm in the Surfaces module in Imaris. Total IBA1+ and MAC2+IBA1+ surface area in the field of view was categorized as plaque-associated or non-plaque-associated based on proximity to plaques (plaque-associated = < 5.8 μm). Percentage of MAC2+ IBA1+ coverage was calculated by dividing MAC2+IBA1+ / total IBA1+ surface area.

Data analysis and statistics. Statistical analysis was performed with Prism Graph Pad (v.8.0.1). To compare two groups, the unpaired Student’s t-test was used. To compare multiple groups, a one-way ANOVA with Tukey’s posthoc test was performed. For all analyses, statistical significance was accepted at $p < 0.05$. All bar graphs are represented as means +/- SEM and significance expressed as follows: *$p < 0.05$, **$p< 0.01$, ***$p < 0.001$. n is given as the number of mice within each group, unless otherwise indicated.

RESULTS

*Lgals3/*MAC2 distinguishes infiltrating cells from microglia in the adult CNS.

We and others have previously identified distinct transcriptional and phenotypic profiles of brain-engrafted peripherally derived myeloid cells from resident microglia in the adult mouse brain; however, these findings have yet to translate into reliable histological markers that distinguish peripheral infiltrates from their microglial counterparts in the CNS (F. C. Bennett et al., 2018; Cronk et al., 2018; Hohsfield et al., 2020; Anat Shemer et al., 2018). In this study, we explored a previously described scRNAseq data set to identify transcripts that distinguish between resident microglia and infiltrating myeloid cells (Syage et al., 2020). scRNAseq data was obtained from the JHMV mouse model which recapitulates many characteristics of human diseases associated with encephalomyelitis and demyelination (Bergmann, Lane, & Stohlman, 2006; Lampert, Sims, & Kniazeff, 1973; Lane & Buchmeier, 1997; Savarin et al., 2010; Weiner, 1973). In brief, intracranial inoculation of susceptible C57BL/6 mice with the neuroadapted JHMV, a member of the Coronaviridae family, results in an acute encephalomyelitis characterized by wide- spread viral replication in astrocytes, microglia, and oligodendroglia with relative sparing of neurons (Bergmann et al., 2006; Lane & Hosking, 2010). In response to JHMV infection, proinflammatory cytokines and chemokines are expressed by activated microglia and astrocytes, resulting in an orchestrated inflammatory response consisting of neutrophils, monocytes/macrophages, and activated virus-specific CD4+ and CD8+ T cells (Bergmann et al., 2006; Hosking & Lane, 2010; Lane & Hosking, 2010).

We recently performed a detailed analysis of immune cell infiltration into the CNS of JHMV-infected mice through scRNAseq, which highlighted the heterogeneity of the immune response following infection with a neurotropic virus, in addition to confirming that monocytes

and neutrophils are the prominent cells entering the CNS (Syage et al., 2020). Here, we employed the scRNAseq data set to identify differentially expressed genes between monocyte/macrophage cells compared to microglia. *Lgals3* transcripts were enriched in infiltrating monocytes and macrophages, and lowly expressed in microglia (specifically in MG3 and Cyc. MG clusters) even under JHMV/inflammatory conditions (**Figure 1a-d**). *Lgals3* encodes galectin-3 (also known as MAC2), which is a member of the lectin family involved in monocyte/macrophage chemoattraction and activation (MacKinnon et al., 2008). Since low levels of *Lgals3* transcripts were detected in some microglia clusters, we next evaluated whether galectin-3/MAC2 expression was present in both monocyte/macrophage and distinct microglial populations. To assess this, we subsequently infected a separate cohort of C57BL/6 mice with JHMV and evaluated the ability of galectin-3/MAC2 to distinguish distinct myeloid cell populations. Histological analyses for MAC2 in non-infected brain sections revealed no MAC2 staining in IBA1+ cells, except in areas associated with ventricles and choroid plexus (**Figure 1e-f**). Analysis of JHMV-infected brain and spinal cord sections showed a clear population of IBA1+/MAC2+ cells that were not present in uninfected animals. IBA1+/MAC2+ cells appear spatially and morphologically distinct from IBA1+/MAC2- cells, which resemble microglia and reside in parenchymal areas (**Figure 1e, f, i**). In the brain, IBA1+/MAC2+ cells accumulated in the brainstem (medulla, pons, midbrain, thalamus, and hypothalamus), cerebellum (near the fourth ventricle), and in white matter tracts (corpus callosum), whereas little to no deposition was observed in the cerebrum at any timepoint (hippocampus, cortex, striatum) with the exception of sites near the lateral ventricle and/or white matter tracts (**Figure 1e, f, h**). Many areas of high MAC2+ cell accumulation appear to be in or near white matter areas (**Figure 1f**). IBA1+/MAC2+ cells appear less ramified with retracted/thickened processes and enlarged cell

somas compared to IBA1+/MAC2- cells (**Figure 1f).** IBA1+/MAC2+ cell infiltration in the brain appears to peak around 14 d.p.i **(Figure 1e, g, h)**; however, the brainstem still shows prominent accumulation at 21 d.p.i. In the spinal cord, IBA1+/MAC2+ cell infiltration peaked at 14 d.p.i. and declined by 21 d.p.i. with cells enriched in white matter tracts within ventral funiculus **(Figure 1i, j).**

MAC2 is a specific and long-lasting marker for bone marrow-derived infiltrating cells.

Beyond acute CNS infiltration, current monocyte markers make it difficult to distinguish between peripheral and resident myeloid cells. CCR2 and CD14 are downregulated following monocyte differentiation into macrophages (Fantuzzi et al., 1999; Steinbach & Thiele, 1994; Wong et al., 1997) and studies using $CCR2^{RFP}$ knock-in mice report that $CCR2^{RFP+}$ cells are not detected in the CNS, even under inflammatory conditions (Saederup et al., 2010), meaning that these markers fail to label monocyte-derived cells past a few days following engraftment in the CNS. Given these difficulties, we next sought to examine whether MAC2 could serve as 1) a marker for BM-derived cells and 2) a long-lasting marker for these cells once engrafted in the brain.

To accomplish this, we utilized BM GFP chimeric mice to assess the ability of this monocyte/macrophage marker candidate to label infiltrating BM-derived cells. CAG-GFP donor BM was administered (via retro-orbital injection) to whole body (WB, with >95% chimerism) irradiated mice and allowed to recover for ~10 months, resulting in long-term GFP chimeric mice. In this model, GFP+ expression indicates that cells derive from the BM. Following recovery, we explored co-localization of MAC2 expression in GFP+ cells in the adult mouse brains of long- term GFP BM chimeric mice and long-term GFP BM chimeric mice that

underwent colony- stimulating factor 1 receptor inhibitor (CSF1Ri)-induced myeloid cell depletion and repopulation (~6 months following CSF1Ri treatment and CNS engraftment) (Figure 2a). In a previous study, we demonstrated that irradiation/BM transplant followed by CSF1Ri treatment results in substantial replacement of the microglial compartment with BM-derived monocytes (Hohsfield et al., 2020), providing a model to evaluate long-term and brain-wide BM-derived monocyte/macrophage engraftment.

Ten-month WB irradiated mice exhibited ~20% infiltration of GFP+ cells, with prominent deposition observed in areas near the lateral ventricle/subventricular zone (SVZ), medial habenula (MHb), internal capsule (IC), and meninges (**Figure 2a, b**). In accordance with our prior data, we observed that these infiltrating GFP+ cells express little to no levels of P2RY12 and TMEM119, two canonical microglial markers (data not shown). Ten-month WB irradiated mice treated with CSF1Ri exhibited 79-96% (mean = 86%) engraftment of GFP+ cells, seen throughout the brain parenchyma (**Figure 2a, d, h-j**). In aged-matched controls, no GFP+ cell deposition is visible (**Figure 2b, h-j**). Notably, we found that MAC2+ staining was still apparent in GFP+/IBA1+ cells, even 6 and 10 months after CNS infiltration was stimulated, while no MAC2 expression was seen in control animals or in GFP-/IBA1+ cells (**Figure 2b-g, h-j**). In 10 mo WB irradiated mice, an average of 89-96% of GFP+ cells express MAC2 near the lateral ventricle/SVZ, MHb, and IC (**Figure 2k-m**). In 10 mo WB irradiated + CSF1Ri treated mice, an average of 85-93% of GFP+ cells express of MAC2 near the lateral ventricle/SVZ, MHb, and IC (**Figure 2k-m**). It should be noted that there are lower and higher levels of MAC2+ staining in GFP+ cells in mice, which likely reflects the more recent infiltration of BM-derived cells into the parenchyma, indicating that MAC2 expression may gradually decrease over time as cells become more CNS parenchymal macrophage- or microglia-like to fill the tissue niche.

Some MAC2 expression is seen in the nuclei of resident microglia, but clearly fills the cell body and processes of GFP+/IBA+ cells. Given the high level of co-expression of MAC2 in GFP BM-derived myeloid cells, these results indicate that MAC2 can serve as a histological marker of BM-derived infiltrating cells and utilized as a potential long-lasting marker to distinguish between peripherally derived monocytes/macrophages and resident microglia.

MAC2 is not a ubiquitous marker for plaque-associated microglia during the early stages of disease in 5xFAD mice.

While we identified MAC2 as a marker for peripheral infiltrates, Lgals3 has also been reported in specific myeloid cell populations under certain conditions. For example, *Lgals3* was identified as an upregulated gene in amyloid-β (Aβ) plaque-associated microglia, also known as disease-associated microglia (DAM) or microglial neurodegenerative (MGnD) phenotype (Butovsky & Weiner, 2018; Krasemann et al., 2017), and in isolated amyloid plaque-containing microglia (Grubman et al., 2021). Moreover, galectin-3/MAC2 staining has been found in microglia in close contact with Aβ plaques in both human and mice (Boza-Serrano et al., 2019). However, it is often difficult to distinguish between monocytes/macrophages and activated microglia, as they share many morphological and gene expression similarities (M. L. Bennett et al., 2016; Butovsky et al., 2014; Buttgereit et al., 2016; Keren-Shaul et al., 2017; Konishi et al., 2017). To directly test *Lgals3*/Galectin-3 expression in the AD brain, we stained for MAC2 in 5xFAD mice, and then used JHMV infection to trigger peripheral infiltration, evaluating whether MAC2 expression is specific to plaque-associated microglia.

5xFAD mice, which express five human APP and PSEN1 transgenes with familial Alzheimer's disease mutations, display extensive extracellular plaque deposition and

microgliosis (Oakley et al., 2006). In these mice, amyloid plaques begin to form around 3 months of age and exhibit significant plaque deposition and microglial activation in the cerebral cortex and brain stem, including the thalamus, midbrain, and hindbrain, by 4 months of age (**Figure 3a**). Here, we i.c. infected 4-month-old 5xFAD mice with JHMV to stimulate monocyte infiltration into the CNS. Brain sections of uninfected and JHMV-infected mice were stained for amyloid plaques (Amylo- Glo), myeloid cells (IBA1), and MAC2. Evaluation of whole brain sagittal sections showed profound MAC2 staining in JHMV-infected 5xFAD **(Figure 3b**), but not uninfected mice (**Figure 3a**). Similar to WT JHMV-infected mice, MAC2+ cell deposition is apparent in areas near ventricles (in the cerebellum near the fourth ventricle, in tissue near the lateral ventricle) and white matter tracts (the corpus callosum, middle longitudinal fasciculus), whereas little to no MAC2 staining is present in 5xFAD controls (**Figure 3a-e**). MAC2+ cells are seen in the choroid plexus of 5xFAD controls, but they do not infiltrate into the parenchyma (**Figure 3c,e**). High resolution images show little to no MAC2+ staining in plaque-associated microglia (1.6% of MAC2 staining in plaque-associated IBA1+ cells) in uninfected 5xFAD mice (**Figure 3f-g**), and an average of 16.4% of MAC2 staining in IBA1+ cells surrounding amyloid plaques in JHMV-infected 5xFAD mice (**Figure 3h-i**). It also appears that not all plaque-associated microglia are MAC2+ nor is there an abundance of MAC2+IBA1+ in plaque-associated regions. MAC2+ staining is also present in non-plaque-associated regions in IBA1+ cells (8.7% MAC2+IBA1+ staining) in JHMV-infected mice (**Figure 3d,h-i**). These findings provide evidence that MAC2 is not a specific marker for plaque-associated microglia and is not expressed by microglia in the young non-infected 5xFAD mouse model, indicating that *Lgals3*/MAC2 expression may reflect peripheral infiltrates honing to plaques.

The effects of aging on MAC2 staining in WT and 5xFAD mice.

Transcriptional profile analysis has revealed an upregulation of *Lgals3* in microglia isolated from mouse models of neurodegenerative disease, including Alzheimer's disease and amyotrophic lateral sclerosis as well as aging, and identified *Lgals3* as a hub gene for primed microglia (Holtman et al., 2015). Safaiyan et al. recently identified white matter-associated microglia (WAM), which accumulate in white matter tracts during aging. *Lgals3* was one of 39 transcripts of the WAM signature that was identified when comparing aged white matter compared to young matter or aged gray matter myeloid cells; and the authors report expression of galectin-3 in IBA1+ cells in old but not young white matter (Safaiyan et al., 2021).

To address whether MAC2 staining also increases with aging under steady-state and diseased conditions, we next stained brain sections from 4, 8, 12, and 18 mo WT and 5xFAD mice with MAC2, IBA1, and Amylo-Glo. Again, we observe that MAC2+IBA1+ cells and staining is most apparent in the choroid plexus of WT and 5xFAD mice, regardless of age (**Figure 4 a-b**). In line with previous studies, our data shows an age-dependent increase in MAC2+IBA1+ cell accumulation in 5xFAD mice in the hippocampus, cortex, and in white matter areas (e.g. fimbria, corpus callosum) within close proximity to the lateral ventricle (**Figure 4b, c, e**). In gray matter regions, the majority of MAC2+ cells are IBA1+ plaque-associated microglia (**Figure 4b, c**). However, there appears to be a lag in the appearance of MAC2 expression and microglial/DAM activation around plaques. For example, prominent MAC2 expression in plaque-associated IBA1+ cells appear at 18 mo of age in the cortex despite the accumulation of these plaque-associated microglia at 4 mo of age (**Figure 4c**). Furthermore, the majority of IBA1+ plaque-associated cells do not express MAC2 (<20% of IBA1+ cells are MAC2+; **Figure 4e**), meaning MAC2 does not account for a significant proportion of

plaque-associated cells. MAC2+IBA1+ cell deposition does not occur in gray matter areas in the aged WT mice (**Figure 4a, d, f**); however, interestingly we do observe MAC2+IBA1+ cells present in white matter areas at 18 mo of age (**Figure 4d**). This is also true for 5xFAD mice (**Figure 4c**). Thus, it appears that MAC2 expression is not a specific response to plaques. Given the proximity of these brain regions to the lateral ventricles and the lack of MAC2 expression in the majority of plaque-associated microglia, we postulate two scenarios: 1) a specific subpopulation of activated microglia (subset of DAM and/or WAM) switch on *Lgals3* and galectin-3/MAC2 expression over time or 2) that MAC2+ cells derive from a different cell source, such as from the periphery. Since microglia and macrophages undergo rapid morphological and transcriptional transformations upon activation, reflective of the highly plastic nature of myeloid cells, defining MAC2 expression as an indicator of cell activation or peripheral infiltration remains difficult. However, given the findings in this study, specifically the spatial and temporal expression of MAC2+IBA1+ cells in areas that are closely associated with peripheral immune cell infiltration in CNS disorders, most prominently in white matter areas in multiple sclerosis, we hypothesize that MAC2 expression labels a subset of peripheral immune cells in the young adult brain that can infiltrate and engraft the brain.

DISCUSSION

Microglia and BM-derived monocytes are implicated in a number of neurological disorders (Herz et al., 2017). In AD, several genome-wide association studies have identified variants associated with myeloid cells that increase disease risk, highlighting the importance of myeloid cells and the growing need to decipher their phenotype and function during disease (Bradshaw et al., 2013; Guerreiro et al., 2013; Jonsson et al., 2013; Lambert et al., 2013). However, myeloid cells are highly dynamic cells which can be influenced at both the transcriptional and protein level by specific diseases during disease induction and progression, thus complicating the use of reliable and stable cell-specific markers and posing challenges to the functional exploration and contributions of these distinct cells. For instance, the presence of peripheral-derived myeloid cells around amyloid plaques and their contribution in AD pathology has been a long-standing question in the field with contrasting results (El Khoury et al., 2007; Hawkes & McLaurin, 2009; Jay et al., 2015; Reed-Geaghan et al., 2020; Simard, Soulet, Gowing, Julien, & Rivest, 2006).

Under steady state conditions, microglia and monocyte/macrophages populations express several overlapping surface markers, including Cd11b, F4/80, CD115 (CSF1R), and IBA1 (Gautier et al., 2012; Prinz, Priller, Sisodia, & Ransohoff, 2011). Recent gene expression studies have identified surface markers and transcription factors unique to resident microglia (e.g., P2RY12, TMEM119, SIGLEC-H, *Sall1*), but several of these markers lose their distinct homeostatic expression levels during disease/cell activation (M. L. Bennett et al., 2016; Butovsky et al., 2014; Buttgereit et al., 2016; Chen & Colonna, 2021; Keren-Shaul et al., 2017; Konishi et al., 2017). Despite the utility of previous approaches (e.g., BM chimeras, parabiosis, and mouse models of fluorescent protein expression or tamoxifen-inducible Cre-recombinase

under monocyte/microglia promoters) in providing myeloid cell-specific labeling/targeting and unprecedented opportunities to study microglia and monocytes (B. Ajami et al., 2007; Jung et al., 2000; Mildner et al., 2007; Wang et al., 2016), the field has lacked a commercially available histological marker for monocyte-derived populations in the CNS.

In this study, our main goal was to identify a marker that can discern between murine microglial and monocyte-derived cell populations during inflammation and disease in the CNS. Given the plasticity of myeloid cells, we recognize that the identification of cell lineage based on a single marker is not ideal (M. L. Bennett et al., 2016; Butovsky et al., 2014); however, previous studies have identified unique single genes and markers for microglia, such as P2ry12 and Tmem119, that have aided investigations and added to the repertoire of tools utilized by CNS myeloid cell researchers (M. L. Bennett et al., 2016; Butovsky et al., 2014). These markers have been indispensable to identifying endogenous and homeostatic microglia in the CNS. Here, we show that *Lgals3* is highly expressed in monocyte/macrophages in the healthy and JHMV-infected brain, and that galectin-3/MAC2 can be used as a histological marker to distinguish peripherally derived myeloid cells from microglia under both steady state and neuroinflammatory conditions. Galectin-3/MAC2 is a β-galactoside-binding lectin that is highly expressed in and secreted by monocytes/macrophages; it is associated with many macrophage functions, including cell adhesion, migration, proliferation, and apoptosis (MacKinnon et al., 2008). However, galectin-3 expression has also been reported in other cell populations, including fibroblasts, osteoblasts, endothelial cells, neuronal cells, and immune cells (neutrophils, eosinophils, basophils, mast cells) (Thomas & Pasquini, 2018). Here, we show that *Lgals3* is not highly expressed in other Cd11b+ cell populations via scRNAseq, including T cells, B cells, NK cells, neutrophils, and microglia, but is highly expressed in several monocyte and macrophage

cell clusters. Although we do not observe significant MAC2+ staining in non-IBA1+ cells in the CNS, careful consideration here is also warranted and IBA1 (or other myeloid cell markers) should be employed in combination with MAC2 to distinguish these myeloid populations.

In line with our study, recent work by Ochocka et al. using scRNAseq and flow cytometry of CD11b+ myeloid cells in naïve and glioma-bearing mice showed that *Lgals3* and galectin-3 are highly expressed by infiltrating monocyte/macrophages at RNA and protein levels, respectively (Ochocka et al., 2021). These authors propose the use of TMEM119 and galectin-3 for efficient and distinguishable separation of microglia and monocyte/macrophages in glioma models and highlighted their ability to achieve distinct spatial distribution of these cells within tumor tissue (Ochocka et al., 2021). Moreover, recent studies in mouse models of diabetes and spinal cord injury have identified unique populations of infiltrating and phagocytic macrophages, distinct from resident microglia, that express *Lgals3*/galectin-3/MAC2. In diabetes, galactin-3 expressing macrophages infiltrate and aggregate near injury sites, implicating these cells in the response to cerebrovascular insults (Mehina et al., 2021). In spinal cord injury, injury-activated macrophages maintain a transcriptionally distinct identify to activated microglia, expressing higher levels of *Lgals3*, *Apoe*, and *Cxcr4*, among other genes (Wahane et al., 2021). In the present study, we also observed distinct spatial distribution of MAC2+ cells in the JHMV-infected brain; cells were sequestered in the brain stem, white matter areas, and regions surrounding the ventricles. Further study is needed to evaluate the distinct contributions of MAC2+ myeloid cells and MAC2- myeloid cells in pathogenesis, but given the role of BM-derived myeloid cells in demyelination (Yamasaki et al., 2014), it is not surprising to find their selective recruitment in these areas. In GFP BM chimeras, MAC2+ cells were observed in the choroid plexus and perivascular spaces in whole body-irradiated mice, respectively,

consistent with their partial cell turnover from BM sources (Goldmann et al., 2016; Van Hove et al., 2019). Identifying MAC2 as a distinct histological marker for monocytes provides investigators with the ability to explore the spatial distribution and dynamics of these peripheral cells without the side effects of irradiation or other experimental caveats (e.g., tamoxifen).

In mice, monocytes express CD11b and CD45, and are divided into two main subpopulations: classical/inflammatory monocytes ($Ly6C^{hi}CCR2+CX3CR1^{lo}$) and non-classical/patrolling monocytes ($Ly6C^{lo}CCR2^{lo}\ CX3CR1^{hi}$) (Geissmann, Jung, & Littman, 2003; Geissmann et al., 2010). Of interest, studies have shown that *Lgals3* is enriched in a population of Ly6C+ monocytes located in the BM and blood (Mildner et al., 2017). Although transcriptional profile analyses of microglia and monocytes have generated several proposed monocyte-specific markers based off of an identified monocyte signature, including *Apoe*, *Ccr2*, *Ms4a7*, and *Clec12a* (F. C. Bennett et al., 2018; Cronk et al., 2018; Hohsfield et al., 2020; Lund et al., 2018; Anat Shemer et al., 2018) these markers have presented a number of limitations: upregulation during disease, downregulation upon macrophage differentiation, or lack of success in staining fixed adult brain tissue. For example, though Cd11a (*Itgal*) is expressed on all peripheral circulating immune cells and not microglia, it could only be detected on infiltrating cells in fixed brain sections using a tedious tyramide amplification strategy, limiting its practical use (Shuka et al., 2019). In addition, Bennett et al. identified MS4A7 as a unique marker for HSC-derived cells, but MS4A7 staining was only shown in blood, fetal brain, and primary human microglia, and RNA *in situ* hybridization was required to show staining in postmortem AD brain samples (F. C. Bennett et al., 2018). CD44 was a marker identified for distinguishing CNS infiltrating from CNS resident cells by Korin et al., however, later found by Mrdjen et al. to be upregulated in microglia during disease or aging (Korin et al., 2017; Mrdjen et al., 2018).

Given that monocytes and macrophages exist as heterogenous populations with varying expression profiles (reflecting functional diversity, differential origins, differentiation status, tissue of residence) and dynamic adaption of their transcription regulatory networks to changing environments (Gosselin et al., 2014; Lavin et al., 2014), it has been challenging for researchers to develop a marker for monocyte-derived cells that remains intact following differentiation and tissue engraftment. Here, we show that MAC2 staining is retained in BM-derived cells 6-10 months following CNS recruitment in the brain, indicating that MAC2 may be a marker that is conserved across several monocyte and macrophages subpopulations, or at least the subsets recruited to the CNS/sites of inflammation.

Transcriptional profile analysis of isolated microglia from mouse models of AD, amyotrophic lateral sclerosis, and aging identified *Lgals3* as a central hub gene in primed microglia, along with *Apoe*, *Axl*, *Clec7a*, and *Itgax* (Holtman et al., 2015). Further comprehensive scRNAseq analysis of microglia in neurodegenerative diseases discovered a unique microglial subset, termed disease-associated microglia (DAM) or microglial neurodegenerative phenotype (MGnD) microglia. These cells exhibit a downregulation in homeostatic microglia genes (e.g., *P2ry12*, *Tmem119*) and upregulation in genes involved in phagocytic, lysosomal, and lipid metabolism pathways (e.g., *Apoe*, *Axl*, *Clec7a*, *Cst7*, *Itgax*, *Lilrb4*) (Keren-Shaul et al., 2017), including *Lgals3* (Butovsky & Weiner, 2018; Krasemann et al., 2017), which is upregulated during later stages of neurodegeneration (Chen & Colonna, 2021). However, a recent study has shown that enzymatic dissociation methods can induce aberrant gene expression signatures in microglia (Marsh et al., 2020), indicating that some scRNAseq findings may be confounded and an artifact of isolation methods, analysis, or sequencing platform. A recent investigation utilizing scRNAseq, snRNAseq and scATACseq

identified distinct microglia subpopulations in 3xTgAD and 5xFAD mice, including a DAM cluster containing *Cst7*, but lacking *Lgals3*; instead, *Lgals3* was found in a small cluster containing *Cd14* and *Itgal* (Balderrama-Gutierrez et al., 2021). Galectin-3 was also shown to be significantly elevated in human AD patients, exhibit preferential expression in microglia in contact with plaques, and serve as a ligand for TREM2 (Boza-Serrano et al., 2019). In contrast, Sobue et al. showed that gene expression levels of *LGALS3*, *AIF1*, and *CD68*, were unchanged in human AD precuneus samples (Sobue et al., 2021). In line with this, using bulk- tissue RNAseq analysis, our lab has shown that while *Lgals3* is upregulated in 5xFAD mice in the hippocampus and thalamus compared to wild types, expression levels do not change following sustained microglial depletion, unlike several homeostatic (e.g., *Csf1r*, *Cx4cr1*, *Hexb*, *Siglech*) and DAM genes (e.g., *Clec7a*, *Cst7*, *Itgax*) which are significantly downregulated by microglial depletion (Spangenberg et al., 2019). These data provide evidence that elevated *Lgals3* in 5xFAD brains may not be specific to microglia. Consistent with spatial transcriptomics and *in situ*sequencing data in $APP_{NL\text{-}G\text{-}F}$ mice, *Lgals3* was not identified in plaque-induced genes (PIGs), consisting of 57 genes that overlap with several DAM genes (W. T. Chen et al., 2020). The current study shows that MAC2 staining is not present in plaque-associated microglia in the young 5xFAD mice, and only appears in plaque-associated IBA1+ cells during JHMV infection or in aged animals (albeit at modest numbers). A recent study - showing clonal hematopoiesis of indeterminate potential (CHIP) is associated with protection against AD – detected mutated marrow-derived cells in the brains of patients which appear indistinguishable from microglia (Bouzid et al., 2021), highlighting the potential role for peripheral infiltrates in replacing defective microglia during aging or disease. Thus, the presence of MAC2+ cells in disease and experimental models should be considered a potential sign of peripheral infiltrates, and

subsequently followed up with BM chimeric models, parabiosis, or BM lineage tracing transgenics. It is possible that microglia may upregulate *Lgals3* under certain conditions, including infection or inflammatory stimulus, or that upregulated mRNA does not effectively translate to protein expression. Likewise, we cannot discount the possibility that microglia in other conditions (stroke, injury, and chronic neurodegenerative disease) may also upregulate *Lgals3*, or that these MAC2+ cells may derive from BM sources. Other explanations for the disparity between *Lgals3* transcript levels and MAC2 staining in plaque-associated microglia could be a result of: 1) microglia and infiltrating peripheral myeloid cells expressing different isoforms of *Lgals3*/galectin-3, in which one isoform is detectable by the MAC2 antibody while the other is not, or 2) different secretion and/or cellular retention rates of *Lgals3*/galectin-3 within these two myeloid cell populations. Moreover, *Lgals3* may also be expressed by discrete microglial populations in the brain–for example, in specialized axon tract- associated microglia (ATM) or P7/early postnatal microglia (termed proliferative region- associated microglia (PAM), which appear as amoeboid cells that transiently reside in axon tracts of the corpus callosum and cerebellum (Hammond et al., 2019; Li et al., 2019), as well as in white matter-associated microglia (WAM), found specifically in white matter areas that increase with aging (Safaiyan et al., 2021). Furthermore, surviving microglia following CSF1Ri-induced depletion have been described as MAC2+ (Zhan, Sohn, Zhou, Li, & Gan, 2019). Given these findings and the data from this current study, we would implore researchers to consider *Lgals3*/MAC2 expression as a potential indicator of peripheral origins, but encourage further validation with other important tools, such as fate-mapping techniques. For example, lineage tracing from *Ms4a3* or *Cxcr4* could be utilized, as it has recently been shown as a specific gene expressed by BM-derived granulocyte-monocyte progenitors (GMPs) or HSC-derived monocytes, respectively, to

efficiently trace monocyte-derived cells (Liu et al., 2019; Werner et al., 2020). Other markers include Cd49d, also expressed by T cells and DCs, and Cd49e, which were identified in peripheral monocyte populations, but not in CNS resident myeloid cell populations utilizing CyTOF (Bahareh Ajami et al., 2018).

In sum, we identify galectin-3/MAC2 as a potential monocyte marker that can be utilized in inflamed CNS tissue. Unlike other markers, BM-derived myeloid cells retain MAC2 expression even as they leave perivascular areas and occupy the parenchymal niche for prolonged periods of time. The ability to discern peripherally derived cells from resident microglia is critical to exploring their distinct roles in health and disease. Growing attention has been placed on understanding CNS myeloid cells and the environmental cues that sculpt their transcriptional and phenotypic profiles, particularly during disease. Detailed knowledge of these distinct myeloid cell populations and our ability to distinguish microglia and monocytes will prove essential in targeting these cells for improved therapeutic strategies.

Acknowledgments

We thank Edna Hingco for her excellent technical assistance. WT and 5xFAD time course tissue was provided by U54 AG054349 (NIA Model Organism Development and Evaluation for Late onset Alzheimer's Disease (MODEL-AD)). K.N.G was supported by the National Institutes of Health (NIH) under awards: R01NS083801 (NINDS), RF1AG056768 (NIA), and RF1AG065329 (NIA). L.A.H. was supported by the Alzheimer's Association Research Fellowship (AARF-16-442762). T.E.L. was supported by the National Institutes of Health (NIH) under awards: R01NS041249 (NINDS) and R35NS116835 (NINDS), the National Multiple

Sclerosis Society (NMSS) Collaborative Research Center grant CA-1607-25040 and The Ray and Tye Noorda Foundation. Y.G. was supported by NIH T32 training grant (NS082174).

Conflict of interest

The authors declare that they have no conflicts of interest.

Author contributions

L.A.H. developed experimental protocols, designed, performed, and analyzed experiments and wrote the manuscript. K.I.T. and Y.G. performed and analyzed experiments. A.R.S. performed experiments and bioinformatic analysis. S.J.K., Y.C., and S.F. performed experiments. M.A.I. contributed to project design. T.E.L. and K.N.G. directed the project, designed the experiments, interpreted the results and wrote the manuscript.

Data availability statement

The data that support the findings of this study are available from TEL and KNG upon reasonable request.

ORCID

Matthew A. Inlay http://orcid.org/0000-0002-0451-2076

Thomas E. Lane http://orcid.org/0000-0003-0392-0825

Kim N. Green http://orcid.org/0000-0002-6049-6744

REFERENCES

1. Ajami, B., Bennett, J. L., Krieger, C., McNagny, K. M., & Rossi, F. M. (2011). Infiltrating monocytes trigger EAE progression, but do not contribute to the resident microglia pool. *Nat Neurosci, 14*(9), 1142-1149. doi:10.1038/nn.2887
2. Ajami, B., Bennett, J. L., Krieger, C., Tetzlaff, W., & Rossi, F. M. (2007). Local self-renewal can sustain CNS microglia maintenance and function throughout adult life. *Nat Neurosci, 10*(12), 1538-1543. doi:10.1038/nn2014
3. Ajami, B., Samusik, N., Wieghofer, P., Ho, P. P., Crotti, A., Bjornson, Z., . . . Steinman, L. (2018). Single-cell mass cytometry reveals distinct populations of brain myeloid cells in mouse neuroinflammation and neurodegeneration models. *Nat Neurosci, 21*(4), 541-551. doi:10.1038/s41593-018-0100-x
4. Balderrama-Gutierrez, G., Liang, H., Rezaie, N., Carvalho, K., Forner, S., Matheos, D., . . . Mortazavi, A. (2021). Single-cell and nucleus RNA-seq in a mouse model of AD reveal activation of distinct glial subpopulations in the presence of plaques and tangles. *bioRxiv*, 2021.2009.2029.462436. doi:10.1101/2021.09.29.462436
5. Bennett, F. C., Bennett, M. L., Yaqoob, F., Mulinyawe, S. B., Grant, G. A., Hayden Gephart, M., . . . Barres, B. A. (2018). A Combination of Ontogeny and CNS Environment Establishes Microglial Identity. *Neuron, 98*(6), 1170-1183.e1178. doi:10.1016/j.neuron.2018.05.014
6. Bennett, M. L., Bennett, F. C., Liddelow, S. A., Ajami, B., Zamanian, J. L., Fernhoff, N. B., . . . Barres, B. A. (2016). New tools for studying microglia in the mouse and human CNS. *Proc Natl Acad Sci U S A, 113*(12), E1738-1746. doi:10.1073/pnas.1525528113

7. Bergmann, C. C., Lane, T. E., & Stohlman, S. A. (2006). Coronavirus infection of the central nervous system: host-virus stand-off. *Nat Rev Microbiol, 4*(2), 121-132. doi:10.1038/nrmicro1343
8. Blanc, C. A., Grist, J. J., Rosen, H., Sears-Kraxberger, I., Steward, O., & Lane, T. E. (2015). Sphingosine-1-phosphate receptor antagonism enhances proliferation and migration of engrafted neural progenitor cells in a model of viral-induced demyelination. *Am J Pathol, 185*(10), 2819-2832. doi:10.1016/j.ajpath.2015.06.009
9. Bouzid, H., Belk, J. A., Jan, M., Qi, Y., Sarnowski, C., Wirth, S., . . . Jaiswal, S. (2021). Clonal hematopoiesis is associated with protection from Alzheimer's disease. *medRxiv*, 2021.2012.2010.21267552. doi:10.1101/2021.12.10.21267552
10. Boza-Serrano, A., Ruiz, R., Sanchez-Varo, R., García-Revilla, J., Yang, Y., Jimenez-Ferrer, I., Deierborg, T. (2019). Galectin-3, a novel endogenous TREM2 ligand, detrimentally regulates inflammatory response in Alzheimer's disease. *Acta neuropathologica, 138*(2), 251- 273. doi:10.1007/s00401-019-02013-z
11. Bradshaw, E. M., Chibnik, L. B., Keenan, B. T., Ottoboni, L., Raj, T., Tang, A., . . . De Jager, P. L. (2013). CD33 Alzheimer's disease locus: altered monocyte function and amyloid biology. *Nat Neurosci, 16*(7), 848-850. doi:10.1038/nn.3435
12. Butovsky, O., Jedrychowski, M. P., Moore, C. S., Cialic, R., Lanser, A. J., Gabriely, G., . . . Weiner, H. L. (2014). Identification of a unique TGF-beta-dependent molecular and functional signature in microglia. *Nat Neurosci, 17*(1), 131-143. doi:10.1038/nn.3599
13. Butovsky, O., & Weiner, H. L. (2018). Microglial signatures and their role in health and disease. *Nat Rev Neurosci, 19*(10), 622-635. doi:10.1038/s41583-018-0057-5

14. Buttgereit, A., Lelios, I., Yu, X., Vrohlings, M., Krakoski, N. R., Gautier, E. L., . . . Greter, M. (2016). Sall1 is a transcriptional regulator defining microglia identity and function. *Nat Immunol, 17*(12), 1397-1406. doi:10.1038/ni.3585

15. Chen, H.-R., Sun, Y.-Y., Chen, C.-W., Kuo, Y.-M., Kuan, I. S., Tiger Li, Z.-R., . . . Kuan, C.-Y. (2020). Fate mapping via CCR2-CreER mice reveals monocyte-to-microglia transition in development and neonatal stroke. *Science Advances, 6*(35), eabb2119. doi:10.1126/sciadv.abb2119

16. Chen, W. T., Lu, A., Craessaerts, K., Pavie, B., Sala Frigerio, C., Corthout, N., . . . De Strooper, B. (2020). Spatial Transcriptomics and In Situ Sequencing to Study Alzheimer's Disease. *Cell, 182*(4), 976-991.e919. doi:10.1016/j.cell.2020.06.038

17. Chen, Y., & Colonna, M. (2021). Microglia in Alzheimer's disease at single-cell level. Are there common patterns in humans and mice? *Journal of Experimental Medicine, 218*(9). doi:10.1084/jem.20202717

18. Chu, H. X., Arumugam, T. V., Gelderblom, M., Magnus, T., Drummond, G. R., & Sobey, C. G. (2014). Role of CCR2 in inflammatory conditions of the central nervous system. *J Cereb Blood Flow Metab, 34*(9), 1425-1429. doi:10.1038/jcbfm.2014.120

19. Cronk, J. C., Filiano, A. J., Louveau, A., Marin, I., Marsh, R., Ji, E., . . . Kipnis, J. (2018). Peripherally derived macrophages can engraft the brain independent of irradiation and maintain an identity distinct from microglia. *J Exp Med, 215*(6), 1627-1647. doi:10.1084/jem.20180247

20. Dickey, L. L., Worne, C. L., Glover, J. L., Lane, T. E., & O'Connell, R. M. (2016). MicroRNA- 155 enhances T cell trafficking and antiviral effector function in a model of

coronavirus- induced neurologic disease. *J Neuroinflammation, 13*(1), 240. doi:10.1186/s12974-016-0699- z

21. El Khoury, J., Toft, M., Hickman, S. E., Means, T. K., Terada, K., Geula, C., & Luster, A. D. (2007). Ccr2 deficiency impairs microglial accumulation and accelerates progression of Alzheimer-like disease. *Nat Med, 13*(4), 432-438. doi:10.1038/nm1555
22. Elmore, M. R., Lee, R. J., West, B. L., & Green, K. N. (2015). Characterizing newly repopulated microglia in the adult mouse: impacts on animal behavior, cell morphology, and neuroinflammation. *PLoS One, 10*(4), e0122912. doi:10.1371/journal.pone.0122912
23. Elmore, M. R., Najafi, A. R., Koike, M. A., Dagher, N. N., Spangenberg, E. E., Rice, R. A., . . . Green, K. N. (2014). Colony-stimulating factor 1 receptor signaling is necessary for microglia viability, unmasking a microglia progenitor cell in the adult brain. *Neuron, 82*(2), 380-397. doi:10.1016/j.neuron.2014.02.040
24. Fantuzzi, L., Borghi, P., Ciolli, V., Pavlakis, G., Belardelli, F., & Gessani, S. (1999). Loss of CCR2 expression and functional response to monocyte chemotactic protein (MCP-1) during the differentiation of human monocytes: role of secreted MCP-1 in the regulation of the chemotactic response. *Blood, 94*(3), 875-883.
25. Gautier, E. L., Shay, T., Miller, J., Greter, M., Jakubzick, C., Ivanov, S., . . . Randolph, G. J. (2012). Gene-expression profiles and transcriptional regulatory pathways that underlie the identity and diversity of mouse tissue macrophages. *Nat Immunol, 13*(11), 1118-1128. doi:10.1038/ni.2419
26. Geissmann, F., Jung, S., & Littman, D. R. (2003). Blood monocytes consist of two principal subsets with distinct migratory properties. *Immunity, 19*(1), 71-82. doi:10.1016/s1074-7613(03)00174-2

27. Geissmann, F., Manz, M. G., Jung, S., Sieweke, M. H., Merad, M., & Ley, K. (2010). Development of monocytes, macrophages, and dendritic cells. *Science, 327*(5966), 656-661. doi:10.1126/science.1178331

28. Ginhoux, F., Greter, M., Leboeuf, M., Nandi, S., See, P., Gokhan, S., . . . Merad, M. (2010). Fate mapping analysis reveals that adult microglia derive from primitive macrophages. *Science, 330*(6005), 841-845. doi:10.1126/science.1194637

29. Goldmann, T., Wieghofer, P., Jordao, M. J., Prutek, F., Hagemeyer, N., Frenzel, K., . . . Prinz, M. (2016). Origin, fate and dynamics of macrophages at central nervous system interfaces. *Nat Immunol, 17*(7), 797-805. doi:10.1038/ni.3423

30. Gomez Perdiguero, E., Klapproth, K., Schulz, C., Busch, K., Azzoni, E., Crozet, L., . . . Rodewald, H.-R. (2015). Tissue-resident macrophages originate from yolk-sac-derived erythro-myeloid progenitors. *Nature, 518*(7540), 547-551. doi:10.1038/nature13989

31. Gosselin, D., Link, V. M., Romanoski, C. E., Fonseca, G. J., Eichenfield, D. Z., Spann, N. J., . . . Glass, C. K. (2014). Environment drives selection and function of enhancers controlling tissue-specific macrophage identities. *Cell, 159*(6), 1327-1340. doi:10.1016/j.cell.2014.11.023

32. Grubman, A., Choo, X. Y., Chew, G., Ouyang, J. F., Sun, G., Croft, N. P., . . . Polo, J. M. (2021). Transcriptional signature in microglia associated with Aβ plaque phagocytosis. *Nat Commun, 12*(1), 3015. doi:10.1038/s41467-021-23111-1

33. Gschwandtner, M., Derler, R., & Midwood, K. S. (2019). More Than Just Attractive: How CCL2 Influences Myeloid Cell Behavior Beyond Chemotaxis. *Front Immunol, 10*(2759). doi:10.3389/fimmu.2019.02759

34. Guerreiro, R., Wojtas, A., Bras, J., Carrasquillo, M., Rogaeva, E., Majounie, E., . . . Hardy, J. (2013). TREM2 variants in Alzheimer's disease. *N Engl J Med, 368*(2), 117-127. doi:10.1056/NEJMoa1211851

35. Haage, V., Semtner, M., Vidal, R. O., Hernandez, D. P., Pong, W. W., Chen, Z., . . . Gutmann, D. H. (2019). Comprehensive gene expression meta-analysis identifies signature genes that distinguish microglia from peripheral monocytes/macrophages in health and glioma. *Acta Neuropathol Commun, 7*(1), 20. doi:10.1186/s40478-019-0665-y

36. Hammond, T. R., Dufort, C., Dissing-Olesen, L., Giera, S., Young, A., Wysoker, A., . . . Stevens, B. (2019). Single-Cell RNA Sequencing of Microglia throughout the Mouse Lifespan and in the Injured Brain Reveals Complex Cell-State Changes. *Immunity, 50*(1), 253-271.e256. doi:10.1016/j.immuni.2018.11.004

37. Hawkes, C. A., & McLaurin, J. (2009). Selective targeting of perivascular macrophages for clearance of beta-amyloid in cerebral amyloid angiopathy. *Proc Natl Acad Sci U S A, 106*(4), 1261-1266. doi:10.1073/pnas.0805453106

38. Held, K. S., Chen, B. P., Kuziel, W. A., Rollins, B. J., & Lane, T. E. (2004). Differential roles of CCL2 and CCR2 in host defense to coronavirus infection. *Virology, 329*(2), 251-260. doi:10.1016/j.virol.2004.09.006

39. Herz, J., Filiano, A. J., Smith, A., Yogev, N., & Kipnis, J. (2017). Myeloid Cells in the Central Nervous System. *Immunity, 46*(6), 943-956. doi:10.1016/j.immuni.2017.06.007

40. Hohsfield, L. A., Najafi, A. R., Ghorbanian, Y., Soni, N., Hingco, E. E., Kim, S. J., . . . Green, K. N. (2020). Effects of long-term and brain-wide colonization of peripheral bone marrow-derived myeloid cells in the CNS. *J Neuroinflammation, 17*(1), 279. doi:10.1186/s12974-020-01931-0

41. Holtman, I. R., Raj, D. D., Miller, J. A., Schaafsma, W., Yin, Z., Brouwer, N., . . . Eggen, B. J. (2015). Induction of a common microglia gene expression signature by aging and neurodegenerative conditions: a co-expression meta-analysis. *Acta Neuropathol Commun, 3*, 31. doi:10.1186/s40478-015-0203-5

42. Honarpisheh, P., Lee, J., Banerjee, A., Blasco-Conesa, M. P., Honarpisheh, P., d'Aigle, J., . . . McCullough, L. D. (2020). Potential caveats of putative microglia-specific markers for assessment of age-related cerebrovascular neuroinflammation. *J Neuroinflammation, 17*(1), 366. doi:10.1186/s12974-020-02019-5

43. Hosking, M. P., & Lane, T. E. (2010). The role of chemokines during viral infection of the CNS. *PLoS Pathog, 6*(7), e1000937. doi:10.1371/journal.ppat.1000937

44. Jay, T. R., Miller, C. M., Cheng, P. J., Graham, L. C., Bemiller, S., Broihier, M. L., . . . Lamb, B. T. (2015). TREM2 deficiency eliminates TREM2+ inflammatory macrophages and ameliorates pathology in Alzheimer's disease mouse models. *J Exp Med, 212*(3), 287-295. doi:10.1084/jem.20142322

45. Jonsson, T., Stefansson, H., Steinberg, S., Jonsdottir, I., Jonsson, P. V., Snaedal, J., . . . Stefansson, K. (2013). Variant of TREM2 associated with the risk of Alzheimer's disease. *N Engl J Med, 368*(2), 107-116. doi:10.1056/NEJMoa1211103

46. Jordao, M. J. C., Sankowski, R., Brendecke, S. M., Sagar, Locatelli, G., Tai, Y. H., . . . Prinz, M. (2019). Single-cell profiling identifies myeloid cell subsets with distinct fates during neuroinflammation. *Science, 363*(6425). doi:10.1126/science.aat7554

47. Jung, S., Aliberti, J., Graemmel, P., Sunshine, M. J., Kreutzberg, G. W., Sher, A., & Littman, D. R. (2000). Analysis of fractalkine receptor CX(3)CR1 function by targeted deletion and

green fluorescent protein reporter gene insertion. *Mol Cell Biol, 20*(11), 4106-4114. doi:10.1128/mcb.20.11.4106-4114.2000

48. Keren-Shaul, H., Spinrad, A., Weiner, A., Matcovitch-Natan, O., Dvir-Szternfeld, R., Ulland, T. K., . . . Amit, I. (2017). A Unique Microglia Type Associated with Restricting Development of Alzheimer's Disease. *Cell, 169*(7), 1276-1290.e1217. doi:10.1016/j.cell.2017.05.018
49. Kierdorf, K., Erny, D., Goldmann, T., Sander, V., Schulz, C., Perdiguero, E. G., . . . Prinz, M. (2013). Microglia emerge from erythromyeloid precursors via Pu.1- and Irf8-dependent pathways. *Nat Neurosci, 16*(3), 273-280. doi:10.1038/nn.3318
50. Kierdorf, K., Masuda, T., Jordão, M. J. C., & Prinz, M. (2019). Macrophages at CNS interfaces: ontogeny and function in health and disease. *Nature Reviews Neuroscience, 20*(9), 547-562. doi:10.1038/s41583-019-0201-x
51. Konishi, H., Kobayashi, M., Kunisawa, T., Imai, K., Sayo, A., Malissen, B., . . . Kiyama, H. (2017). Siglec-H is a microglia-specific marker that discriminates microglia from CNS-associated macrophages and CNS-infiltrating monocytes. *Glia, 65*(12), 1927-1943. doi:10.1002/glia.23204
52. Korin, B., Ben-Shaanan, T. L., Schiller, M., Dubovik, T., Azulay-Debby, H., Boshnak, N. T., . . . Rolls, A. (2017). High-dimensional, single-cell characterization of the brain's immune compartment. *Nat Neurosci, 20*(9), 1300-1309. doi:10.1038/nn.4610
53. Krasemann, S., Madore, C., Cialic, R., Baufeld, C., Calcagno, N., El Fatimy, R., . . . Butovsky, O. (2017). The TREM2-APOE Pathway Drives the Transcriptional Phenotype of Dysfunctional Microglia in Neurodegenerative Diseases. *Immunity, 47*(3), 566-581.e569. doi:10.1016/j.immuni.2017.08.008

54. Lambert, J. C., Ibrahim-Verbaas, C. A., Harold, D., Naj, A. C., Sims, R., Bellenguez, C., . . . Amouyel, P. (2013). Meta-analysis of 74,046 individuals identifies 11 new susceptibility loci for Alzheimer's disease. *Nat Genet, 45*(12), 1452-1458. doi:10.1038/ng.2802

55. Lampert, P. W., Sims, J. K., & Kniazeff, A. J. (1973). Mechanism of demyelination in JHM virus encephalomyelitis. Electron microscopic studies. *Acta neuropathologica, 24*(1), 76-85. doi:10.1007/bf00691421

56. Lane, T. E., & Buchmeier, M. J. (1997). Murine coronavirus infection: a paradigm for virus-induced demyelinating disease. *Trends Microbiol, 5*(1), 9-14. doi:10.1016/s0966-842x(97)81768-4

57. Lane, T. E., & Hosking, M. P. (2010). The pathogenesis of murine coronavirus infection of the central nervous system. *Crit Rev Immunol, 30*(2), 119-130. doi:10.1615/critrevimmunol.v30.i2.20

58. Lavin, Y., Winter, D., Blecher-Gonen, R., David, E., Keren-Shaul, H., Merad, M., . . . Amit, I. (2014). Tissue-resident macrophage enhancer landscapes are shaped by the local microenvironment. *Cell, 159*(6), 1312-1326. doi:10.1016/j.cell.2014.11.018

59. Li, Q., Cheng, Z., Zhou, L., Darmanis, S., Neff, N. F., Okamoto, J., . . . Barres, B. A. (2019). Developmental Heterogeneity of Microglia and Brain Myeloid Cells Revealed by Deep Single- Cell RNA Sequencing. *Neuron, 101*(2), 207-223.e210. doi:10.1016/j.neuron.2018.12.006

60. Liu, Z., Gu, Y., Chakarov, S., Bleriot, C., Kwok, I., Chen, X., . . . Ginhoux, F. (2019). Fate Mapping via Ms4a3-Expression History Traces Monocyte-Derived Cells. *Cell, 178*(6), 1509-1525.e1519. doi:10.1016/j.cell.2019.08.009

61. Lund, H., Pieber, M., Parsa, R., Han, J., Grommisch, D., Ewing, E., . . . Harris, R. A. (2018). Competitive repopulation of an empty microglial niche yields functionally distinct subsets of microglia-like cells. *Nat Commun, 9*(1), 4845. doi:10.1038/s41467-018-07295-7

62. MacKinnon, A. C., Farnworth, S. L., Hodkinson, P. S., Henderson, N. C., Atkinson, K. M., Leffler, H., Sethi, T. (2008). Regulation of alternative macrophage activation by galectin- 3. *Journal of immunology (Baltimore, Md. : 1950), 180*(4), 2650-2658. doi:10.4049/jimmunol.180.4.2650

63. Marro, B. S., Grist, J. J., & Lane, T. E. (2016). Inducible Expression of CXCL1 within the Central Nervous System Amplifies Viral-Induced Demyelination. *J Immunol, 196*(4), 1855-1864. doi:10.4049/jimmunol.1501802

64. Marsh, S. E., Kamath, T., Walker, A. J., Dissing-Olesen, L., Hammond, T. R., Young, A. M. H., . . . Stevens, B. (2020). Single Cell Sequencing Reveals Glial Specific Responses to Tissue Processing & Enzymatic Dissociation in Mice and Humans. *bioRxiv*, 2020.2012.2003.408542. doi:10.1101/2020.12.03.408542

65. Masuda, T., Sankowski, R., Staszewski, O., Bottcher, C., Amann, L., Sagar, . . . Prinz, M. (2019). Spatial and temporal heterogeneity of mouse and human microglia at single-cell resolution. *Nature, 566*(7744), 388-392. doi:10.1038/s41586-019-0924-x

66. Mehina, E. M. F., Taylor, S., Boghozian, R., White, E., Choi, S. E., Cheema, M. S., . . . Brown, C. E. (2021). Invasion of phagocytic Galectin 3 expressing macrophages in the diabetic brain disrupts vascular repair. *Science Advances, 7*(34), eabg2712. doi:doi:10.1126/sciadv.abg2712

67. Mildner, A., Schmidt, H., Nitsche, M., Merkler, D., Hanisch, U. K., Mack, M., . . . Prinz, M. (2007). Microglia in the adult brain arise from Ly-6ChiCCR2+ monocytes only under defined host conditions. *Nat Neurosci, 10*(12), 1544-1553. doi:10.1038/nn2015

68. Mildner, A., Schönheit, J., Giladi, A., David, E., Lara-Astiaso, D., Lorenzo-Vivas, E., . . . Jung, S. (2017). Genomic Characterization of Murine Monocytes Reveals C/EBPβ Transcription Factor Dependence of Ly6C(-) Cells. *Immunity, 46*(5), 849-862.e847. doi:10.1016/j.immuni.2017.04.018

69. Mrdjen, D., Pavlovic, A., Hartmann, F. J., Schreiner, B., Utz, S. G., Leung, B. P., . . . Becher, B. (2018). High-Dimensional Single-Cell Mapping of Central Nervous System Immune Cells Reveals Distinct Myeloid Subsets in Health, Aging, and Disease. *Immunity, 48*(2), 380-395.e386. doi:10.1016/j.immuni.2018.01.011

70. Munro, D. A. D., Bradford, B. M., Mariani, S. A., Hampton, D. W., Vink, C. S., Chandran, S., . . . Priller, J. (2020). CNS macrophages differentially rely on an intronic Csf1r enhancer for their development. *Development, 147*(23). doi:10.1242/dev.194449

71. Oakley, H., Cole, S. L., Logan, S., Maus, E., Shao, P., Craft, J., . . . Vassar, R. (2006). Intraneuronal beta-amyloid aggregates, neurodegeneration, and neuron loss in transgenic mice with five familial Alzheimer's disease mutations: potential factors in amyloid plaque formation. *J Neurosci, 26*(40), 10129-10140. doi:10.1523/jneurosci.1202-06.2006

72. Ochocka, N., Segit, P., Walentynowicz, K. A., Wojnicki, K., Cyranowski, S., Swatler, J., . . . Kaminska, B. (2021). Single-cell RNA sequencing reveals functional heterogeneity of glioma-associated brain macrophages. *Nat Commun, 12*(1), 1151. doi:10.1038/s41467-021-21407-w

73. Prinz, M., & Priller, J. (2014). Microglia and brain macrophages in the molecular age: from origin to neuropsychiatric disease. *Nat Rev Neurosci, 15*(5), 300-312. doi:10.1038/nrn3722

74. Prinz, M., Priller, J., Sisodia, S. S., & Ransohoff, R. M. (2011). Heterogeneity of CNS myeloid cells and their roles in neurodegeneration. *Nat Neurosci, 14*(10), 1227-1235. doi:10.1038/nn.2923

75. Ransohoff, R. M., & Cardona, A. E. (2010). The myeloid cells of the central nervous system parenchyma. *Nature, 468*(7321), 253-262. doi:10.1038/nature09615

76. Reed-Geaghan, E. G., Croxford, A. L., Becher, B., & Landreth, G. E. (2020). Plaque-associated myeloid cells derive from resident microglia in an Alzheimer's disease model. *J Exp Med, 217*(4). doi:10.1084/jem.20191374

77. Rojo, R., Sauter, K. A., Lefevre, L., Hume, D. A., & Pridans, C. (2018). Maternal tamoxifen treatment expands the macrophage population of early mouse embryos. *bioRxiv*, 296749. doi:10.1101/296749

78. Saederup, N., Cardona, A. E., Croft, K., Mizutani, M., Cotleur, A. C., Tsou, C. L., . . . Charo, I. F. (2010). Selective chemokine receptor usage by central nervous system myeloid cells in CCR2-red fluorescent protein knock-in mice. *PLoS One, 5*(10), e13693. doi:10.1371/journal.pone.0013693

79. Safaiyan, S., Besson-Girard, S., Kaya, T., Cantuti-Castelvetri, L., Liu, L., Ji, H., . . . Simons, M. (2021). White matter aging drives microglial diversity. *Neuron, 109*(7), 1100-1117.e1110. doi:10.1016/j.neuron.2021.01.027

80. Savarin, C., Stohlman, S. A., Atkinson, R., Ransohoff, R. M., & Bergmann, C. C. (2010). Monocytes regulate T cell migration through the glia limitans during acute viral encephalitis. *J Virol, 84*(10), 4878-4888. doi:10.1128/jvi.00051-10

81. Shemer, A., Erny, D., Jung, S., & Prinz, M. (2015). Microglia Plasticity During Health and Disease: An Immunological Perspective. *Trends Immunol, 36*(10), 614-624. doi:10.1016/j.it.2015.08.003

82. Shemer, A., Grozovski, J., Tay, T. L., Tao, J., Volaski, A., Süß, P., . . . Jung, S. (2018). Engrafted parenchymal brain macrophages differ from microglia in transcriptome, chromatin landscape and response to challenge. *Nat Commun, 9*(1), 5206. doi:10.1038/s41467-018-07548-5

83. Shukla, A. K., McIntyre, L. L., Marsh, S. E., Schneider, C. A., Hoover, E. M., Walsh, C. M., . . . Inlay, M. A. (2019). CD11a expression distinguishes infiltrating myeloid cells from plaque-associated microglia in Alzheimer's disease. *Glia, 67*(5), 844-856. doi:10.1002/glia.23575

84. Simard, A. R., Soulet, D., Gowing, G., Julien, J. P., & Rivest, S. (2006). Bone marrow-derived microglia play a critical role in restricting senile plaque formation in Alzheimer's disease. *Neuron, 49*(4), 489-502. doi:10.1016/j.neuron.2006.01.022

85. Sobue, A., Komine, O., Hara, Y., Endo, F., Mizoguchi, H., Watanabe, S., . . . Yamanaka, K. (2021). Microglial gene signature reveals loss of homeostatic microglia associated with neurodegeneration of Alzheimer's disease. *Acta Neuropathol Commun, 9*(1), 1. doi:10.1186/s40478-020-01099-x

86. Spangenberg, E., Severson, P. L., Hohsfield, L. A., Crapser, J., Zhang, J., Burton, E. A., . . . Green, K. N. (2019). Sustained microglial depletion with CSF1R inhibitor impairs parenchymal plaque development in an Alzheimer's disease model. *Nat Commun, 10*(1), 3758. doi:10.1038/s41467-019-11674-z

87. Steinbach, F., & Thiele, B. (1994). Phenotypic investigation of mononuclear phagocytes by flow cytometry. *J Immunol Methods, 174*(1-2), 109-122. doi:10.1016/0022-1759(94)90015-9

88. Syage, A. R., Ekiz, H. A., Skinner, D. D., Stone, C., O'Connell, R. M., & Lane, T. E. (2020). Single-Cell RNA Sequencing Reveals the Diversity of the Immunological Landscape following Central Nervous System Infection by a Murine Coronavirus. *J Virol, 94*(24). doi:10.1128/jvi.01295-20

89. Thomas, L., & Pasquini, L. A. (2018). Galectin-3-Mediated Glial Crosstalk Drives Oligodendrocyte Differentiation and (Re)myelination. *Front Cell Neurosci, 12*, 297. doi:10.3389/fncel.2018.00297

90. Utz, S. G., See, P., Mildenberger, W., Thion, M. S., Silvin, A., Lutz, M., . . . Greter, M. (2020). Early Fate Defines Microglia and Non-parenchymal Brain Macrophage Development. *Cell, 181*(3), 557-573.e518. doi:10.1016/j.cell.2020.03.021

91. Van Hove, H., Martens, L., Scheyltjens, I., De Vlaminck, K., Pombo Antunes, A. R., De Prijck, S., . . . Movahedi, K. (2019). A single-cell atlas of mouse brain macrophages reveals unique transcriptional identities shaped by ontogeny and tissue environment. *Nat Neurosci, 22*(6), 1021-1035. doi:10.1038/s41593-019-0393-4

92. Wahane, S., Zhou, X., Zhou, X., Guo, L., Friedl, M.-S., Kluge, M., . . . Zou, H. (2021). Diversified transcriptional responses of myeloid and glial cells in spinal cord injury shaped by HDAC3 activity. *Science Advances, 7*(9), eabd8811. doi:doi:10.1126/sciadv.abd8811

93. Wang, Y., Ulland, T. K., Ulrich, J. D., Song, W., Tzaferis, J. A., Hole, J. T., . . . Colonna, M. (2016). TREM2-mediated early microglial response limits diffusion and toxicity of amyloid plaques. *J Exp Med, 213*(5), 667-675. doi:10.1084/jem.20151948

94. Weiner, L. P. (1973). Pathogenesis of demyelination induced by a mouse hepatitis. *Arch Neurol, 28*(5), 298-303. doi:10.1001/archneur.1973.00490230034003

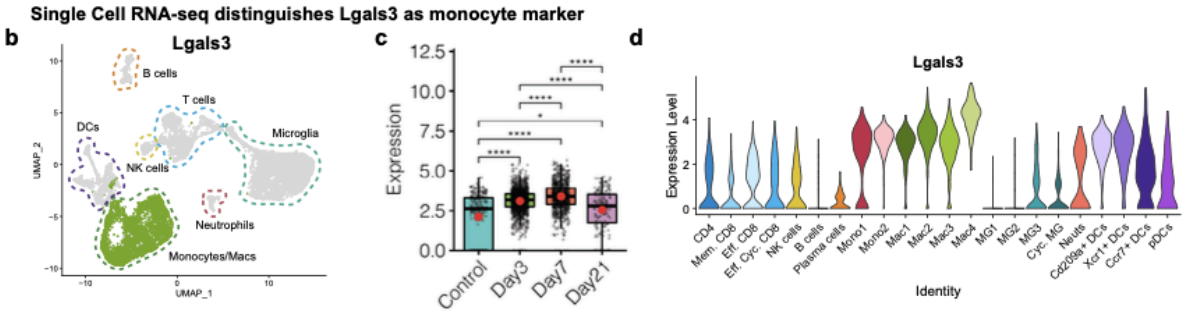
95. Werner, Y., Mass, E., Ashok Kumar, P., Ulas, T., Händler, K., Horne, A., . . . Stumm, R. (2020). Cxcr4 distinguishes HSC-derived monocytes from microglia and reveals monocyte immune responses to experimental stroke. *Nat Neurosci, 23*(3), 351-362. doi:10.1038/s41593- 020-0585-y

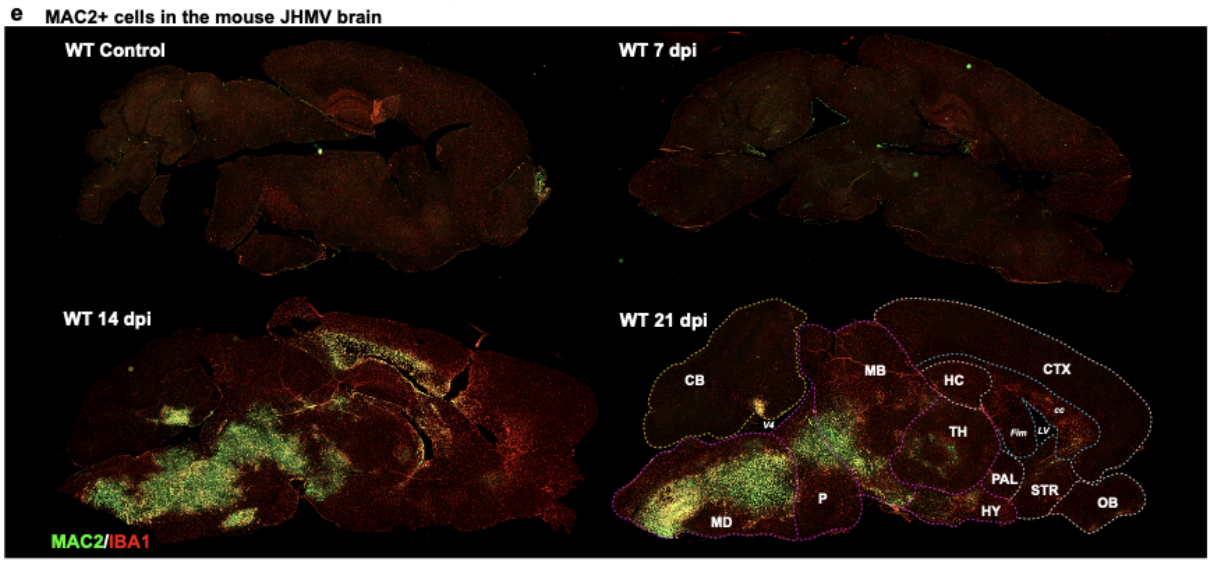
96. Wong, L. M., Myers, S. J., Tsou, C. L., Gosling, J., Arai, H., & Charo, I. F. (1997). Organization and differential expression of the human monocyte chemoattractant protein 1 receptor gene. Evidence for the role of the carboxyl-terminal tail in receptor trafficking. *J Biol Chem, 272*(2), 1038-1045. doi:10.1074/jbc.272.2.1038

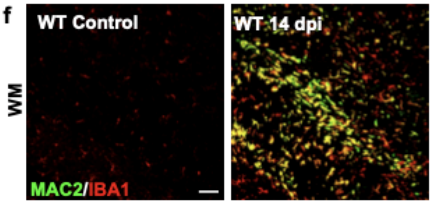
97. Yamasaki, R., Lu, H., Butovsky, O., Ohno, N., Rietsch, A. M., Cialic, R., . . . Ransohoff, R. M. (2014). Differential roles of microglia and monocytes in the inflamed central nervous system. *J Exp Med, 211*(8), 1533. doi:10.1084/jem.20132477

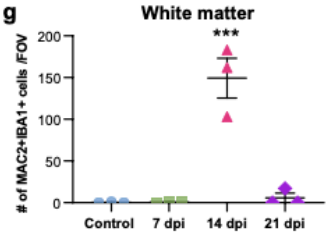
98. Zhan, L., Sohn, P. D., Zhou, Y., Li, Y., & Gan, L. (2019). A Mac2-positive progenitor-like microglial population survives independent of CSF1R signaling in adult mouse brain. *bioRxiv*, 722090. doi:10.1101/722090





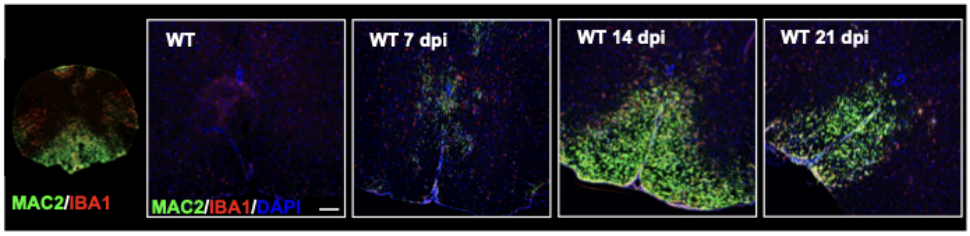






h MAC2+ distribution in JHMV mouse brain

	Animal group			
Brain region	Control	7 dpi	14 dpi	21 dpi
Brainstem	-	-	+++	+++
Cerebellum	-	-	++	+
White matter	-	-	+++	+
Cerebrum	-	-	-	-



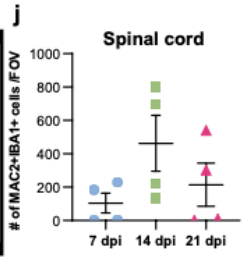


Figure 1. *Lgals3*/MAC2 distinguishes infiltrating cells from microglia in the adult CNS. (a) Schematic of experimental design of intracranial (i.c.) infection of five to six-week-old C57BL/6 wild type (WT) mice with 250 PFU of the neurotropic JHM-J2.2v-1 strain of mouse hepatitis virus (JHMV). Brains and spinal cords were collected at 7, 14, 21 days post infection (d.p.i.). (b) UMAP plot displays aggregate data of CD45+ cells and shows scaled expression of transcripts encoding *Lgals3* in monocyte/macrophage (Monocytes/Macs) clusters (Syage et al., 2020). (c) Temporal analysis of expression of transcripts encoding *Lgals3*. Transcript levels were elevated at defined timepoints during JHMV infection. Data is presented as normalized expression values, and random noise was added to show data point distribution. Box plots show interquartile range and median value (bold horizontal bar). Red dots indicate the average expression value per sample. Wilcoxon's test was used for statistical analysis. (d) Violin plot shows gene expression of *Lgals3* in all CD45+ cells on the single-cell level and that *Lgals3* is upregulated in monocytes and macrophage clusters. (e) Representative whole sagittal brain sections of MAC2 (green) and IBA1 (red) staining in WT non-infected and JHMV-infected mice at 7, 14, and 21 d.p.i. (f) High resolution 20x confocal images of MAC2+ (green) and IBA1+ (red) cells in the white matter tracts of WT non-infected and JHMV-infected at 14 d.p.i. (g) Quantification of MAC+IBA1+ cells per field of view (FOV) in white matter tracts of brains in WT control and JHMV-infected mice.(h) Table of the relative MAC2+ cell distribution in distinct brain regions. – indicates no accumulation. + indicates low accumulation. ++ indicates moderate accumulation. +++ indicates extensive accumulation. (i) Representative confocal images of MAC2+ (green) and IBA1+ (red) cells in the spinal cords of WT control and JHMV-infected mice at various timepoints post infection. (j) Quantification of (i). Mouse, syringe and virus illustrations were obtained from Servier Medical Art at smart.servier.com. IBA1, ionized calcium adapter molecule 1; CB, cerebellum; cc, corpus callosum; CTX, cortex; Fim, fimbria; HC, hippocampus; HY, hypothalamus; LV, lateral ventricle; MB, midbrain; MD, medulla; OB, olfactory bulb; P, pons; PAL, pallidum; STR, striatum; TH, thalamus; V4, fourth ventricle. Data are represented as mean ± SEM (n=3-4 mice/timepoint). * $p < 0.05$, *** $p < 0.001$, **** $p < 0.0001$, compared to control unless otherwise indicated. Scale bar in (f) ~100 μm; in (i) inserts ~160 μm.

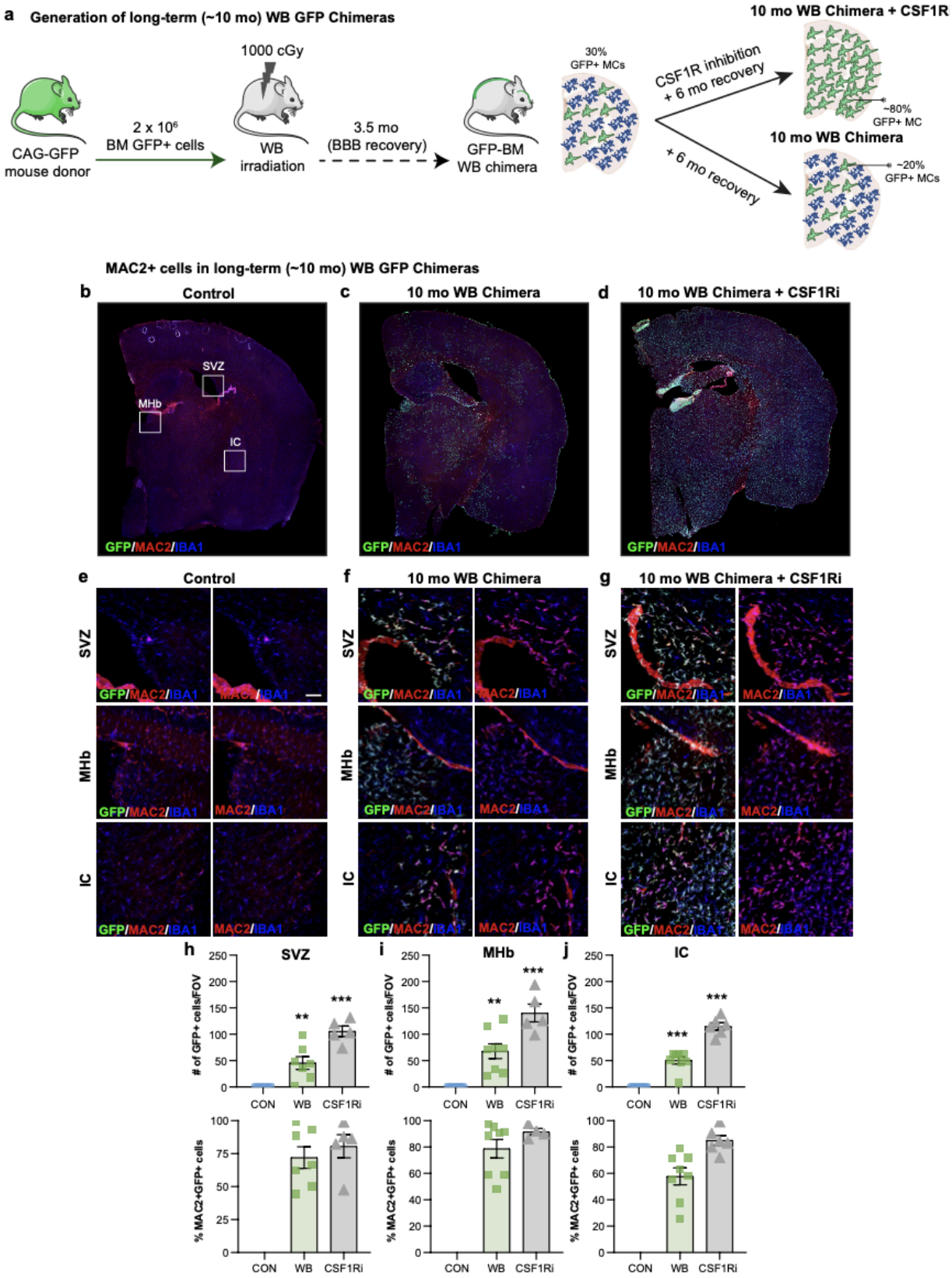

a
Generation of long-term (~10 mo) WB GFP Chimeras
CAG-GFP mouse donor
2 x 10⁶ BM GFP+ cells
1000 cGy
WB irradiation
3.5 mo (BBB recovery)
GFP-BM WB chimera
30% GFP+ MCs
CSF1R inhibition + 6 mo recovery
10 mo WB Chimera + CSF1R
~80% GFP+ MC
+ 6 mo recovery
10 mo WB Chimera
~20% GFP+ MCs
MAC2+ cells in long-term (~10 mo) WB GFP Chimeras
b
Control
c
10 mo WB Chimera
d
10 mo WB Chimera + CSF1Ri
SVZ
MHb
IC
GFP/MAC2/IBA1
e
Control
f
10 mo WB Chimera
g
10 mo WB Chimera + CSF1Ri
SVZ
MHb
IC
GFP/MAC2/IBA1
MAC2/IBA1
h
SVZ
i
MHb
j
IC
# of GFP+ cells/FOV
% MAC2+GFP+ cells
CON
WB
CSF1Ri

Figure 2. MAC2 is a specific and long-lasting marker for bone marrow-derived infiltrating cells.(a) Schematic of experimental design for the generation of long-term green fluorescent protein (GFP) bone marrow (BM) chimeras. Treatment of BM chimeras with colony-stimulating factor 1 receptor (CSF1R) inhibitor results in extensive parenchymal engraftment of BM-derived peripheral myeloid cells in the brain (Hohsfield et al., 2020). Four-month-old wild type (WT) mice underwent whole body (WB) irradiation (1000 cGy) and BM transplant via retro-orbital injection of 2 × 106BM cells from age- and sex- matched CAG-GFP mice. Following a 3.5 mo recovery, mice were treated with CSF1R inhibitor PLX3397 (600 ppm) for 14d, and then placed on control diet for 6 mo. (b-g) Representative images of whole coronal brain sections (b-d) and high resolution 20x confocal (e-g) images of GFP+ (green), MAC2+ (red) and IBA1+ (red) cells in control (b, e), ~10 mo WB chimeras (c, f), and ~10 mo WB chimeric mice treated with a CSF1R inhibitor (d, g). White boxes in (b) indicate brain regions of interest shown in (e-g). Images show that MAC2+ cells co-localize with GFP BM-derived cells in the brain parenchyma. (h-j) Quantification of the number of GFP+ cells per field of view (FOV) in the subventricular zone (SVZ) (h), medial habenula (MHb) (i), and internal capsule (IC) (j) in control, ~10 mo WB chimeras, and ~10 mo WB chimeric mice treated with a CSF1R inhibitor. (k-m) Percentage of GFP+ cells that express MAC or MAC2+ cells that express GFP in the subventricular zone (SVZ) (k), medial habenula (MHb) (l), and internal capsule (IC) (m) in control, ~10 mo WB chimeras, and ~10 mo WB chimeric mice treated with a CSF1R inhibitor. Data are represented as mean ± SEM (n=5–9). ** $p < 0.01$, *** $p < 0.001$, compared to control. Scale bar ~60 μm.

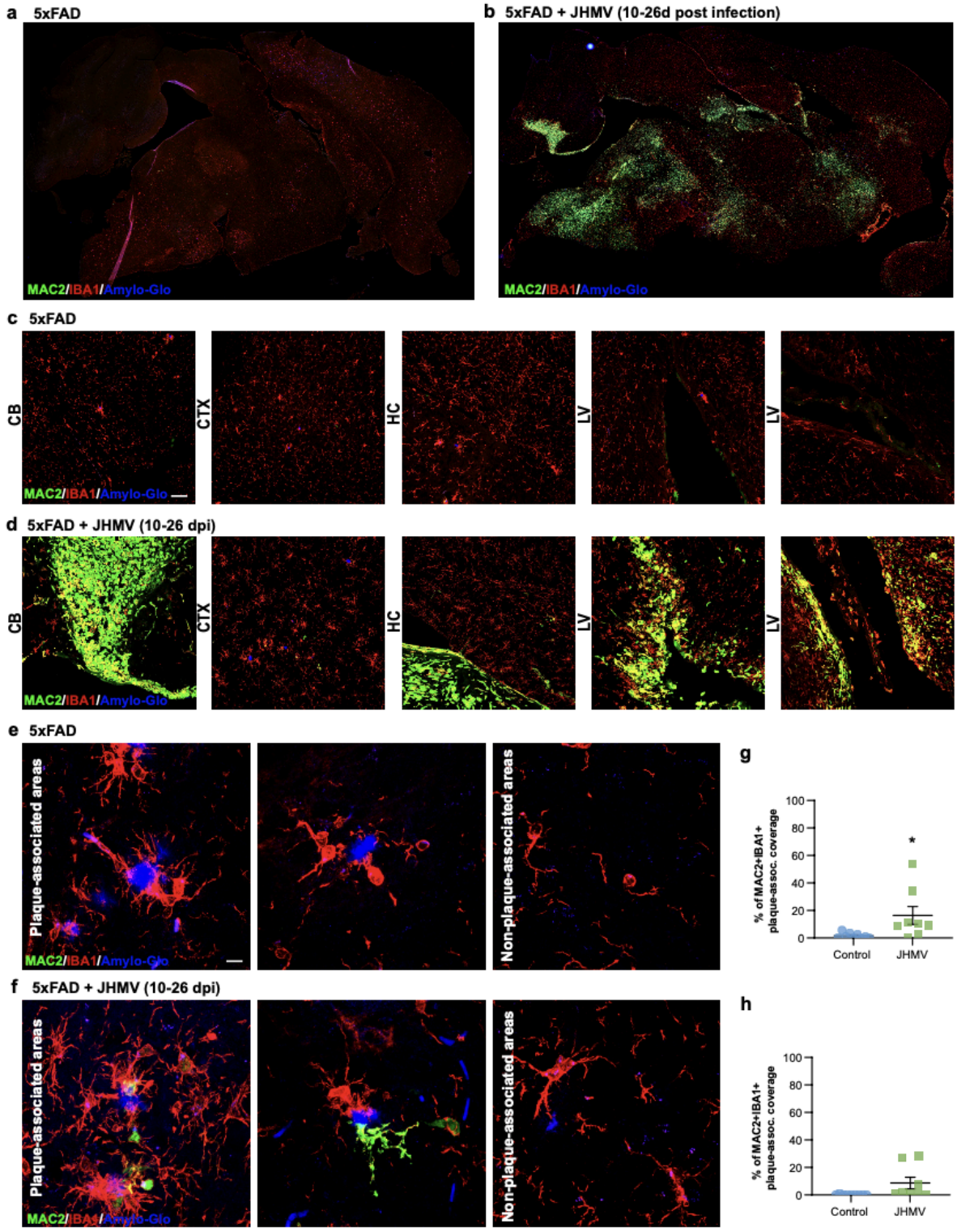

a 5xFAD
b 5xFAD + JHMV (10-26d post infection)
MAC2/IBA1/Amylo-Glo
c 5xFAD
CB
CTX
HC
LV
LV
d 5xFAD + JHMV (10-26 dpi)
e 5xFAD
Plaque-associated areas
Non-plaque-associated areas
f 5xFAD + JHMV (10-26 dpi)
g
% of MAC2+IBA1+ plaque-assoc. coverage
100
80
60
40
20
0
*
Control
JHMV
h

Figure 3. MAC2 is not a ubiquitous marker for plaque-associated microglia during the early stages of disease in 5xFAD mice. Four-month-old 5xFAD mice were infected intracranially with 200 PFU of JHMV strain and brains evaluated at 10-25 d.p.i. (a-d) Representative whole sagittal brain section (a-b) and 20x confocal (c-d) images of Amylo-Glo (amyloid, blue), MAC2 (green), and IBA1 (red) staining in control (a, c) and JHMV-infected (b, d) 5xFAD mice. (e) Quantification of the number of MAC2+IBA1+ cells per field of view (FOV) in the cerebellum (CB), cortex (CTX), hippocampus (HC), and lateral ventricle (LV). (f,h) Representative high resolution 100x confocal images of Amylo-Glo+ plaques (amyloid, blue), MAC2+ (green) cells, and IBA1+ (red) cells in plaque-associated and non-plaque-associated areas in the brains of control (f) and JHMV- infected (h) 5xFAD mice. Images show that MAC2+ cells do not label plaque-associated microglia in non-infected 5xFAD mice. (g,i) Quantification of % MAC2+IBA1+ staining in IBA1+ cells and in plaque-associated (g) and non-plaque-associated (i) areas of the cortex and hippocampus. Multiple field of views in these brain regions were quantified across three animals from each group. Data are represented as mean ± SEM (n=8-9). * $p < 0.05$. Scale bar in (c) ~60 μm; in (e) ~10 μm.

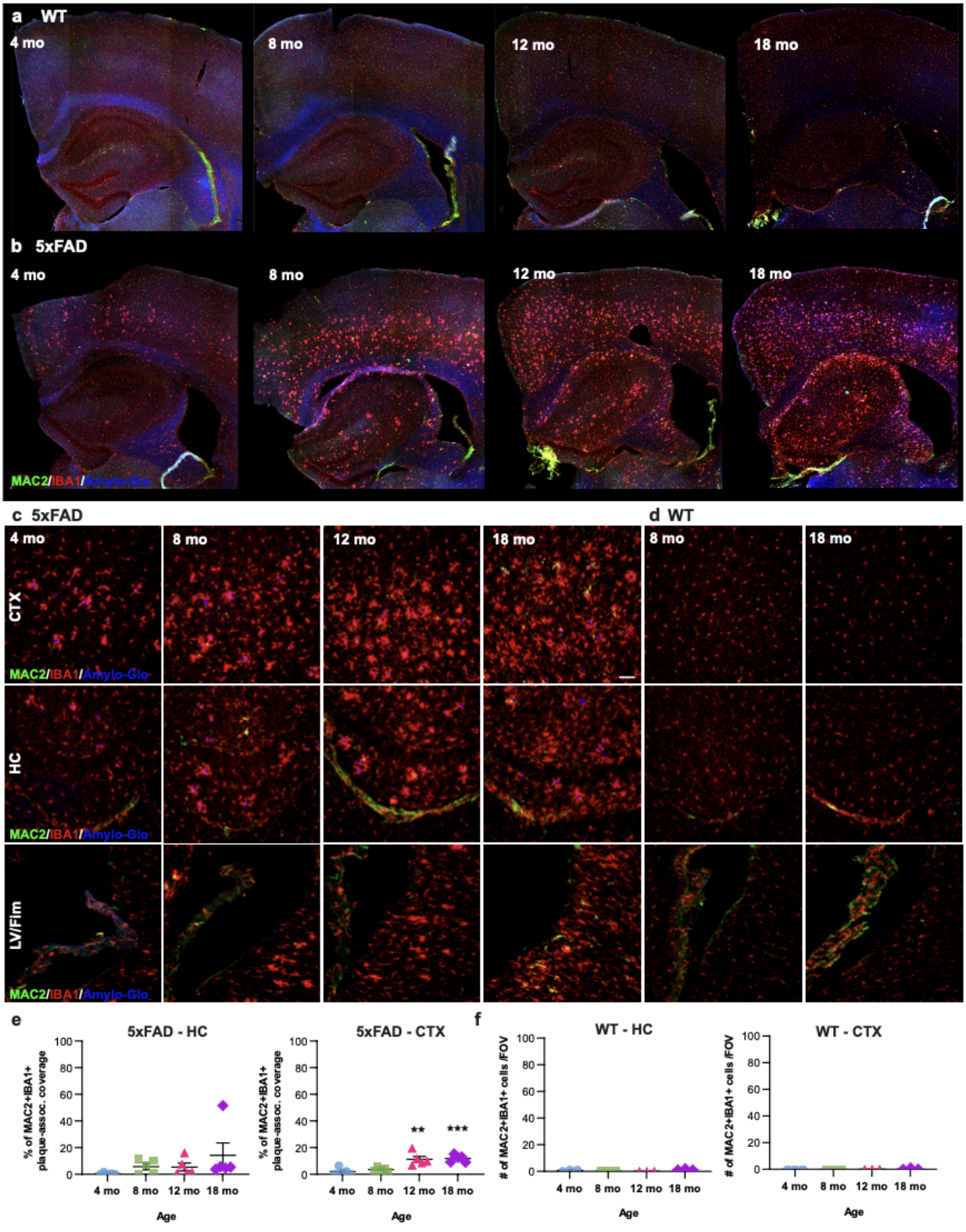

a WT
4 mo
8 mo
12 mo
18 mo
b 5xFAD
4 mo
8 mo
12 mo
18 mo
MAC2/IBA1/Amylo-Glo
c 5xFAD
d WT
4 mo
8 mo
12 mo
18 mo
CTX
HC
LV/Fim
MAC2/IBA1/Amylo-Glo
e
5xFAD - HC
5xFAD - CTX
% of MAC2+IBA1+ plaque-assoc. coverage
4 mo
8 mo
12 mo
18 mo
Age
**
***
f
WT - HC
WT - CTX
# of MAC2+IBA1+ cells /FOV

Figure 4. The effects of aging on MAC2 staining in WT and 5xFAD mice. Brains of wild type (WT) and 5xFAD mice at 4, 8, 12, and 18 months (mo) of age were evaluated for MAC2 staining in plaque-associated microglia. (a-b) Representative images of MAC2 (green), IBA1 (red, myeloid cells), and Amylo-Glo (blue, amyloid plaques) staining in brain sections of WT (a) and 5xFAD (b) mice. (c-d) Representative 20x confocal images of MAC2, IBA1, and Amylo-Glo staining in the cortex (CTX), hippocampus (HC), and lateral ventricle (LV)/fimbria (Fim) of WT (d) and 5xFAD (c) mice shows the age-dependent increase in MAC2 staining in 5xFAD mice. (e-f) Quantification of plaque-associated MAC2+IBA1+ staining and MAC2+IBA1+ cells in 5xFAD and WT mice, respectively. Female (pink) and male (blue) mice are indicated by color scheme. Data are represented as mean ± SEM (n=3-5). ** $p < 0.01$, *** $p < 0.001$, compared to 4 mo. Scale bar in (c) ~60 μm.

CHAPTER 4

CHARACTERIZING THE EFFECTS OF MOUSE-ADAPTED SARS-COV-2 INFECTION ON ALZHEIMER'S DISEASE- ASSOCIATED NEUROPATHOLOGY

© 2024 Susana Furman

Characterizing the effects of mouse-adapted SARS-CoV-2 infection on Alzheimer's disease-associated neuropathology

Susana Furman[1], Gema M. Olivarria[1], Yuting Cheng[2], Collin Pachow[2], Kellie Fernandez[2], Dominic Ibarra Javonillo[1], Kim N. Green[1], Thomas E. Lane[1,3]

[1]Department of Neurobiology and Behavior, University of California, Irvine, Irvine, California, USA

[2]Department of Molecular Biology and Biochemistry, School of Biological Sciences, University of California, Irvine, Irvine, California, USA

[3]Center for Virus Research, University of California, Irvine 92697

*Address Correspondence:

Thomas E. Lane, Ph.D.

Department of Neurobiology & Behavior

School of Biological Sciences

University of California, Irvine

Email: tlane@uci.edu

Key words: COVID-19, coronavirus, Alzheimer's disease, neuroinflammation

ABSTRACT

Transgenic animal models of Alzheimer's disease (AD) offer the opportunity to better evaluate comorbidities that promote progression of disease. Accumulating evidence has suggested that viral infection may contribute to the onset of AD as well as impact pre-existing neuropathology. Evidence from both *in vivo* and *in vitro* studies indicates that infections significantly exacerbate AD-like pathological changes, suggesting that infection-mediated inflammation may increase the susceptibility of developing AD later in life. This is further highlighted in the face of the ongoing COVID-19 pandemic as SARS-CoV-2 infection is associated with a worsening of clinical symptoms in elderly patients with dementia. Therefore, understanding how SARS-CoV-2 infection influences AD-associated neuropathology represents a critical knowledge gap and emphasizes the importance of performing discovery-based research using viral infection of a clinically relevant mouse model of AD to address these questions. The current study employed intranasal infection of 5xFAD mice with a mouse-adapted SARS-CoV-2 (MA10) to assess effects on neuroinflammation and AD-associated pathology. MA10 infection of aged-matched (10-14 month) wildtype (WT) C57BL/6 mice or 5xFAD mice resulted in a dramatic increase in expression of transcripts associated with modulation of the immune system and other inflammatory pathways in the lungs that eventually returned to baseline levels of expression after initial infection. Interestingly, while viral RNA was not detected within the brains of infected mice, MA10 infection led to lasting gene expression changes in the brain and these changes are associated with neuronal dysfunction**.** However, changes in gene expression were not associated with detectable changes in activated microglia and astrocytes, or inflammatory monocyte/macrophages in infected mice. Additionally, no changes were observed in Aβ plaques or dystrophic neurites in the brains of 5xFAD mice. No evidence of over neuronal

degeneration was found; moreover, no overt changes in synapse number were noted. These findings indicate that experimental infection of mice with MA10 is associated with detectable and long lasting changes in the brain associated with neuronal dysfunction, even though gene expression changes do not directly translate into altered neuropathological changes. Moreover, this study provides evidence that viral infection that results from a lower viral dose or less severe variants of SARS-CoV-2 may not necessarily lead to permanent or long term deleterious consequences in the brain.

INTRODUCTION

Alzheimer's disease (AD) is the most common cause of age-related dementia and impairs memory formation, and other intellectual functions leading to a decline in quality of life and ability to perform daily tasks. Pathology includes the aberrant accumulation of amyloid plaques and neurofibrillary tangles (NFTs) accompanied with neuronal loss and neuroinflammation. [1] AD is a complex multifactorial disease, where a wide range of risk factors are likely to influence its onset. While age has been established as the most important risk factor [2], a wide variety of genetic [3–7] and environmental factors [8–14] have been associated with an increased risk of AD. Some studies have suggested possible links between viral infection and either onset or exacerbation of pathology and clinical symptoms associated with various human neurodegenerative diseases including AD [15,16]. The viral hypothesis of AD proposes that some infectious agents contribute to AD pathogenesis, and numerous studies have implicated several infectious agents in AD [17–22]. Evidence also suggests that other viruses and their viral proteins may have amyloidogenic properties that can lead to the formation of amyloid aggregates [23–25]. The increasing number of studies associating infections to neurodegeneration and AD necessitates further investigation on the contribution of infections to AD and other dementias.

The etiological agent of COVID-19 is severe acute respiratory syndrome coronavirus 2 (SARS-CoV-2). In 2020, COVID-19 rapidly developed into a global pandemic [26] affecting hundreds of millions of people worldwide [27]. In the majority of individuals, infection presents with mild-to-moderate respiratory disease and other flu-like symptoms [28,29], with more severe presentations resulting in respiratory distress syndrome (ARDS) leading to respiratory failure [30]. Although COVID-19 symptoms are mostly respiratory in nature, neurological symptoms and complications have also been documented [31–35], with the majority occurring in patients with

severe disease [36]. Common neurological symptoms include headache, dizziness, as well as olfactory and gustatory dysfunction.[37,38] However more severe disease has also been associated with ischemic strokes, cerebrovascular disease, coagulation abnormalities, seizures, meningitis and encephalitis. [34,39–46]

Several risk factors have been associated with severe disease, and evidence suggests that increased age is associated with not only a higher risk of disease severity, but also mortality [47–49] . Pre-existing dementia also appears to be a contributing risk factor for COVID-19. Infection is associated with a worsening of clinical symptoms in elderly patients with dementia and increased mortality [50,51], and among patients with dementia, AD was the most prevalent cognitive impairment in those that died of COVID-19 [52]. COVID-19 appears to impact brain structure and function, and while definitive mechanisms between COVID-19 and neurodegeneration remain poorly understood, several suggest that COVID-19 may induce or accelerate neurodegenerative processes, including those related to dementia and Alzheimer's disease.

Many neurodegenerative disorders, including AD, are associated with abnormal protein folding and aggregation, with increased risk linked to exposure to infectious agents such as viruses and bacteria [15,17–22,53]. Recent evidence suggests that various viruses, including coronaviruses like SARS-CoV-1 [23,24] and more recently SARS-CoV-2 [54] possess viral proteins that exhibit amyloidogenic properties and can lead to the formation of amyloid aggregates.

Neuroinflammation is also present in a variety of neurodegenerative diseases and influenced by reactive microglia and astrocytes that lose their homeostatic functions. This leads to the release of increased amounts of proinflammatory cytokines, which consequently damage the blood-brain barrier (BBB) and lead to synaptic dysfunction, neurotoxicity and neuronal death [55]. In the context of COVID-19, CNS cells including glial cells and neurons have been

identified as likely targets for SARS-COV-2 infection in both patients and animal models [56–59] and post-mortem analysis of brains from COVID-19 patients have reported gliosis, axonal damage and BBB disruption [60–62] . Infection of laboratory animals has also shown BBB-disruption, gliosis in the absence of direct viral neuroinvasion across a variety of anatomical regions, including the hippocampus. Additionally decreased hippocampal neurogenesis, synaptic loss, and memory deficits have been observed. [63–66] Cases where direct viral infiltration in the brain was observed, also noted similar results including hippocampal gliosis. Additionally an increase in expression of AD risk genes was noted. [67]

The association of COVID-19 with neuroinflammation and specific neurodegenerative processes could result in hippocampal injury and neuronal/synaptic dysfunction, and therefore we hypothesized that infection of SARS-CoV-2 would impact brain function. Here we investigated CNS changes associated with intranasal inoculation with mouse-adapted SARS-CoV-2 (MA10) to model the effects of COVID-19 on the CNS, and evaluated the impacts of chronic infection on gene expression, neuroinflammation , cell death, and synaptic function in aged standard laboratory mice (C57BL/6) as well as AD associated pathology in an established preclinical AD mouse model (5xFAD).

MATERIALS AND METHODS:

Mice and viral infection: All animal experiments performed were approved by UC Irvine Institutional Animal Care and Use Committee. Male and female 10-14 month old C57BL/6 wildtype WT and 5xFAD hemizygous (B6.Cg-Tg(APPSwFlLon,PSEN1*M146L*L286V)6799Vas/Mmjax were group housed by sex in single use disposable plastic cages and provided ad-libitum water. SARS-Related Coronavirus 2, Mouse-Adapted, MA10 Variant (in isolate USA-WA1/2020 backbone), Infectious Clone (ic2019-nCoV MA10) in Calu-3 Cells, NR-55329 contributed by Ralph S. Baric was obtained from BEI. Mice were anesthetized through an intraperitoneal injection of a mixture of ketamine and xylazine and inoculated with 5 x 10^3 PFU of SARS2MA10 in 50µl of 1x PBS or sham inoculated. Infected and uninfected mice were visually examined daily for signs of clinical illness and euthanized early if they reached a predetermined euthanasia criteria.

Histology immunohistochemical staining: Mice were euthanized at defined time points and tissues were collected and placed in either cold TRIzol for RNA extraction and qPCR analysis or 4% paraformaldehyde for histological analysis. Fixed half brains were cryoprotected in 30% sucrose solution, embedded in O.C.T and sliced via cryostat in 15µm sagittal sections. Brain sections were desiccated overnight. Slides were rinsed with 1X TBS to remove residual O.C.T. Samples were then blocked with 5% normal goat serum and 0.1% Triton-X in TBS followed by overnight incubation in the same block with appropriate primary antibodies. On the second day, slides were treated with appropriate secondary antibodies following TBS rinsing (Supplementary figure 1: S1). Amylo-Glo staining (TR-300-AG; Biosensis) and TUNEL assay (12156792910 Sigma Aldrich) were performed according to the manufacturer's instructions.

Imaging and quantitative analysis: High resolution fluorescent images were obtained at 20X magnification using a Leica TCS SPE-II confocal microscope and LAS-X software. With confocal imaging, one field of view (FOV) per brain region was captured per mouse. Three brain regions per mouse were imaged; cortex (CRTX), dentate gyrus (DG) and subiculum (SUB). Cell counts and plaque burden were quantified using the spots module in Imaris. Volumetric measurements were automatically acquired using the surfaces module with confocal images of each brain region.

Super-Resolution Lattice Structure Illumination Microscopy (Lattice-SIM) was performed using an Elyra 7 microscope system. The same three distinct anatomical regions (CRTX, DG, and SUB) per mouse were imaged at 40X magnification. Images were processed using ZEN SIM2 on the ZEN software before being analyzed on Imaris. For quantification of both pre- and post-synaptic puncta (synaptophysin and PSD95), the Imaris spots module was used to count the number of puncta for each z-stack. Z-stacks were 5-8uM and the number of co-localized spots was normalized to z-stack volume. Overlapping puncta were defined as spots that were <0.2 uM apart.

RNA extraction and sequencing: Mouse tissue was added to TRIzol and homogenization was performed with the Bead Ruptor 12 (Omni International) and 1.4mm ceramic beads (Omni- International, 19-627). RNA from mouse tissue was extracted via RNeasy minikit (Qiagen, 74106) using the “Purification of Total RNA, Including Small RNAs, from Animal Tissues" protocol, with Buffer RWT substituted by Buffer RW1. Library preparation, RNA sequencing, and read mapping analysis were performed by Novagene Co. Gene expression values were normalized into log2 FPKM (fragments per kilobase of transcript per million mapped reads). Heatmaps were created using Morpheus (Morpheus,

https://software.broadinstitute.org/morpheus). Volcano plots were created using custom code in R. Differentially expressed genes were selected as significant with a log2(Fold Change) > 0.5 and a false discovery rate (FDR) <0.05. From the comparisons, lists of genes of interest were chosen to plot a heatmap of their expression and a GO term enrichment analysis using enrichR (https://amp.pharm.mssm.edu/Enrichr/).

cDNA synthesis and gene expression analysis via pcr: cDNA was made following the "First Strand cDNA Synthesis" protocol by New England Biolabs, using AMV Reverse Transcriptase (New England Biolabs, M0277L), Random Hexamers (Invitrogen, N8080127), RNAse inhibitor (New England BiolabsM0314L) and AMV Buffer (New England Biolabs B0277A). qPCRs were performed using the QIAquant 96 2 plex and iTaq Universal SYBER Green Supermix (BioRad, 1725120). Standard protocol for iTaq Universal SYBER GREEN Supermix was followed. Reactions were 10µl, and the machine was set to run for 1 cycle (95°C for 3 min), followed by 40 cycles (95°C for 15 s, then 58°C for 30 s). Sequences for mouse GAPDH, forward primer:AACTTTGGCATTGTGGAAGG, reverse primer: GGATGCAGGGATGATGTTCT; SARS-CoV-2 Nucleocapsid primers were purchased from Integrated DNA Technologies, forward (IDT, 10006821) and reverse (IDT, 10006822).

Statistical analysis: The sample sizes are limited but similar to those found in prior studies conducted by our lab and were not predetermined using statistical methods [68]. GraphPad Prism was used to perform statistical analysis on immunohistochemical data. Data were analyzed using two-way ANOVA, and Tukey's post-hoc tests used to evaluate biologically relevant interactions. Each data set was examined for sex-differences, and if none were found, both male and female data were combined. P-value of <0.05 was considered statistically significant. Data for each experiment is presented as MEAN±SEM.

RESULTS

MA10 infection elicits mild disease in infected mice and genotype does not affect mortality. WT and transgenic 5xFAD male and female mice (10-14 months of age) were intranasally infected (i.n.) with 5 x 10^3 PFU of MA10. Mice were monitored and euthanized at two experimental timepoints, 7 and 21 days post infection (dpi). Two primary organs were harvested-lungs and brains. Tissues from a small subcohort of animals were utilized for bulk-RNA Seq while the rest of tissue was utilized to assess pathological changes (Figure 1A). Disease was mild in both WT and 5xFAD, however mortality was observed in both infected groups. Additionally, no significant differences in mortality were observed between infected groups (Figure 2B). Viral replication was examined via qPCR in lungs and brains. qPCR indicated no viral RNA in either the lungs or brains of infected mice at either timepoints (data not shown).

MA10 infection in lungs of WT and 5xFAD mice is associated with differential expression of genes involved in modulation of the immune system and inflammatory pathways. RNA was isolated from lungs at days 7 and 21 dpi. and analysis of differentially expressed genes (DEG) per time point was performed. Volcano plots of lung gene expression in MA10- infected vs. four control groups at the predetermined experimental timepoints were plotted; WT-7dpi, 5xFAD-7dpi, WT-21 dpi and 5xFAD-21dpi. Only the 7dpi groups show clear, but unique differential expression of genes in each group. At 21 dpi., there were no significant DEGs in the lungs on MA10 infected WT and three unidentified genes for 5xFAD mice, in comparison to their uninfected counterparts suggesting a return to baseline gene expression with no significant long-term changes (Figure 2A). Heatmaps were created to compare significant DEGs from these two 7dpi groups of mice. DEGs were selected as significant if $\log_2$Fold Change

was greater than 0.5 and false discovery rate/ adjusted p-value as less than 0.05 (FC>0.5, FDR<0.05). Genes that met such criteria were then used to plot heatmaps of their expression (Figure 2B). In the WT-7dpi group of mice, analysis revealed upregulation in pathways associated with a decrease in immune cell (both B and T cell) proliferation as well as chemokine and chemokine receptor activity including chemokines; CXCL9, CXCL10, CCL2, CCL7, and CCL8, and chemokine receptors CXCR3, CCR2 (Figure 2C). Interestingly, in the lungs of both groups, analysis revealed downregulation of pathways associated with insulin-like-growth factor (Igf-1) binding (Figure 2C-D).

MA10 infection leads to lasting gene expression changes in the brain and these changes are associated with neuronal dysfunction. RNA isolation and analysis of differentially expressed genes was performed on half-brains with the same criteria as previously described. Volcano plots of brain gene expression in MA10- infected vs four control groups at the predetermined experimental timepoints were plotted; WT-7dpi, 5xFAD-7dpi (Figure 3A), WT-21dpi and 5xFAD-21dpi (Figure 4A). Heatmaps were also created comparing significant DEGs from these four groups of mice; 7dpi group (Figure 3B) and 21dpi group (Figure 4B). In the WT-7dpi group of mice, analysis indicated upregulation in pathways associated with voltage-gated calcium channel activity, neurotransmitter receptor activity, abnormal operant conditioning, reduced long-term potentiation and abnormal hippocampal mossy fiber morphology (Figure 3C). In the 5xFAD-7dpi group of mice, analysis indicated downregulation in pathways associated with abnormal postsynaptic currents, neuron morphology, impaired coordination and increased anxiety-related responses. Additionally there was a downregulation in pathways associated with neurotransmitter receptor activity, synaptic transmission and plasticity as well as axonogenesis (Figure 3D). Unlike differential expression of genes in lungs,

that appeared to have no significant differences at the 21dpi time point, brains of both groups WT-21dpi and 5xFAD-21dpi groups did indicate lasting changes in gene expression (Figure 4A); however heatmap analysis indicated that the 5xFAD group had significantly more lasting differentially expressed genes in comparison to the WT group (Figure 4B). Moreover, when examining pathways of interest, the WT-21dpi group showed only one down-regulated gene (UQCRF51) that is associated with multiple neurodegenerative diseases in addition to AD; Parkinson's disease (PD) and Huntington's disease (HD) (Figure 4C). On the other hand, analysis on the 5xFAD-21dpi group indicated a downregulation of many more pathways most of which were associated with neuronal and synaptic dysfunction , impaired coordination and anxiety related responses, and both amyloid and tau binding (Figure 4D).

MA10 infection does not affect astrocyte cell number or volume in the brain of WT or 5xFAD mice at 21 dpi. Other studies have indicated the presence of gliosis and other CNS changes in infected animal models in the absence of virus in the brain at various time points. [63–67] Given that 21 dpi was the experimental time point where changes in gene expression persisted in comparison to lungs, histopathological changes were assessed in a separate batch of animals at this particular time point. Mice were intranasally infected with either saline or MA10 as previously described. WT and 5xFAD mice of both sexes were aged to (10-14 months), a similar age as the cohort used for bulk RNASeq analysis (12 months). Brains were immunolabeled for a variety of CNS cells; IBA1+ microglia, GFAP+ astrocytes, Mac2+ monocytes, and NeuN+ neurons. A TUNEL assay was performed to stain for the presence of DNA damage/apoptotic cells. As the 5xFAD mouse model not only exhibits gliosis but also robust Aβ pathology and dystrophic neurites [69,70], brains were also immunolabeled for LAMP1+ lysosomes to asses dystrophic neurites, and stained for Aβ plaques with an Amyloglo stain to assess for the presence

or changes in these specific AD associated pathologies in both WT and 5xFAD mice. Quantification and volumetric measurements were performed on these with the exception of NeuN+ neurons and TUNEL+ cells, where only quantification was performed. Three distinct anatomical regions of the brain were chosen given that past studies of laboratory animals with SARS-CoV-2 or SARS-CoV-2-MA10 (MA10) indicated CNS changes as a result of infection in the cortex and hippocampus of infected animals. [63–67] Additionally, the 5xFAD model develops early and robust Aβ plaques in the subiculum [70], so therefore the regions chosen to assess histopathological changes were cortex (CRTX), dentate gyrus (DG), and subiculum (SUB).

Representative images of GFAP+astrocytes (red) with Amyloglo counterstain (DAPI, blue) for Aβ plaques were acquired for three distinct anatomical regions previously mentioned (Figure 5A-C). GFAP is expressed by hippocampal astrocytes, and in the cortex only expressed by reactive astrocytes. Immunostaining and quantification does not indicate changes in astrocyte count as a result of MA10 infection in the hippocampus or cortex (Figure 5D). Additionally, no significant changes in average astrocyte volume were observed as a result of infection (Figure 5E). In uninfected mice, genotype does have a significant effect in leading to an increased astrocyte number and volume in the cortex of 5xFAD mice, decreased astrocyte count in dentate gyrus, and an increased astrocyte volume in the subiculum (Figure 5D-E).

MA10 infection does not affect microglia or infiltrating monocyte cell number or volume in the brains of WT or 5xFAD mice at 21 dpi. Representative images of IBA1+ microglia (green), Mac2+ monocytes (red) with Amyloglo counterstain (DAPI, blue) for Aβ plaques were acquired for three distinct anatomical regions previously mentioned (Figure 6A-C). Immunostaining and quantification does not indicate changes in microglia count or volume as a result of MA10 infection in the hippocampus or cortex (Figure 6D-E). In uninfected mice,

genotype does have a significant effect in leading to an increased microglia number and volume in all 3 regions in 5xFAD mice (Figure 6D-E).

Mac2 is a unique marker for peripheral monocyte-derived macrophages with the Mac2 protein highly expressed in these infiltrating cells but not microglia. Several studies have shown that under inflammatory conditions peripherally derived monocytes enter the brain. [71–73] Immunostaining and quantification does not indicate changes in peripheral monocyte count or volume as a result of MA10 infection in the hippocampus or cortex. In uninfected mice, genotype does have a significant effect in leading to an increased monocyte number and volume in all 3 regions in 5xFAD mice (Figure 6 F-G).

MA10 infection does not affect dystrophic neurite or plaque burden in the brain 5xFAD mice at 21 dpi. Dense core Aβ plaques, a key feature of AD pathology, are surrounded by dystrophic neurites, which are abnormal swollen neuritic processes that can be immunostained by lysosome-associated membrane protein 1 (LAMP1). Representative images of LAMP1+ lysosomes (red), with Amyloglo counterstain (DAPI, blue) for Aβ plaques were acquired for three distinct anatomical regions previously mentioned (Figure 7A-C). Immunostaining and quantification does not indicate changes in count or volume of dystrophic neurites as a result of MA10 infection in the hippocampus or cortex (Figure 7D-E). Aβ plaques quantifications and volumetric measurements were performed in the same manner. There is no difference in Aβ plaques count or volume as a result of MA10 infection in the examined regions (Figure 7F-G). Dystrophic neurites and Aβ plaque pathology are only present in 5xFAD, and infection does not affect or induce this particular pathology in WT mice (Figure 7A-C).

MA10 infection does not affect apoptosis or neuron number in the brain of WT or 5xFAD mice at 21dpi. Given that BulkRNASeq analysis pointed to a variety of pathways

associated with neuronal dysfunction at 21 dpi, quantification of neurons was performed to assess any over neurodegeneration associated with any drastic decrease in NeuN+ neuron count in the cortex and subiculum of MA10 infected mice. Additionally, a TUNEL assay was performed to evaluate whether other more general cell death/apoptosis was occurring that could contribute to CNS impairment as a result of MA10 infection. Representative images of NeuN+ neurons (green), TUNEL+ apoptotic cells (red) and Amyloglo counterstain (DAPI, blue) for Aβ plaques were acquired for the same three distinct anatomical regions (Figure 8A-C). Quantitative analysis of NeuN+ neurons was not performed on DG gyrus, as cells in this region are too tightly clustered for definitive and consistent analysis performed by Imaris software. Immunostaining and quantification of NeuN+ cells does not indicate changes in neuron count as a result of MA10 infection in the subiculum or cortex (Figure 8E). TUNEL staining and quantification of TUNEL+ cells did not indicate a significant change in cell death as a result of MA10 infection. In uninfected mice, genotype does have a significant effect, indicating an increased TUNEL+ cell number in all 3 regions in 5xFAD mice compared to their WT counterparts (Figure 8D).

MA10 infection does not change synapse numbers in the brain of WT or 5xFAD mice at 21 dpi. Considering that there was no overt indication of neuronal death, as an expected decrease in neuron counts, or any evidence of apoptosis as quantified by TUNEL, other approaches to assess neuronal dysfunction were explored. Synaptic puncta were quantified within the same three anatomical regions as described before (CRTX, DG, and SUB) via co-localization of the presynaptic marker, Synaptophysin, and postsynaptic marker PSD95. Representative images of synaptophysin puncta (magenta), and PSD95 positive puncta (turquoise) were acquired for the anatomical regions previously mentioned (Figure 9A-C).

Immunostaining and quantification did not indicate changes in synapse numbers in the brains of either WT or 5xFAD mice at 21 dpi (Figure 9D).

DISCUSSION

While COVID-19 most commonly presents with respiratory symptoms, neurological symptoms have been extensively documented, with symptoms manifesting during the initial period of disease and lasting beyond viral clearance [32–35,37,38,74,75]. The full extent of neuropathological changes in the CNS that results from SARS-COV-2 infection is still not fully understood. Given the association of COVID-19 with neuroinflammation and other neurodegenerative processes, it is imperative that the changes in the CNS resulting from infection and mechanisms contributing to neurodegenerative processes be examined. To accomplish this, this study utilized a novel mouse-adapted SARS-COV-2 (MA10) to infect aged C57BL/6 (WT) mice and a pre-clinical AD mouse model of the same genetic background (5xFAD) to examine the effects on gene expression and characterize neuropathological changes in the brain after chronic infection. This article provides evidence of several findings.

Infection with MA10 elicits mild disease in aged mice, and while mortality was observed in infected animals, it did not differ significantly because of genotype; infected 5xFAD mice did not have a higher mortality rate than WT mice. This was surprising because patients with dementia have been observed to experience more severe clinical disease and increased mortality due to infection. Additionally, among patients with dementia, AD was the most prevalent cognitive impairment observed in those who succumbed to COVID-19 [50–52]. However, the findings indicating higher mortality in patients with pre-existing dementia could be do to a variety of factors not applicable to mice in controlled environments, including an inability to modify behavior to prevent infection, leading to a higher proportion on elderly patients with COVID-19 in comparison to the general population and therefore a higher recorded mortality rate in this population.

Additionally, acute MA10 infection is associated with differential expression of genes involved in modulation of the immune system and inflammatory pathways in lungs of infected mice. In the WT-7dpi group of mice, analysis revealed upregulation in pathways associated with a decrease in immune cell (both B and T cell) proliferation as well upregulation in pathways associated with chemokine and chemokine receptor activity including; CXCL9, CXCL10, CXCL11,CXCL12, CCL2, CCL7, and CCL8, and chemokine receptors such as CXCR3, CCR2. Studies have indicated that COVID-19 leads to immune dysregulation that results from T-cell depletion in the serum [76], as well as a decrease in circulating T cells in the lymph nodes and spleen [77]. Others have noted reduced B cell numbers in serum in COVID-19 as a result of hypoxia [78]. Given this, it was not surprising to find a similar result in the lungs of infected animals. Additionally, chemokines are important inflammatory mediators that aid in the immune response to clear pathogens. Reports also cite a dysregulated immune response defined by elevated chemokine expression profiles [79,80]. Certain chemokines including CCL2, CCL7, CCL8,CXCLl9, have been shown to be elevated in mild cases of COVID-19 as well as CXCL10 in severe disease [81]. CCL2 and CXCL10 are known to inhibit myeloid progenitor cells leading to lymphopenia in other coronavirus infections including SARS-CoV-1 and MERS-CoV [82–84]. CCR2 and CXCR3 have also been shown to be upregulated in MERS-CoV infections [85]. Furthermore they have been reported to be upregulated in other respiratory viruses such as RSV [86]. Analysis in the lungs of both groups on mice also revealed downregulation of pathways associated with insulin-like-growth factor (Igf-1) binding .Other studies have noted that SARS-CoV-2 infection is associated with Igf-1 signaling pathways impairment in a variety of tissues in patients and animal models, and these impairments were associated with excessive interferon responses and more severe COVID-19 [87,88]. It is still unclear if the disrupted immune

regulation persists beyond acute infection, and if these effects are organ or tissue specific. However, our data, at least in infected lung tissue, indicates that these changes in gene expression are only present in the acute phase of infection. As observed in the lungs of infected animals at 21 dpi, there are no significant gene expression changes, as outlined by our criteria.

There is a wide range of memory impairments following COVID-19 noted across studies. Neurological symptoms following infection also include long and short-term memory deficits, impaired visuospatial memory and other memory deficits associated with anxiety [89–91]. Additionally, other studies have linked persistent cognitive impairments to the severity of pulmonary dysfunction and related respiratory symptoms [36,92]. Similar results indicating cognitive impairments have also been reported by other groups utilizing animal models, where memory deficits were observed in infected mice [66]. However, evidence has not yet fully elucidated the molecular or cellular processes involved in the development of impaired cognition and how they may lead to memory dysfunction. Some groups have provided supporting evidence suggesting impaired hippocampal neurogenesis as a possible mechanism leading to memory impairment [65,66].

In this study, the brains of MA10 infected mice in both acute and chronic phases of infection indicated changes in gene expression that were associated with neuronal dysfunction. In the acute phase, RNASeq analysis indicates an upregulation in genes associated with reduced long-term potentiation (LTP) in WT mice, and downregulation genes associated with neuronal plasticity in 5xFAD mice. LTP is a well-characterized form of synaptic plasticity and has been considered as a cellular mechanism underlying learning and memory, and LTP dysfunction is thought to be an underlying cause of memory loss [93]. Therefore it would not be surprising if

impairments in LTP and other genes associated with synaptic plasticity were contributing factors to impaired memory noted in both human and animal studies.

In the chronic MA10 infection, similar pathways associated with neuronal and synaptic dysfunction were seen in the brains of infected 5xFAD mice. The 5xFAD mice surprisingly had significantly more genes affected at 21 dpi in comparison to WT mice. In WT mice, one particular gene of interest associated with three prominent neurodegenerative diseases was still downregulated at 21 dpi, UQCRFS1. Dysfunction of UQCRFS1has been implicated with reduced or disrupted mitochondrial function, [94] and mitochondrial dysfunction has been linked to not only AD, but also PD and HD [95–97]. Interestingly, downregulation of UQCRFS1 has also been directly observed in an ovine HD model as well. [98]

Next, this study aimed to determine whether the gene expression changes indicating neuronal and synaptic dysfunction were also due to, or associated with changes in neuroinflammation or other AD associated pathology. Given that both astrocytes and microglia can contribute to neuroinflammatory and neurodegenerative processes [99–102] changes in astrocyte and microglia number and volume were quantified. MA10 infection did not appear to elicit changes in either astrocyte number or volume, and even though one study has associated infection with trending increases in astrocyte number and increased GFAP expression in the brains of infected laboratory mice [63,67]; however others have not found any significant increases in astrocyte numbers [65,66] . Perhaps it is possible that astrogliosis does occur but only at earlier time points of infection, and returns to pre-infection levels after infection resolves and therefore could not be detected at later time points . In uninfected mice, genotype does have a significant effect, leading to an increased astrocyte number and volume in the cortex of 5xFAD mice. Aβ

plaques are only present in 5xFAD mice and so this result is expected considering that GFAP+ astrocytes numbers are closely linked to Aβ plaque numbers [70].

Furthermore, in uninfected mice, genotype does have a significant effect in leading to an increased microglia number and volume in all 3 regions in 5xFAD mice. Microglia are known to surround dense core plaques, and remain stable in WT mice across their lifespans, but increase in 5xFAD mice, where numbers closely correlate with plaque load [70]. However, the fact that there were no significant changes in microglia number or volume detected was surprising, as many past studies have described increases in microglia number and morphological changes in acute and chronic timepoints [63–67] , suggesting that MA10 infection can elicit long lasting microgliosis. In fact, one particular study has provided evidence that the secretion of the pro-inflammatory cytokine IL-1β by microglia, not neurons or astrocytes, contributes to synaptic loss in the brains of infected mice [65]. IL-1β is associated with impaired neurogenesis and hippocampal dependent memory [103], has been correlated with Aβ accumulation and neurofibrillary tangles (NFTs) [104] and can result in the aberrant release of glutamate that results in neuronal death in many neurodegenerative disease [105] . However, our inability to detect microgliosis here could be due to a variety of factors. The results in the studies described above mostly revealed evidence of microgliosis in acute infections, and in the ones focusing on later time points, significantly higher viral doses and/or different viral variants were used. It is possible that lower infectious doses, like previously described in our methods, are not high enough to elicit neuroinflammation in the brains of infected animals. Additionally, other studies have used different variants of SARS-CoV-2 and there is established evidence that there are differences in symptom and disease severity due to different viral variants [106,107] . This points to the possibility that lower doses of

SARS-CoV-2 do not elicit the same injury to the CNS; shorter periods of gliosis and/or that different pathways of injury that still result in some neuronal dysfunction.

Considering that no evidence of gliosis was found in our experimental animals, other changes in the CNS were considered. As previously stated, peripherally derived monocytes can enter the brain under inflammatory conditions [71–73] and given that the brains of 5xFAD mice are already in a neuroinflammatory state [69,70] it was not surprising that in uninfected mice, genotype does have a significant effect in leading to an increased monocyte number and volume in all 3 regions in 5xFAD mice. Of course, the presence of these cells in the brains of uninfected WT mice has been observed, but they seem to be present mostly in the choroid plexus, not in cortex or hippocampus like 5xFAD mice [73]. In the context of MA10 infection, there is no increase in peripheral monocyte (Mac2+ cells) count or volume in the hippocampus or cortex in either WT or 5xFAD. This could be due to several reasons. It is possible that the lower viral dose used on these mice did not elicit enough neuroinflammation to lead to the infiltration of these Mac2+ cells, or the initial acute inflammation only occurs in the early stages of infection. Therefore, even if Mac2+ cells might have been present during acute infection, their presence might have been only for a short period of time and therefore could not be detected at a later time point.

Taking into consideration that bulkRNASeq analysis of MA10 infected brains indicated neuronal and synaptic dysfunction, we wondered whether dystrophic neurites or Aβ plaque pathology was affected by MA10 infection, given that dystrophic neurites associated with Aβ plaques and can disrupt neuronal function eventually leading to neuronal death [108,109]. MA10 infection did not induce or affect dystrophic neurites or Aβ plaque pathology in WT or 5xFAD mice respectively. We believed MA10 could perhaps affect these given that some coronavirus viral proteins are believed to be amyloidogenic [24] and animal studies indicate that MA10

infection appears to affect other AD-associated pathology including tau [64,67]. Additionally, we believed that perhaps infection might result in decreases in neuron number and other apoptotic cells; however upon analysis this was not the case, but in uninfected mice genotype has a significant effect. However other studies have found similar results, citing no changes in cortical neuron counts in the brains of infected animals, but instead a higher burden of hyperphosphorylated tau especially in regions adjacent to endothelial cells [64,67]. Considering that there was no overt indication of neuronal death, changes in synapse number were examined, however no evidence of synapse loss was found. This could argue that MA10 infection does not induce overt neurodegeneration as there is no rapid change in neuron number or apoptosis, and although no synaptic loss was observed, infection could possibly lead to other detrimental changes in neuronal function with the development of hyperphosphorylated tau as major contributor, which our study did not assess.

In summary, COVID-19 predominantly presents with respiratory symptoms, however neurological manifestations have been extensively documented, persisting even after viral clearance. The neuropathological impact of SARS-CoV-2 on the central nervous system (CNS) remains poorly understood. This study investigates CNS changes and neurodegenerative processes associated with COVID-19 using a mouse-adapted SARS-CoV-2 (MA10) to infect aged laboratory mice. Infected mice displayed differential gene expression in the lungs during acute infection, aligning with observed immune dysregulation in COVID-19 patients/ While changes in the lungs were short lived, changes in the brains were longer lasting but did not translate to changes in neuropathology. These findings underscore the need for further research to elucidate the molecular mechanisms underlying COVID-19-related CNS changes and their long-term impact on neurodegenerative processes.

REFERENCES:

1. De-Paula, V. J., Radanovic, M., Diniz, B. S. & Forlenza, O. V. Alzheimer's Disease. in *Protein Aggregation and Fibrillogenesis in Cerebral and Systemic Amyloid Disease* (ed. Harris, J. R.) 329–352 (Springer Netherlands, Dordrecht, 2012). doi:10.1007/978-94-007-5416-4_14.
2. Henderson, A. S. The risk factors for Alzheimer's disease: a review and a hypothesis. *Acta Psychiatr. Scand.* **78**, 257–275 (1988).
3. Bellenguez, C. *et al.* New insights into the genetic etiology of Alzheimer's disease and related dementias. *Nat. Genet.* **54**, 412–436 (2022).
4. Goate, A. *et al.* Segregation of a missense mutation in the amyloid precursor protein gene with familial Alzheimer's disease. *Nature* **349**, 704–706 (1991).
5. St George-Hyslop, P. *et al.* Genetic evidence for a novel familial Alzheimer's disease locus on chromosome 14. *Nat. Genet.* **2**, 330–334 (1992).
6. Sherrington, R. *et al.* Alzheimer's Disease Associated with Mutations in Presenilin 2 is Rare and Variably Penetrant. *Hum. Mol. Genet.* **5**, 985–988 (1996).
7. Kim, J., Basak, J. M. & Holtzman, D. M. The Role of Apolipoprotein E in Alzheimer's Disease. *Neuron* **63**, 287–303 (2009).
8. Newman, A. B. *et al.* Dementia and Alzheimer's disease incidence in relationship to cardiovascular disease in the Cardiovascular Health Study cohort. *J. Am. Geriatr. Soc.* **53**, 1101–1107 (2005).
9. Alford, S., Patel, D., Perakakis, N. & Mantzoros, C. S. Obesity as a risk factor for Alzheimer's disease: weighing the evidence. *Obes. Rev.* **19**, 269–280 (2018).
10. Lee, H. J. *et al.* Diabetes and Alzheimer's Disease: Mechanisms and Nutritional Aspects.

Clin. Nutr. Res. **7**, 229–240 (2018).

11. Moulton, P. V. & Yang, W. Air Pollution, Oxidative Stress, and Alzheimer's Disease. *J. Environ. Public Health* **2012**, 472751 (2012).
12. Hu, N. *et al.* Nutrition and the Risk of Alzheimer's Disease. *BioMed Res. Int.* **2013**, e524820 (2013).
13. Ramos-Cejudo, J. *et al.* Traumatic Brain Injury and Alzheimer's Disease: The Cerebrovascular Link. *EBioMedicine* **28**, 21–30 (2018).
14. Huat, T. J. *et al.* Metal Toxicity Links to Alzheimer's Disease and Neuroinflammation. *J. Mol. Biol.* **431**, 1843–1868 (2019).
15. Levine, K. S. *et al.* Virus exposure and neurodegenerative disease risk across national biobanks. *Neuron* **111**, 1086-1093.e2 (2023).
16. Lotz, S. K., Blackhurst, B. M., Reagin, K. L. & Funk, K. E. Microbial Infections Are a Risk Factor for Neurodegenerative Diseases. *Front. Cell. Neurosci.* **15**, 691136 (2021).
17. Carbone, I. *et al.* Herpes virus in Alzheimer's disease: relation to progression of the disease. *Neurobiol. Aging* **35**, 122–129 (2014).
18. Dhingra, V., Li, Q., Allison, A. B., Stallknecht, D. E. & Fu, Z. F. Proteomic Profiling and Neurodegeneration in West-Nile-Virus-Infected Neurons. *J. Biomed. Biotechnol.* **2005**, 271–279 (2005).
19. Esiri, M. M., Biddolph, S. C. & Morris, C. S. Prevalence of Alzheimer plaques in AIDS. *J. Neurol. Neurosurg. Psychiatry* **65**, 29–33 (1998).
20. Little, C. S., Hammond, C. J., MacIntyre, A., Balin, B. J. & Appelt, D. M. Chlamydia pneumoniae induces Alzheimer-like amyloid plaques in brains of BALB/c mice. *Neurobiol. Aging* **25**, 419–429 (2004).

21. Miklossy, J. Historic evidence to support a causal relationship between spirochetal infections and Alzheimer's disease. *Front. Aging Neurosci.* **7**, 46 (2015).

22. Miklossy, J. *et al.* Beta-amyloid deposition and Alzheimer's type changes induced by Borrelia spirochetes. *Neurobiol. Aging* **27**, 228–236 (2006).

23. Chevalier, C. *et al.* PB1-F2 Influenza A Virus Protein Adopts a β-Sheet Conformation and Forms Amyloid Fibers in Membrane Environments. *J. Biol. Chem.* **285**, 13233–13243 (2010).

24. Ghosh, A. *et al.* Self-assembly of a nine-residue amyloid-forming peptide fragment of SARS corona virus E-protein: mechanism of self aggregation and amyloid-inhibition of hIAPP. *Biochemistry* **54**, 2249–2261 (2015).

25. Pham, C. L. *et al.* Viral M45 and necroptosis-associated proteins form heteromeric amyloid assemblies. *EMBO Rep.* **20**, e46518 (2019).

26. Solomon, M. & Liang, C. Human coronaviruses: The emergence of SARS-CoV-2 and management of COVID-19. *Virus Res.* **319**, 198882 (2022).

27. COVID - Coronavirus Statistics - Worldometer. https://www.worldometers.info/coronavirus/.

28. Huang, C. *et al.* Clinical features of patients infected with 2019 novel coronavirus in Wuhan, China. *The Lancet* **395**, 497–506 (2020).

29. Guan, W. *et al.* Clinical Characteristics of Coronavirus Disease 2019 in China. *N. Engl. J. Med.* **382**, 1708–1720 (2020).

30. Diamond, M., Peniston, H. L., Sanghavi, D. & Mahapatra, S. Acute Respiratory Distress Syndrome. in *StatPearls* (StatPearls Publishing, Treasure Island (FL), 2022).

31. Chen, T. *et al.* Clinical characteristics of 113 deceased patients with coronavirus disease

2019: retrospective study. *BMJ* **368**, m1091 (2020).

32. Harapan, B. N. & Yoo, H. J. Neurological symptoms, manifestations, and complications associated with severe acute respiratory syndrome coronavirus 2 (SARS-CoV-2) and coronavirus disease 19 (COVID-19). *J. Neurol.* **268**, 3059–3071 (2021).
33. Johansson, A., Mohamed, M. S., Moulin, T. C. & Schiöth, H. B. Neurological manifestations of COVID-19: A comprehensive literature review and discussion of mechanisms. *J. Neuroimmunol.* **358**, 577658 (2021).
34. Mao, L. *et al.* Neurologic Manifestations of Hospitalized Patients With Coronavirus Disease 2019 in Wuhan, China. *JAMA Neurol.* **77**, 683–690 (2020).
35. Zubair, A. S. *et al.* Neuropathogenesis and Neurologic Manifestations of the Coronaviruses in the Age of Coronavirus Disease 2019 A Review. *JAMA Neurol.* **77**, 1018–1027 (2020).
36. Liotta, E. M. *et al.* Frequent neurologic manifestations and encephalopathy-associated morbidity in Covid-19 patients. *Ann. Clin. Transl. Neurol.* **7**, 2221–2230 (2020).
37. Cooper, K. W. *et al.* COVID-19 and the Chemical Senses: Supporting Players Take Center Stage. *Neuron* **107**, 219–233 (2020).
38. Karadaş, Ö., Öztürk, B. & Sonkaya, A. R. A prospective clinical study of detailed neurological manifestations in patients with COVID-19. *Neurol. Sci. Off. J. Ital. Neurol. Soc. Ital. Soc. Clin. Neurophysiol.* **41**, 1991–1995 (2020).
39. Duong, L., Xu, P. & Liu, A. Meningoencephalitis without respiratory failure in a young female patient with COVID-19 infection in Downtown Los Angeles, early April 2020. *Brain. Behav. Immun.* **87**, 33 (2020).
40. Fan, H., Tang, X., Song, Y., Liu, P. & Chen, Y. Influence of COVID-19 on Cerebrovascular Disease and its Possible Mechanism. *Neuropsychiatr. Dis. Treat.* **16**, 1359–1367 (2020).

41. Favas, T. T. *et al.* Neurological manifestations of COVID-19: a systematic review and meta-analysis of proportions. *Neurol. Sci. Off. J. Ital. Neurol. Soc. Ital. Soc. Clin. Neurophysiol.* **41**, 3437–3470 (2020).

42. Lyons, S. *et al.* Seizure with CSF lymphocytosis as a presenting feature of COVID-19 in an otherwise healthy young man. *Seizure* **80**, 113–114 (2020).

43. Merkler, A. E. *et al.* Risk of Ischemic Stroke in Patients With Coronavirus Disease 2019 (COVID-19) vs Patients With Influenza. *JAMA Neurol.* (2020) doi:10.1001/jamaneurol.2020.2730.

44. Moriguchi, T. *et al.* A first case of meningitis/encephalitis associated with SARS-Coronavirus-2. *Int. J. Infect. Dis. IJID Off. Publ. Int. Soc. Infect. Dis.* **94**, 55–58 (2020).

45. Sohal, S. & Mansur, M. COVID-19 Presenting with Seizures. *IDCases* **20**, e00782 (2020).

46. Tang, N., Li, D., Wang, X. & Sun, Z. Abnormal coagulation parameters are associated with poor prognosis in patients with novel coronavirus pneumonia. *J. Thromb. Haemost. JTH* **18**, 844–847 (2020).

47. Chen, Y. *et al.* Aging in COVID-19: Vulnerability, immunity and intervention. *Ageing Res. Rev.* **65**, 101205 (2021).

48. Mueller, A. L., McNamara, M. S. & Sinclair, D. A. Why does COVID-19 disproportionately affect older people? *Aging* **12**, 9959–9981 (2020).

49. O'Driscoll, M. *et al.* Age-specific mortality and immunity patterns of SARS-CoV-2. *Nature* **590**, 140–145 (2021).

50. Atkins, J. L. *et al.* Preexisting Comorbidities Predicting COVID-19 and Mortality in the UK Biobank Community Cohort. *J. Gerontol. A. Biol. Sci. Med. Sci.* **75**, 2224–2230 (2020).

51. Wang, Q., Davis, P. B., Gurney, M. E. & Xu, R. COVID-19 and dementia: Analyses of risk, disparity, and outcomes from electronic health records in the US. *Alzheimers Dement. J. Alzheimers Assoc.* **17**, 1297–1306 (2021).

52. Martín-Jiménez, P. *et al.* Cognitive Impairment Is a Common Comorbidity in Deceased COVID-19 Patients: A Hospital-Based Retrospective Cohort Study. *J. Alzheimers Dis. JAD* **78**, 1367–1372 (2020).

53. de Souza Rolim, T. *et al.* Oral infections and orofacial pain in Alzheimer's disease: a case-control study. *J. Alzheimers Dis. JAD* **38**, 823–829 (2014).

54. Bhardwaj, T. *et al.* Amyloidogenic proteins in the SARS-CoV and SARS-CoV-2 proteomes. *Nat. Commun.* **14**, 945 (2023).

55. Kiraly, M., Foss, J. F. & Giordano, T. Neuroinflammation, Its Role in Alzheimer's Disease and Therapeutic Strategies. *J. Prev. Alzheimers Dis.* **10**, 686–698 (2023).

56. Singh, M., Bansal, V. & Feschotte, C. A Single-Cell RNA Expression Map of Human Coronavirus Entry Factors. *Cell Rep.* **32**, 108175 (2020).

57. Chen, R. *et al.* The spatial and cell-type distribution of SARS-CoV-2 receptor ACE2 in human and mouse brain. 2020.04.07.030650 Preprint at https://doi.org/10.1101/2020.04.07.030650 (2020).

58. Cama, V. F. *et al.* The microglial NLRP3 inflammasome is involved in human SARS-CoV-2 cerebral pathogenicity: A report of three post-mortem cases. *J. Neuroimmunol.* **361**, 577728 (2021).

59. de Melo, G. D. *et al.* COVID-19–related anosmia is associated with viral persistence and inflammation in human olfactory epithelium and brain infection in hamsters. *Sci. Transl. Med.* **13**, eabf8396 (2021).

60. Matschke, J. *et al.* Neuropathology of patients with COVID-19 in Germany: a post-mortem case series. *Lancet Neurol.* **19**, 919–929 (2020).

61. Bellon, M. *et al.* Cerebrospinal Fluid Features in Severe Acute Respiratory Syndrome Coronavirus 2 (SARS-CoV-2) Reverse Transcription Polymerase Chain Reaction (RT-PCR) Positive Patients. *Clin. Infect. Dis. Off. Publ. Infect. Dis. Soc. Am.* **73**, e3102–e3105 (2021).

62. Schwabenland, M. *et al.* Deep spatial profiling of human COVID-19 brains reveals neuroinflammation with distinct microanatomical microglia-T-cell interactions. *Immunity* **54**, 1594-1610.e11 (2021).

63. Amruta, N. *et al.* Mouse Adapted SARS-CoV-2 (MA10) Viral Infection Induces Neuroinflammation in Standard Laboratory Mice. *Viruses* **15**, 114 (2022).

64. Käufer, C. *et al.* Microgliosis and neuronal proteinopathy in brain persist beyond viral clearance in SARS-CoV-2 hamster model. *EBioMedicine* **79**, 103999 (2022).

65. Klein, R. *et al.* COVID-19 induces neuroinflammation and loss of hippocampal neurogenesis. *Res. Sq.* rs.3.rs-1031824 (2021) doi:10.21203/rs.3.rs-1031824/v1.

66. Vanderheiden, A. *et al.* Vaccination prevents IL-1β-mediated cognitive deficits after COVID-19. *Res. Sq.* rs.3.rs-3353171 (2023) doi:10.21203/rs.3.rs-3353171/v1.

67. Green, R. *et al.* SARS-CoV-2 infection increases the gene expression profile for Alzheimer's disease risk. *Mol. Ther. Methods Clin. Dev.* **27**, 217–229 (2022).

68. Olivarria, G. M. *et al.* Microglia Do Not Restrict SARS-CoV-2 Replication following Infection of the Central Nervous System of K18-Human ACE2 Transgenic Mice. *J. Virol.* **96**, e0196921 (2022).

69. Oakley, H. *et al.* Intraneuronal β-Amyloid Aggregates, Neurodegeneration, and Neuron Loss in Transgenic Mice with Five Familial Alzheimer's Disease Mutations: Potential

Factors in Amyloid Plaque Formation. *J. Neurosci.* **26**, 10129–10140 (2006).

70. Forner, S. *et al.* Systematic phenotyping and characterization of the 5xFAD mouse model of Alzheimer's disease. *Sci. Data* **8**, 270 (2021).
71. Ajami, B. *et al.* Single-cell mass cytometry reveals distinct populations of brain myeloid cells in mouse neuroinflammation and neurodegeneration models. *Nat. Neurosci.* **21**, 541–551 (2018).
72. Jordão, M. J. C. *et al.* Single-cell profiling identifies myeloid cell subsets with distinct fates during neuroinflammation. *Science* **363**, eaat7554 (2019).
73. Hohsfield, L. A. *et al.* MAC2 is a long-lasting marker of peripheral cell infiltrates into the mouse CNS after bone marrow transplantation and coronavirus infection. *Glia* **70**, 875–891 (2022).
74. Keyhanian, K. *et al.* SARS-CoV-2 and nervous system: From pathogenesis to clinical manifestation. *J. Neuroimmunol.* **350**, 577436 (2020).
75. Butt, I., Sawlani, V. & Geberhiwot, T. Prolonged confusional state as first manifestation of COVID-19. *Ann. Clin. Transl. Neurol.* **7**, 1450–1452 (2020).
76. Zhang, W. *et al.* The use of anti-inflammatory drugs in the treatment of people with severe coronavirus disease 2019 (COVID-19): The Perspectives of clinical immunologists from China. *Clin. Immunol. Orlando Fla* **214**, 108393 (2020).
77. Xu, Z. *et al.* Pathological findings of COVID-19 associated with acute respiratory distress syndrome. *Lancet Respir. Med.* **8**, 420–422 (2020).
78. Kotagiri, P. *et al.* The impact of hypoxia on B cells in COVID-19. *eBioMedicine* **77**, (2022).
79. Channappanavar, R. & Perlman, S. Pathogenic human coronavirus infections: causes and consequences of cytokine storm and immunopathology. *Semin. Immunopathol.* **39**, 529–539

(2017).

80. Lowery, S. A., Sariol, A. & Perlman, S. Innate immune and inflammatory responses to SARS-CoV-2: Implications for COVID-19. *Cell Host Microbe* **29**, 1052–1062 (2021).

81. Khalil, B. A., Elemam, N. M. & Maghazachi, A. A. Chemokines and chemokine receptors during COVID-19 infection. *Comput. Struct. Biotechnol. J.* **19**, 976–988 (2021).

82. Zhou, J. *et al.* Active replication of Middle East respiratory syndrome coronavirus and aberrant induction of inflammatory cytokines and chemokines in human macrophages: implications for pathogenesis. *J. Infect. Dis.* **209**, 1331–1342 (2014).

83. Broxmeyer, H. E. *et al.* Comparative analysis of the human macrophage inflammatory protein family of cytokines (chemokines) on proliferation of human myeloid progenitor cells. Interacting effects involving suppression, synergistic suppression, and blocking of suppression. *J. Immunol. Baltim. Md 1950* **150**, 3448–3458 (1993).

84. Peiris, J. S. M., Guan, Y. & Yuen, K. Y. Severe acute respiratory syndrome. *Nat. Med.* **10**, S88-97 (2004).

85. Jafarzadeh, A., Chauhan, P., Saha, B., Jafarzadeh, S. & Nemati, M. Contribution of monocytes and macrophages to the local tissue inflammation and cytokine storm in COVID-19: Lessons from SARS and MERS, and potential therapeutic interventions. *Life Sci.* **257**, 118102 (2020).

86. Morrison, P. T. *et al.* Chemokine-receptor upregulation and disease severity in respiratory syncytial virus infection. *Clin. Immunol. Orlando Fla* **128**, 85–93 (2008).

87. Shin, J. *et al.* SARS-CoV-2 infection impairs the insulin/IGF signaling pathway in the lung, liver, adipose tissue, and pancreatic cells via IRF1. *Metab. - Clin. Exp.* **133**, (2022).

88. Hazrati, E. *et al.* The effect of IGF-1 plasma concentration on COVID-19 severity. *Microb.*

Pathog. **164**, 105416 (2022).

89. Llana, T., Zorzo, C., Mendez-Lopez, M. & Mendez, M. Memory alterations after COVID-19 infection: a systematic review. *Appl. Neuropsychol. Adult* **31**, 292–305 (2024).
90. Beaud, V. *et al.* Pattern of cognitive deficits in severe COVID-19. *J. Neurol. Neurosurg. Psychiatry* **92**, 567–568 (2021).
91. Jaywant, A. *et al.* Frequency and profile of objective cognitive deficits in hospitalized patients recovering from COVID-19. *Neuropsychopharmacol. Off. Publ. Am. Coll. Neuropsychopharmacol.* **46**, 2235–2240 (2021).
92. Miskowiak, K. W. *et al.* Cognitive impairments four months after COVID-19 hospital discharge: Pattern, severity and association with illness variables. *Eur. Neuropsychopharmacol. J. Eur. Coll. Neuropsychopharmacol.* **46**, 39–48 (2021).
93. Malenka, R. C. & Nicoll, R. A. Long-term potentiation--a decade of progress? *Science* **285**, 1870–1874 (1999).
94. Giannos, P., Prokopidis, K., Raleigh, S. M., Kelaiditi, E. & Hill, M. Altered mitochondrial microenvironment at the spotlight of musculoskeletal aging and Alzheimer's disease. *Sci. Rep.* **12**, 11290 (2022).
95. Wang, W., Zhao, F., Ma, X., Perry, G. & Zhu, X. Mitochondria dysfunction in the pathogenesis of Alzheimer's disease: recent advances. *Mol. Neurodegener.* **15**, 30 (2020).
96. Toomey, C. E. *et al.* Mitochondrial dysfunction is a key pathological driver of early stage Parkinson's. *Acta Neuropathol. Commun.* **10**, 134 (2022).
97. Quintanilla, R. A. & Johnson, G. V. W. Role of Mitochondrial Dysfunction in the Pathogenesis of Huntington's Disease. *Brain Res. Bull.* **80**, 242–247 (2009).
98. Jiang, A. *et al.* Evidence for glutamate excitotoxicity that occurs before the onset of striatal

cell loss and motor symptoms in an ovine Huntington's Disease model. 2023.06.20.545648 Preprint at https://doi.org/10.1101/2023.06.20.545648 (2023).

99. González-Reyes, R. E., Nava-Mesa, M. O., Vargas-Sánchez, K., Ariza-Salamanca, D. & Mora-Muñoz, L. Involvement of Astrocytes in Alzheimer's Disease from a Neuroinflammatory and Oxidative Stress Perspective. *Front. Mol. Neurosci.* **10**, 427 (2017).

100. Wang, W.-Y., Tan, M.-S., Yu, J.-T. & Tan, L. Role of pro-inflammatory cytokines released from microglia in Alzheimer's disease. *Ann. Transl. Med.* **3**, 136 (2015).

101. Shao, Y., Gearing, M. & Mirra, S. S. Astrocyte-apolipoprotein E associations in senile plaques in Alzheimer disease and vascular lesions: a regional immunohistochemical study. *J. Neuropathol. Exp. Neurol.* **56**, 376–381 (1997).

102. McGeer, P. L., Itagaki, S., Tago, H. & McGeer, E. G. Reactive microglia in patients with senile dementia of the Alzheimer type are positive for the histocompatibility glycoprotein HLA-DR. *Neurosci. Lett.* **79**, 195–200 (1987).

103. Garber, C. *et al.* Astrocytes decrease adult neurogenesis during virus-induced memory dysfunction via IL-1. *Nat. Immunol.* **19**, 151–161 (2018).

104. Griffin, W. S. T. & Mrak, R. E. Interleukin-1 in the genesis and progression of and risk for development of neuronal degeneration in Alzheimer's disease. *J. Leukoc. Biol.* **72**, 233–238 (2002).

105. Bading, H. Therapeutic targeting of the pathological triad of extrasynaptic NMDA receptor signaling in neurodegenerations. *J. Exp. Med.* **214**, 569–578 (2017).

106. Arabi, M. *et al.* Severity of the Omicron SARS-CoV-2 variant compared with the previous lineages: A systematic review. *J. Cell. Mol. Med.* **27**, 1443–1464 (2023).

107. Qiu, Y. *et al.* Comparison of the disease severity with infection of severe acute respiratory syndrome coronavirus 2 (SARS-CoV-2) Delta and Omicron variants: A meta-analysis. *MedComm – Future Med.* **2**, e39 (2023).

108. Sanchez-Varo, R. *et al.* Abnormal accumulation of autophagic vesicles correlates with axonal and synaptic pathology in young Alzheimer's mice hippocampus. *Acta Neuropathol. (Berl.)* **123**, 53–70 (2012).

109. Tsering, W. & Prokop, S. Neuritic Plaques — Gateways to Understanding Alzheimer's Disease. *Mol. Neurobiol.* **61**, 2808–2821 (2024).

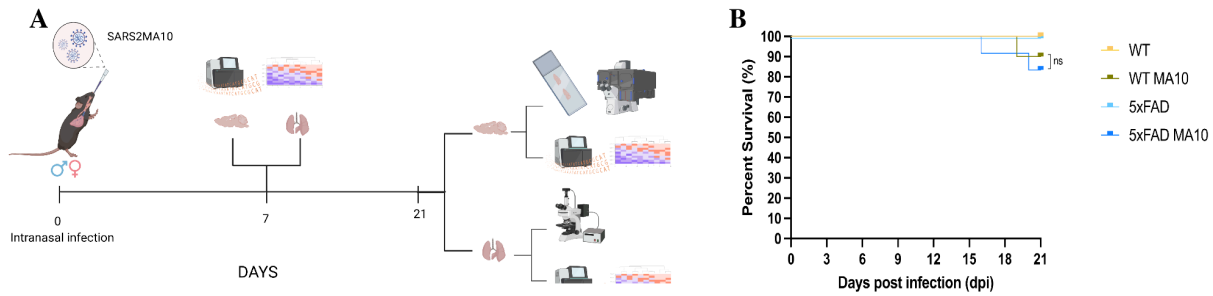
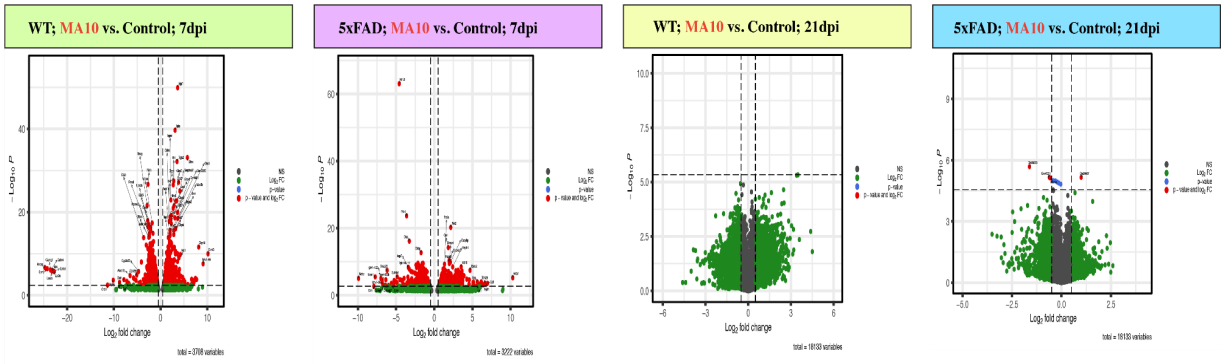
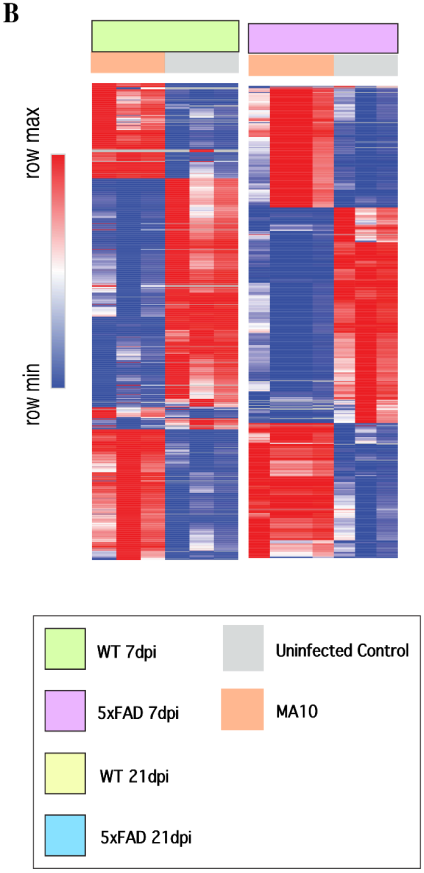


Figure 1. MA10 infection elicits mild disease in infected mice and genotype does not affect mortality. (A) Schematic depicting experimental setup. Male and female 10-14 month-old WT and 5xFAD mice were intranasally infected with a dose of 5 x103 PFU of SARS-CoV-2 MA10 (MA10) and lungs and brains harvested at 7 and 21 days post infection (dpi). (B) Percent survival of uninfected WT and 5xFAD and their MA10 infected counterparts shows that genotype (WT vs. 5xFAD) does not affect percent survival of infected mice.

A



B



C

WT; MA10 vs. Control; 7dpi

Table of significant pathways of interest for Mammalian Phenotype

term	genes
Decreased CD8-positive, alpha-beta T cell number MP:0008079	CD274, PLAG1, NLRC5, ITGAL, ETS1, DLL1, ADAM28, BCLAF1, CXCR2, JAK3, PRKCH, STAT1, STAT2, THEMIS, TAP1, VAV1, PSMB9, CXCL10, CDK6, PTPRC, CD8A, LCK, IRF1, IL2RB, FAS, MDM4, LCP2
Decreased T cell proliferation MP:0005095	PRKCH, THEMIS, ITGAL, ETS1, VAV1, BCLAF1, RAP1A, CDK6, PTPRC, LCK, IMPDH1, BCL6B, IL2RB, LEPR, LCP2, CCR5, JAK3, LAT, CCR2
Decreased B cell number MP:0005017	[PRKCH, ITGA4, STAT1, ITGAL, ETS1, FLI1, ARNTL, RASGRP3, DOCK10, PTPRC, FUBP1, KIT, CXCR2, BCL3, IL2RB, S1PR1, FAS, CYCS, TRIB2, JAK3, MYBL1, SH2B3

Table of significant pathways of interest for GO Molecular Function

term	genes
Insulin-Like Growth Factor II Binding (GO:0031995)	IGFBP5, IGFBP4, IGFBP3, IGFBP2, IGFBP6
Insulin-Like Growth Factor I Binding (GO:0031994)	IGFBP5, IGFBP4, IGFBP3, IGFBP2, IGFBP6, LRP2
Insulin-Like Growth Factor Binding (GO:0005520)	IGFBP5, IGFBP4, IGFBP3, IGFBP2, LRP2, IGFBP6
Chemokine Activity (GO:0008009)	CXCL10, CXCL9, CXCL11, CCL8, CXCL12, CCL7, CCL2
Chemokine Receptor Activity (GO:0004950)	CXCR3, CXCR2, CCR5, CCR2

D

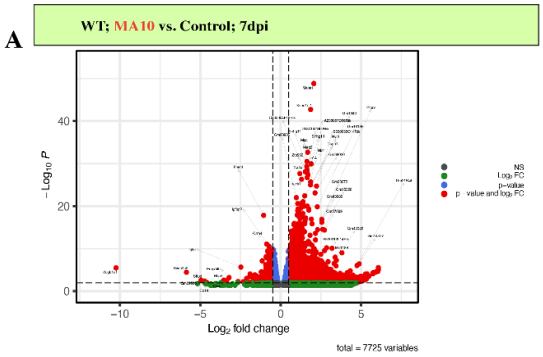
5xFAD; MA10 vs. Control; 7dpi

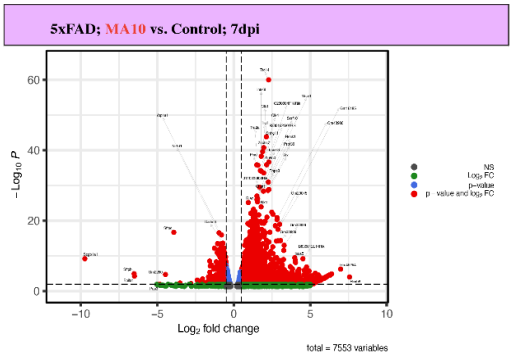
Table of significant pathways of interest for GO Molecular Function

term	genes
Insulin-Like Growth Factor I Binding (GO:0031994)	IGFBP4, ITGB4, IGFBP6
Insulin-Like Growth Factor Binding (GO:0005520)	IGFBP4, ITGB4, IGFBP6
Insulin-Like Growth Factor II Binding (GO:0031995)	IGFBP4, IGFBP6

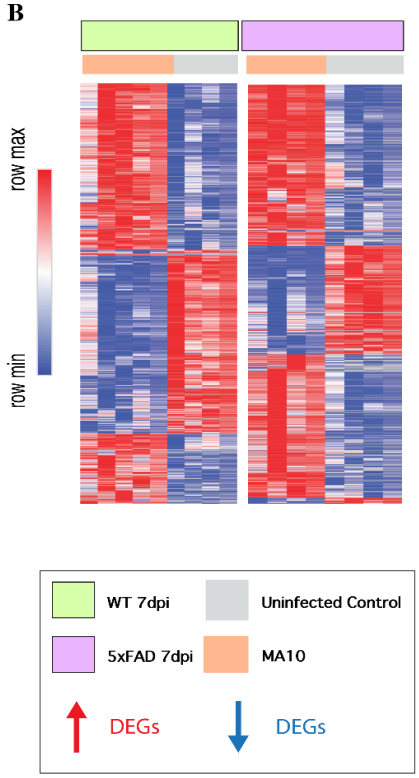
Figure 2. MA10 infection in lungs of WT and 5xFAD mice is associated with differential expression of genes involved in modulation of immune system responses and other inflammatory pathways. RNA sequencing was performed on lungs from SARS-CoV2-MA10 (MA10) infected 12 month- old wild-type (WT) and 5xFAD male mice at 7 and 21 days post infection (dpi). (A) Volcano plot of differentially expressed genes (DEG) displaying fold change (FC) of genes (log2 scale) and P values (various time points; WT-7dpi, 5xFAD-7dpi, WT-21dpi, and 5xFAD-21dpi. (B) Heatmap of selected (FC=0.5, FDR<0.05) DEG from WT MA10 infected and 5xFAD MA10 infected mice versus uninfected controls at 7dpi. Colors corresponding to upregulation (red) and downregulation (blue).

A





B



C

WT; MA10 vs. Control; 7dpi

Table of significant pathways of interest for GO Molecular Function

term	genes
Voltage-Gated Calcium Channel Activity (GO:0005245)	RYR1, CACNA2D1, CACNA1B, CACNA1D, CACNA1C, OPRM1, CACNA1F, PKD2, CACNA1E, CACNA1H, CACNB4, SCN9A, SCN7A, SCN3A
Neurotransmitter Receptor Activity Involved In Regulation Of Postsynaptic Membrane Potential (GO:0099529)	GABRA2, GRIA2, GRIN2A, GRIK2, GRIN2B, GRIA3

Table of significant pathways of interest for Mammalian Phenotype

term	genes
Abnormal operant conditioning behavior MP:0002803	GABRB1, HTR1B, DRD1, OPRM1, GRIN2B
Reduced long term potentiation MP:0001473	SLC24A2, TRPC5, MBNL2, DGKB, BDNF, ROCK2, FMR1, ATRX, CACNA1B, UBE3A, GRIK2, OPRM1, AKAP5, GRIN2B, SHISA7, CCDC88A, GRIN2A, GRM5, CREB1, NETO1, ST8SIA4, RARB
Abnormal hippocampal mossy fiber morphology MP:0002761	KCNJ6, FMR1, LRRK2, DCX, PLXNA2, LYST, PLXNA3

D

5xFAD; MA10 vs. Control; 7dpi

Table of significant pathways of interest for Mammalian Phenotype

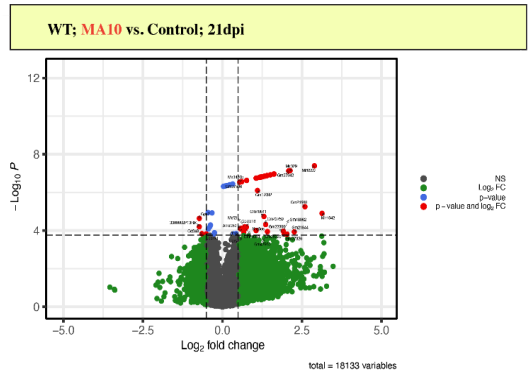
term	genes
Abnormal inhibitory postsynaptic currents MP:0002945	CHRM3, GABBR2, DAGLA, SLC32A1, SYT1, CHRNA4, NRXN2, DNM1, LRFN3, SV2A, NOVA2, CSPG5, LHX6, PIP5K1C, GABRD, PACSIN1
Abnormal miniature inhibitory postsynaptic currents MP:0009435	BCKDK, IGSF21, NLGN2, CLSTN3, KCTD13, ATP1A3, LHX6, TBR1, REM2, ATP6V0A1, PACSIN1
Abnormal miniature excitatory postsynaptic currents MP:0004753	SYT1, CLSTN3, DNM1, SCAMP5, LRFN3, CACNG8, LRFN4, GPRIN1, KCTD13, SLC17A7, PIP5K1C, VAMP2, REM2, ATP6V0A1, PACSIN1
Abnormal cholinergic neuron morphology MP:0001038	ACVRL1, NGFR, ARX, LMNA, LHX8
Impaired coordination MP:0001405	RTN4R, CAMK2B, BARHL2, PPM1L, NXPH3, ARX, SEZ6, CEND1, ATP1A3, RGS4, CALB2, NEUROD2, GRM2, BRINP1, EFNB3, NAGLU, FRZB, LMNA, PSAP, NKX2-1, SLC17A7, WASF1, EMD, LRRC4B, CADPS2, GAA, EN2, SEZ6L, TUBB4A, BCKDK, OLFM2, SLC7A8, GPRIN1, EEF1A2, CBLN1
Increased anxiety-related response MP:0001363	APP, CHRNA4, ARX, NAB2, IGHMBP2, NRXN2, PDXP, EMC10, ATP1A1, SPPL3, NEUROD2, NAGLU, PLAU, SLITRK1, NPY, PENK, SLC17A7, GABRD, GABBR2, CADPS2, KCNIP3, TBR1, SEZ6L, ADORA2A, DNAJC30, ITM2C

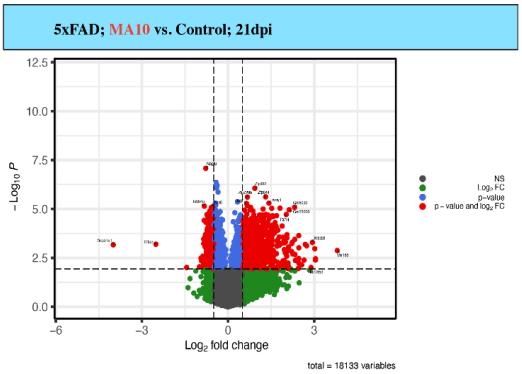
Table of significant pathways of interest for GO Biological Processes

term	genes
Regulation Of Neurotransmitter Receptor Activity (GO:0099601)	PRRT1, APP, NLGN2, SHISA8, CACNG7, CACNG8, PTK2B, NPTX1, DLGAP3, NPTX2, NPTXR, CNIH3, CACNG5
Chemical Synaptic Transmission (GO:0007268)	CHRM3, NLGN2, CHRNA4, STXBP1, CHRM4, NRXN2, SLC1A6, HAPLN4, GRM2, GRM4, RPS6KA1, PENK, SLC17A7, NPTX1, NPTX2, SNCB, GABRD, SYT5, GABBR2, PTPRN2, SLC32A1, SYT1, GRID1, PDYN, HTR5A, SYN1, GRIN1, CORT, TH, SST, GIPC1, KCNK3, SCN2B, CBLN1
Regulation Of Neuronal Synaptic Plasticity (GO:0048168)	CAMK2B, APP, SYNGR1, RAB3A, NCDN, SYP, NOL3, EPHB2, SHISA8, SLC8A2, GRIN1
Axonogenesis (GO:0007409)	EPHB6, SEMA6B, APP, LYPLA2, SEMA7A, RAB3A, EPHA8, MAP1S, APLP1, SEMA4C, WNT7A, CCK, MYPN, NELL2, EFNB1, NELL1, EFNA3, EFNB3, EFNA2, TUBB3, SLITRK1, EPHB2, LGR6, SCN1B

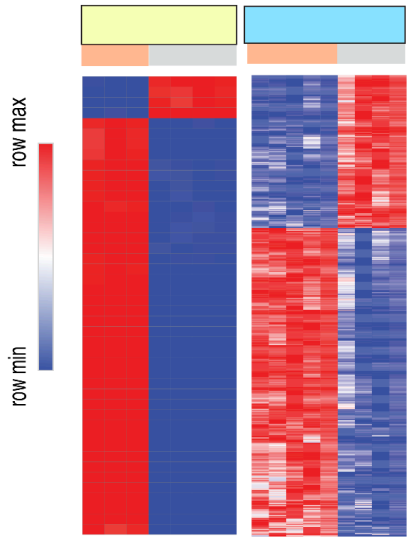
Figure 3. MA10 infection in brains of WT and 5xFAD mice is associated with differential expression of genes involved in regulation of synaptic activity at 7dpi. RNA sequencing was performed on brains from SARS-CoV2-MA10 (MA10) infected 12 month- old wild-type (WT) and 5xFAD male mice at 7 days post infection (dpi). (A) Volcano plot of differentially expressed genes (DEG) displaying fold change of genes (log2 scale) and P values (5xFAD-7dpi. (B) Heatmap of selected (FC=0.5, FDR<0.05) DEGs from WT MA10 infected and 5xFAD MA10 infected mice versus uninfected controls at 7dpi respectively. Tables displaying associated genes with (C) enriched pathways of interest examined via GO enrichment in WT MA10 and other enriched pathways of interest in (D) 5xFAD MA10 infected mice versus uninfected controls at 7dpi. Colors corresponding to upregulation (red) and downregulation (blue).

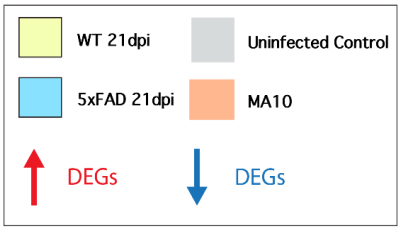
A





B





C

WT; MA10 vs. Control; 21dpi

Table of significant Enriched pathways of interest

term	genes
Parkinson's disease	UQCRFS1
Alzheimer's disease	UQCRFS1
Huntington's disease	UQCRFS1

D

5xFAD; MA10 vs. Control; 21dpi

Table of significant pathways of interest for Mammalian Phenotype

term	genes
Abnormal neuron physiology MP:0004811	NTRK1, GRN, GPR37, GPR88, ATP1A3, TBR1, SORCS2, CLN6, SLC8A2, STX1B, TUBA1A, GPRIN1, PSAP, ORAI1, DRD2, WASF1, HCN2
Abnormal CNS synaptic transmission MP:0002206	SYT2, DAGLA, GPR37, CLSTN1, SEZ6, ATP1A3, DOC2B, DNM1, SLC8A2, STX1B, SLC17A7, DRD2, WASF1, VAMP2, REM2
Abnormal excitatory postsynaptic currents MP:0002910	PRKCG, APP, GABBR2, DAGLA, SYT2, CLSTN1, GPR88, SEZ6, TBR1, MAPK8IP2, STX1B, DNER, SLC17A7, DRD2, LRRC4B
Abnormal inhibitory postsynaptic currents MP:0002945	GABBR2, DAGLA, GPR37, SYT2, SLC32A1, CHRNA4, GPR88, NRXN2, DOC2B, DNM1, LRFN3, SV2A, NOVA2
impaired coordination MP:0001405	CSF1R, GRN, PPM1L, GPR88, SEZ6, CEND1, ATP1A3, ADCY5, RGS4, NAGLU, DNER, PSAP, SLC17A7, DRD2, WASF1, LRRC4B, GPR37, SYT2, KCNJ11, GAA, ATP2B2, ATP1B2, MAPK8IP2, SEZ6L, SSTR2, TUBB4A, BCKDK, FA2H, OLFM2, SLC7A8, GPRIN1, EEF1A2, GARS, HCN2
increased anxiety-related response MP:0001363	APP, GABBR2, CSF1R, GRN, KCNJ11, CHRNA4, WFS1, NRXN2, EMC10, TBR1, ATP1A1, COMT, SEZ6L, SSTR2, SPPL3, NAGLU, ADORA2A, PLAU, DNAJC30, SLITRK1, PENK, MAP6, SLC17A7

Table of significant pathways of interest for GO Biological Processes

term	genes
Synapse Organization (GO:0050808)	KIRREL3, C1QB, CX3CR1, APP, NLGN2, DCTN1, WNT7B, NRXN2, CX3CL1, SLC8A2, SLITRK1, SPOCK2, DNER, GPC4, DRD2, SNCB, LRRC4B
Chemical Synaptic Transmission (GO:0007268)	CHRNB2, SYT5, GABBR2, PTPRN2, NLGN2, SLC32A1, CNP, CHRNA4, GRID1, STXBP1, NRXN2, SLC1A4, PDYN, HAPLN4, SYN1, GRIN1, SST, PENK, SLC17A7, NPTX1, DRD2, NPTX2, SNCB, SCN2B
Regulation Of Neuronal Synaptic Plasticity (GO:0048168)	APP, SYNGR1, RAB3A, NCDN, SYP, DRD2, SLC8A2, GRIN1

Table of significant pathways of interest for GO Molecular Function

term	genes
Amyloid-Beta Binding (GO:0001540)	NGFR, RAMP3, CLSTN1, ITGB2, ATP1A3, MAPK8IP2, CLU, LDLR, GRIN1
Tau Protein Binding (GO:0048156)	GSK3A, HSP90AB1, DCTN1, MAP1A, MARK4, CLU

Figure 4. MA10 infection in brains of WT and 5xFAD mice is associated with differential expression of genes involved in regulation of synaptic activity at 21 dpi. RNA sequencing was performed on brains from SARS-CoV2-MA10 (MA10) infected 12 month- old wild-type (WT) and 5xFAD male mice at 21 days post infection (dpi). (A) Volcano plot of differentially expressed genes (DEG) displaying fold change of genes (log2 scale) and P values (5xFAD-21dpi. (B) Heatmap of selected (FC=0.5, FDR<0.05) DEGs from WT MA10 infected and 5xFAD MA10 infected mice versus uninfected controls at 21dpi respectively. Tables displaying associated genes with (C) enriched pathways of interest examined in WT MA10 and other enriched pathways of interest examined via GO enrichment in (D) 5xFAD MA10 infected mice versus uninfected controls at 21dpi. Colors corresponding to upregulation (red) and downregulation (blue).

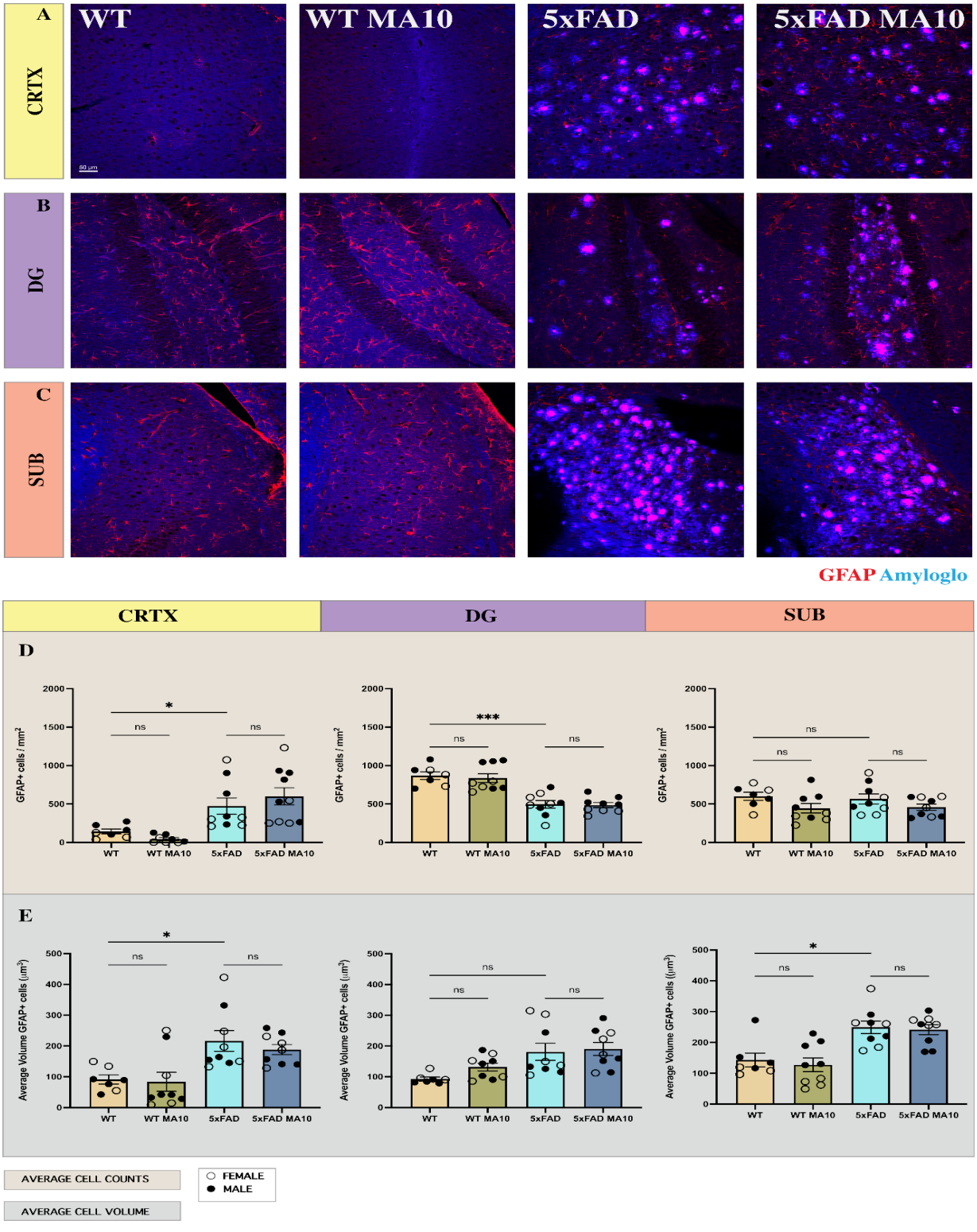
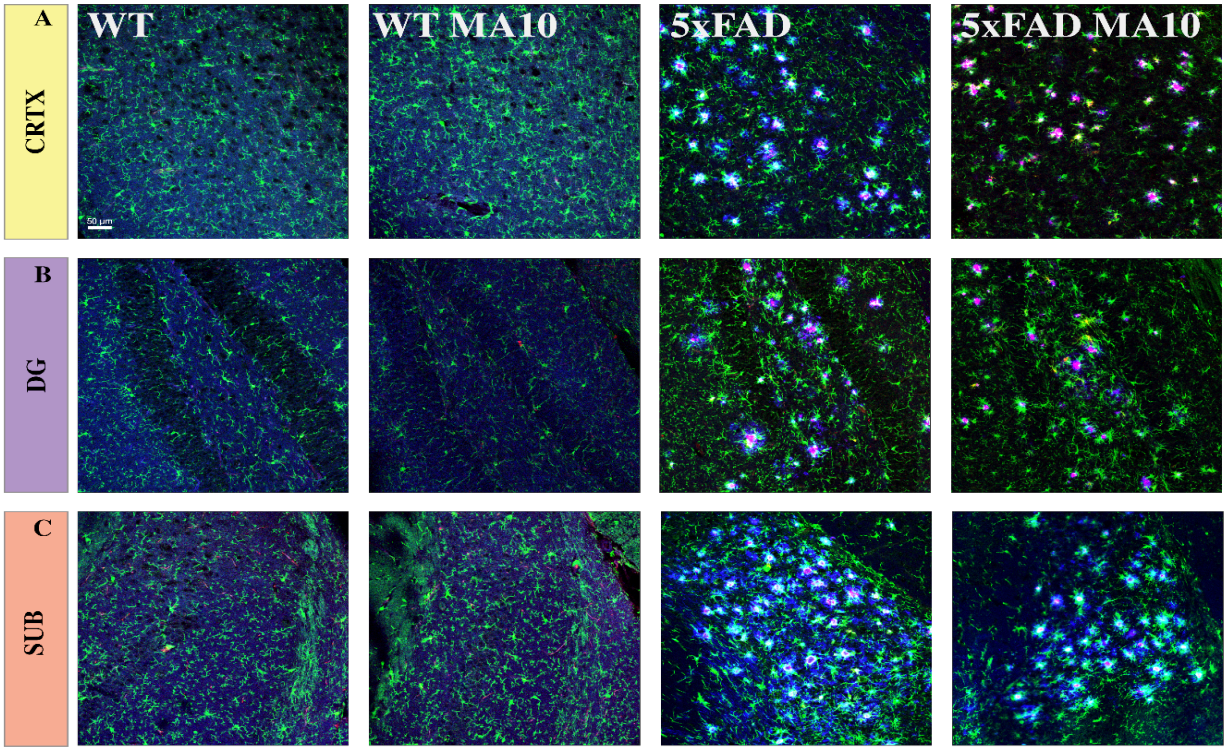
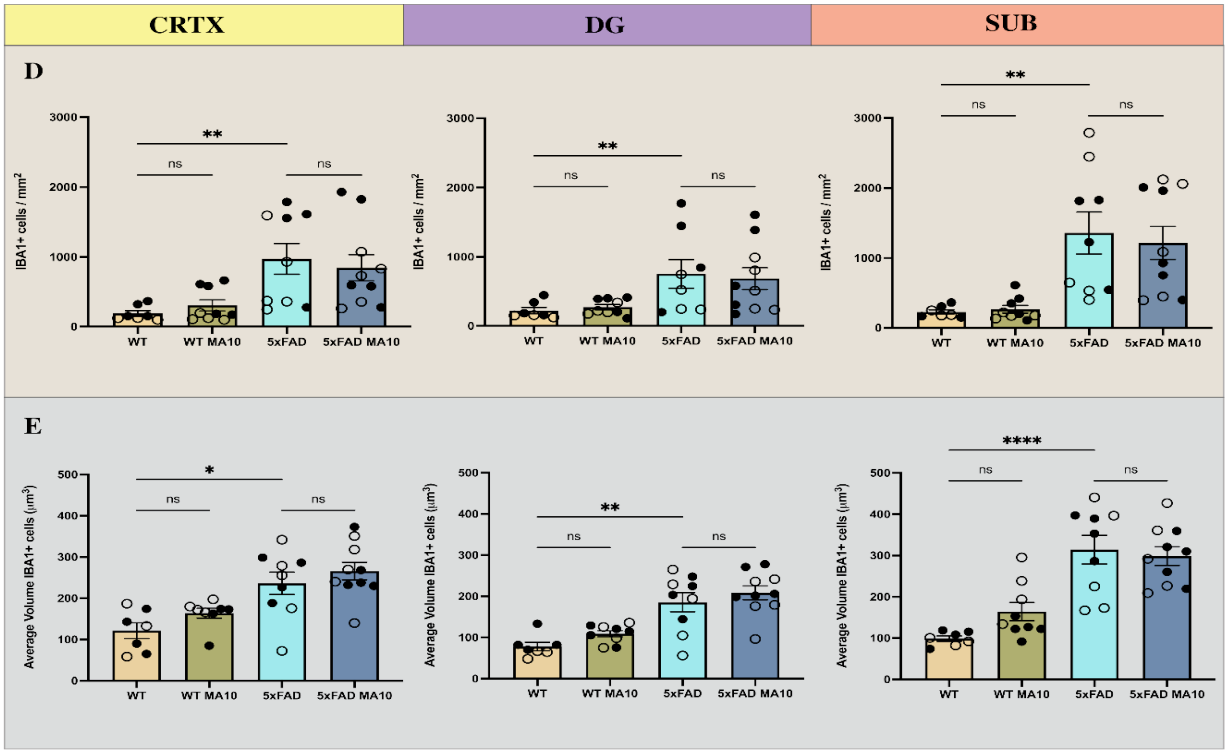

A
CRTX
WT
WT MA10
5xFAD
5xFAD MA10
B
DG
C
SUB
GFAP Amyloglo
CRTX
DG
SUB
D
GFAP+ cells / mm²
E
Average Volume GFAP+ cells (µm³)
WT
WT MA10
5xFAD
5xFAD MA10
ns
*
***
AVERAGE CELL COUNTS
AVERAGE CELL VOLUME
FEMALE
MALE

Figure 5. Effects of MA10 infection on GFAP staining in WT and 5xFAD mice. Brains of uninfected and MA10 infected mice at 21 days post infection were immunostained for GFAP to assess changes in astrocytes. Plaques were stained via Amyloglo. (A-C) Representative images at 20X magnification of 10-14 month- old WT and 5xFAD cortex (CRTX), dentate gyrus (DG), and subiculum (SUB) respectively. (D) GFAP immunostaining for astrocyte number, and average astrocyte volume (E) does not indicate changes in either in any of these distinct anatomical brain regions as a result of MA10 infection, but there is an effect in number and volume of astrocytes as a result of genotype (WT vs. 5xFAD). Immunohistological data were analyzed using two-way ANOVA. Tukey's post-hoc test was employed to examine biologically relevant interactions. Female and male mice are indicated by open or closed circles respectively. Data are represented as MEAN ±SEM. * $p < .05$, ** $p < .01$, *** $p < .001$, **** $p < .0001$. Scale bar in (A) = 50 μm.


A
CRTX
WT
WT MA10
5xFAD
5xFAD MA10
50 µm
B
DG
C
SUB
IBA1 Mac2 Amyloglo


CRTX
DG
SUB
D
IBA1+ cells / mm²
3000
2000
1000
0
**
ns
WT
WT MA10
5xFAD
5xFAD MA10
E
Average Volume IBA1+ cells (µm³)
500
400
300
200
100
0
*
**
****
AVERAGE CELL COUNTS
AVERAGE CELL VOLUME
FEMALE
MALE

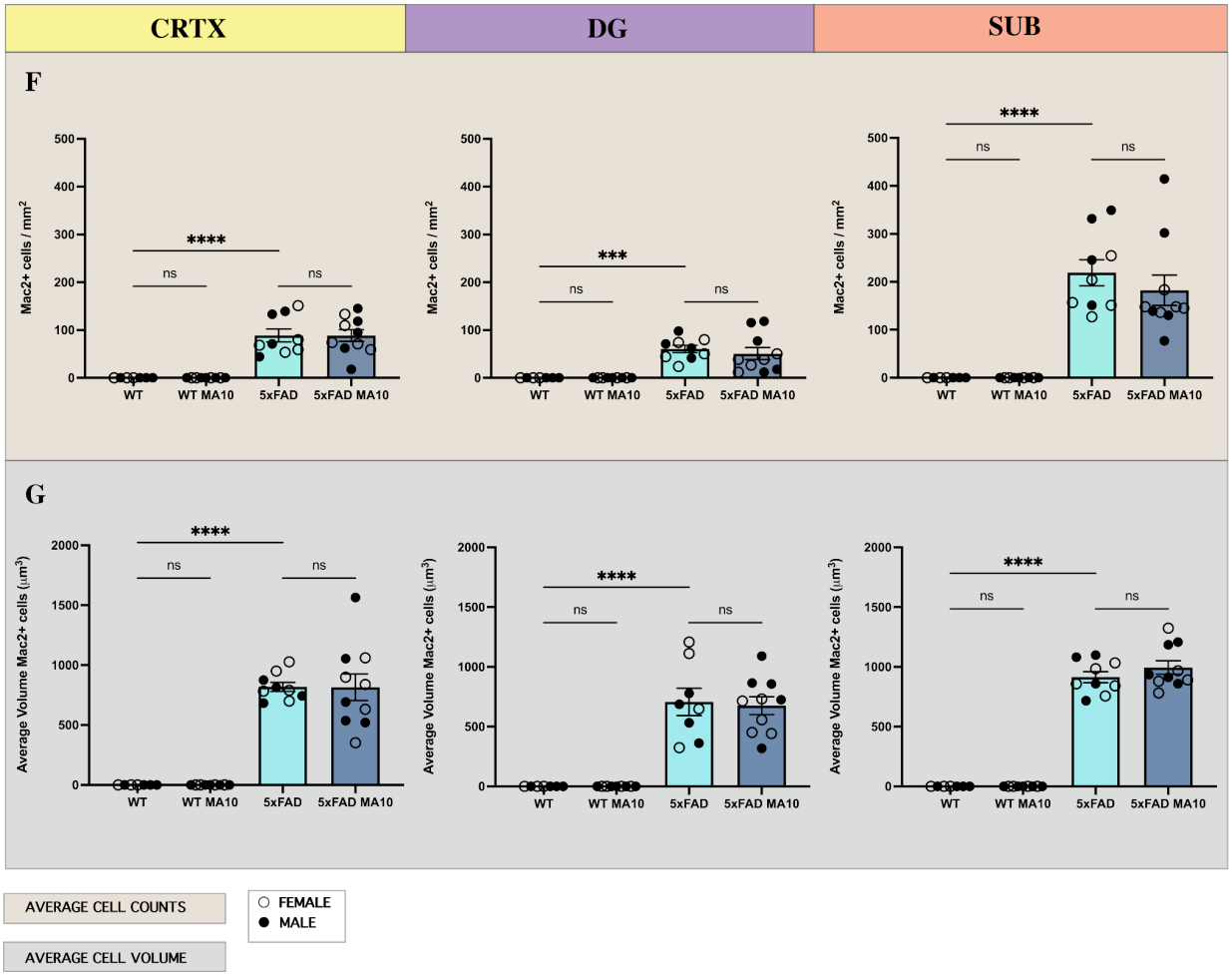
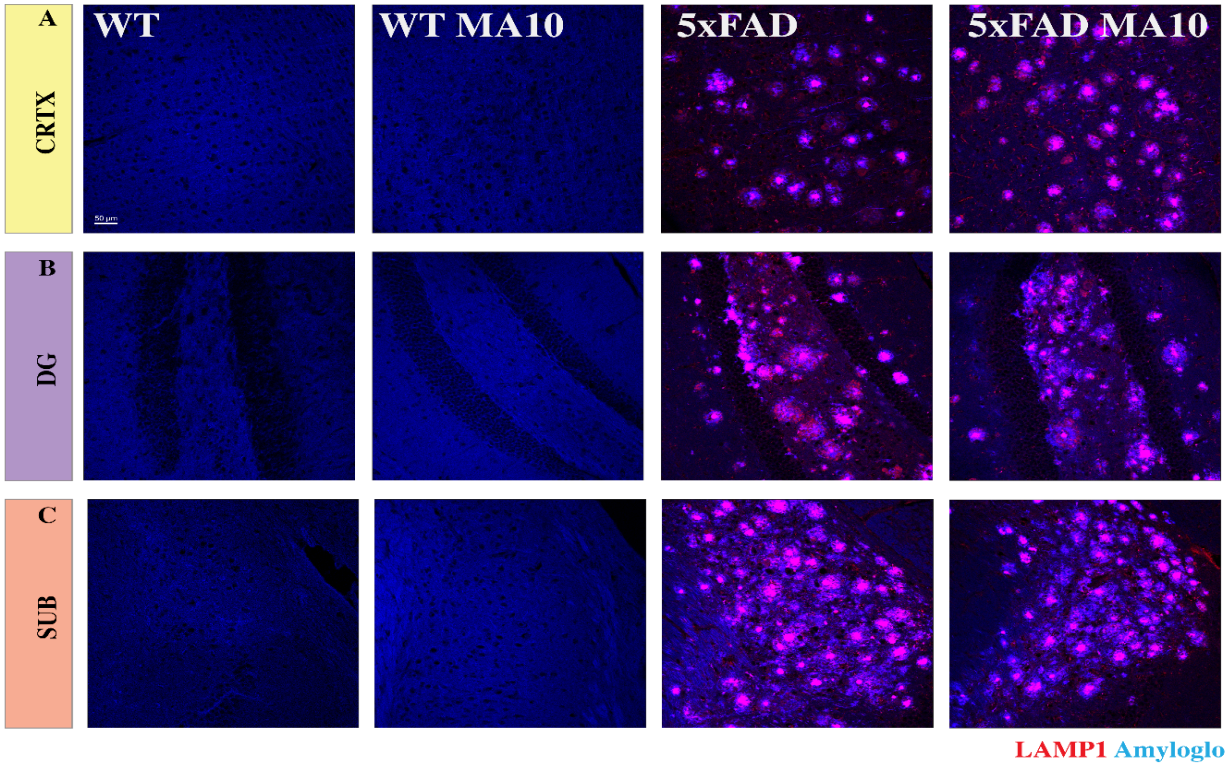
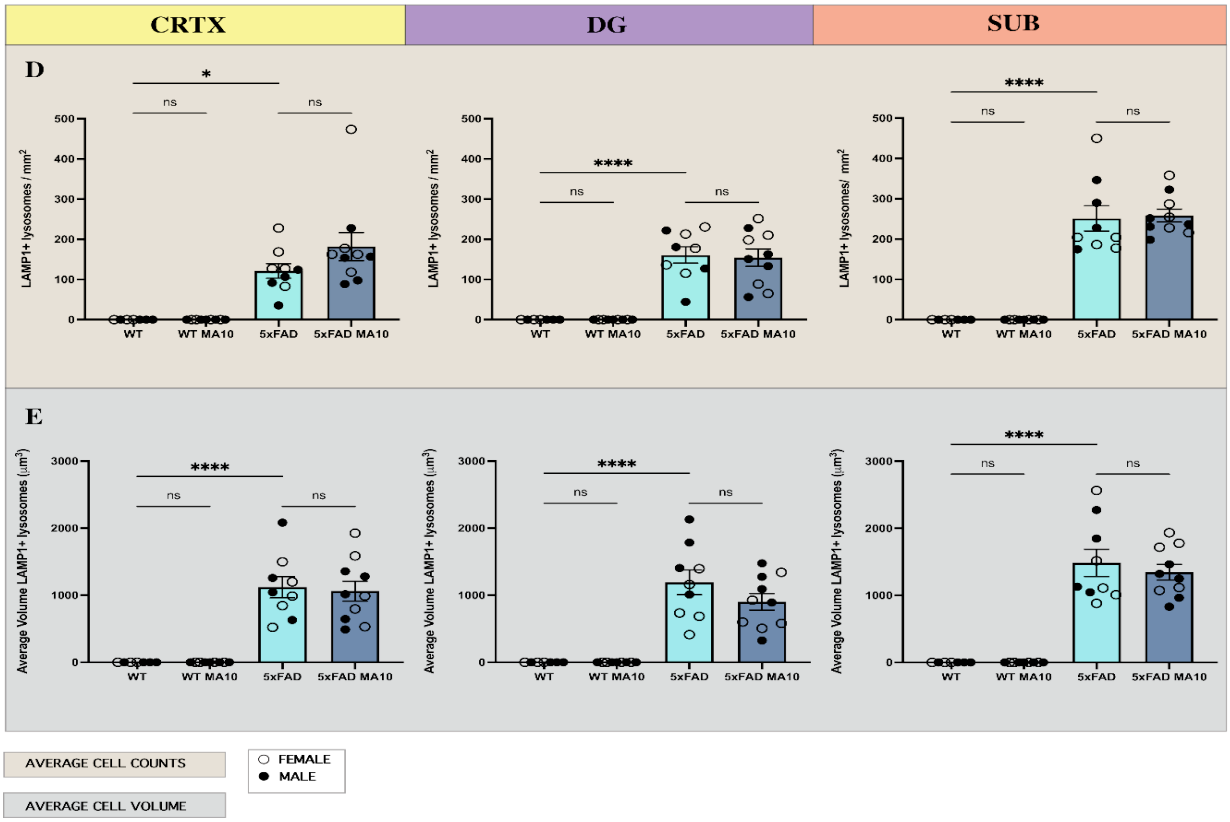


Figure 6. Effects of MA10 infection on IBA1 and Mac2 staining in WT and 5xFAD mice. Brains of uninfected and MA10 infected mice at 21 days post infection were immunostained for IBA1 and MAC2 to assess changes in microglia and infiltrating monocytes. Plaques were stained via Amyloglo. (A-C) Representative images at 20X magnification of 10-14 month- old WT and 5xFAD cortex (CRTX), dentate gyrus (DG), and subiculum (SUB) respectively. (D) IBA1 immunostaining for microglia number, average microglia volume (E) as well as (F) Mac2 immunostaining for monocyte number and average monocyte volume (G) does not indicate changes in either in any of these distinct anatomical brain regions as a result of MA10 infection, but there is an effect in number and volume of both microglia and monocytes as a result of genotype (WT vs. 5xFAD). Immunohistological data were analyzed using two-way ANOVA. Tukey's post-hoc test was employed to examine biologically relevant interactions. Female and male mice are indicated by open or closed circles respectively. Data are represented as MEAN ±SEM. * $p < .05$, ** $p < .01$, *** $p < .001$, **** $p < .0001$. Scale bar in (A) = 50 µm.


A
CRTX
WT
WT MA10
5xFAD
5xFAD MA10
B
DG
C
SUB
LAMP1 Amyloglo


CRTX
DG
SUB
D
LAMP1+ lysosomes / mm2
LAMP1+ lysosomes/ mm2
WT
WT MA10
5xFAD
5xFAD MA10
ns
*
****
E
Average Volume LAMP1+ lysosomes (µm3)
AVERAGE CELL COUNTS
AVERAGE CELL VOLUME
FEMALE
MALE

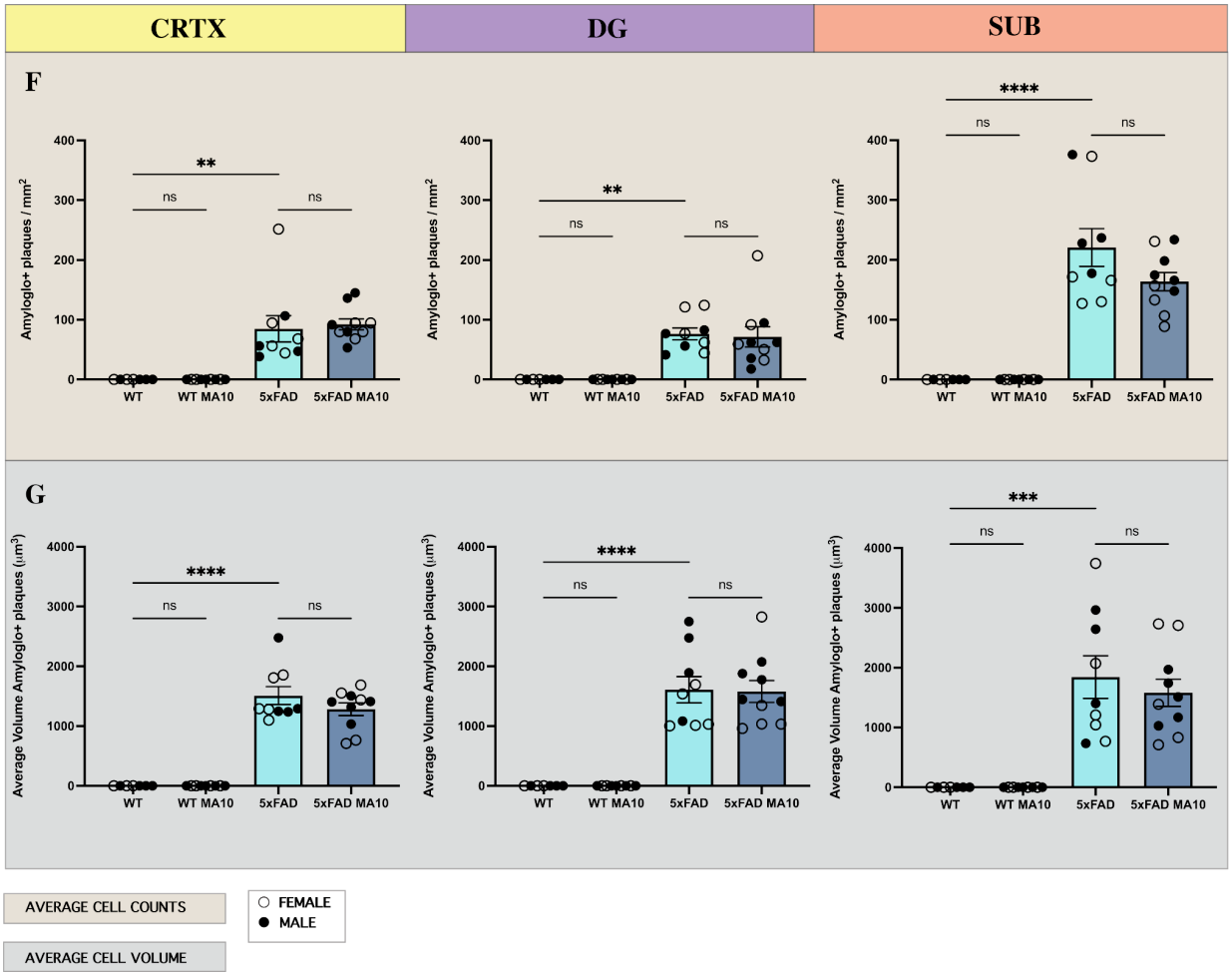
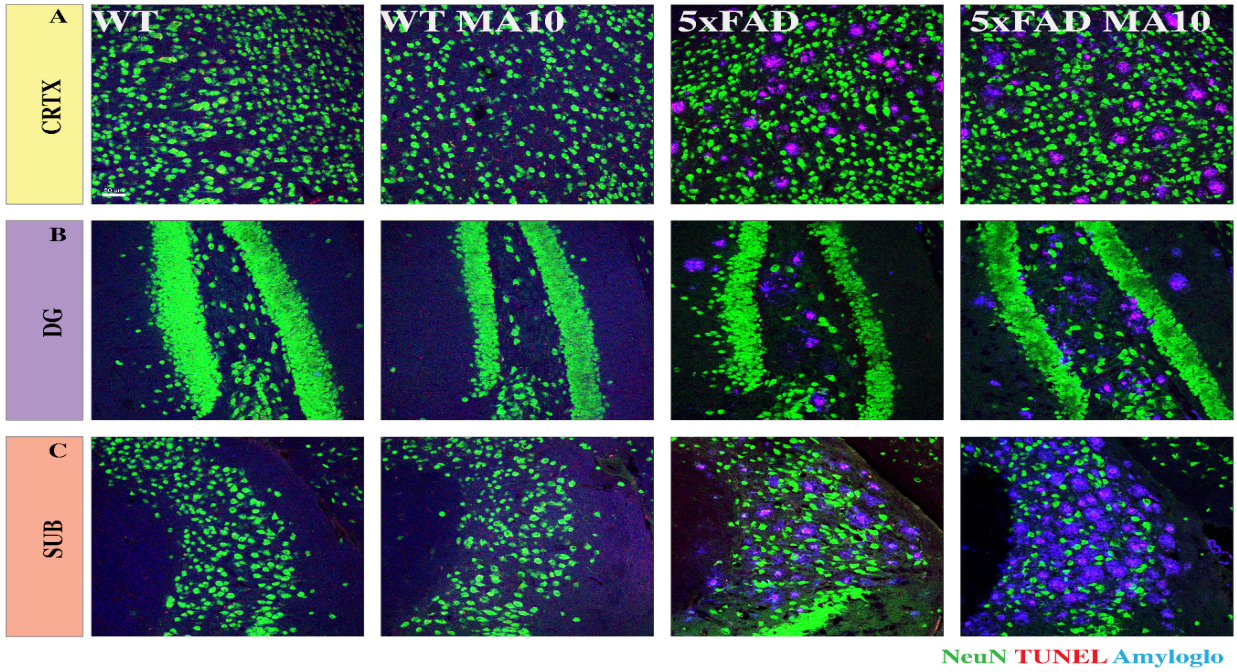


Figure 7. Effects of MA10 infection on dystrophic neurites and amyloid beta plaques in WT and 5xFAD mice. Brains of uninfected and MA10 infected mice at 21 days post infection were immunostained for LAMP1 to assess changes in dystrohpic neurites. Plaques were stained via Amyloglo. (A-C) Representative images at 20X magnification of 10-14 month-old WT and 5xFAD cortex (CRTX), dentate gyrus (DG), and subiculum (SUB) respectively. (D) LAMP1 immunostaining for dystrophic neurite number and volume (E) as well as (F) Amyloglo staining for plaque number and average volume (G) does not indicate changes in either in any of these distinct anatomical brain regions as a result of MA10 infection, but there is an effect in number and volume of both dystrohpic neurites and plaques as a result ofgenotype (WT vs. 5xFAD). Immunohistological data were analyzed using two-way ANOVA. Tukey's post- hoc test was employed to examine biologically relevant interactions. Female and male mice are indicated by open or closed circles respectively. Data are represented as MEAN ±SEM. * $p < .05$, ** $p < .01$, *** $p < .001$, **** $p < .0001$. Scale bar in (A) = 50 µm.


A
CRTX
WT
WT MA10
5xFAD
5xFAD MA10
B
DG
C
SUB
NeuN TUNEL Amyloglo

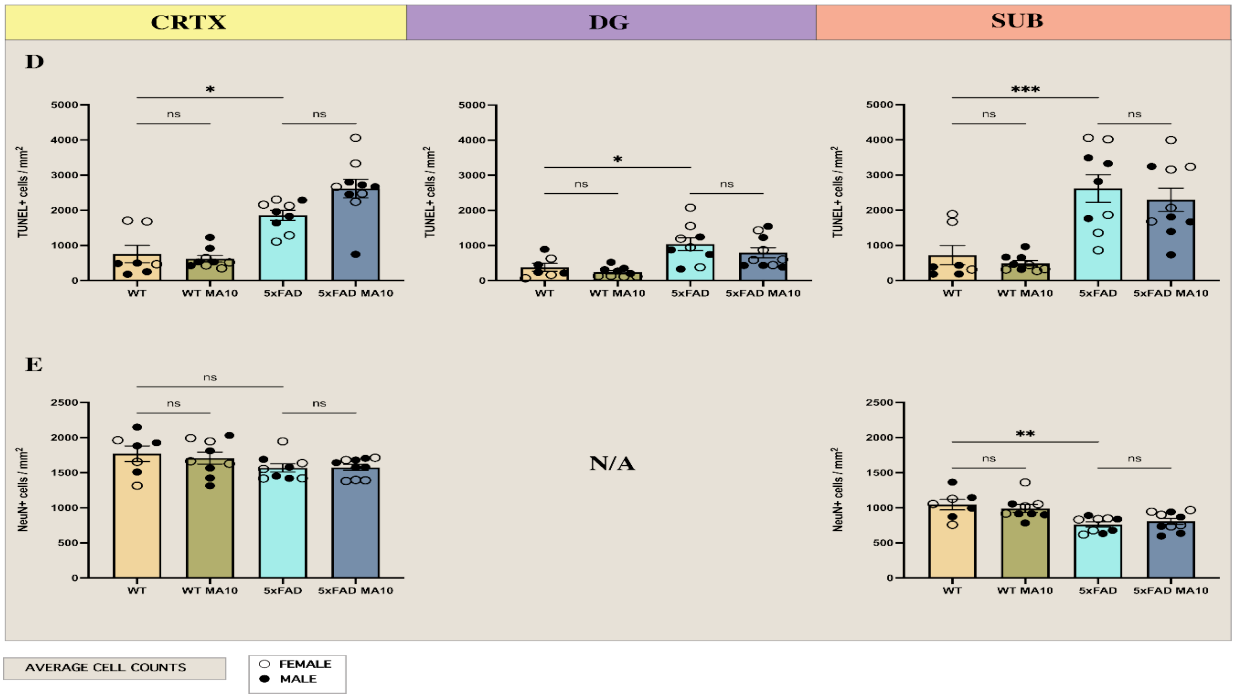
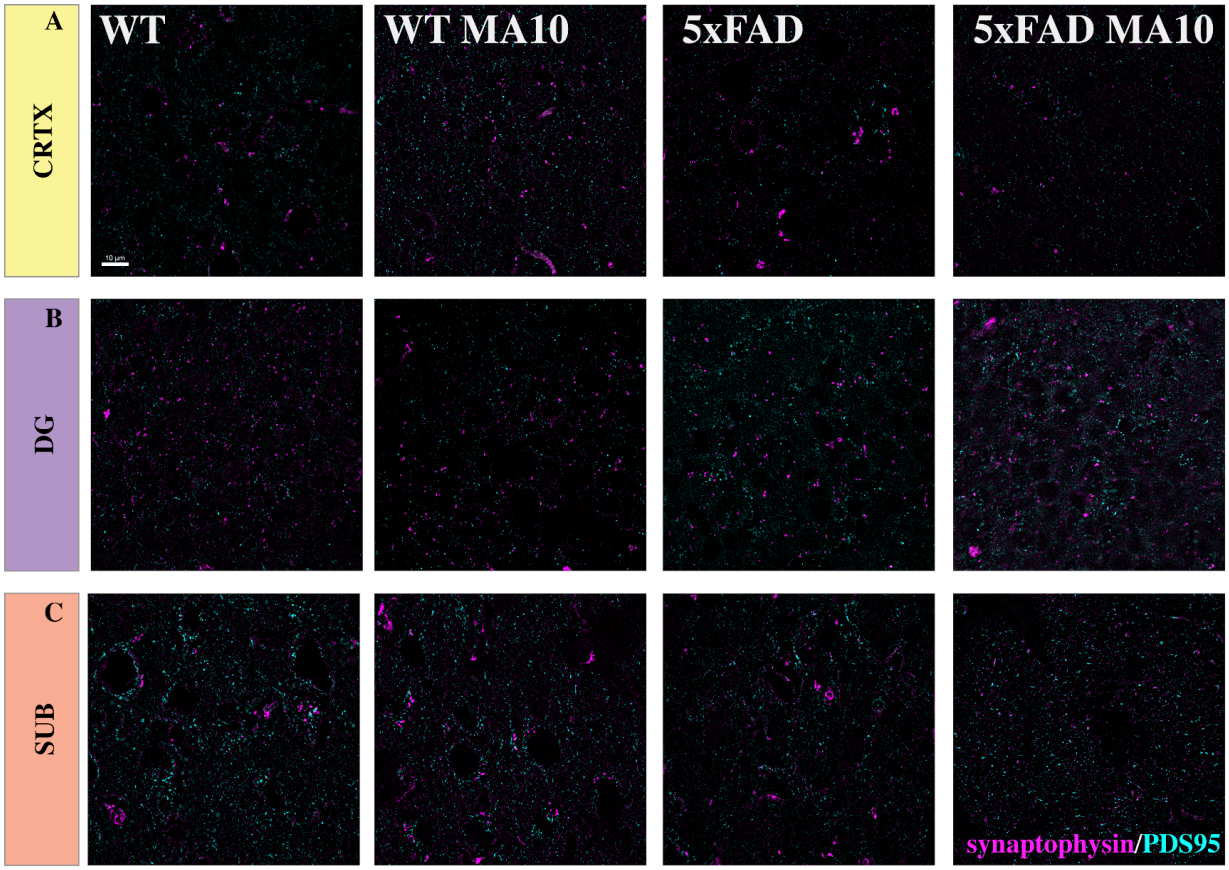

CRTX
DG
SUB
D
TUNEL+ cells / mm2
WT
WT MA10
5xFAD
5xFAD MA10
ns
*
***
E
NeuN+ cells / mm2
**
N/A
AVERAGE CELL COUNTS
FEMALE
MALE

Figure 8. Effects of MA10 infection on neurons and cell death in WT and 5xFAD mice. Brains of uninfected and MA10 infected mice at 21 days post infection were immunostained for NeuN to assess changes in mature neurons. Cell death was assessed via TUNEL assay to detect apoptotic cells. Plaques were stained via Amyloglo. (A-C) Representative images at 20X magnification of 10-14 month- old WT and 5xFAD cortex (CRTX), dentate gyrus (DG), and subiculum (SUB) respectively. (D) TUNEL staining for apoptotic cell number, does not indicate changes in either in any of these distinct anatomical brain regions as a result of MA10 infection but there is an effect in the number of apoptotic (TUNEL+) cells as a result of genotype (WT vs. 5xFAD). (E) NeuN immunostaining for mature neuron number was quantified only in CRTX and subiculum SUB. There are no changes in neuron number in these regions as a result of MA10 infection but there is an effect in number as a result of genotype (WT vs. 5xFAD) in SUB. Immunohistological data were analyzed using two-way ANOVA. Tukey's post-hoc test was employed to examine biologically relevant interactions. Female and male mice are indicated by open or closed circles respectively. Data are represented as MEAN ±SEM. * $p < .05$, ** $p < .01$, *** $p < .001$, **** $p < .0001$. Scale bar in (A) = 50 μm.


A
CRTX
WT
WT MA10
5xFAD
5xFAD MA10
B
DG
C
SUB
synaptophysin/PDS95

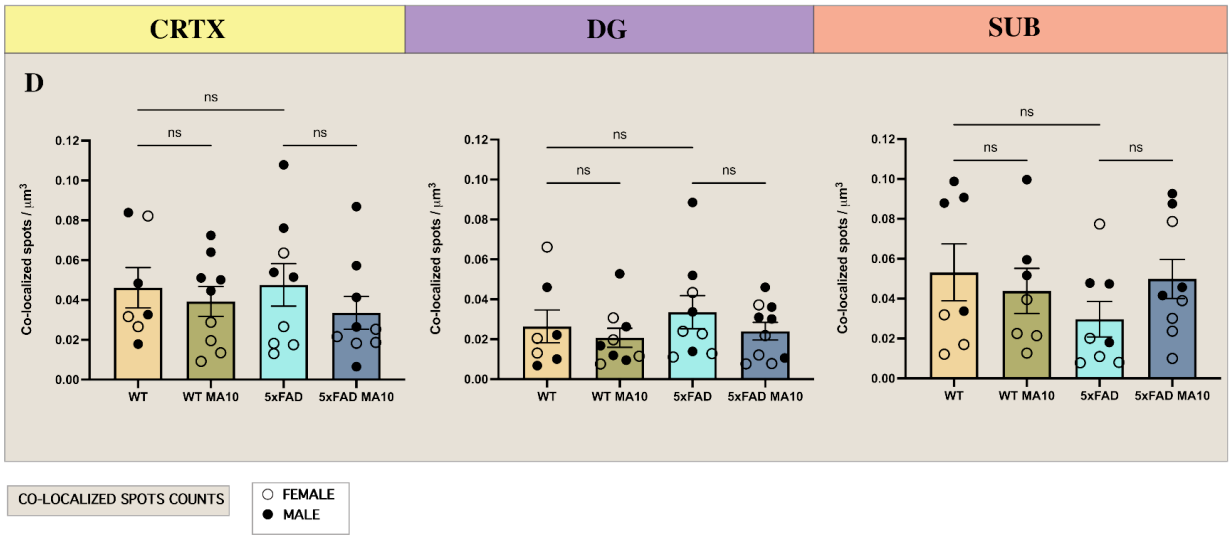

CRTX
DG
SUB
D
Co-localized spots / µm³
ns
WT
WT MA10
5xFAD
5xFAD MA10
CO-LOCALIZED SPOTS COUNTS
FEMALE
MALE

Figure 9. Effects of MA10 infection on synapses in WT and 5xFAD mice. Brains of uninfected and MA10 infected mice at 21 days post infection were immunostained with synaptophysin for presynaptic elements (magenta) and PSD-95 for postsynaptic elements (turquoise). (A-C) Representative super-resolution images at 40X objective of 10-14 month- old WT and 5xFAD cortex (CRTX), dentate gyrus (DG), and subiculum (SUB) respectively. (D)Quantification of synaptophysin+ and PSD-95+ spots per µm3 did not show a change in co-localized spots in any brain region as a result of MA10 infection. Immunohistological data were analyzed using two-way ANOVA. Tukey's post-hoc test was employed to examine biologically relevant interactions. Female and male mice are indicated by open or closed circles respectively. Data are represented as MEAN ±SEM. * $p < .05$, ** $p < .01$, *** $p < .001$, **** $p < .0001$. Scale bar in (A) = 10 µm.

Supplementary Table 1: Corresponding primary, secondary antibodies, and associated information

Primary Antibody	Source	Catalog #	Dilution	Secondary antibody	Source	Catalog #	Dilution
IBA1	Wako	019-19741	1:500	Goat anti-rabbit IgG, AlexaFluor 488	Thermo Fisher	A11008	1:200
GFAP	Abcam	ab134436	1:1000	Goat anti-chicken IgY Alexa Fluor 594	Abcam	ab150172	1:400
Mac2	Cedar lane	CL8942AP	1:500	Goat anti-rat IgG Alexa Fluor 594	Abcam	ab150160	1:200
PSD95	Abcam	ab18258	1:500	Goat anti-rabbit IgG, AlexaFluor 488	Thermo Fisher	A11008	1:200
synaptophysin	Sigma-Aldrich	S5768	1:1000	Goat anti-mouse IgG Alexa Fluor 555	Thermo Fisher	A21424	1:200
NeuN	Abcam	ab104225	1:100	Goat anti-rabbit IgG, AlexaFluor 488	Thermo Fisher	A11008	1:350
LAMP1	Abcam	ab25245	1:200	Goat anti-rat IgG Alexa Fluor 594	Abcam	ab150160	1:200

CHAPTER 5

SUMMARY

5.1 Summary and Significance

Microglia Do Not Restrict SARS-CoV-2 Replication following Infection of the Central Nervous System of K18-Human ACE2 Transgenic Mice

SARS-CoV-2 is the causative agent of COVID-19, a disease that rapidly became a global pandemic and that currently has affected hundreds of millions of people worldwide. While most cases of COVID-19 present with mild-to-moderate respiratory disease [1,2], some severe cases can result in respiratory failure [3]. However, it became clear that other organ systems including the CNS are possible targets of infection [4–6] [7] given that neurological symptoms and complications have been extensively documented since the beginning of the pandemic [8,9,9–12], with the majority of neurological manifestations occurring in patients with severe disease [13]. Additionally, SARS-CoV-2 uses angiotensin converting enzyme 2 (ACE2), which is mainly expressed in alveolar epithelial cells of the lungs [14] , but can be expressed in other tissues, including the brain [15] and particular CNS cells such as microglia and neurons [16,17]. Microglia are the resident immune cells in the CNS, they monitor the CNS and play a role in homeostasis as well as respond to injury and inflammation [18,19], and experimental CNS infection of susceptible mice with neurotropic strains of other murine coronaviruses has been established to induce widespread activation of microglia with the release of pro-inflammatory chemokines and cytokines as well as the activation of both the innate and adaptive immune responses [20–22]. Several animal models have been shown to be susceptible to SARS-CoV-2 infection [23–30], yet rodent models are still favored in laboratory conditions. Although rodents allow for more accessible studies, SARS-CoV-2 is unable to effectively bind to the murine ACE2 receptor [31]. Given the urgent need for preclinical mouse models, human ACE2 (hACE2) transgenic mouse models e.g. k18-hACE2, expressing the human ACE2 receptor, became an early suitable option to model COVID-19 [32–34].

Studies in Chapter 2, aimed to explore the immune response in susceptible k18-hACE2 mice and the contributions of microglia in host defense and neuroinflammation in this model system. Importantly, at the time these experiments were initiated and conducted (2020-2021), the k18-ACE2 model was the "go to" model employed by the majority of investigators world-wide studying in vivo pathogenesis of SARS-CoV-2.

Intranasal inoculation of K18-hACE2 mice with SARS-CoV-2 resulted in significant weight loss and viral replication within the lungs, which was associated with a robust inflammatory response. This response included the presence of T cells, along with elevated expression of proinflammatory cytokines and chemokines, including ifλ, CXCL10, CXCR2, and CCL2. Notably, the presence of CD8+ T cells and increased expression of CXCL10 suggest a targeted immune response, consistent with previous findings on the role of CXCL10 in attracting virus-specific T cells during murine coronavirus infections [35–37]. CCL2 has been shown to attract monocytes/macrophages in the same context [38–41], and CXCR2 most likely reflects the presence of inflammatory neutrophils [20].

Examination of the brains of SARS-CoV-2-infected K18-hACE2 mice revealed extensive viral replication and spread within neurons. Virus was detected in different anatomical regions and indicates that neurons are primary targets for SARS-CoV-2 infection within the brains of K18hACE2 mice. Additionally, microglial activation was evident, contributing to the neuroinflammatory environment. Microglia have been implicated in aiding in the control of viral replication and spread of other murine coronaviruses, via enhancing antiviral T cell responses [42–44] , and so we wanted to evaluate their role in controlling SARS-CoV-2 replication within the CNS. We showed that pharmacological depletion of microglia with CSF1R inhibitor in chow (PLX5622) prior to SARS-CoV-2 infection, did not affect viral replication, but did result in a

marked reduction in proinflammatory chemokine and cytokine expression within the brains compared to infected control chow animals, including monocyte/macrophage chemoattractants CCL2 and CCL5 and this corresponded with an overall reduction in numbers of these cells in the brains of PLX5622-treated mice. These findings support the notion that microglia do contribute to the neuroinflammatory response, in part, through influencing expression of chemokines/cytokines in response to SARS-CoV-2 infection of the CNS of K18-hACE2 mice, and highlighting the complexity of the CNS immune response to SARS-CoV-2.

These observations further highlight the importance of transgenic models, particularly the K18-hACE2 mouse, in elucidating the pathogenesis of COVID-19 early in the pandemic. However, the ability of the virus to efficiently infect and replicate within the CNS in these models contrasts with clinical findings in COVID-19 patients, where extensive CNS infection is rare. Therefore, the development of more suitable animal models that more accurately reflect human SARS-CoV-2 CNS infection and immune responses are crucial for advancing our understanding of COVID-19 pathogenesis and developing effective therapeutic interventions.

Characterizing the effects of mouse-adapted SARS-CoV-2 infection on Alzheimer's disease-associated neuropathology

Alzheimer's disease (AD), the leading cause of age-related dementia, impairs memory and cognitive functions, reducing quality of life and the ability to perform daily tasks. Its pathology includes amyloid plaques, neurofibrillary tangles (NFTs), neuronal loss, and neuroinflammation [45]. AD is a multifactorial disease influenced by numerous risk factors including genetic and environmental [46–58]. Some studies have suggested possible links between viral infection and either onset or exacerbation of pathology and clinical symptoms associated

with various human neurodegenerative diseases including AD [59,60]. Many neurodegenerative disorders, including AD, are associated with abnormal protein folding and aggregation, with increased risk linked to exposure to infectious agents such as viruses and bacteria [59,61–67]. Additionally, evidence indicates that some viruses and their proteins possess amyloidogenic properties, potentially leading to amyloid aggregate formation [68–70]. Furthermore, neuroinflammatory processes and the release of increased amounts of proinflammatory cytokines, can negatively impact the brain in a variety of manners, including synaptic dysfunction, neurotoxicity and neuronal death [71]. In the context of COVID-19, post-mortem analyses of COVID-19 patients' brains show gliosis, axonal damage, and BBB disruption. Laboratory animal infections have demonstrated similar findings; BBB disruption, gliosis, decreased hippocampal neurogenesis, synaptic loss, and memory deficits, even without direct viral neuroinvasion. The increasing number of studies associating infections, including SARS-CoV-2, to neurodegeneration further necessitates further investigation on the contribution of these infections to AD and other dementias, especially the recent evidence linking COVID-19 with neuroinflammation and specific neurodegenerative processes [72–76]. Given this evidence, this study aimed to investigate CNS changes associated with intranasal inoculation with mouse-adapted SARS-CoV-2 (MA10) to model the effects of COVID-19 on the CNS in laboratory mice. Here we evaluated the impacts of chronic infection on gene expression, neuroinflammation , cell death, and synaptic function in aged standard laboratory mice (C57BL/6) as well as AD associated pathology in an established preclinical AD mouse model (5xFAD) to determine the long term impact of SARS-CoV-2 infection in the brain and investigate possible molecular and cellular mechanisms contributing to neurodegeneration.

Intranasal inoculation of WT and 5xFAD mice with SARS-CoV-2- MA10 resulted in mild disease in aged mice, with no differences in mortality associated with genotype. Additionally, we observed a dramatic increase in expression of gene transcripts associated with modulation of the immune system and other inflammatory pathways in the lungs of MA10 infected animals during initial phases of infection that eventually returned to baseline levels of expression after infection had resolved. Furthermore, we aimed to determine if infection led to long lasting changes in gene expression in the brains of infected animals, that could account for the cognitive deficits that have been observed in COVID-19 patients. We found that although viral RNA was not detected within the brains of infected mice, MA10 infection led to lasting gene expression changes in the brain and these changes are associated with neuronal dysfunction**.** In the acute phase of infection, RNASeq analysis indicates an upregulation in genes associated with reduced long-term potentiation (LTP) in WT mice, and downregulation genes associated with neuronal plasticity in 5xFAD mice. LTP, a key form of synaptic plasticity, is considered a cellular mechanism for learning and memory and dysfunction in LTP is thought to cause memory loss [77]. Thus, impairments in LTP and related genes likely contribute to memory deficits observed in both human and animal studies. In the chronic time point of MA10 infection, similar pathways associated with neuronal and synaptic dysfunction were seen in the brains of infected 5xFAD mice; however, 5xFAD mice had significantly more genes affected compared to WT mice. In WT mice, one particular gene of interest associated with three prominent neurodegenerative diseases was still downregulated, UQCRFS1. Dysfunction of UQCRFS1has been implicated with reduced or disrupted mitochondrial function, [78] which has been linked to many neurodegenerative diseases [79–81].

Next, this study aimed to determine whether the gene expression changes indicating neuronal and synaptic dysfunction were also due to, or associated with changes in neuroinflammation or other AD associated pathology. However, changes in gene expression were not associated with detectable changes in activated microglia and astrocytes, or inflammatory monocyte/macrophages in infected mice. Additionally, no changes were observed in Aβ plaques or dystrophic neurites in the brains of 5xFAD mice. No evidence of overt neuronal degeneration was found; moreover, no overt changes in synapse number were noted. These findings indicate that experimental infection of mice with MA10 is associated with detectable and long-lasting changes in the brain associated with neuronal dysfunction, even though gene expression changes do not directly translate into altered neuropathological changes. However, these long-lasting changes in gene expression associated with clear neuronal and synaptic dysfunction provide some mechanistic insights that aid in our understanding how cognitive dysfunction may result from COVID-19. Moreover, this study provides evidence that viral infection that results from a lower viral dose or less severe variants of SARS-CoV-2 may not necessarily lead to permanent or long-term deleterious consequences in the brain.

5.2 Future Directions

Our overall findings indicate SARS-CoV-2 infection is associated with detectable and long-lasting transcriptional changes in the brain associated with neuronal dysfunction and other neurodegenerative processes; however, specific molecular and cellular mechanisms contributing to these changes remain unclear given that we have not yet determined the spatial context and within which particular cell populations these transcriptional changes occur.

Some studies have implicated microglia activation as a key driver in neurodegeneration and cognitive deficits observed as a result of SARS-CoV-2 infection[74] and therefore our laboratory will continue to explore the contribution of microglia to changes in the brain in the context of SARS-CoV-2 infection. In addition, our laboratory will continue to examine and characterize other changes in the CNS associated with SARS-CoV-2 infection that could mechanistically explain the observed transcriptional changes associated neuronal dysfunction, including the use of spatial transcriptomics techniques to examine the positional context of transcriptional activity within particular cell populations and specific anatomical regions of the brain. Lastly, we will continue to further characterize the effects of SARS-CoV-2 infection on other neuropathological changes within the CNS and how these changes could contribute to cognitive deficits. This includes examining for evidence of endothelial and vascular damage and BBB dysfunction as well as other axonal damage.

5.3 References

1. Huang, C. *et al.* Clinical features of patients infected with 2019 novel coronavirus in Wuhan, China. *The Lancet* **395**, 497–506 (2020).
2. Guan, W. *et al.* Clinical Characteristics of Coronavirus Disease 2019 in China. *N. Engl. J. Med.* **382**, 1708–1720 (2020).
3. Diamond, M., Peniston, H. L., Sanghavi, D. & Mahapatra, S. Acute Respiratory Distress Syndrome. in *StatPearls* (StatPearls Publishing, Treasure Island (FL), 2022).
4. Gupta, A. *et al.* Extrapulmonary manifestations of COVID-19. *Nat. Med.* **26**, 1017–1032 (2020).
5. Tavazzi, G. *et al.* Myocardial localization of coronavirus in COVID-19 cardiogenic shock. *Eur. J. Heart Fail.* **22**, 911–915 (2020).
6. Xiao, F. *et al.* Evidence for Gastrointestinal Infection of SARS-CoV-2. *Gastroenterology* **158**, 1831-1833.e3 (2020).
7. Du, Y. *et al.* Clinical Features of 85 Fatal Cases of COVID-19 from Wuhan. A Retrospective Observational Study. *Am. J. Respir. Crit. Care Med.* **201**, 1372–1379 (2020).
8. Chen, T. *et al.* Clinical characteristics of 113 deceased patients with coronavirus disease 2019: retrospective study. *BMJ* **368**, m1091 (2020).
9. Harapan, B. N. & Yoo, H. J. Neurological symptoms, manifestations, and complications associated with severe acute respiratory syndrome coronavirus 2 (SARS-CoV-2) and coronavirus disease 19 (COVID-19). *J. Neurol.* **268**, 3059–3071 (2021).
10. Johansson, A., Mohamed, M. S., Moulin, T. C. & Schiöth, H. B. Neurological manifestations of COVID-19: A comprehensive literature review and discussion of mechanisms. *J. Neuroimmunol.* **358**, 577658 (2021).

11. Mao, L. *et al.* Neurologic Manifestations of Hospitalized Patients With Coronavirus Disease 2019 in Wuhan, China. *JAMA Neurol.* **77**, 683–690 (2020).
12. Zubair, A. S. *et al.* Neuropathogenesis and Neurologic Manifestations of the Coronaviruses in the Age of Coronavirus Disease 2019 A Review. *JAMA Neurol.* **77**, 1018–1027 (2020).
13. Liotta, E. M. *et al.* Frequent neurologic manifestations and encephalopathy-associated morbidity in Covid-19 patients. *Ann. Clin. Transl. Neurol.* **7**, 2221–2230 (2020).
14. Hamming, I. *et al.* Tissue distribution of ACE2 protein, the functional receptor for SARS coronavirus. A first step in understanding SARS pathogenesis. *J. Pathol.* **203**, 631–637 (2004).
15. Li, M.-Y., Li, L., Zhang, Y. & Wang, X.-S. Expression of the SARS-CoV-2 cell receptor gene ACE2 in a wide variety of human tissues. *Infect. Dis. Poverty* **9**, 45 (2020).
16. Singh, M., Bansal, V. & Feschotte, C. A Single-Cell RNA Expression Map of Human Coronavirus Entry Factors. *Cell Rep.* **32**, 108175 (2020).
17. Chen, R. *et al.* The spatial and cell-type distribution of SARS-CoV-2 receptor ACE2 in human and mouse brain. 2020.04.07.030650 Preprint at https://doi.org/10.1101/2020.04.07.030650 (2020).
18. Tremblay, M.-È. *et al.* The role of microglia in the healthy brain. *J. Neurosci. Off. J. Soc. Neurosci.* **31**, 16064–16069 (2011).
19. Nimmerjahn, A., Kirchhoff, F. & Helmchen, F. Resting microglial cells are highly dynamic surveillants of brain parenchyma in vivo. *Science* **308**, 1314–1318 (2005).
20. Hosking, M. P., Liu, L., Ransohoff, R. M. & Lane, T. E. A protective role for ELR+ chemokines during acute viral encephalomyelitis. *PLoS Pathog.* **5**, e1000648 (2009).
21. Lane, T. E., Hardison, J. L. & Walsh, K. B. Functional diversity of chemokines and

chemokine receptors in response to viral infection of the central nervous system. *Curr. Top. Microbiol. Immunol.* **303**, 1–27 (2006).

22. Skinner, D., Marro, B. S. & Lane, T. E. Chemokine CXCL10 and Coronavirus-Induced Neurologic Disease. *Viral Immunol.* **32**, 25–37 (2019).
23. Kim, Y.-I. *et al.* Infection and Rapid Transmission of SARS-CoV-2 in Ferrets. *Cell Host Microbe* **27**, 704-709.e2 (2020).
24. Munster, V. J. *et al.* Respiratory disease in rhesus macaques inoculated with SARS-CoV-2. *Nature* **585**, 268–272 (2020).
25. Rockx, B. *et al.* Comparative pathogenesis of COVID-19, MERS, and SARS in a nonhuman primate model. *Science* **368**, 1012–1015 (2020).
26. Yu, P. *et al.* Age-related rhesus macaque models of COVID-19. *Anim. Models Exp. Med.* **3**, 93–97 (2020).
27. Oreshkova, N. *et al.* SARS-CoV-2 infection in farmed minks, the Netherlands, April and May 2020. *Euro Surveill. Bull. Eur. Sur Mal. Transm. Eur. Commun. Dis. Bull.* **25**, (2020).
28. Shi, J. *et al.* Susceptibility of ferrets, cats, dogs, and other domesticated animals to SARS–coronavirus 2. *Science* **368**, 1016–1020 (2020).
29. Li, W. *et al.* Bats are natural reservoirs of SARS-like coronaviruses. *Science* **310**, 676–679 (2005).
30. Andersen, K. G., Rambaut, A., Lipkin, W. I., Holmes, E. C. & Garry, R. F. The proximal origin of SARS-CoV-2. *Nat. Med.* **26**, 450–452 (2020).
31. Wan, Y., Shang, J., Graham, R., Baric, R. S. & Li, F. Receptor Recognition by the Novel Coronavirus from Wuhan: an Analysis Based on Decade-Long Structural Studies of SARS Coronavirus. *J. Virol.* **94**, e00127-20 (2020).

32. Tseng, C.-T. K. *et al.* Severe acute respiratory syndrome coronavirus infection of mice transgenic for the human Angiotensin-converting enzyme 2 virus receptor. *J. Virol.* **81**, 1162–1173 (2007).

33. McCray, P. B. *et al.* Lethal infection of K18-hACE2 mice infected with severe acute respiratory syndrome coronavirus. *J. Virol.* **81**, 813–821 (2007).

34. Bao, L. *et al.* The pathogenicity of SARS-CoV-2 in hACE2 transgenic mice. *Nature* **583**, 830–833 (2020).

35. Liu, M. T. *et al.* Cutting Edge: The T Cell Chemoattractant IFN-Inducible Protein 10 Is Essential in Host Defense Against Viral-Induced Neurologic Disease1. *J. Immunol.* **165**, 2327–2330 (2000).

36. Stiles, L. N., Hardison, J. L., Schaumburg, C. S., Whitman, L. M. & Lane, T. E. T Cell Antiviral Effector Function Is Not Dependent on CXCL10 Following Murine Coronavirus Infection1. *J. Immunol.* **177**, 8372–8380 (2006).

37. Stiles, L. N., Liu, M. T., Kane, J. A. C. & Lane, T. E. CXCL10 and trafficking of virus-specific T cells during coronavirus-induced demyelination. *Autoimmunity* **42**, 484–491 (2009).

38. Trujillo, J. A., Fleming, E. L. & Perlman, S. Transgenic CCL2 Expression in the Central Nervous System Results in a Dysregulated Immune Response and Enhanced Lethality after Coronavirus Infection. *J. Virol.* **87**, 2376–2389 (2013).

39. Kim, T. S. & Perlman, S. Viral Expression of CCL2 Is Sufficient To Induce Demyelination in RAG1−/− Mice Infected with a Neurotropic Coronavirus. *J. Virol.* **79**, 7113–7120 (2005).

40. Held, K. S., Chen, B. P., Kuziel, W. A., Rollins, B. J. & Lane, T. E. Differential roles of CCL2 and CCR2 in host defense to coronavirus infection. *Virology* **329**, 251–260 (2004).

41. Chen, B. P., Kuziel, W. A. & Lane, T. E. Lack of CCR2 Results in Increased Mortality and Impaired Leukocyte Activation and Trafficking Following Infection of the Central Nervous System with a Neurotropic Coronavirus1. *J. Immunol.* **167**, 4585–4592 (2001).
42. Winkler, E. S. *et al.* Publisher Correction: SARS-CoV-2 infection of human ACE2-transgenic mice causes severe lung inflammation and impaired function. *Nat. Immunol.* **21**, 1470–1470 (2020).
43. Jiang, R.-D. *et al.* Pathogenesis of SARS-CoV-2 in Transgenic Mice Expressing Human Angiotensin-Converting Enzyme 2. *Cell* **182**, 50-58.e8 (2020).
44. Reichard, R. R. *et al.* Neuropathology of COVID-19: a spectrum of vascular and acute disseminated encephalomyelitis (ADEM)-like pathology. *Acta Neuropathol. (Berl.)* **140**, 1–6 (2020).
45. De-Paula, V. J., Radanovic, M., Diniz, B. S. & Forlenza, O. V. Alzheimer's Disease. in *Protein Aggregation and Fibrillogenesis in Cerebral and Systemic Amyloid Disease* (ed. Harris, J. R.) 329–352 (Springer Netherlands, Dordrecht, 2012). doi:10.1007/978-94-007-5416-4_14.
46. Newman, A. B. *et al.* Dementia and Alzheimer's disease incidence in relationship to cardiovascular disease in the Cardiovascular Health Study cohort. *J. Am. Geriatr. Soc.* **53**, 1101–1107 (2005).
47. Alford, S., Patel, D., Perakakis, N. & Mantzoros, C. S. Obesity as a risk factor for Alzheimer's disease: weighing the evidence. *Obes. Rev.* **19**, 269–280 (2018).
48. Lee, H. J. *et al.* Diabetes and Alzheimer's Disease: Mechanisms and Nutritional Aspects. *Clin. Nutr. Res.* **7**, 229–240 (2018).
49. Moulton, P. V. & Yang, W. Air Pollution, Oxidative Stress, and Alzheimer's Disease. *J.*

Environ. Public Health **2012**, 472751 (2012).

50. Hu, N. *et al.* Nutrition and the Risk of Alzheimer's Disease. *BioMed Res. Int.* **2013**, e524820 (2013).
51. Ramos-Cejudo, J. *et al.* Traumatic Brain Injury and Alzheimer's Disease: The Cerebrovascular Link. *EBioMedicine* **28**, 21–30 (2018).
52. Huat, T. J. *et al.* Metal Toxicity Links to Alzheimer's Disease and Neuroinflammation. *J. Mol. Biol.* **431**, 1843–1868 (2019).
53. Bellenguez, C. *et al.* New insights into the genetic etiology of Alzheimer's disease and related dementias. *Nat. Genet.* **54**, 412–436 (2022).
54. Goate, A. *et al.* Segregation of a missense mutation in the amyloid precursor protein gene with familial Alzheimer's disease. *Nature* **349**, 704–706 (1991).
55. St George-Hyslop, P. *et al.* Genetic evidence for a novel familial Alzheimer's disease locus on chromosome 14. *Nat. Genet.* **2**, 330–334 (1992).
56. Sherrington, R. *et al.* Alzheimer's Disease Associated with Mutations in Presenilin 2 is Rare and Variably Penetrant. *Hum. Mol. Genet.* **5**, 985–988 (1996).
57. Kim, J., Basak, J. M. & Holtzman, D. M. The Role of Apolipoprotein E in Alzheimer's Disease. *Neuron* **63**, 287–303 (2009).
58. Henderson, A. S. The risk factors for Alzheimer's disease: a review and a hypothesis. *Acta Psychiatr. Scand.* **78**, 257–275 (1988).
59. Levine, K. S. *et al.* Virus exposure and neurodegenerative disease risk across national biobanks. *Neuron* **111**, 1086-1093.e2 (2023).
60. Lotz, S. K., Blackhurst, B. M., Reagin, K. L. & Funk, K. E. Microbial Infections Are a Risk Factor for Neurodegenerative Diseases. *Front. Cell. Neurosci.* **15**, 691136 (2021).

61. Carbone, I. *et al.* Herpes virus in Alzheimer's disease: relation to progression of the disease. *Neurobiol. Aging* **35**, 122–129 (2014).

62. de Souza Rolim, T. *et al.* Oral infections and orofacial pain in Alzheimer's disease: a case-control study. *J. Alzheimers Dis. JAD* **38**, 823–829 (2014).

63. Dhingra, V., Li, Q., Allison, A. B., Stallknecht, D. E. & Fu, Z. F. Proteomic Profiling and Neurodegeneration in West-Nile-Virus-Infected Neurons. *J. Biomed. Biotechnol.* **2005**, 271–279 (2005).

64. Esiri, M. M., Biddolph, S. C. & Morris, C. S. Prevalence of Alzheimer plaques in AIDS. *J. Neurol. Neurosurg. Psychiatry* **65**, 29–33 (1998).

65. Little, C. S., Hammond, C. J., MacIntyre, A., Balin, B. J. & Appelt, D. M. Chlamydia pneumoniae induces Alzheimer-like amyloid plaques in brains of BALB/c mice. *Neurobiol. Aging* **25**, 419–429 (2004).

66. Miklossy, J. Historic evidence to support a causal relationship between spirochetal infections and Alzheimer's disease. *Front. Aging Neurosci.* **7**, 46 (2015).

67. Miklossy, J. *et al.* Beta-amyloid deposition and Alzheimer's type changes induced by Borrelia spirochetes. *Neurobiol. Aging* **27**, 228–236 (2006).

68. Chevalier, C. *et al.* PB1-F2 Influenza A Virus Protein Adopts a β-Sheet Conformation and Forms Amyloid Fibers in Membrane Environments. *J. Biol. Chem.* **285**, 13233–13243 (2010).

69. Ghosh, A. *et al.* Self-assembly of a nine-residue amyloid-forming peptide fragment of SARS corona virus E-protein: mechanism of self aggregation and amyloid-inhibition of hIAPP. *Biochemistry* **54**, 2249–2261 (2015).

70. Pham, C. L. *et al.* Viral M45 and necroptosis-associated proteins form heteromeric amyloid

assemblies. *EMBO Rep.* **20**, e46518 (2019).

71. Kiraly, M., Foss, J. F. & Giordano, T. Neuroinflammation, Its Role in Alzheimer's Disease and Therapeutic Strategies. *J. Prev. Alzheimers Dis.* **10**, 686–698 (2023).
72. Amruta, N. *et al.* Mouse Adapted SARS-CoV-2 (MA10) Viral Infection Induces Neuroinflammation in Standard Laboratory Mice. *Viruses* **15**, 114 (2022).
73. Klein, R. *et al.* COVID-19 induces neuroinflammation and loss of hippocampal neurogenesis. *Res. Sq.* rs.3.rs-1031824 (2021) doi:10.21203/rs.3.rs-1031824/v1.
74. Vanderheiden, A. *et al.* Vaccination prevents IL-1β-mediated cognitive deficits after COVID-19. *Res. Sq.* rs.3.rs-3353171 (2023) doi:10.21203/rs.3.rs-3353171/v1.
75. Green, R. *et al.* SARS-CoV-2 infection increases the gene expression profile for Alzheimer's disease risk. *Mol. Ther. Methods Clin. Dev.* **27**, 217–229 (2022).
76. Käufer, C. *et al.* Microgliosis and neuronal proteinopathy in brain persist beyond viral clearance in SARS-CoV-2 hamster model. *EBioMedicine* **79**, 103999 (2022).
77. Malenka, R. C. & Nicoll, R. A. Long-term potentiation--a decade of progress? *Science* **285**, 1870–1874 (1999).
78. Giannos, P., Prokopidis, K., Raleigh, S. M., Kelaiditi, E. & Hill, M. Altered mitochondrial microenvironment at the spotlight of musculoskeletal aging and Alzheimer's disease. *Sci. Rep.* **12**, 11290 (2022).
79. Wang, W., Zhao, F., Ma, X., Perry, G. & Zhu, X. Mitochondria dysfunction in the pathogenesis of Alzheimer's disease: recent advances. *Mol. Neurodegener.* **15**, 30 (2020).
80. Toomey, C. E. *et al.* Mitochondrial dysfunction is a key pathological driver of early stage Parkinson's. *Acta Neuropathol. Commun.* **10**, 134 (2022).
81. Quintanilla, R. A. & Johnson, G. V. W. Role of Mitochondrial Dysfunction in the

Pathogenesis of Huntington's Disease. *Brain Res. Bull.* **80**, 242–247 (2009).